COPY NO. 34

NASA CR 152240
REPORT MDC A5702 • JULY 1979

INVESTIGATION OF GROUND EFFECTS ON LARGE AND SMALL SCALE MODELS OF A THREE FAN V/STOL AIRCRAFT CONFIGURATION

MCDONNELL DOUGLAS CORPORATION

COPY NO. 36

NASA CR 152240
REPORT MDC A5702 • JULY 1979

INVESTIGATION OF GROUND EFFECTS ON LARGE AND SMALL SCALE MODELS OF A THREE FAN V/STOL AIRCRAFT CONFIGURATION

Contract No. NAS 2-9690

PREPARED BY

E.P. Schuster
T.D. Carter
D.W. Esker

MCDONNELL AIRCRAFT COMPANY

Box 516, Saint Louis, Missouri 63166 – Tel. (314)232-0232

MCDONNELL DOUGLAS

SUMMARY

Exhaust jet induced forces and moments imposed upon V/STOL aircraft operating in ground proximity may seriously degrade vertical lift performance and aircraft control capability. Empirical scale model investigations have shown the induced aerodynamics to be highly sensitive to aircraft geometry and the propulsion system arrangement. This report describes induced lift investigations of a subsonic, three fan, lift/cruise, V/STOL aircraft configuration conducted with both large and small scale models. The aircraft is a multimission design incorporating a nose mounted lift fan and two lift/cruise units located over the wing.

Follow-on tests of an existing NASA powered model (70 percent scale) were conducted at the NASA Ames Static Test Facility to establish ground effect performance. Concurrently, model tests of the same aircraft configuration at 4.1 percent scale were carried out at McDonnell Aircraft Company. Results of the large and small scale tests are presented for the baseline aircraft and for several variations of the lower surface geometry.

Configuration effects were assessed for lift improvement devices, lift/cruise nozzle rails, nozzle perimeter plates, and alternate nose fan exit hubs. Tests were conducted at four model heights (H/D = 0.95, 1.53, 3.06 and 6.45, where D is the average nozzle exit diameter equal to 0.997 m.)

Significant test results include:

- Based on the small scale model tests, static induced lift for three fan operation is estimated to be negative three percent at landing gear height (H/D = 1.2) and varies little above H/D = 1.5.
- The large and small scale model induced lift trends show agreement with respect to variations of model height and model lower surface geometry.
- In general, the large scale data exhibit greater lift loss than the small scale data at all heights tested. The difference between the large and small scale model results is not interpreted as only the effect of model scale and model differences, but also a consequence of uncertainty in the large scale model lift measurements.
- Lift improvement devices provide positive lift increments for H/D values below 1.5.
- Rails located between the lift/cruise nozzles are effective in generating positive lift increments at H/D = 0.95.
- An increase in lift fan thrust in close ground proximity is a result of fan exit hub base pressurization.

TABLE OF CONTENTS

LIST OF PAGES

LIST OF FIGURES

LIST OF FIGURES (continued)

LIST OF FIGURES (continued)

LIST OF FIGURES (continued)

NOMENCLATURE

GENERAL SYMBOLS

Symbol	Description	Units
AF	Total measured axial force	N (lbf)
AFAN	Fan exit area	M^2 (in^2)
ATE	Turbine Exit Area	M^2 (in^2)
b	Wing Span	M (in)
B.L.	Butt line	M (in)
c	Chord	M (in)
$\bar{c}$	Mean aerodynamic chord	M (in)
CF	Rake thrust coefficient	---
CAF	Fan mass flow coefficient	---
CAT	Turbine mass flow coefficient	---
C_v	Velocity Coefficient	
C_w	Discharge Coefficient	
D	Average nozzle exit diameter, 0.997m (39.25 in)	M (in)
EGT	Exhaust gas temperature	°C (°F)
F_G	Force, thrust	N (lbf)
F_H	Pressure integrated hub force	N (lbf)
F.S.	Fuselage station	M (in)
H	Model height above ground measured from left/cruise nozzle exit	M (ft)
L	Lift	N (lbf)
L/C	Lift/cruise	---
L/H	Left lift/cruise unit	---
LID	Lift improvement device	---
L.S.	Model lower surface	---
LSPM	Large scale powered model	---
MCAIR	McDonnell Aircraft Company	---
MF	Rake calculated fan exit Mach number	---
MI	Ideal Mach number at nozzle entrance	---

NOMENCLATURE

GENERAL SYMBOLS (Continued)

Symbol	Description	Units
M_p	Airframe Pitching Moment	N-M (in-lbf)
MT	Rake calculated turbine exit Mach number	---
N_F	Fan speed	rpm
NF	Total measured normal force	N (lbf)
P_{amb}	Ambient static pressure	N/M^2 (psi)
P_{hub}	Nose fan exit hub pressure	N/M^2 (psi)
PM_i	Induced pitching moment	N-M (in-lbf)
PSFE	Static pressure, arithmetic average at fan exit rake	N/M^2 (psi)
PSNI	Static pressure, mass weighted average at nozzle entrance	N/M^2 (psi)
PSTE	Static pressure, arithmetic average at turbine exit rake	N/M^2 (psi)
PTFE	Total pressure, area weighted average at fan exit rake	N/M^2 (psi)
PTTE	Total pressure, area weighted average at turbine exit rake	N/M^2 (psi)
PTNI	Total pressure, mass weighted average at nozzle entrance	N/M^2 (psi)
SF	Total measured side force	N (lbf)
T_I	Inlet total temperature	°K (°R)
T_J	Mass averaged exhaust jet temperature	°K (°R)
TTFE	Total temperature, area weighted average at fan exit rake	°K (°R)
TTNI	Total temperature, mass weighted average at nozzle entrance	°K (°R)
TTTE	Total temperature, area weighted average at turbine exit rake	°K (°R)
VI	Ideal airflow velocity at nozzle entrance	M/sec (ft/sec)
V/STOL	Vertical/short takeoff and landing	---
WBF	Bellmouth measured fan airflow	Kg/sec (lbm/sec)

NOMENCLATURE

GENERAL SYMBOLS (Continued)

Symbol	Description	Units
WF	Rake calculated fan exit airflow	Kg/sec (lbm/sec)
W. L.	Water line	---
WT	Rake calculated turbine exit airflow	Kg/sec (lbm/sec)
VI	Rake calculated ideal airflow velocity	M/sec (ft/sec)

GREEK SYMBOLS

Δ	Incremental	---
δ	Relative static pressure (P (psi)/14.696)	---
δ_{LC}	Lift cruise unit hood geometric deflection	deg
δ_{NL}	Nose lift unit lower geometric deflection	deg
δ_{Y}	Nozzle yaw vane deflection	deg
θ	Relative total temperature (T (°R)/518.7)	---

EQUATIONS

$$C_F = \frac{\sqrt{(SF)^2 + (AF)^2 + (NF)^2}}{(WF + WT)\ VI}$$

$$CAF = \frac{WBF}{WF}$$

$$CAT = \frac{WBT}{WT}$$

$$MF = \sqrt{\frac{2.0\ (PTFE/PSFE)^{0.2857} - 2.0}{0.4}}$$

$$MI = \sqrt{\frac{2.0\ (PTNI/PSNI)^{0.2857} - 2.0}{0.4}}$$

$$MT = \sqrt{\frac{2.0\ (PTTE/PSTE)^{0.2857} - 2.0}{0.4}}$$

$$PM_i = M_p - F_{G_{NOSE}}\ (4.045) + (F_{G_{L/H}} + F_{G_{R/H}})(2.097)$$

$$VI = (MI)\sqrt{\frac{2403.1\ (TTNI)_2}{1 + 0.2\ (MI)}}$$

$$WF = \frac{(PSFE)\ (AFANE)}{\sqrt{TTTE}}\ (0.9188)\ (MF)\ \sqrt{1 + 0.2\ (MF)^2}$$

$$WT = \frac{(PSTE\ (ATE)}{\sqrt{TTTE}}\ (0.9057\ (MT)\ \sqrt{1 + 0.18\ (MT)^2}$$

1. INTRODUCTION

Exhaust jet induced forces and moments imposed upon V/STOL aircraft operating in ground proximity may seriously degrade vertical lift performance and aircraft control capability. The induced effects are a result of the interactions of the nozzle exhaust, ground and aircraft surfaces which produce a complex flow field beneath the aircraft. A number of empirical, small scale investigations, References 1-4, have shown that the induced aerodynamics are highly sensitive to aircraft geometry and the propulsion system arrangement. Accordingly, accurate ground effect characteristics are required for meaningful evaluation of competitive V/STOL aircraft designs.

The lift/cruise fan V/STOL aircraft concept is a design which NASA and McDonnell Aircraft Company (MCAIR) have investigated over the last decade involving both conceptual design studies and component hardware tests. In 1974, NASA, with MCAIR as contractor, built and tested a 70 percent scale powered model of a 3 fan, lift/cruise aircraft configuration. Figure 1-1 is a schematic of the aircraft model which is a subsonic, low wing, multimission design. The propulsion system arrangement consists of a nose mounted lift fan and two lift/cruise fan units located over the wing. The initial studies of this large scale powered model (LSPM) included both low speed tests in the 40 x 80 ft wind tunnel and outside static ground effect testing at the static test facility at NASA-Ames Research Center. The ground effect test results, Reference 5, indicated some unusual characteristics.

It was found in this initial test that the effect of ground height on total lift was less than one percent over the range of test heights, H/D between 1 and 6.45. Pressure and temperature measurements at the exit of each fan, however, indicated that the total thrust of the fan propulsion units fell off as ground height was reduced and decreased to 93% of the out-of-ground effect level at an H/D of 2.5. Between 2.5 and 1.0 H/D, the total thrust increased, primarily due to a large thrust increase indicated on the nose mounted lift fan. The difference between the balance measured total lift and the rake measured thrust was attributed to a positive lift force on the aircraft lower surface resulting from impingement of the jet exhaust flows. It was further postulated that the increase in nose fan thrust level at low ground heights was due to ground effect pressurization of the nose fan exit hub area. These initial LSPM results were at variance with subsequent test data obtained on a small scale, flat plate model of a generically similar 3 fan aircraft, Reference 4. The flat plate model results indicated a lift loss of nine percent at an H/D of 1.0.

FIGURE 1-1
3-FAN V/STOL AIRCRAFT
70% Scale Powered Model

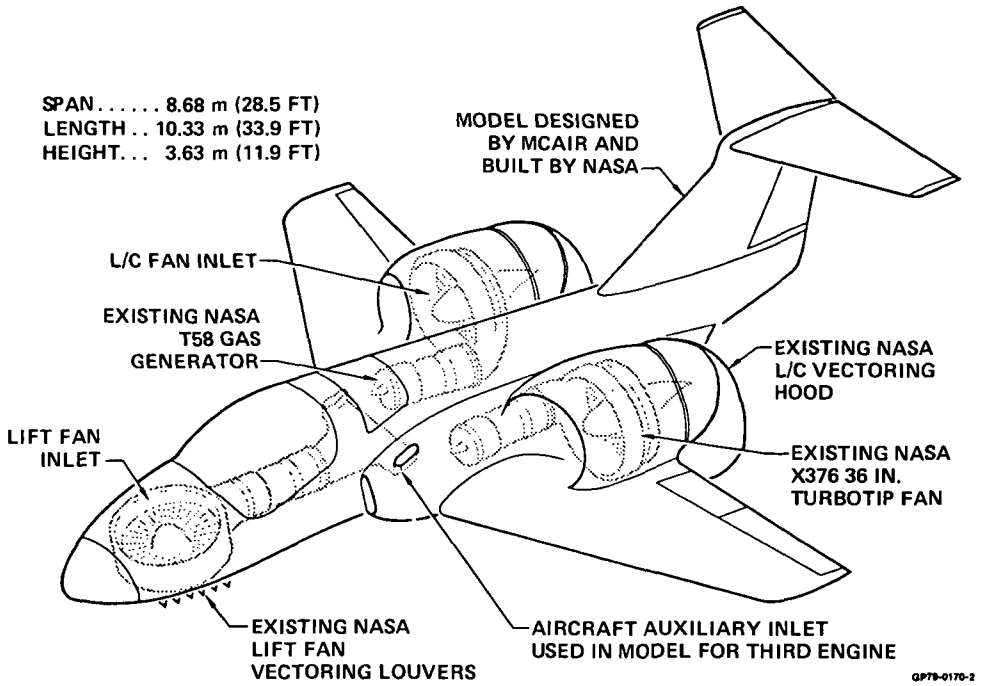

Questions concerning the proper induced lift characteristics to be assigned the three fan aircraft provided the impetus for further investigations of this configuration. An experimental approach was taken which involved both follow-on tests of the LSPM at NASA-Ames and a small scale three-dimensional model of the LSPM configuration at MCAIR. The scope of the effort was designed to establish test technique, investigate in particular the nose fan characteristics in ground effect and further to identify where possible the effects of model scale on induced lift characteristics.

The LSPM follow-on test program at NASA-Ames was performed somewhat differently than the initial program. In the follow-on program, the individual propulsion units installed in the LSPM were removed from the model and isolated calibrations of each were performed in and out of ground effect. This effort established thrust and mass flow coefficients for the fan exit pressure and temperature rakes and thereby means were provided to remove the direct thrust forces from the LSPM total lift measurements.

Modifications to the LSPM included addition of instrumentation to record the lower airframe surface pressure and temperature distributions and means to change the thrust vector angles on the lift/cruise units from 84° to 90°. Additional hardware was fabricated to investigate changes to the model lower surface geometry and included

a rectangular lift improvement device, lift/cruise nozzle rails, nozzle perimeter plates which closed gaps surrounding the lift/cruise nozzle exits and a hemispherical nose lift fan exit hub.

Concurrently, tests of a 4.1 percent scale model of the three fan LSPM were carried out in the MCAIR Propulsion Subsystem Test Facility. This model was instrumented to provide lower airframe surface pressure measurements and was tested over the same range of model heights and lower surface geometry variations as covered in the LSPM test program. The effect of the LSPM support struts on induced lift was also evaluated during the small scale program.

The results of both the follow-on LSPM tests and the small scale test program and comparisons are presented in this report. The results of the isolated fan calibrations are reported under separate cover as Reference 6.

An exploratory investigation of the flow field below the large scale powered model was carried out concurrently with the induced lift program. Velocity measurements in the nozzle exhaust and fountain upwash regions were obtained by means of a laser Doppler velocimeter. A description of this flow field study is presented in Reference 7.

The overall program was conducted under Contract NAS 2-9690. Mr. L. Stewart Rolls and Mr. Bruno Gambucci of NASA-Ames Research Center served successively as Technical Monitor. MCAIR established the design modifications to the LSPM test apparatus. Fabrication and assembly of the LSPM test hardware were performed at NASA-Ames. The LSPM tests were carried out by NASA personnel with MCAIR support between 4 June 1978 and 28 July 1978. Data analysis and documentation were performed by MCAIR. The complete small scale test program was carried out by MCAIR.

A description of the test apparatus used in these two programs is presented in Section 2. In Section 3 the calibration tests performed for both the large and small scale model programs are summarized, the program test results and discussion are presented in Section 4 and the conclusions in Section 5. Schedules of test runs for the two test series are presented in Appendix A.

2. EXPERIMENTAL APPARATUS

The experimental hardware, instrumentation, data acquisition and test facilities utilized for the LSPM and the 4.1 percent scale model test programs are described in this section.

2.1 LARGE SCALE POWERED MODEL (LSPM) DESCRIPTION

The LSPM configuration represents a subsonic, fixed low wing, lift/cruise fan V/STOL aircraft design reduced to 70 percent scale. The model was originally built at NASA-Ames in 1974. The main features of the model include three gas generator driven turbotip fans and variable geometry for all control surfaces and vectoring system components. The size and detail design of the model were based on utilization of existing propulsion system components, including the gas generators, turbotip fans and vectoring system components supplied by NASA-Ames. The physical size and performance characteristics of the T58-GE-8B gas generator and low pressure ratio (1.08) GE-X376B turbotip fan were the predominant considerations in sizing the model. A schematic of the model illustrating the major propulsion system components is shown in Figure 2-1. The basic geometry and overall dimensions of the model configuration are shown in Figure 2-2.

Modifications of the model were made for this program to permit testing of a variety of devices including:

- o Lift Improvement Devices (LID)
- o Lift/cruise nozzle rails
- o Lift/cruise nozzle perimeter plates
- o Hemispherical nose fan exit hub.

A brief description of the model and propulsion system components is presented below. A detailed description is available in Reference 5.

2.1.1 LSPM AIRFRAME - The fuselage shape of the aircraft accommodates side-by-side seating in the forward fuselage, and provides volume in the center fuselage for satisfying the needs of the multimission role. This wide bodied design permits installation of the lift fan unit in the forward fuselage section of the aircraft.

The model incorporated a low wing with lower surface flush with the bottom of the center fuselage. The wing had an aspect ratio of 4.5, a taper ratio of 0.30, and a quarter chord line sweep of 25°. Total wing planform area was 16.75 m^2 (180.3 ft^2). The wing had different airfoil sections inboard and outboard of the lift/cruise fan nacelle/wing intersection. The inboard panel utilized an NACA 4416 airfoil section, and the outboard wing panel used modified supercritical airfoil sections at root and tip.

FIGURE 2-1
LARGE SCALE POWERED MODEL PROPULSION SYSTEM

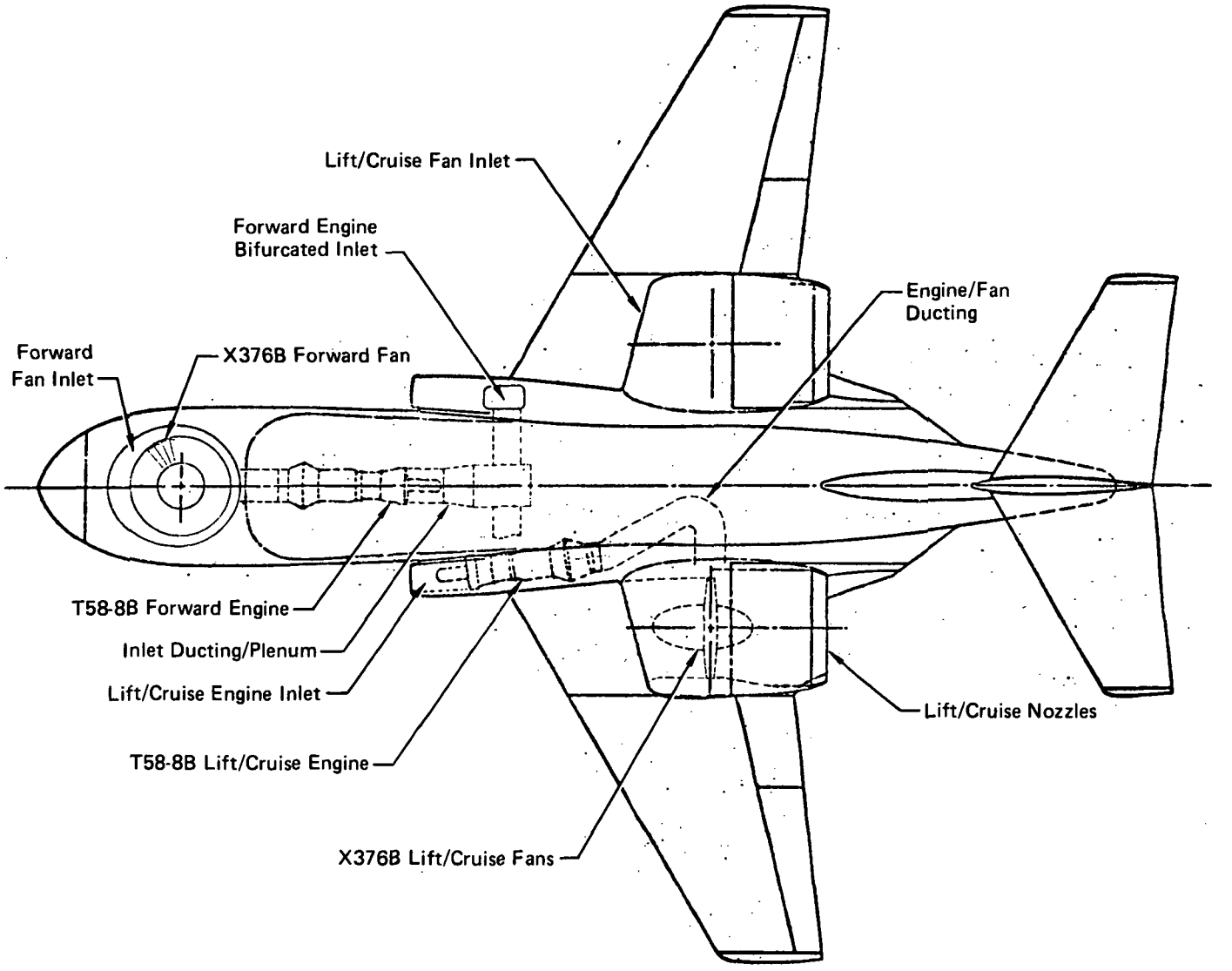

FIGURE 2-2
LARGE SCALE POWERED MODEL
Basic Geometry

	Wing	Horizontal Tail	Vertical Tail
Area, m^2 (ft^2)	16.572 (180.32)	4.006 (43.12)	3.096 (33.32)
Aspect Ratio	4.500	3.665	0.688
Taper Ratio	0.300	0.405	0.433
b, m (ft)	8.682 (28.49)	3.832 (12.57)	1.459 (4.787)
C_{root}, m (ft)	2.968 (9.738)	1.488 (4.882)	2.960 (9.711)
C_{tip}, m (ft)	0.890 (2.920)	0.603 (1.978)	1.282 (4.206)
$\bar{C}$, m (ft)	2.116 (6.942)	1.108 (3.635)	2.232 (7.323)
Λ C/4	25.00°	25.20°	45.50°

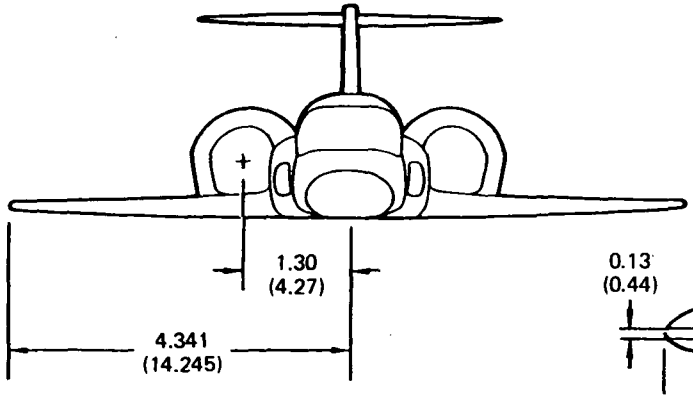

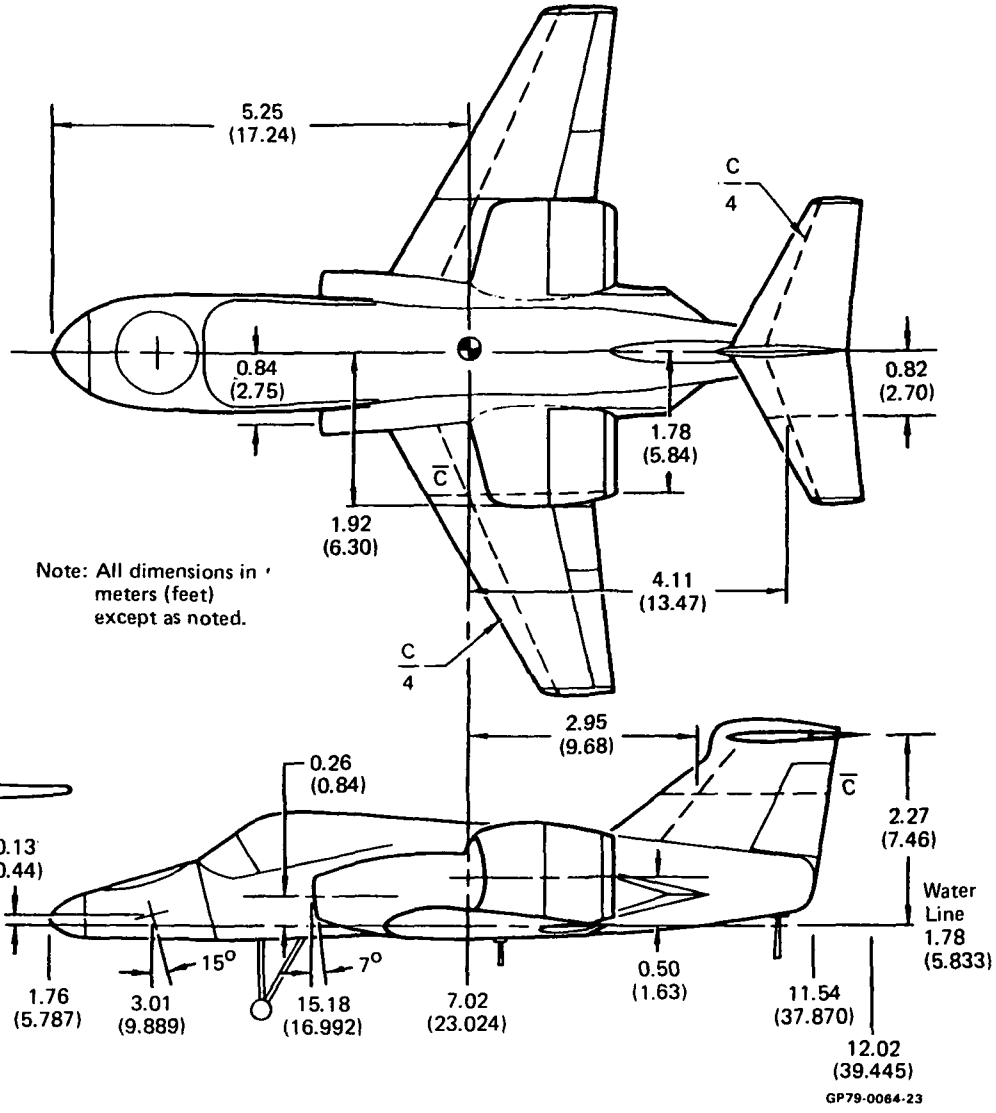

Note: All dimensions in meters (feet) except as noted.

The empennage consisted of a "T" tail configuration with a movable horizontal stabilator and vertical stabilizer with movable rudder. The vertical tail utilized a NACA 65A010 airfoil section and the horizontal tail was a symmetrical NACA 64A0XX airfoil section with thickness ratio of 0.10 at the root and 0.08 at the tip.

2.1.2 LSPM AIR INDUCTION SYSTEM - The model air induction system consisted of the lift/cruise fan inlets, the nose fan inlet, and gas generator inlets for each installation as shown in Figures 2-3 and 2-4.

FIGURE 2-3
LSPM FAN INLET SYSTEMS

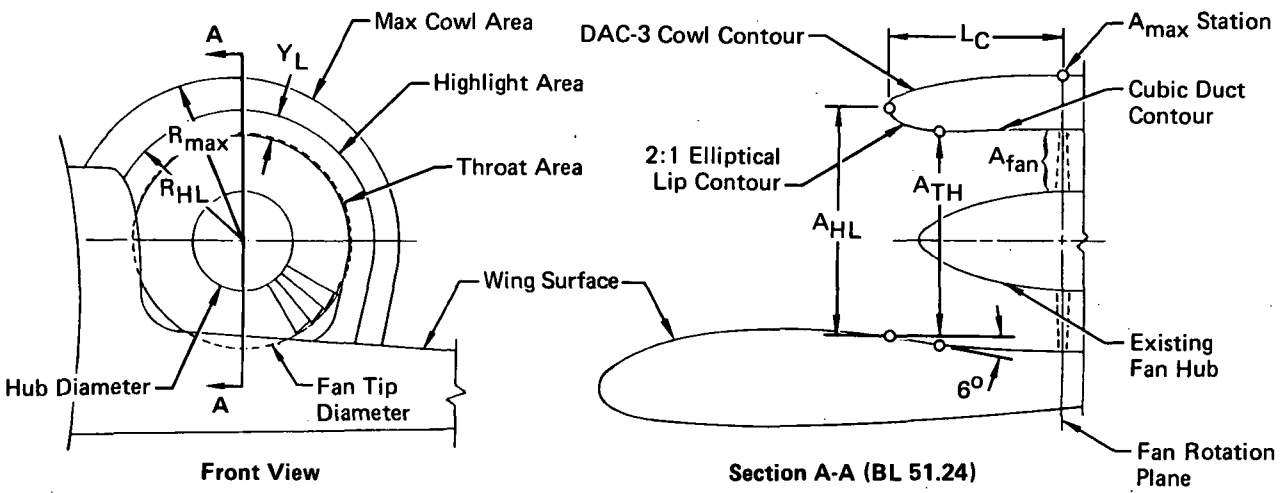

Lift/Cruise Fan Inlet

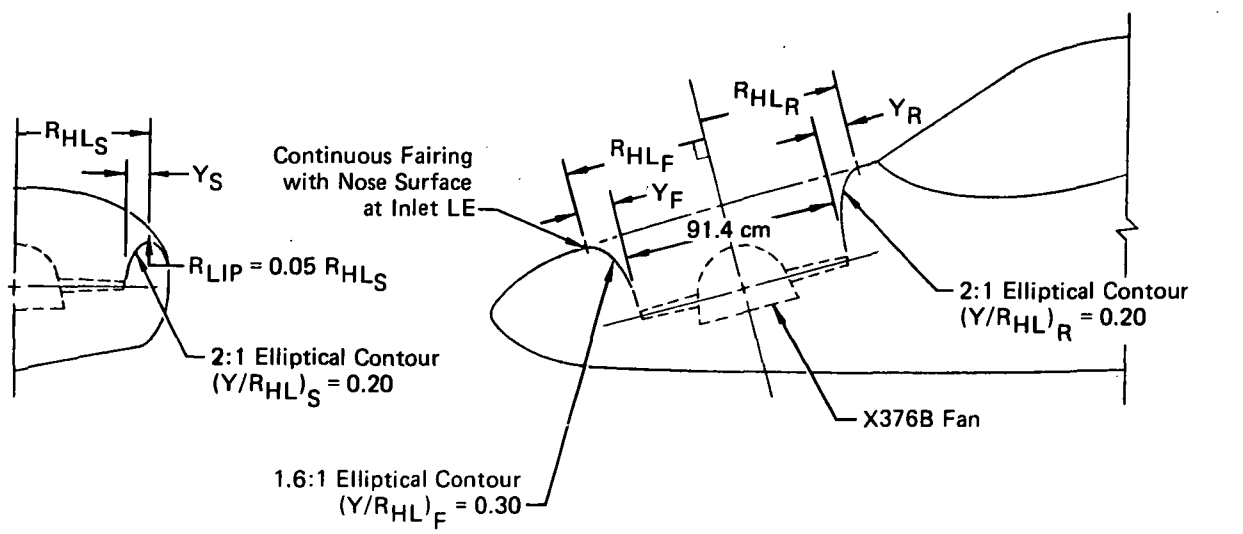

Nose Fan Inlet

FIGURE 2-4
LIFT/CRUISE GAS GENERATOR INLET DESIGN GEOMETRY

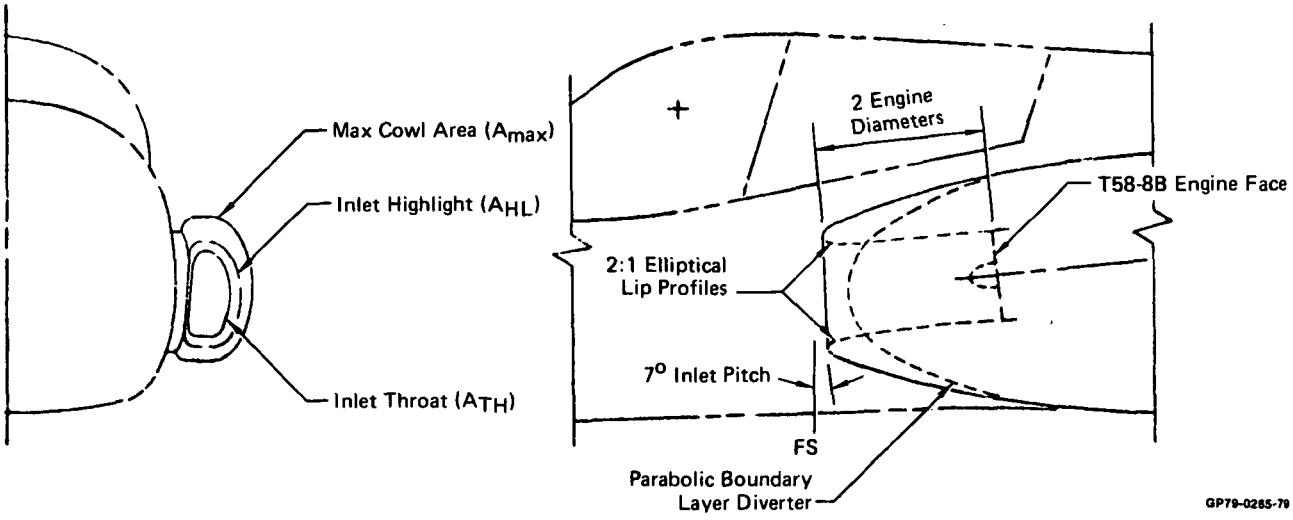

The lift/cruise fan inlets were located over the wing and adjacent to the fuselage in a fully integrated design concept. They were fixed geometry inlets with an internal contraction ratio (A_{HL}/A_{TH}) of 1.25, a 2:1 elliptical lip profile and cubic duct contours internally. A low drag modified elliptical cowl contour was used externally.

The lift/cruise engine inlets were side mounted with fixed geometry. They also had an inlet contraction ratio of 1.25, a 2:1 elliptical internal lip shape, and low drag, modified elliptical cowl contours external. Parabolic boundary layer diverters were incorporated between the inlets and the fuselage.

The nose fan inlet was located in the nose of the aircraft just downstream of the radome and forward of the canopy. It was a flush mounted inlet with an overall resultant contraction ratio (A_{HL}/A_{FAN}) of 2.09. The forward section of the inlet had a lip thickness ratio (Y/R_{HL}) of 0.30. This decreased to a minimum thickness ratio of 0.20 at the sides, and remained constant over the aft section of the inlet. The inlet had a 1.6:1 elliptical tip profile at the leading edge which increased to a 2:1 elliptical profile at the side. The 2:1 profile was maintained over the aft section of the inlet.

The nose fan gas generator inlet design consisted of two flush mounted inlets, each ducted into a common plenum located upstream of the aft facing gas generator (Figure 2-1). The inlets were located on the upper surface of the lift/cruise gas generator nacelles at the approximate wing leading edge station. Each inlet had a contraction ratio (A_{HL}/A_{TH}) of 4.0 and a diffusion ratio (A_{PLENUM}/A_{TH}) into the plenum of 1.5.

2.1.3 LSPM PROPULSION UNITS - Three identical 91.44 cm diameter GE-X376B turbotip fans were installed in the model, each one driven by a modified T58-GE-8B gas generator. The engine and fan for each lift unit were interconnected with steel ducts and bellows arranged as shown in Figure 2-1. The gas generators, turbotip fans, interconnect ducting and bellows were existing hardware items supplied by the Large Scale Aerodynamics Branch (LSAB) of NASA-Ames. The design characteristics of the gas generator and fan are presented in Figure 2-5. The performance values given are engine specification values, and are presented for reference only.

2.1.4 LSPM THRUST VECTORING NOZZLES - The exhaust nozzle systems installed on the LSPM included two lift/cruise nozzles and a nose lift nozzle illustrated in Figures 2-6 and 2-7. The lift/cruise nozzle consisted of a fan exit diffuser, circular hood deflector and exit cone. The diffuser was formed by the combination of the fan exit hub and constant diameter outer duct and had an area ratio of 1.5. The hood element was formed of multiple constant area segments and had a radius of curvature to duct diameter ratio of 0.54.

For this test program, an additional 5° hood element was fabricated to change the geometric deflection angle, δ_{LC}, to 95° and the thrust vector angle from 84° to 90°.

The nozzle exit cone was detachable, and was equipped with two 10% thickness to length ratio, articulated yaw vanes. These vanes provided lateral vectoring to produce yawing moments. The nozzle cone had a fixed nozzle exit area of 0.7677 m^2 (1190 $in.^2$) with an exit contraction ratio (A_{HOOD}/A_{NOZ}) of 1.16.

The nose lift unit thrust vectoring nozzle system utilized a remotely activated louver system. Fourteen low camber louvers, each with a thickness ratio of 10%, provided thrust vectoring over a range from 105° to 30°. Two 10% thickness ratio, articulated yaw vanes located beneath the louvers provided yaw vectoring of 0°, $\pm$6° and $\pm$12°. The yaw vanes were of the same design as those on the lift/cruise units, and were detachable from the model.

An alternate hemispherical shaped hub was fabricated for the nose fan installation to evaluate the effects of hub shape on fan performance. Figure 2-8 is a photograph of the original flat plate hub and the new hemispherical hub. Figure 2-9 shows the nose fan exit louver nozzle and hub installation.

FIGURE 2-5
GAS GENERATOR AND TURBOTIP FAN DESIGN CHARACTERISTICS

T58-GE-8B Gas Generator

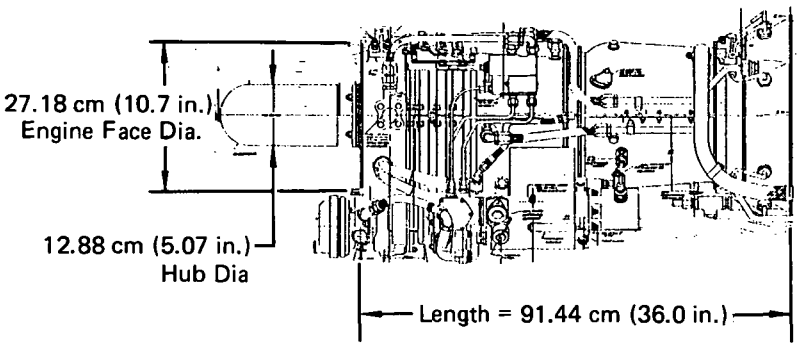

Design Point Performance (Intermediate Power)

Air Flow	5.62 kg/sec
Compressor Pressure Ratio	8.0:1
Turbine Inlet Temperature	932°C
Exhaust Gas Temperature	677°C
Engine Speed	19,500 rpm

GE-X376B Turbotip Fan

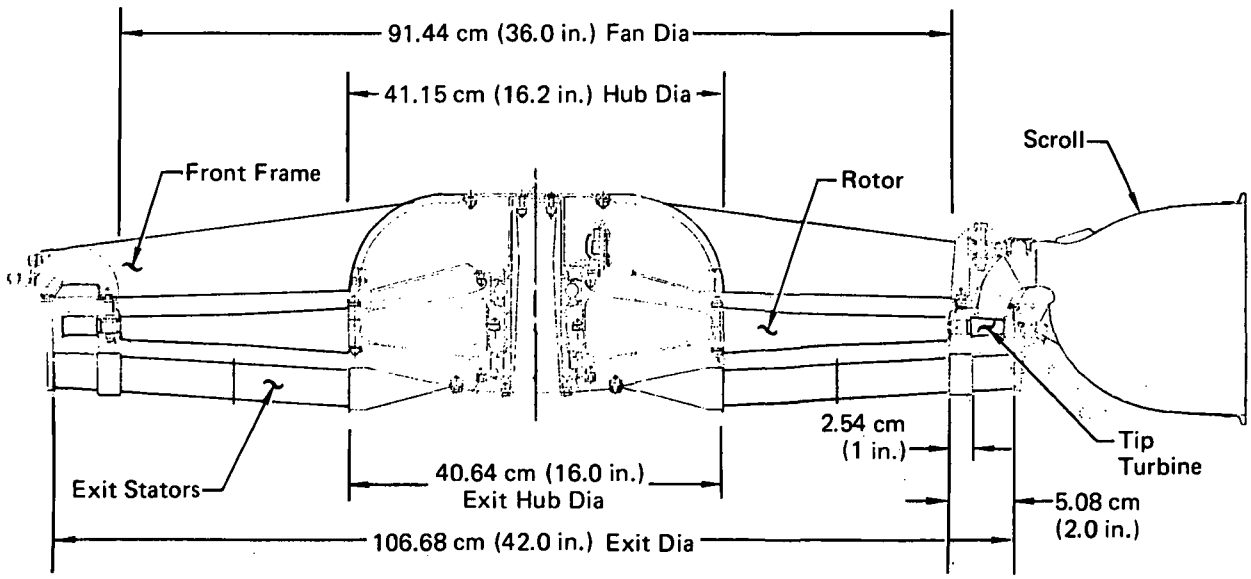

Design Point Performance (100% Speed)

Air Flow	69.4 kg/sec
Fan Pressure Ratio	1.08
Admission Arc	180°
Fan Speed (100%)	4074 rpm

GP79-0064-4

FIGURE 2-6
LIFT/CRUISE UNIT VECTORING SYSTEM GEOMETRY

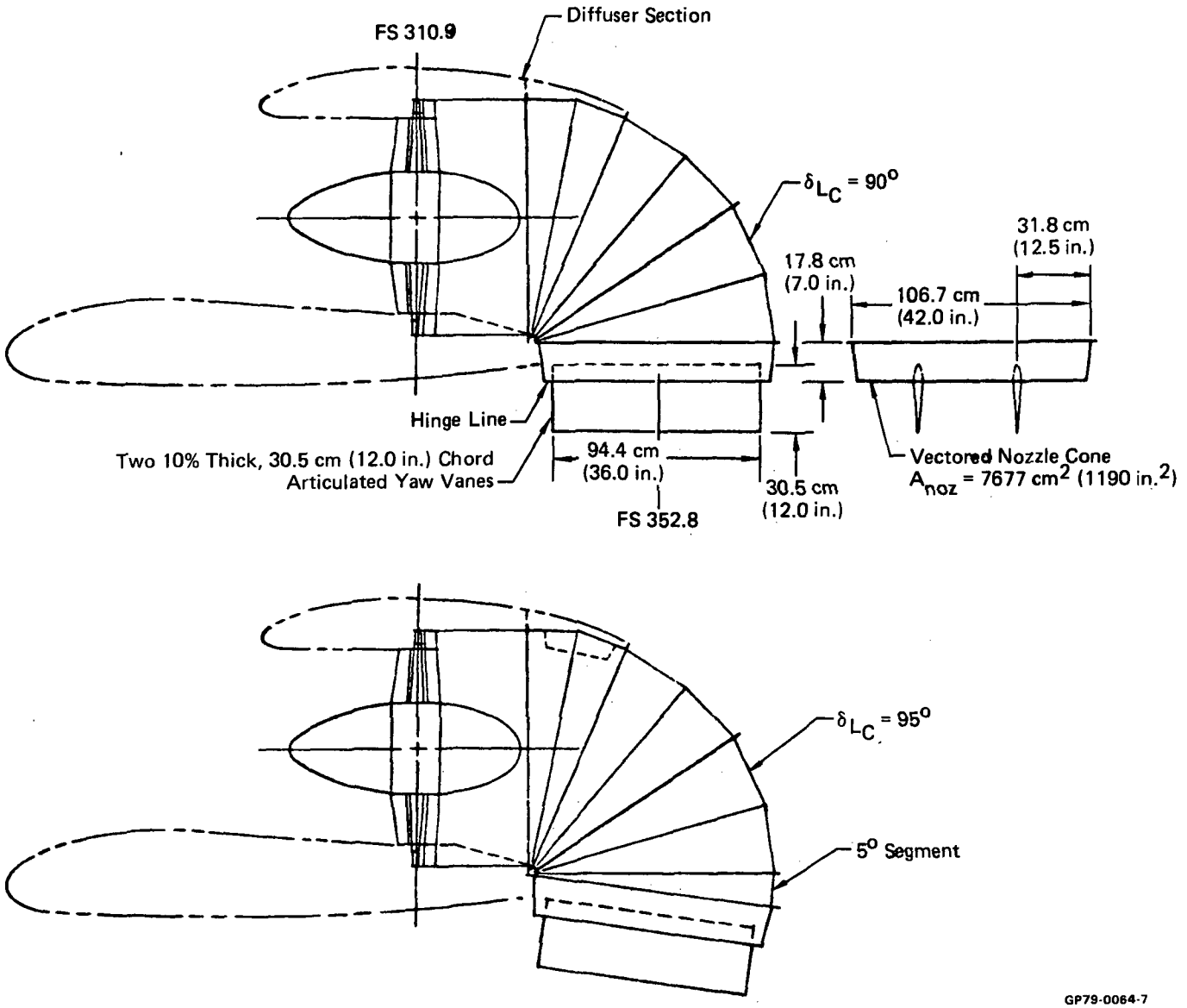

FIGURE 2-7
NOSE LIFT UNIT VECTORING SYSTEM GEOMETRY

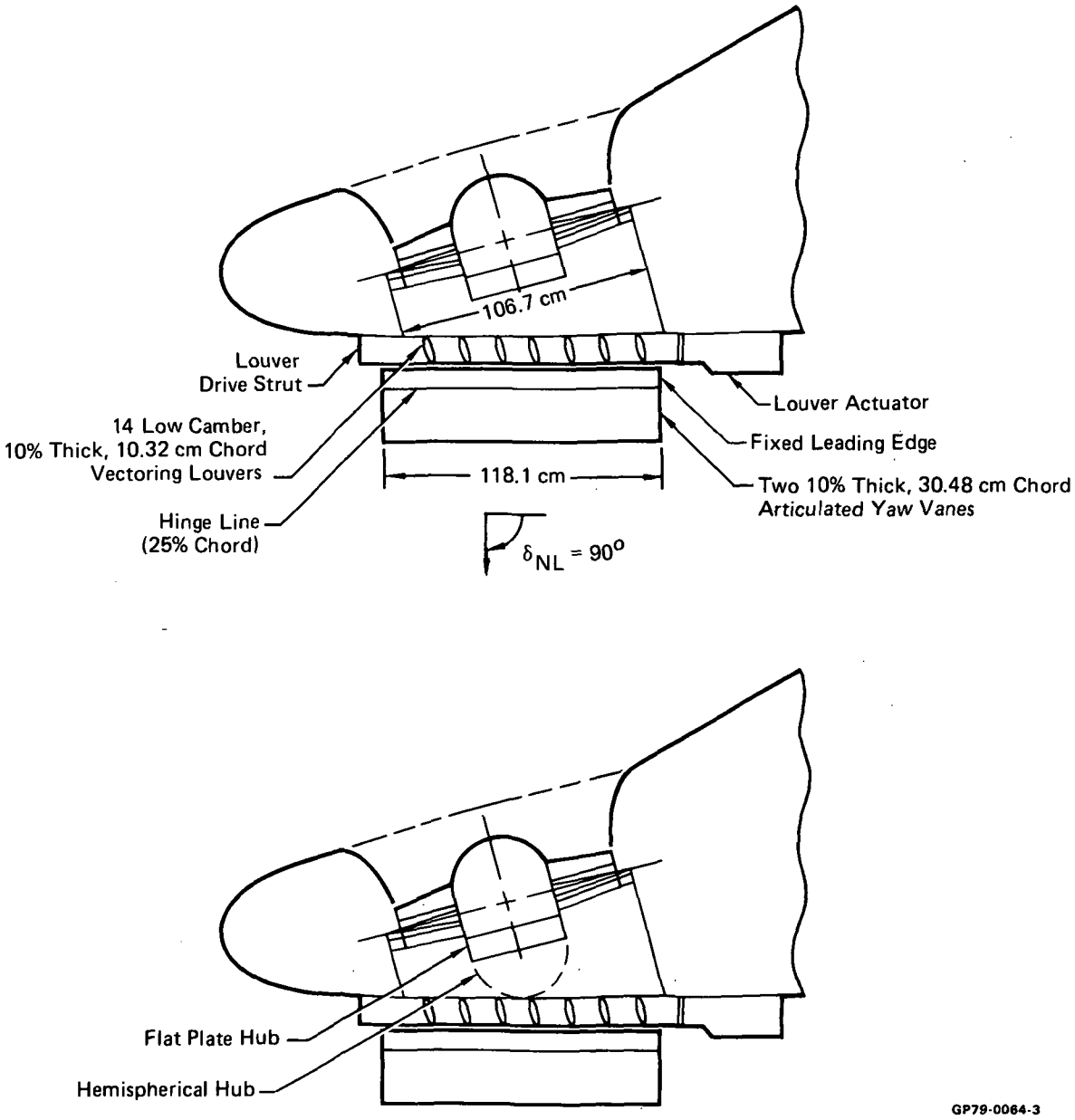

FIGURE 2-8
NOSE FAN EXIT HUBS HEMISPHERICAL AND FLAT PLATE

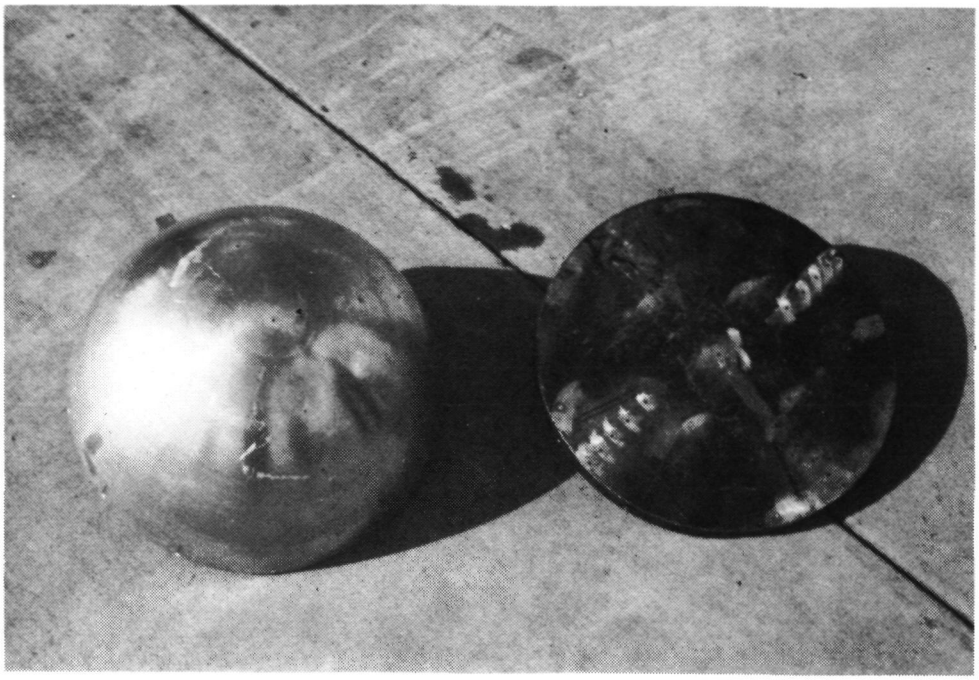

GP79-0064-16

FIGURE 2-9
NOSE FAN EXIT LOUVER INSTALLATION

GP79-0064-17

2.1.5 LSPM LIFT MODIFICATION DEVICES - A fully removable rectangular lift improvement device (LID) was fabricated for this program and is shown schematically in Figure 2-10. It consisted of two longitudinal strakes and a forward and aft fence. This boxlike arrangement was configured into 2 sided and 3 sided LIDs by removing the fore and aft fences. The LID had an overall length of 4.3 meters, a width of 1.1 meters and a height of 0.3 meters. The 4 sided LID installed on the model is shown in Figure 2-11.

FIGURE 2-10
RECTANGULAR LIFT IMPROVEMENT DEVICE (LID)

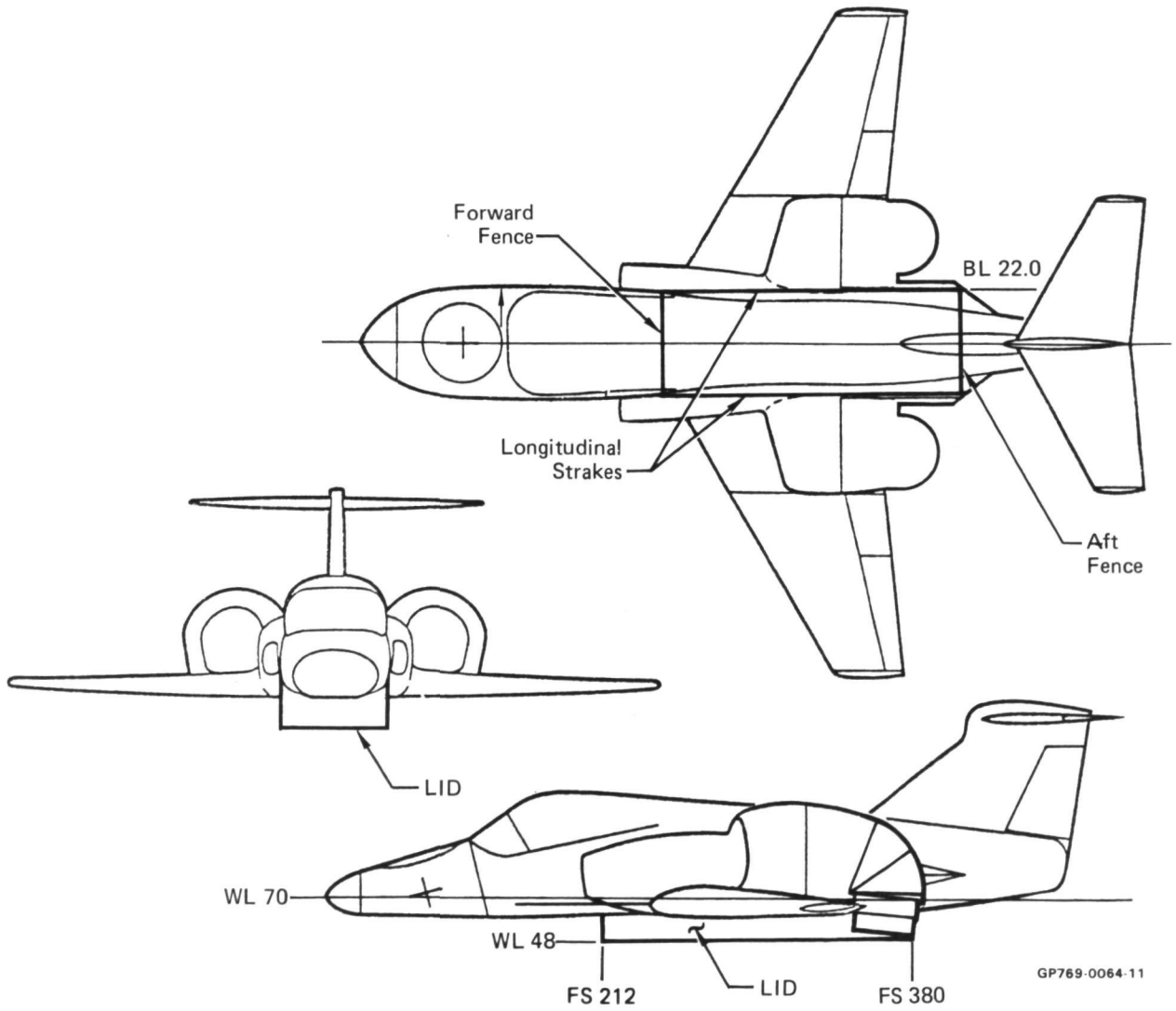

FIGURE 2-11
LID INSTALLATION ON LSPM

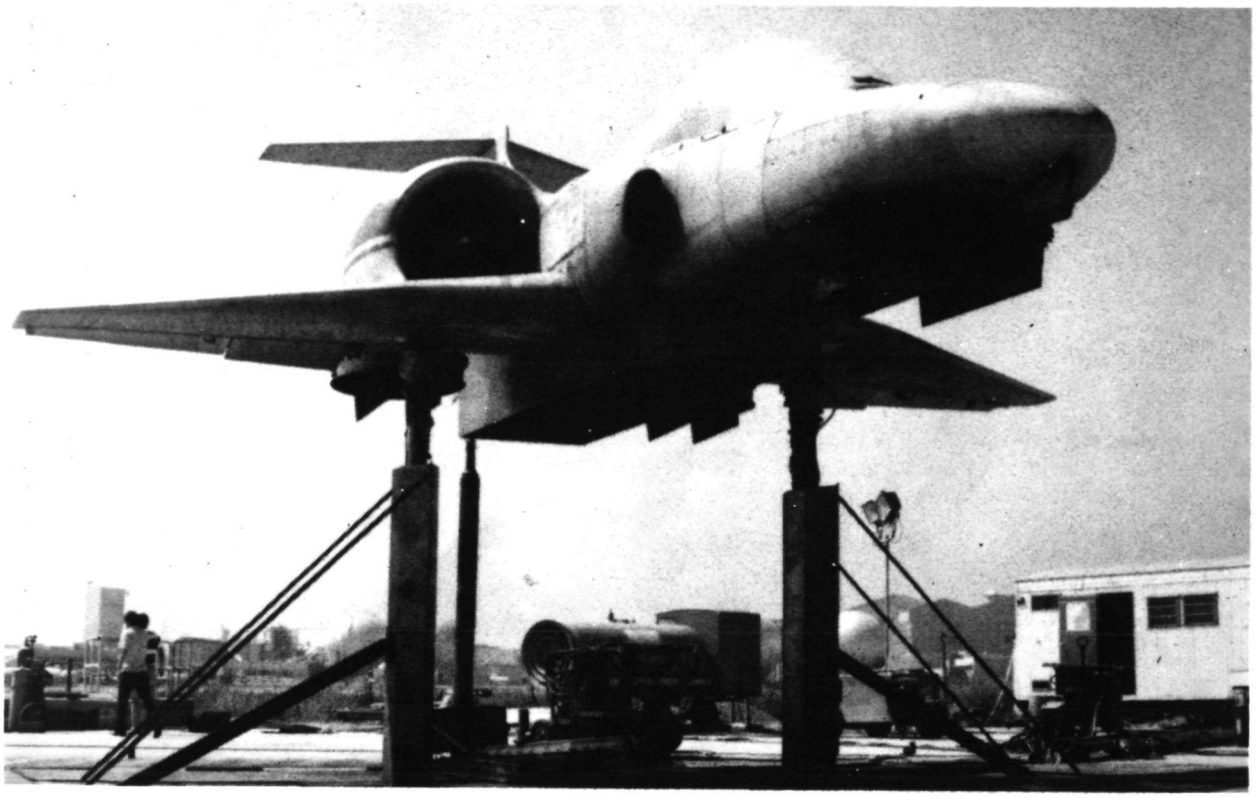

GP79-0064-19

The lift/cruise nozzle rails are detailed in Figure 2-12. The rails simulate the inboard walls of an advanced vectoring nozzle and supporting structure which would be used on a production aircraft. Previous small scale tests had indicated that the rails influenced induced lift performance and as a consequence it was decided to evaluate rails on the NASA-Ames 70% three fan configuration. Figure 2-13 shows the rail installation on the left lift/cruise unit of the LSPM. Also evident in the photograph is the additional 5° hood segment for the lift/cruise nozzle.

Figure 2-14 is a bottom view of the right lift/cruise nozzle. This view shows that the nozzle exit was not immediately adjacent to the model wing or fuselage. The open area around the nozzle allows the nozzle efflux to entrain ambient air from above and thus less air is induced to flow underneath the wings and fuselage. This in turn may cause a reduction in the negative pressure underneath the fuselage and wing. The open area also decreased the amount of model planform area adjacent to the nozzle where the high negative pressures exist. To determine if the open area significantly affects the lift losses, perimeter plates were placed around the nozzles as shown in Figure 2-15. These plates were tested only at the lowest model height.

ORIGINAL PAGE
BLACK AND WHITE PHOTOGRAPH

FIGURE 2-12
LIFT/CRUISE NOZZLE RAILS

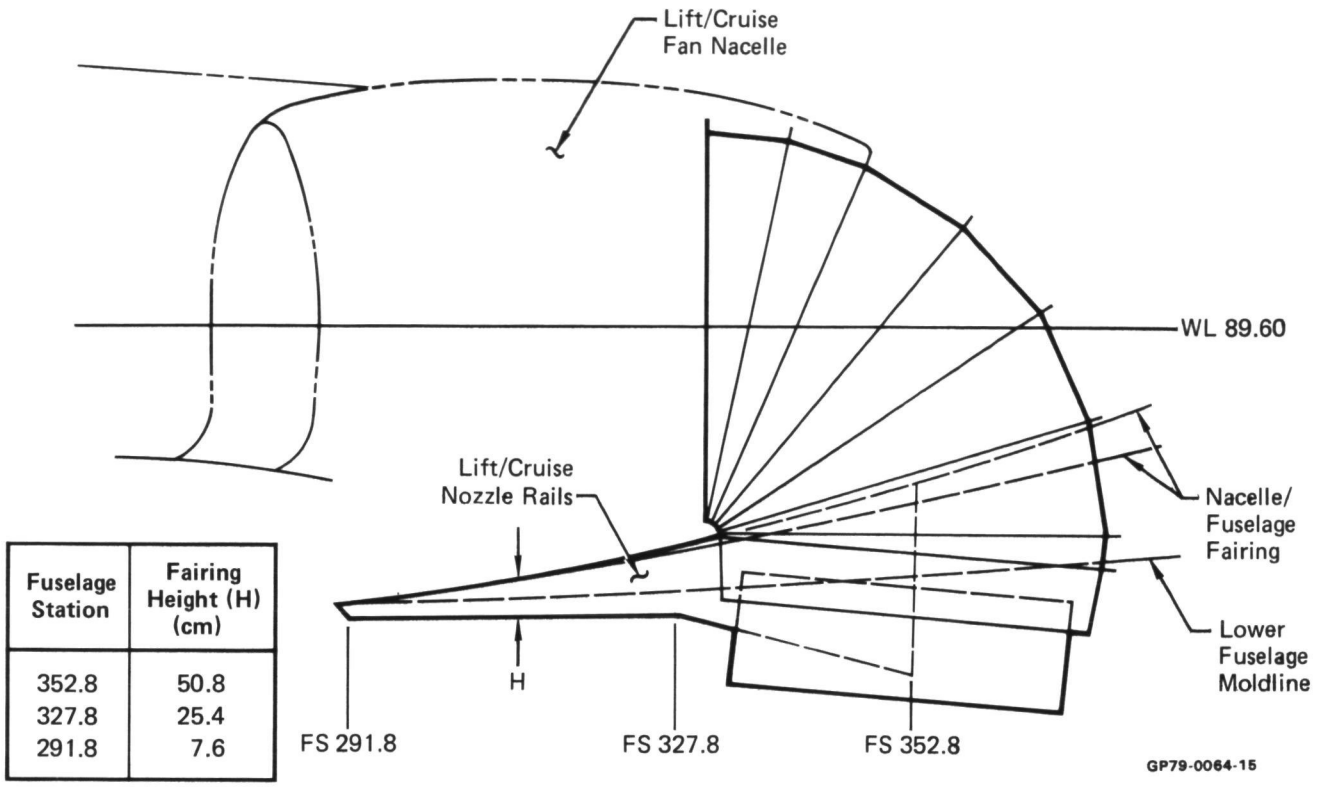

Fuselage Station	Fairing Height (H) (cm)
352.8	50.8
327.8	25.4
291.8	7.6

FIGURE 2-13
LIFT/CRUISE NOZZLE RAIL INSTALLATION

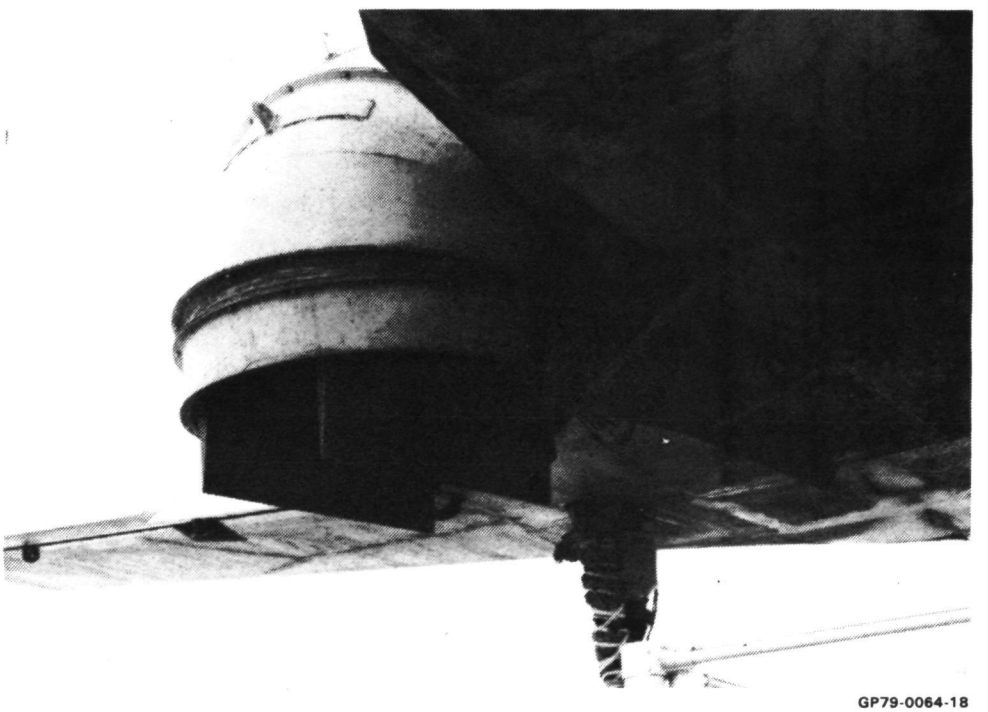

FIGURE 2-14
LIFT/CRUISE NOZZLE EXIT GEOMETRY

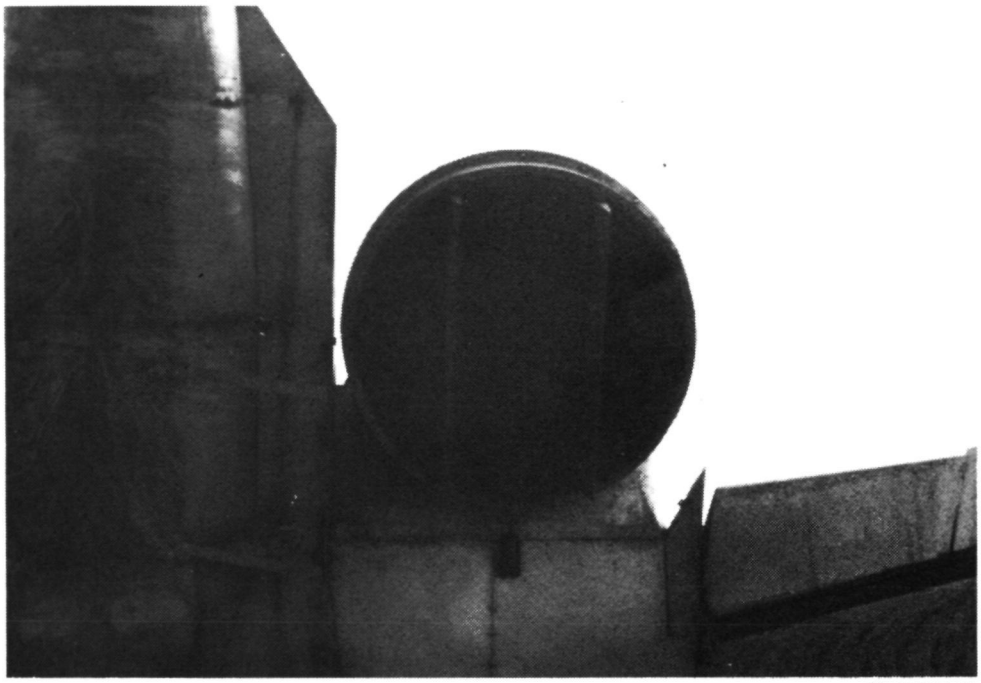

GP79-0064-20

FIGURE 2-15
LIFT/CRUISE NOZZLE PARIMETER PLATE INSTALLATION

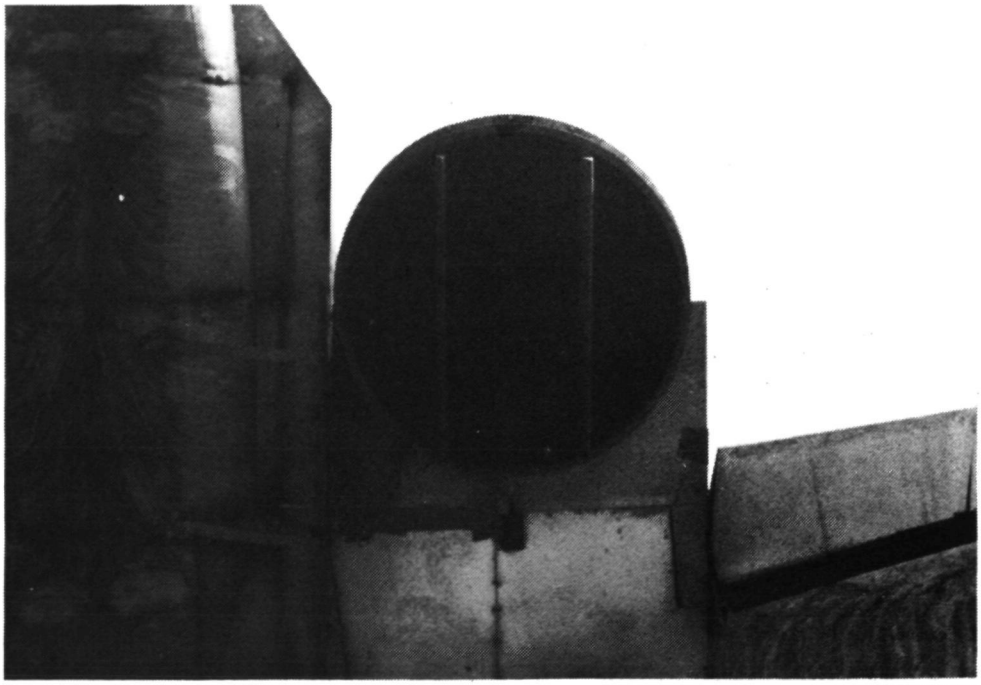

GP79-0064-21

2.2 LARGE SCALE POWERED MODEL INSTRUMENTATION

The LSPM was instrumented with temperature and pressure pickups located at various positions on the airframe and propulsion system components for the purpose of establishing propulsion system thrust and airframe pressure distributions in ground effect. In addition the total lift imposed on the model was measured by means of three load cells located just beneath the model on each supporting strut. A description of the pressure and temperature instrumentation, load cells and data acquisition system is provided in the following paragraphs.

2.2.1 LSPM AIRFRAME INSTRUMENTATION

Wing Lower Model Surface - A total of 80 static pressure ports and 27 thermocouples were installed on the lower left fuselage surface and underneath the left wing. The detailed locations are shown in Figures 2-16 and 2-17.

Upper Wing Surface - Fifteen static pressure ports are located on the upper left wing surface. Detailed locations are shown in Figure 2-18.

FIGURE 2-16
LSPM PRESSURE TAP LOCATIONS LOWER FUSELAGE SURFACE

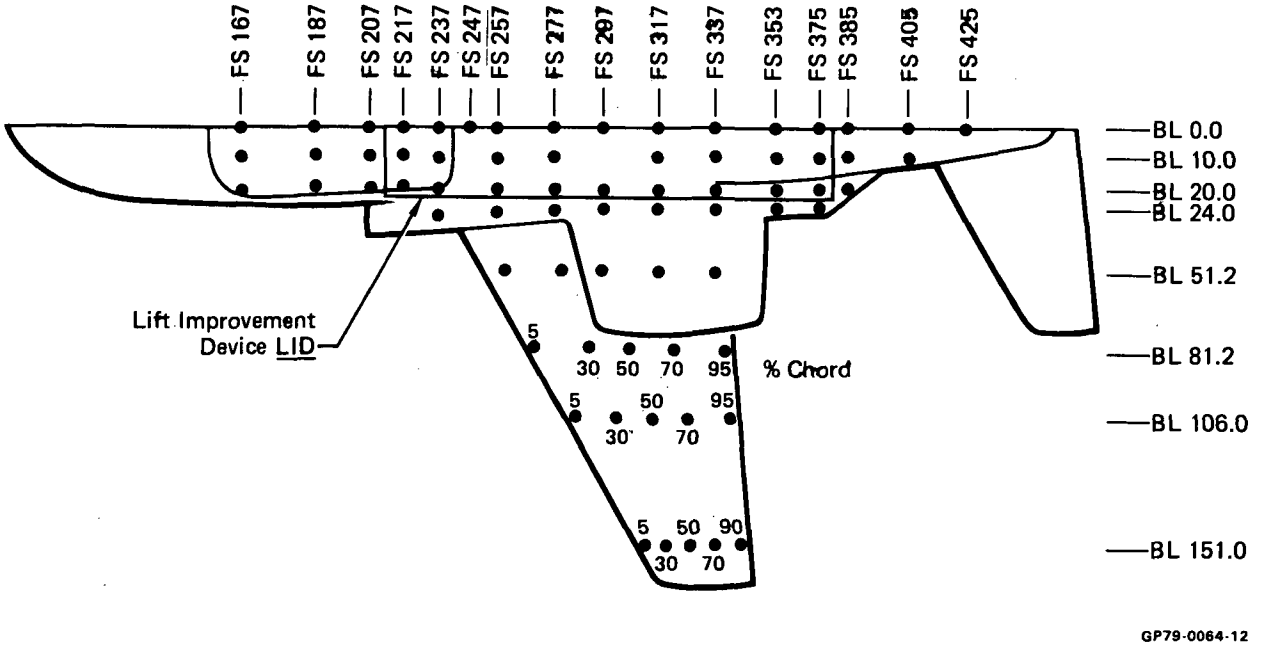

FIGURE 2-17
LSPM THERMOCOUPLE LOCATIONS LOWER FUSELAGE SURFACE

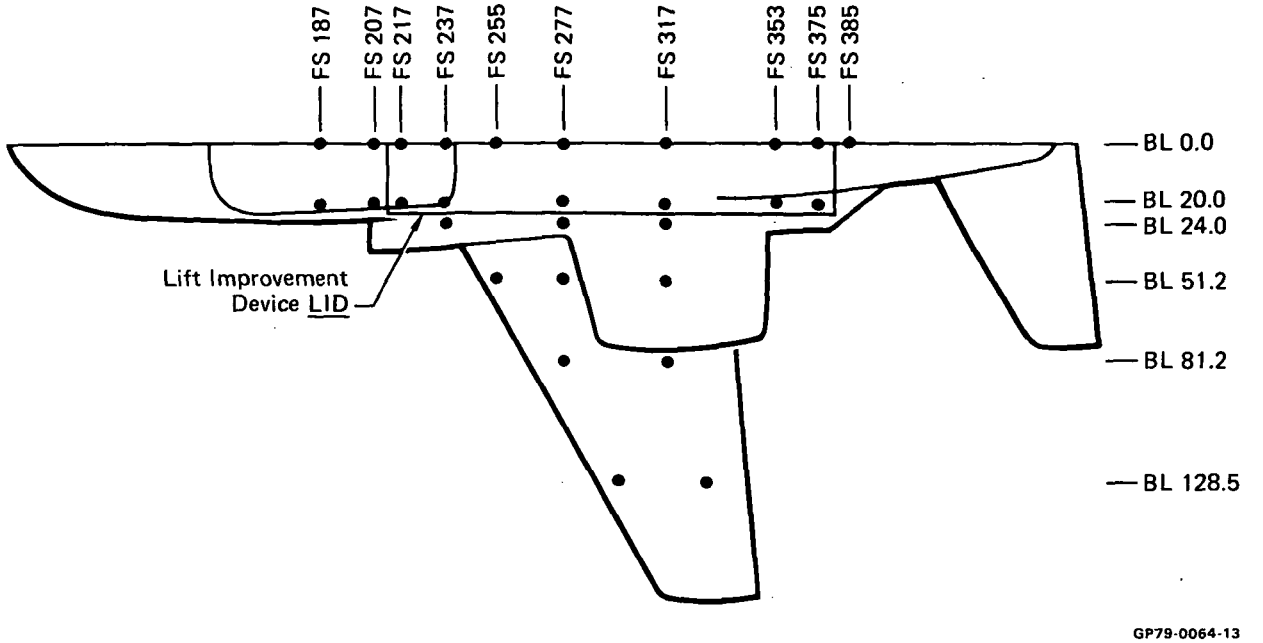

FIGURE 2-18
UPPER WING SURFACE STATIC PRESSURES

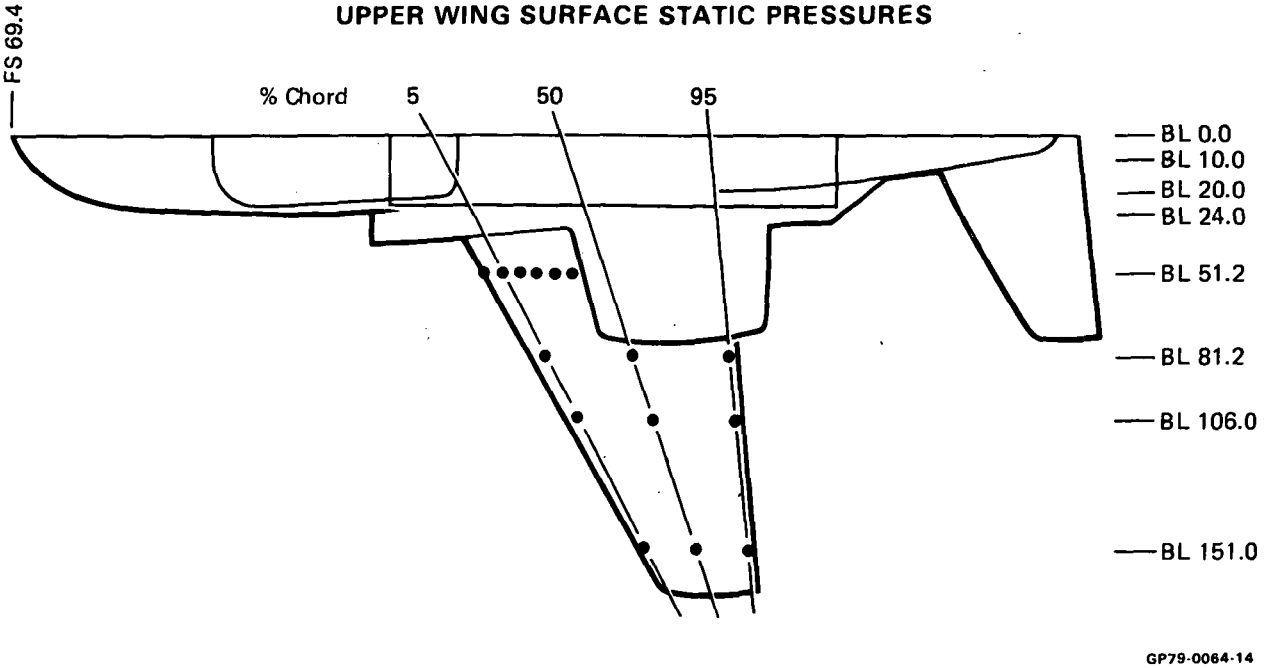

Airframe Total Lift - Three load cells, one mounted on each of the support struts, were used to measure the total lift on the model. Each load cell was a 3-component strain gauge balance with 26,690 newton (6000 lbf.) normal force, 17,790 newton (4000 lbf.) axial force, and 13,345 newton (3000 lbf.) side force capability. The load cells were installed directly below the test model between the struts and model monitoring pads. Metal shrouds were installed around each cell and cooling air was supplied to maintain near constant load cell temperature.

2.2.2 LSPM PROPULSION SYSTEM INSTRUMENTATION - The propulsion system instrumentation included static pressure, total pressure, and total temperature measurements at various locations of the three propulsion units. The components of the propulsion system that were instrumented included:

- o Left lift/cruise nacelle
- o Nose and left fan face
- o Left, right, and nose fan and tip turbine exits
- o Left fan nozzle exits

Left Lift/Cruise Nacelle - Nineteen static pressure ports are located on the left hand nacelle duct wall and upper cowling. Detailed locations are shown in Figure 2-19.

Fan Face - The left lift/cruise fan face and nose lift fan face were both instrumented with identical inlet total pressure rakes. An 8 leg, 48 total pressure probe rake, along with a 4 leg-8 total temperature probe rake, were installed at each fan face. Due to data channel limitations only 16 of the 48 total pressures were recorded for each fan face rake. Four wall static pressure ports were also located at the rake station of each inlet. The instrumentation locations for the fan face rakes are presented in Figure 2-20.

Engine Face - The left lift/cruise engine face and the nose fan engine face were both instrumented with inlet performance rakes. A 4 leg, 16 total pressure probe rake, along with a 4 leg-8 total temperature rake, were installed just upstream of the engine face on each unit. Two wall static ports were also located at the rake station of each engine. The instrumentation locations for these engine face rakes are presented in Figure 2-21. For this test, only total temperature measurements were made at the engine faces.

Fan and Tip Turbine Exit - All three turbotip fan units on the model were instrumented at the fan and tip turbine stator exits. Each fan exit had a 6 leg-30 probe total pressure rake, a 3 leg-9 probe total temperature rake, and 12 exit static pressure ports, 6 on the hub and 6 on the outer wall. The tip turbine exit instru-

FIGURE 2-19
LEFT LIFT/CRUISE NACELLE AND INLET DUCT SURFACE PRESSURES

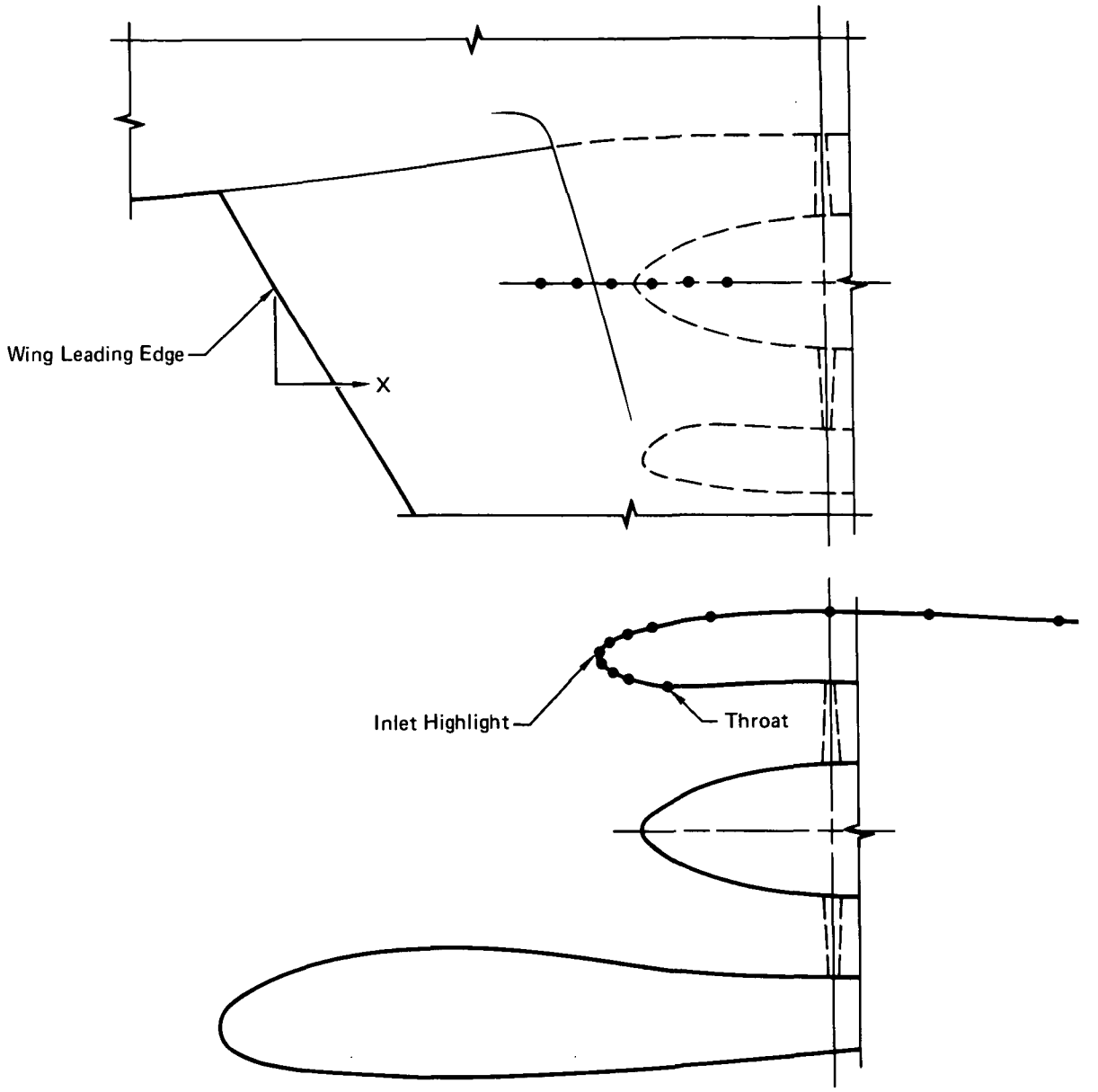

mentation consisted of 4 equal-area-weighted total pressure probes, 4 total temperature probes, and 5 outer wall static pressure ports. The fan and tip turbine exit instrumentation was used to measure the basic performance of the turbotip fans including the airflow and fan pressure rise. The detailed location of the fan and tip turbine exit instrumentation is presented in Figure 2-22. A cross-sectional drawing of the turbotip fan illustrating the positioning of both the inlet and fan exit rakes is presented in Figure 2-23.

FIGURE 2-20
FAN FACE INSTRUMENTATION

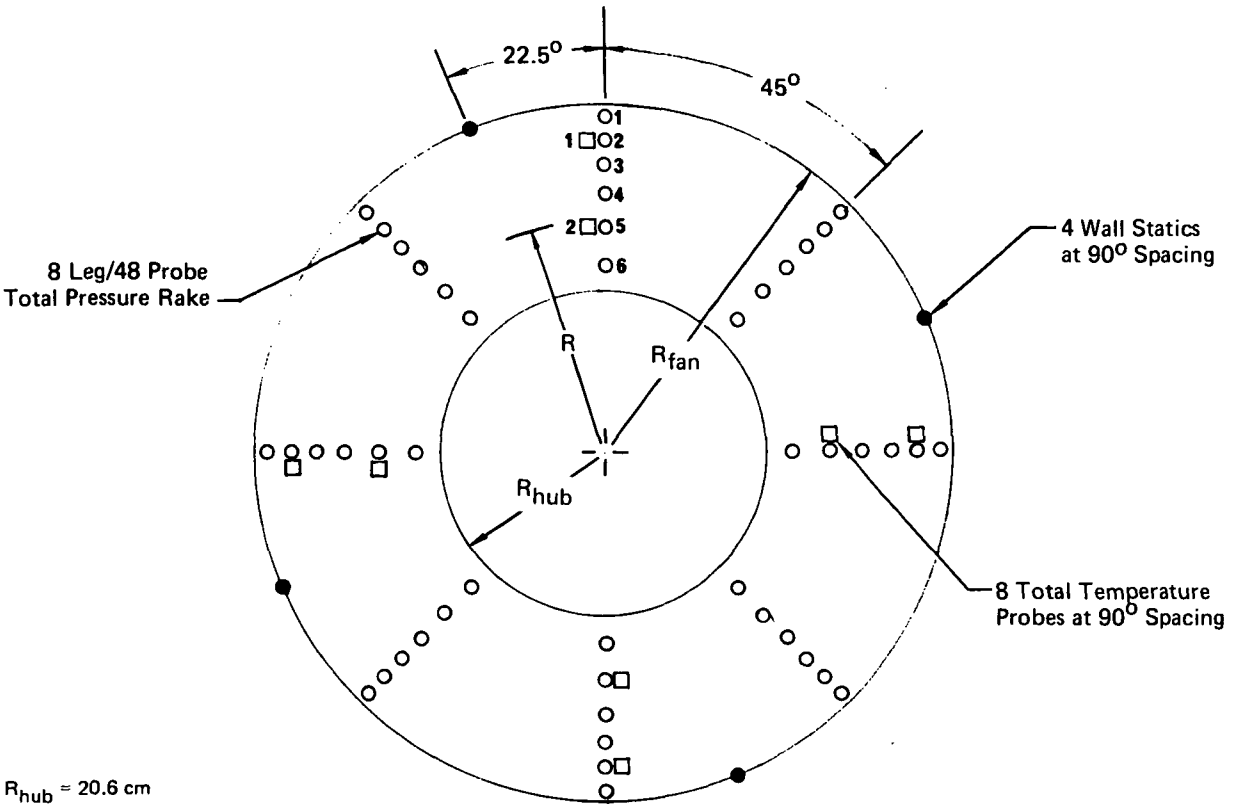

Thermocouple Locations

T/C No.	Radius (cm)
1	40.92
2	29.03

Pressure Tube Locations

Probe No.	Radius (cm)
1	44.17
2	40.92
3	37.39
4	33.45
5	29.03
6	23.77

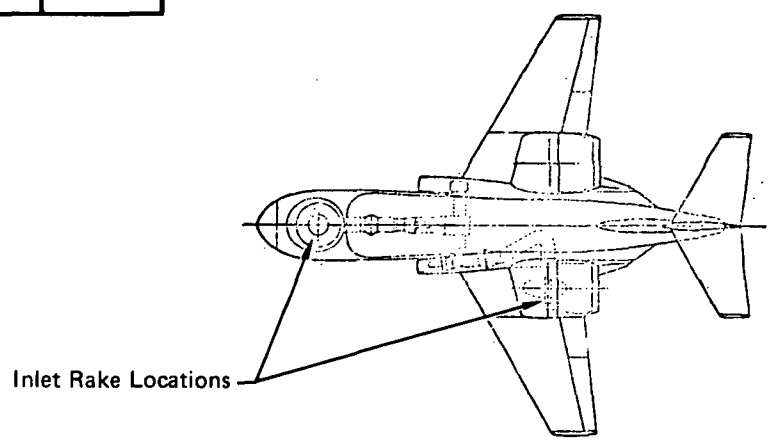

GP769-0064-31

FIGURE 2-21
ENGINE FACE INSTRUMENTATION

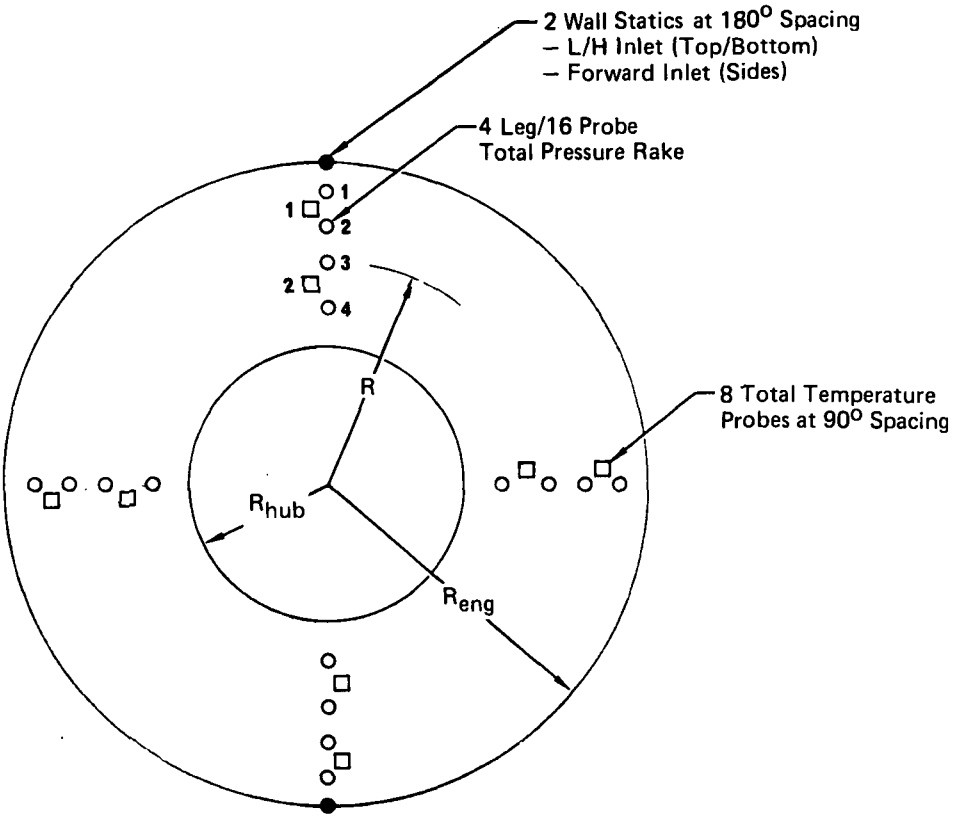

Thermocouple Locations

T/C No.	Radius (cm)	
	L/C	Fwd
1	12.19	11.73
2	8.56	8.51

R_{hub} = 6.45 cm
R_{eng} = 13.59 cm

Pressure Tube Locations

Probe No.	Radius (cm)	
	L/C	Fwd
1	13.26	12.67
2	11.18	10.97
3	9.37	9.19
4	7.98	7.72

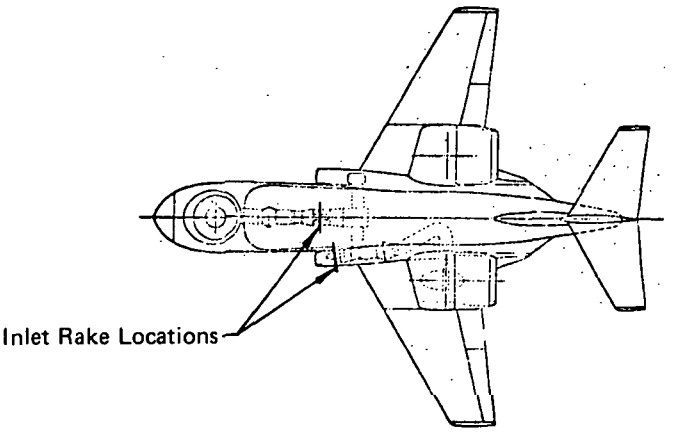

GP79-0064-30

FIGURE 2-22
FAN AND TIP TURBINE EXIT INSTRUMENTATION

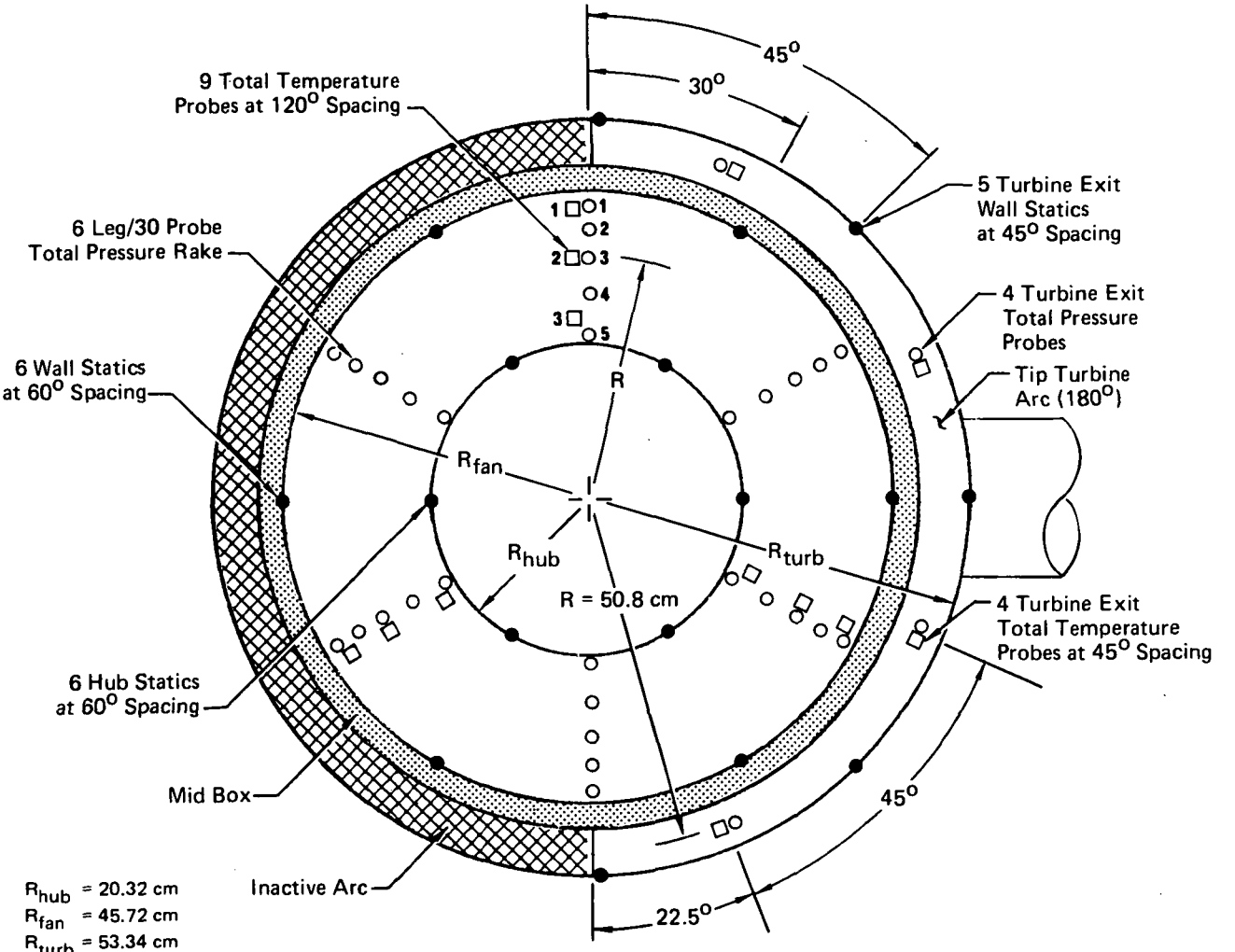

Thermocouple Locations

T/C No.	Radius (cm)	
	L/C	Fwd
1	40.64	41.73
2	33.07	34.11
3	27.18	28.32

Pressure Tube Locations

Tube No.	Radius (cm)	
	L/C	Fwd
1	43.61	44.81
2	37.54	38.71
3	32.41	33.96
4	28.12	29.49
5	24.28	25.65

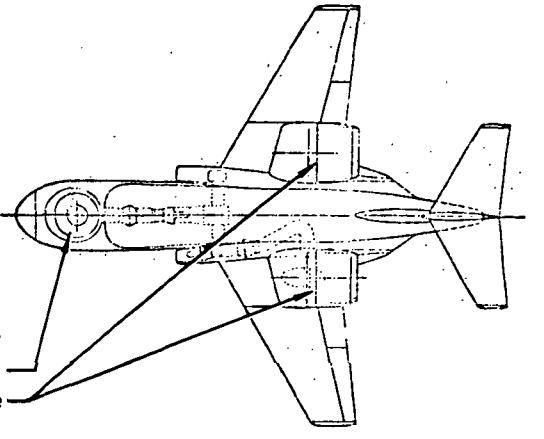

GP79-0064-29

FIGURE 2-23
FAN INLET AND EXIT INSTRUMENTATION INSTALLATION
Left Lift/Cruise and Nose Fan Units

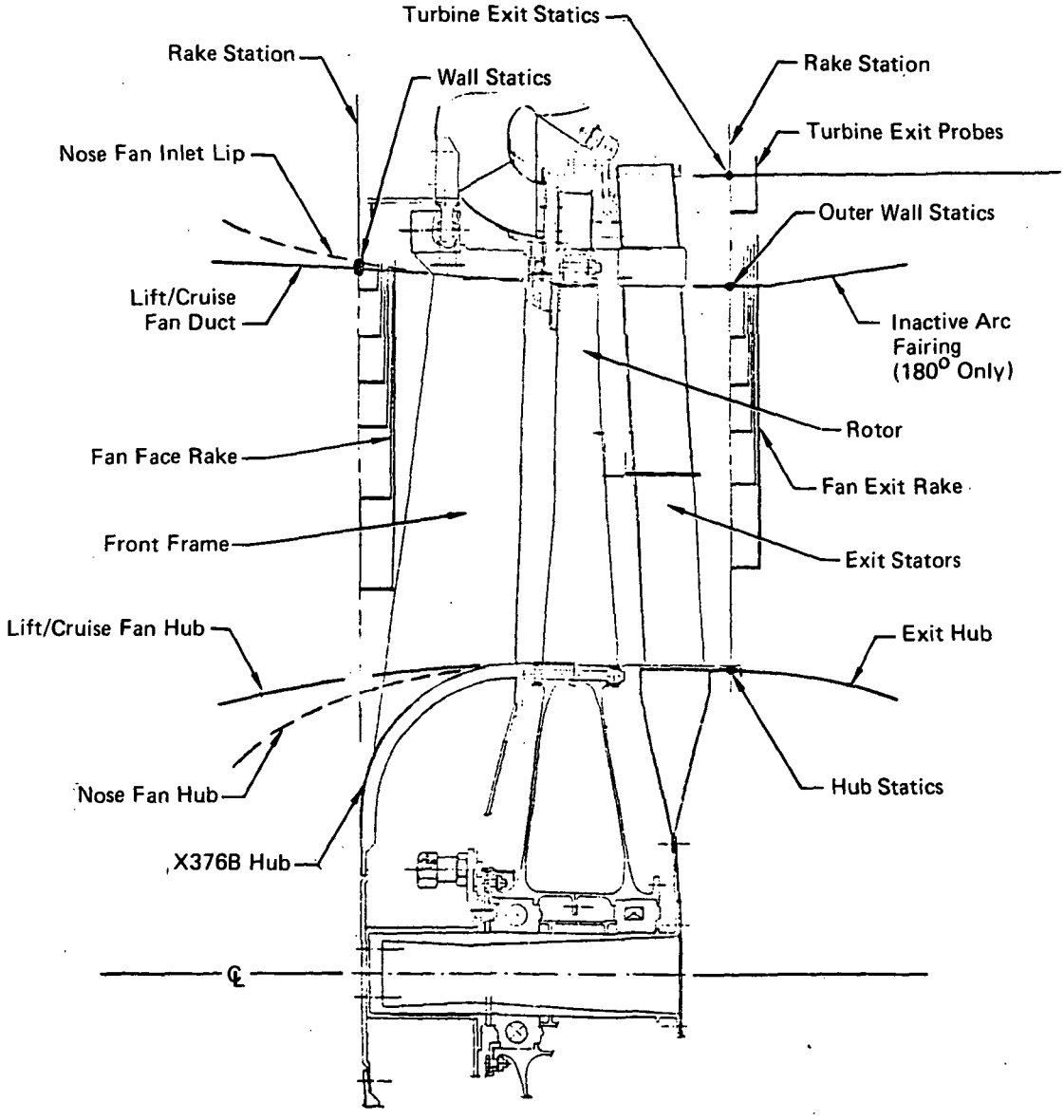

GP79-0064-27

Engine Exit - The left lift/cruise and nose fan engine exhaust ducts were each instrumented with three wall static pressure ports, located approximately one duct diameter downstream of the engine exit. The pressure port locations are shown in Figure 2-24. In addition to these static pressure measurements, the eight-probe engine EGT harness was utilized on all three engines to measure the engine exhaust gas total temperatures.

Nose Fan Exit Hubs - The nose fan exit hubs (flat plate and hemispherical) were instrumented with 21 static pressure taps for the purpose of assessing hub pressurization in ground effects. The details of this instrumentation are presented in Figures 2-25 and 2-26.

Nozzle Exits - The left lift/cruise unit was instrumented at the nozzle exit for the purpose of assessing the nozzle exit flow profiles. The left lift/cruise nozzle exit includes 10 total pressure probes attached to the leading edge of the two fixed yaw vane struts, and 4 external nozzle exit base pressure static ports. The details of the nozzle exit instrumentation are presented in Figure 2-27.

2.3 LSPM DATA ACQUISITION AND TEST FACILITY

The experimental test parameters were measured, digitized, and recorded on paper punch tape utilizing a VIDAR Corporation digital data system. This system consists of analog signal conditioning, an integrating digital voltmeter, and a Teletype Paper-Tape punch. A total of 99 data recording channels are available with this system. The first 20 channels of the VIDAR system are multiple scan channels and the remaining channels are single scan. The multi scan channels were used to record the primary test measurements including fan speeds, load cell readings and pressure and temperature scanners.

The LSPM tests were conducted at the NASA-Ames Research Center Static Test Facility, designated as test site number N-249. This site is used primarily to evaluate static performance of powered models prior to entry into the NASA-Ames 40 x 80 wind tunnel. This facility includes an enclosed trailer that serves as the control room and houses the data acquisition systems. Auxiliary equipment located at the site includes an engine starter unit, 400 cycle A/C power unit, and fuel tanker.

2.4 4.1 PERCENT SCALE MODEL DESCRIPTION

A schematic of the 4.1 percent scale model test apparatus is shown in Figure 2-28. The test hardware consisted of three basic elements, a metric airframe model attached to a force balance, a non-metric exhaust jet system which simulated the nozzle flows of the LSPM fan propulsion units and a large rectangular flat plate which provided ground surface simulation.

FIGURE 2-24
ENGINE EXIT INSTRUMENTATION

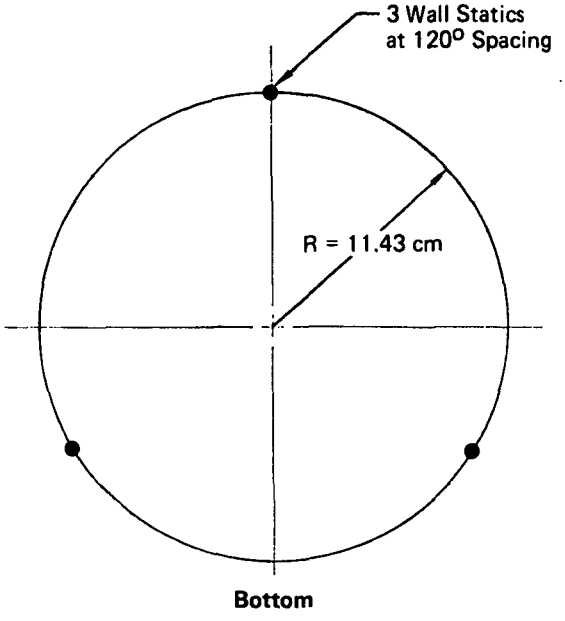

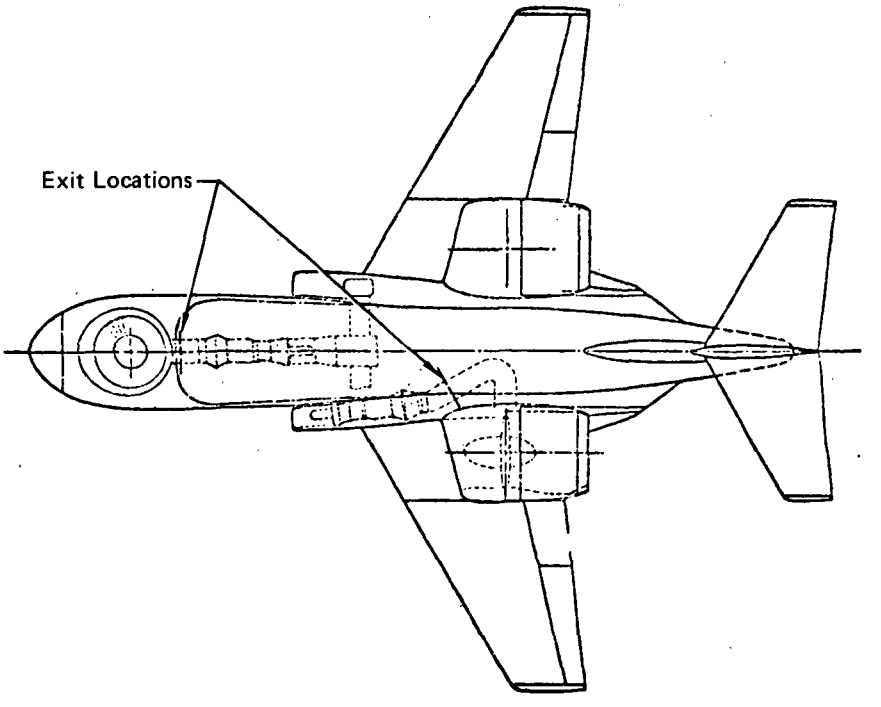

GP79-0064-32

FIGURE 2-25
NOSE FAN EXIT HUB PRESSURE INSTRUMENTATION FLAT PLATE HUB

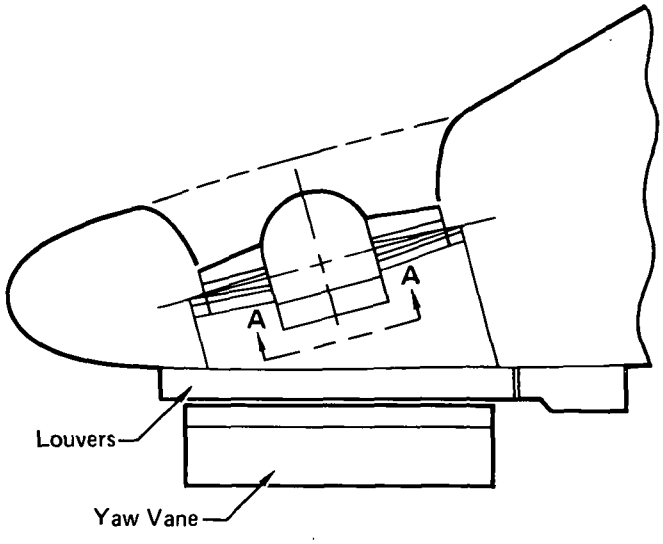

Aircraft Left Side

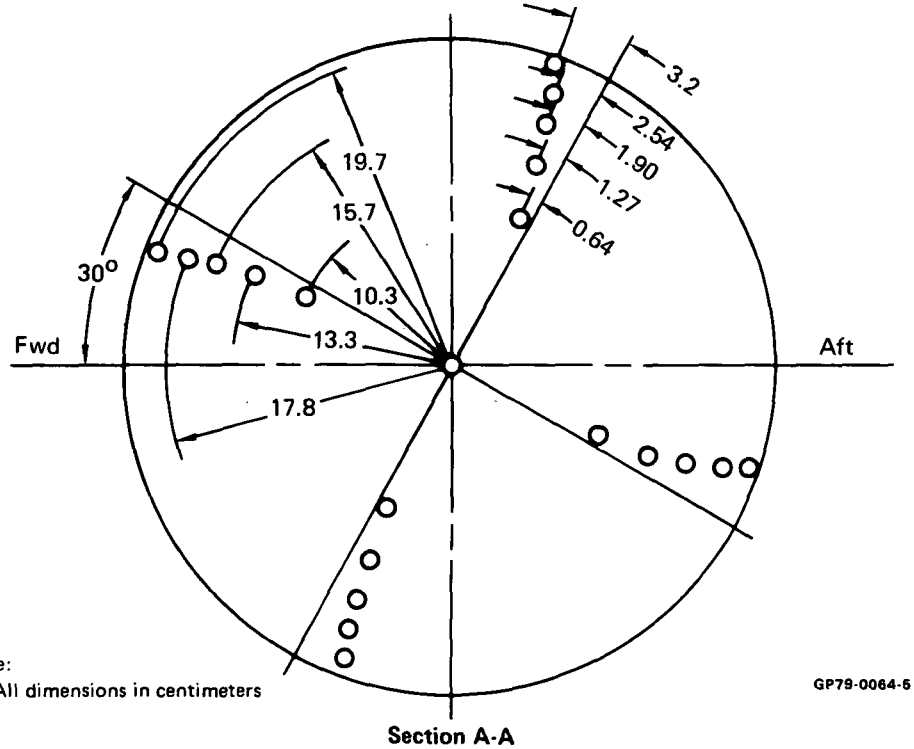

Note:
All dimensions in centimeters

GP79-0064-5

Section A-A

FIGURE 2-26
NOSE FAN EXIT HUB PRESSURE INSTRUMENTATION HEMISPHERICAL HUB

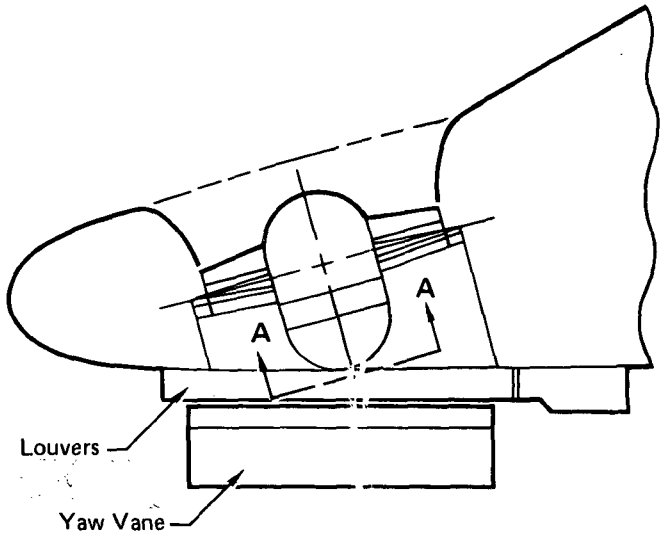

Aircraft Left Side

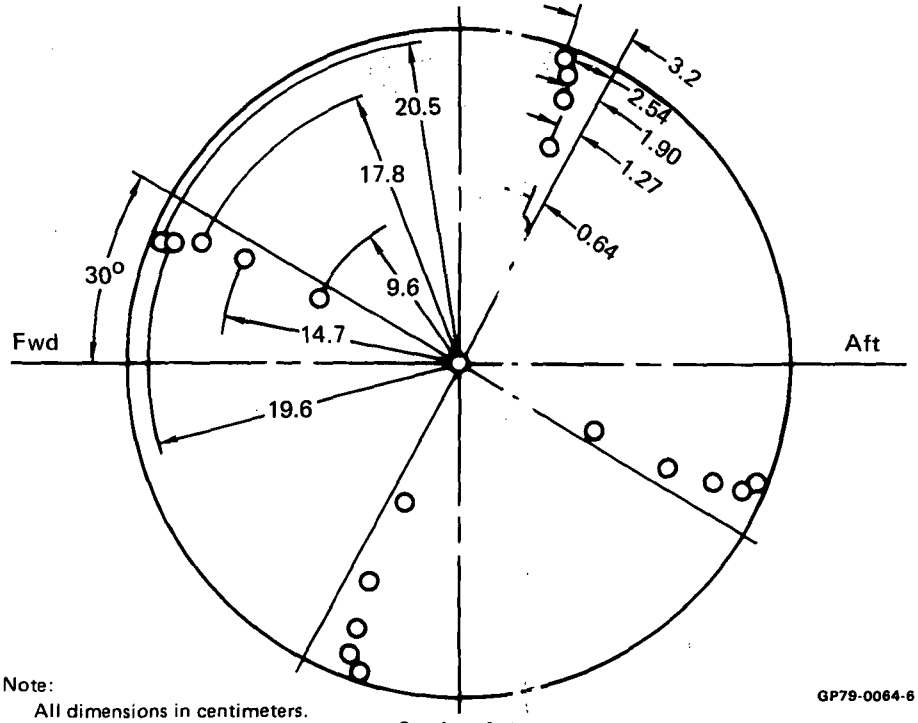

Note:
All dimensions in centimeters.

GP79-0064-6

Section A-A

FIGURE 2-27
LIFT/CRUISE NOZZLE EXIT INSTRUMENTATION

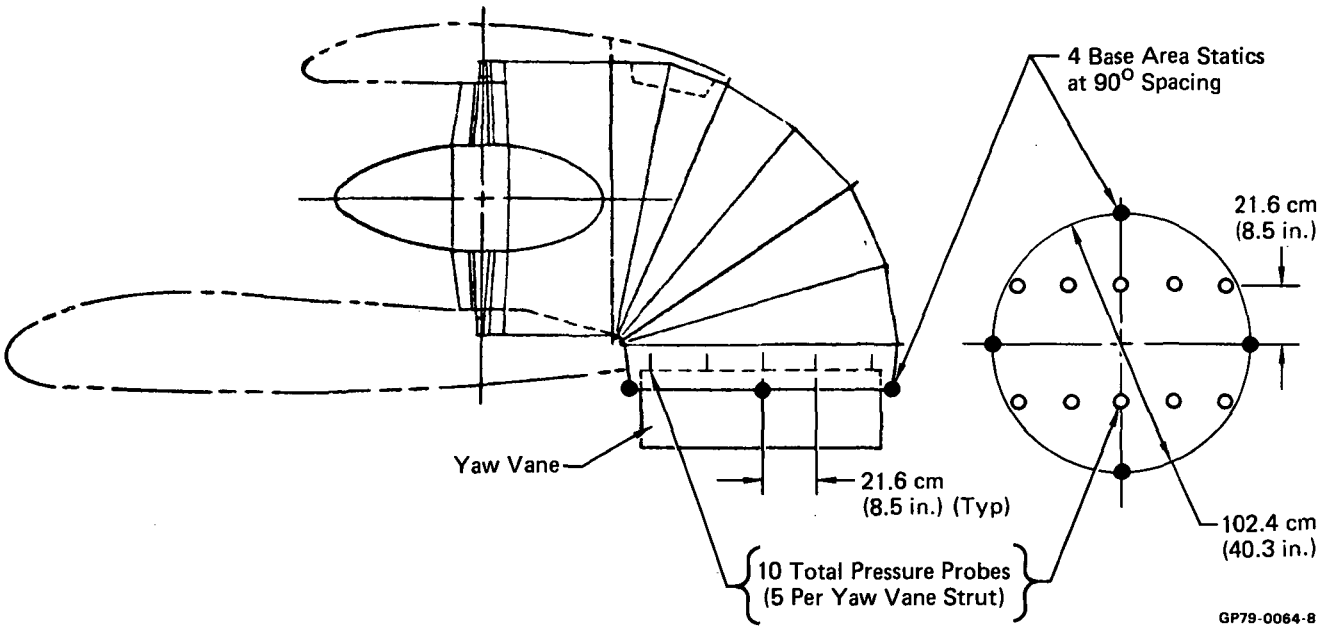

FIGURE 2-28
4.1 PERCENT SCALE MODEL TEST APPARATUS

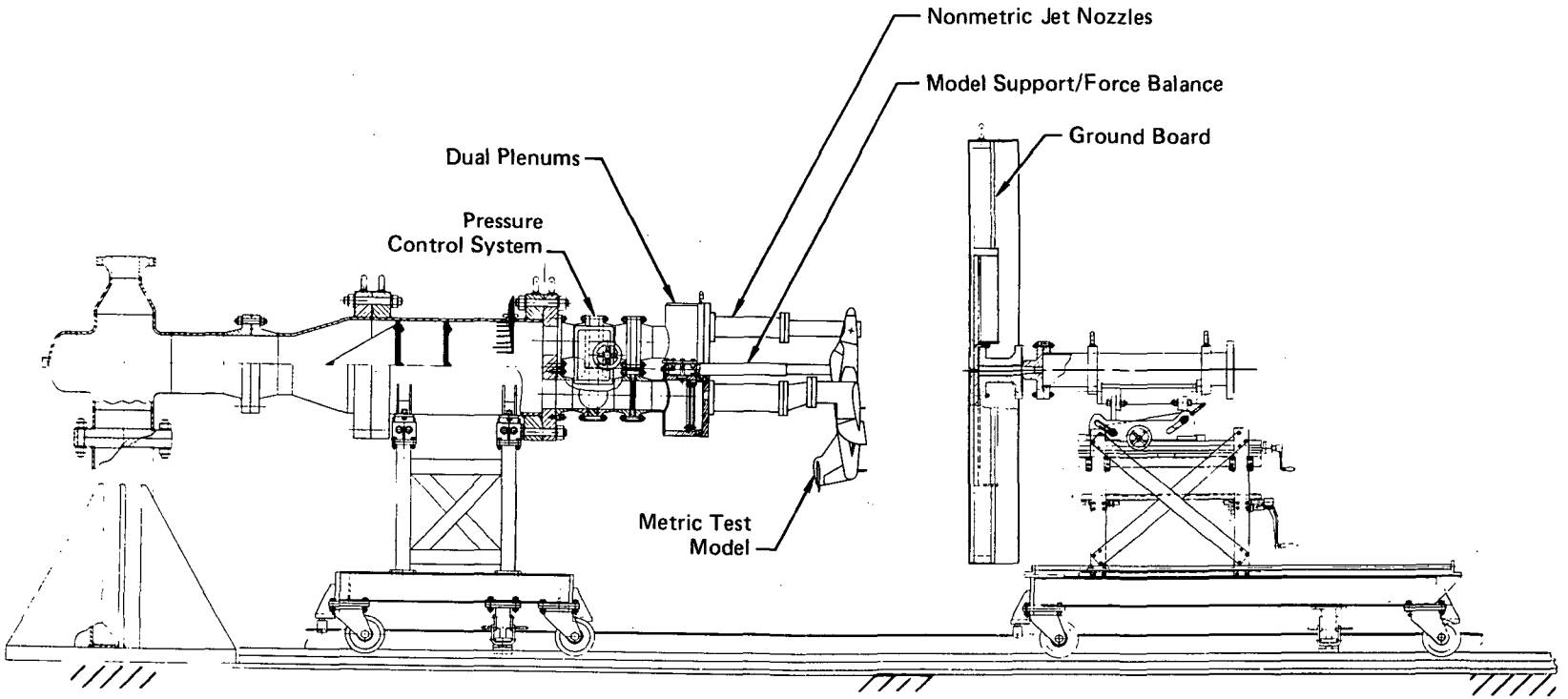

An existing MCAIR three fan aircraft model was modified for this program which provided a 4.1 percent scale airframe model of the NASA-Ames three fan V/STOL aircraft configuration. Provisions to accommodate the air supply piping for the three exhaust jets were built into the airframe model.

The primary features of the LSPM nozzle exhaust system were maintained on the small scale hardware illustrated in Figure 2-29. The two lift/cruise circular hood deflector nozzles were fabricated for this program whereas the nose nozzle was an existing MCAIR test article.

FIGURE 2-29
4.1 PERCENT SCALE MODEL SCHEMATIC

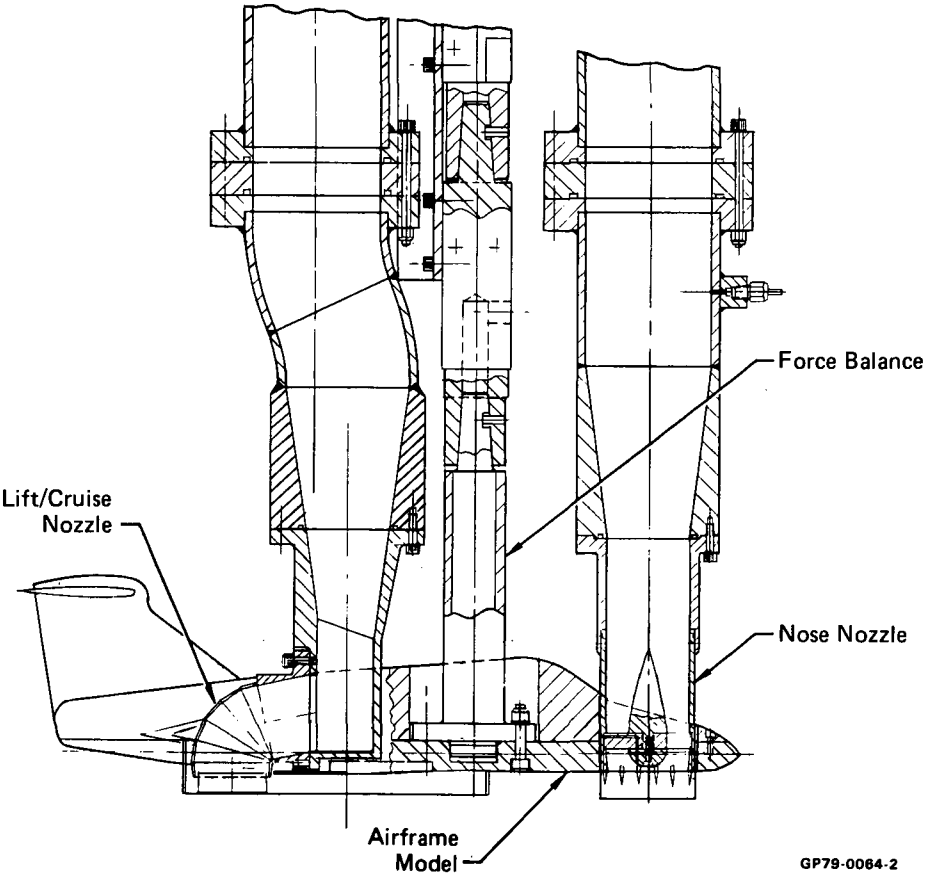

The lift/cruise nozzles were scaled versions of the LSPM units incorporating the segmented hood design and twin exit yaw vanes. The nose nozzle incorporated a hub centerbody and thrust vectoring louvers at the exit, however, its geometry deviated in three respects from the LSPM nose installation. The LSPM exit louver system utilized fourteen low camber vanes whereas the small scale nozzle utilized six vanes in the louver. The LSPM nose nozzle also had twin yaw vane elements whereas a single yaw vane was used on the small scale nozzle. Finally, the small scale nose nozzle was a straight duct design with uncambered louvers in contrast to the LSPM which utilized cambered vanes which vectored the fan exhaust approximately 15° from the fan centerline direction to vertical. The differences between the small scale and LSPM nozzle arrangements were not considered to be significant with respect to induced ground effects. This consideration is based upon previous small scale investigations (Reference 4) of the effects of nose nozzle geometry and exit flow profile on the induced lift characteristics of the three fan aircraft.

Test apparatus to simulate the rectangular LID, nozzle rails and lift/cruise perimeter plates utilized on the LSPM were also fabricated and tested during the small scale test program.

Evaluation of the effects of the LSPM support struts on the induced lift measurements was an additional objective of the small scale test program. Strut hardware was built for four different heights corresponding to H/D values of 0.95, 1.53, 3.06 and 6.45. The model and strut hardware are shown in Figure 2-30 for each model height. The support struts were mounted on the ground board and were separated from the model by small gaps. With no physical connection between model and support strut, the model force balance measured only the effects caused by the presence or absence of the struts.

Figure 2-31 presents photographs of the model lower surface showing the installation of the two, three and four sided LIDs and nozzle rails. Figure 2-32 shows the model with and without the lift/cruise nozzle perimeter plates installed.

2.5 4.1 PERCENT SCALE MODEL INSTRUMENTATION

The primary data recorded during the small scale model tests included the airframe model forces, nozzle pressure ratios and airframe lower surface pressure distributions. A six component force balance was utilized to record the forces and moments induced on the airframe model. The balance used during this test was a Task Corporation Model 23A unit.

FIGURE 2-30
4.1 PERCENT SCALE MODEL AND STRUT HARDWARE

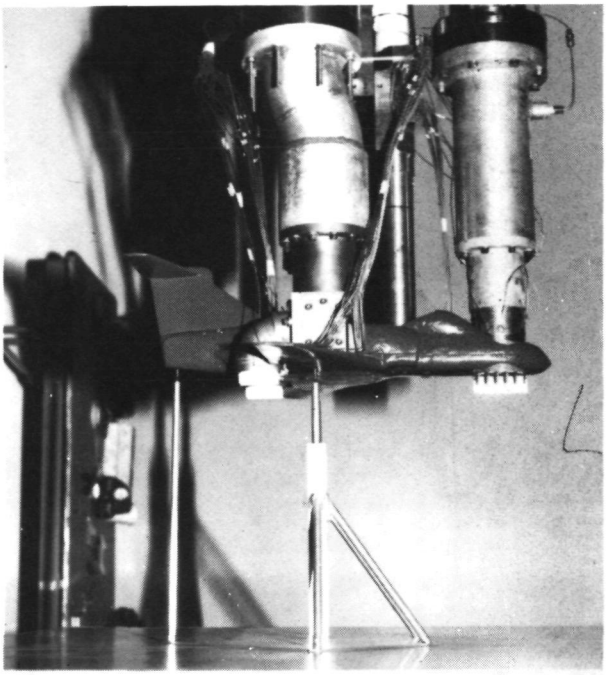

H/D = 6.45

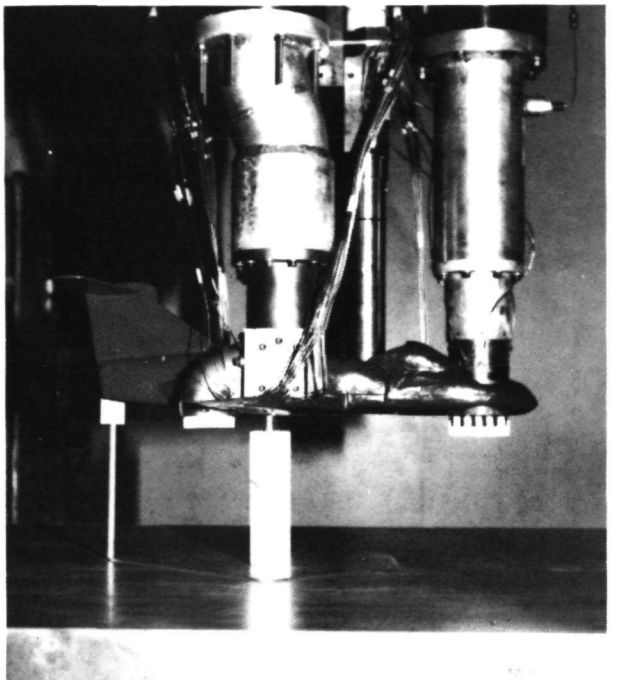

H/D = 3.06

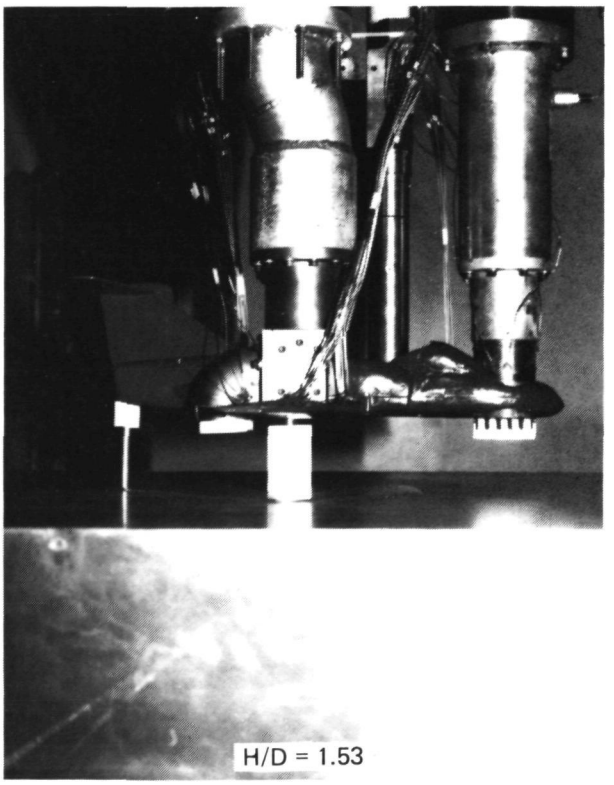

H/D = 1.53

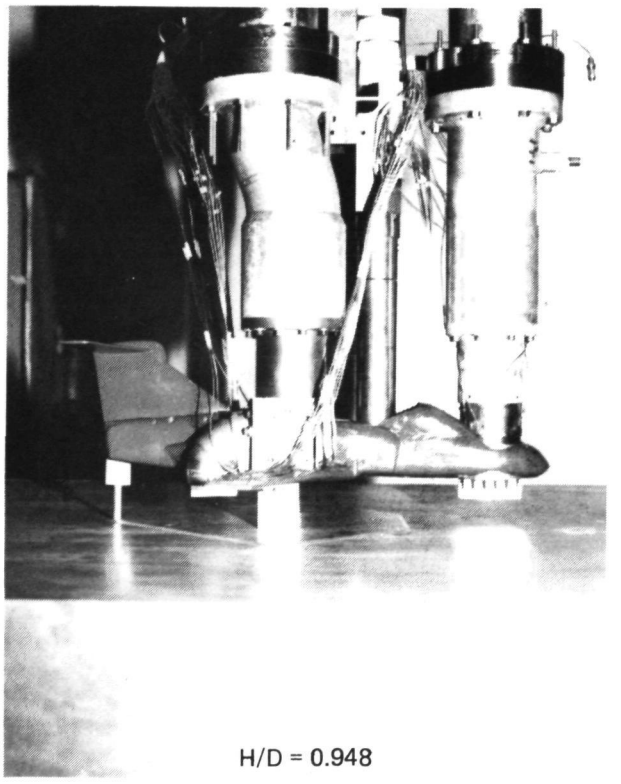

H/D = 0.948

GP79-0064-24

FIGURE 2-31
4.1 PERCENT SCALE MODEL LID APPARATUS

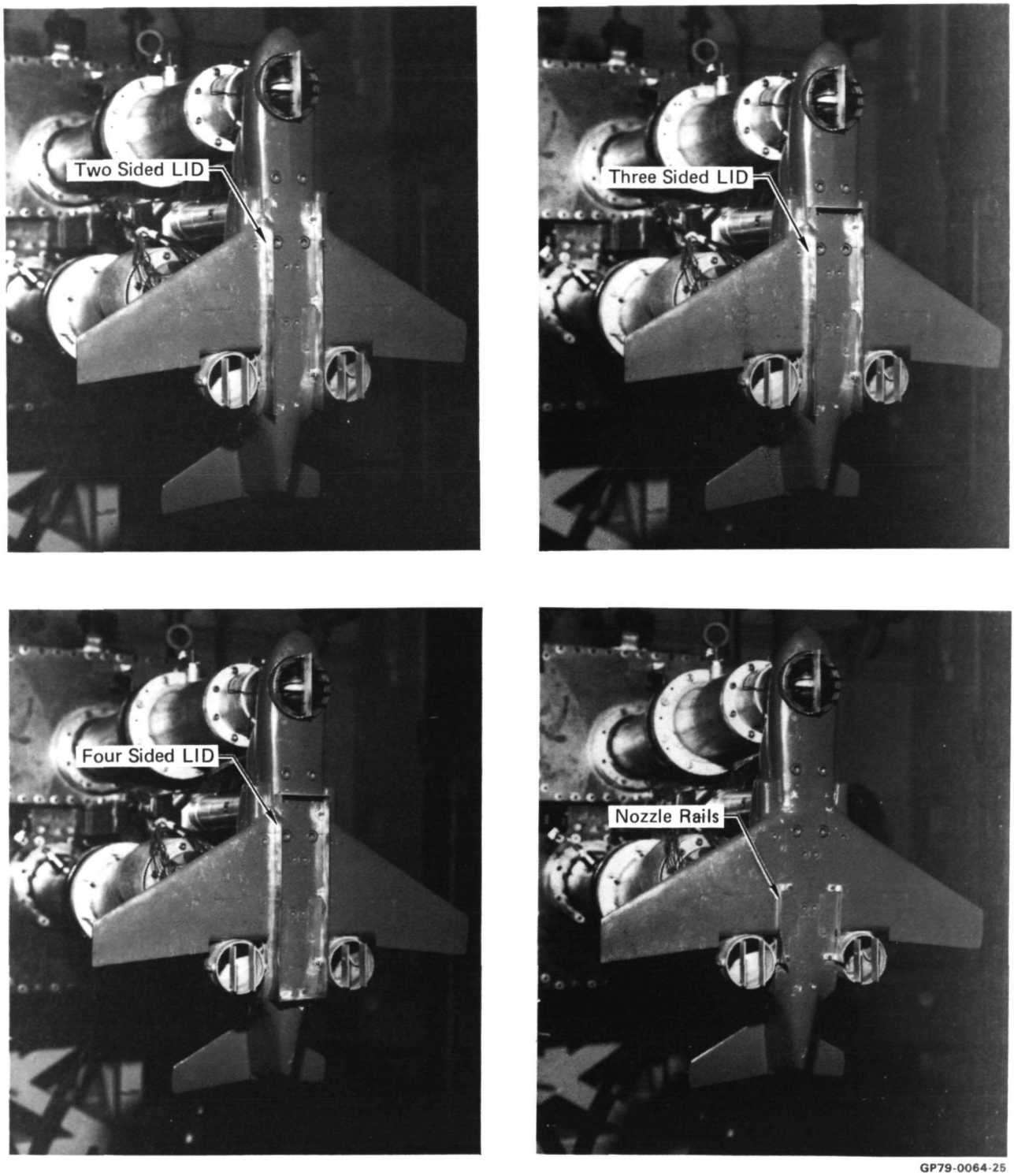

GP79-0064-25

FIGURE 2-32
4.1 PERCENT SCALE MODEL LIFT/CRUISE NOZZLE PERIMETER PLATES

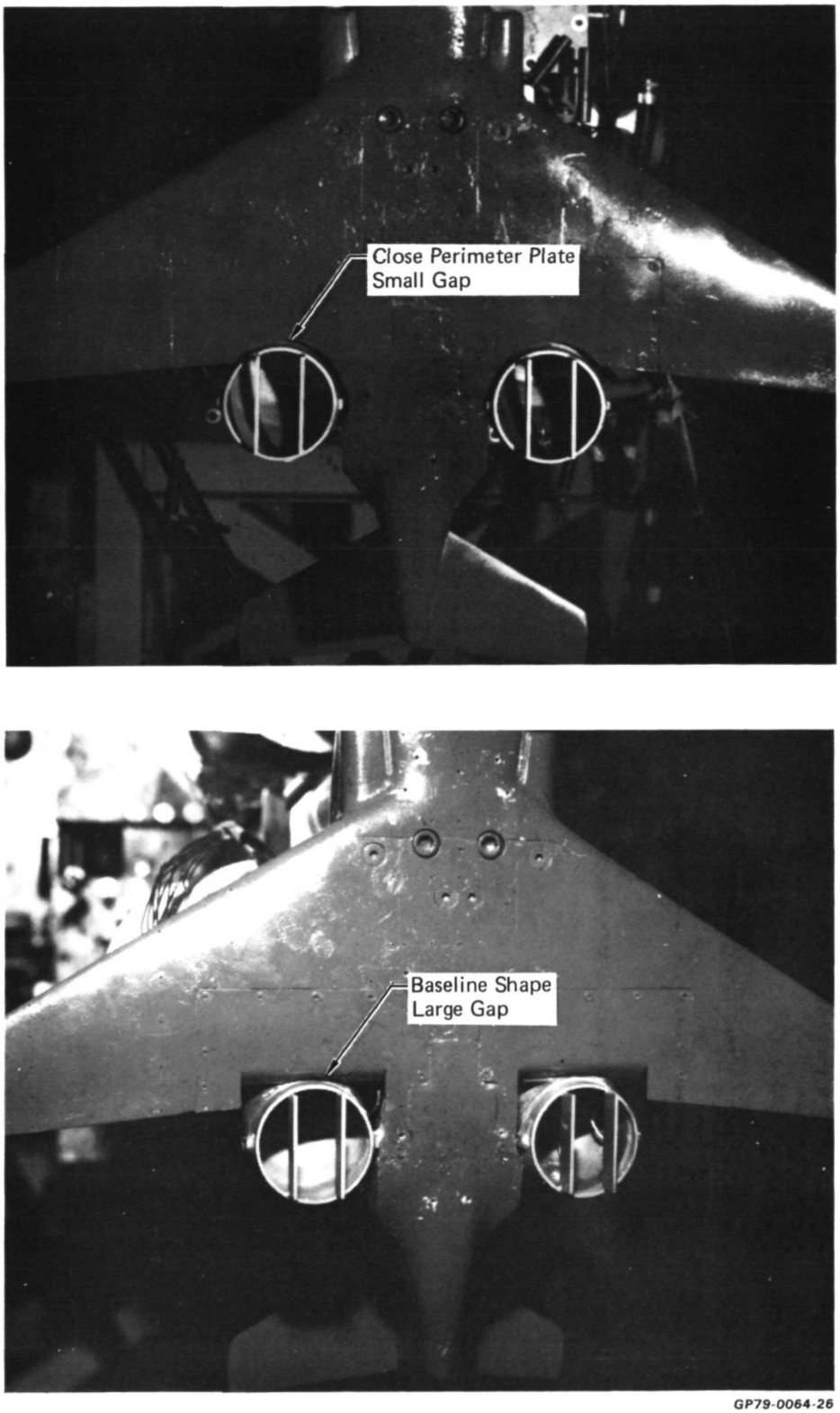

GP79-0064-26

FIGURE 2-33
4.1 PERCENT SCALE MODEL LOWER SURFACE PRESSURE INSTRUMENTATION

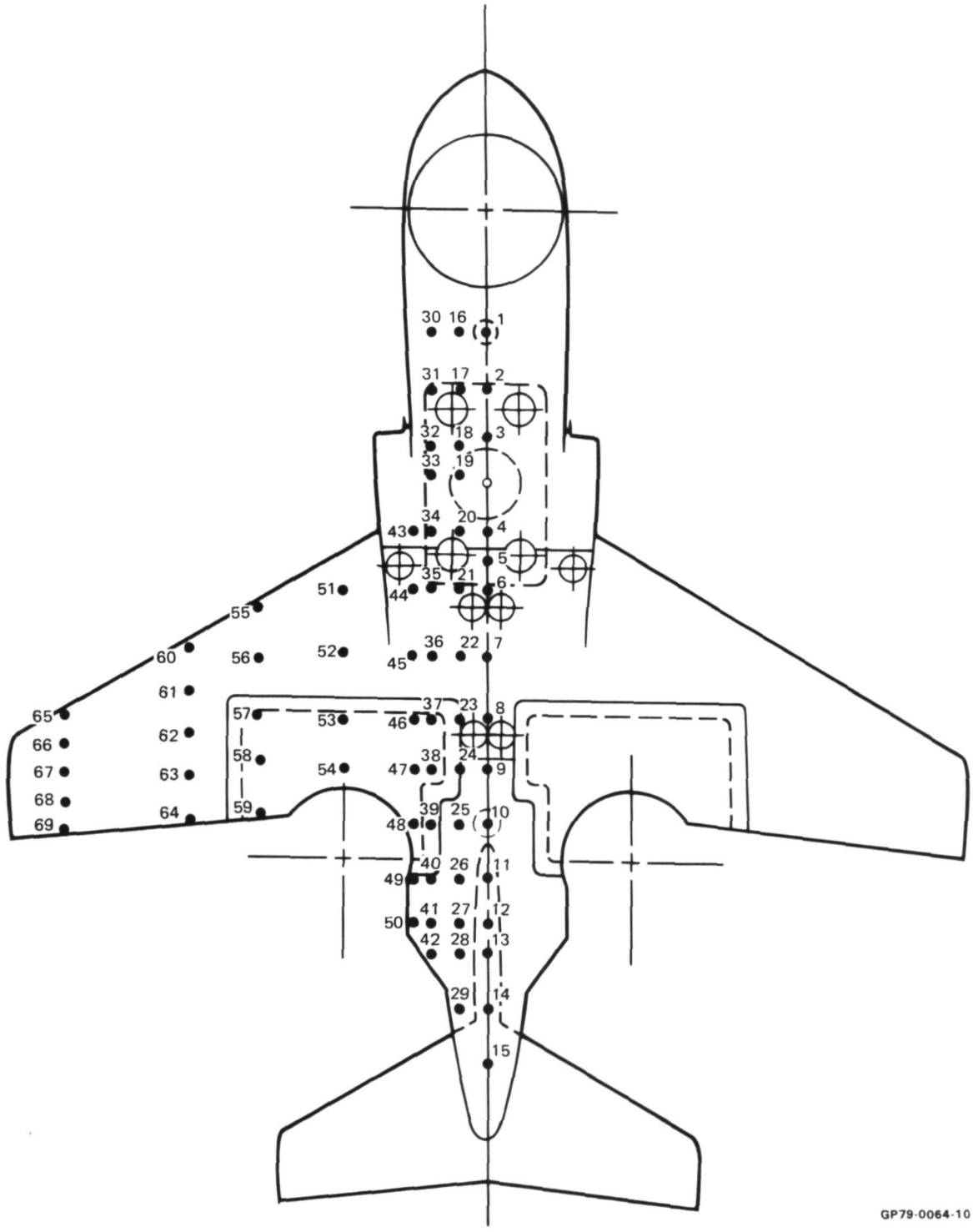

Nozzle total pressure ratios were recorded using standard pressure transducers and pitot tubes located in each nozzle entrance station.

Pressure data were obtained from 69 static taps located on the lower surface of the model, as shown on Figure 2-33. Correspondence with the LSPM lower surface pressure array was achieved for the most part, however space restrictions due to the force balance attachment did not permit complete duplication. The information from the static taps was used to develop lower surface pressure contour plots and also secondary induced force measurements through integration of the pressure-area values.

2.6 DESCRIPTION OF THE MCAIR JET INTERACTION TEST FACILITY

The MCAIR Jet Interaction Test Apparatus is a facility where the lift losses on a V/STOL airframe can be measured accurately and directly by an airframe force balance.

The airframe force balance is a six component device which measures forces and moments about three axes. The lift jet nozzles are isolated from the airframe model by very small adjustable gaps. This arrangement of metric model and non-metric nozzles allows the model balance to measure the propulsion induced forces and moments, exclusive of the nozzle thrust.

The lift jet nozzles are mounted on two plenum assemblies which provide rigid structural support and uniform nozzle airflow. The two plenum assemblies provide the capability of varying the spacing of the nozzles and, since each plenum has a remotely actuated control valve also provides the capability of operating the nozzles at different nozzle pressure ratios. The plenums are attached to the facility settling chamber which supplies them with pressure regulated air.

Four ground planes are available for use with the test apparatus. Two stationary ground planes (241 x 223 cm and 122 x 122 cm) are provided which allow the jet interaction testing to be performed in ground effects at various heights and inclination angles. The testing described herein used the 122 x 122 cm stationary ground plane. The height of the static groundboards can be remotely varied, while the inclination angle (pitch or bank) is changed manually. A six component force balance can be installed on the static ground planes to measure the forces and moments at ground level. Two movable ground planes are also provided on a hydraulically actuated support cart which allows dynamic simulation testing to be performed at various heave, pitch and bank angle amplitudes and frequencies.

3. PROPULSION SYSTEM AND FACILITY CALIBRATIONS

Determination of propulsion induced aerodynamics with a metric powered model as the LSPM, requires measurement of both the total lift forces on the model and the thrust produced by the propulsion units as a function of ground height. Since the induced effects are defined as the difference between total lift and thrust, this technique has inherently greater data uncertainty than the non-metric propulsion system approach used in the 4.1 percent scale model test program. Careful calibration of the powered model propulsion units and operational checks of the total lift measurement system can reduce the uncertainty of the induced lift data.

Accordingly, tests of each of the LSPM propulsion units were performed on an isolated basis to establish thrust and mass flow performance in and out of ground effect. Known loads were applied to the LSPM at several model heights to operationally check the load cells used to measure total lift and to establish an uncertainty level for the lift measurement. In addition, calibrations of the three test nozzles used in the 4.1 percent scale model were carried out in and out of ground proximity. A description of the calibration tests are provided in the following paragraphs.

3.1 LSPM PROPULSION SYSTEM CALIBRATION

Following completion of the LSPM static ground effects test phase, each of the propulsion units, including fan, gas generator, exhaust nozzle and fan exit instrumentation, was removed from the LSPM and installed individually on a thrust stand rig and operated in and out of ground effects. The thrust performance of each unit was measured with load cells, whereas the mass flow processed by the fan and gas generator was established by bellmouth inlets. The measured thrust and mass flows were then compared to ideal thrust and mass flow values computed using the fan exit pressure and temperature data. These comparisons then established thrust and mass flow coefficients for the fan exit rake instrumentation. The results of these tests are presented in Reference 6. The coefficients were in turn utilized with rake computed data obtained during the LSPM ground effects tests to establish the installed thrust performance of each propulsion unit.

The essential test results in the form of rake coefficient variation with ground height are presented in Figures 3-1 through 3-4 for each of the fan units (Reference 6). The rake thrust coefficient, CF, and the fan and turbine mass flow coefficients, CAF and CAT are defined under EQUATIONS. The data of Figures 3-1 and 3-2 indicate that the thrust coefficients for the two lift/cruise nozzles remain relatively constant with ground height down to an H/D value of 1.02, the lowest height tested. The LSPM nose fan unit thrust coefficient variation with ground height,

FIGURE 3-1
X376B/T58 LEFT LIFT/CRUISE UNIT
FAN EXIT RAKE THRUST AND MASS FLOW COEFFICIENTS
$\delta_{LC} = 95°$ $\delta_y = 0°$ $N_F/\sqrt{\theta_{T_i}} = 3600$ RPM

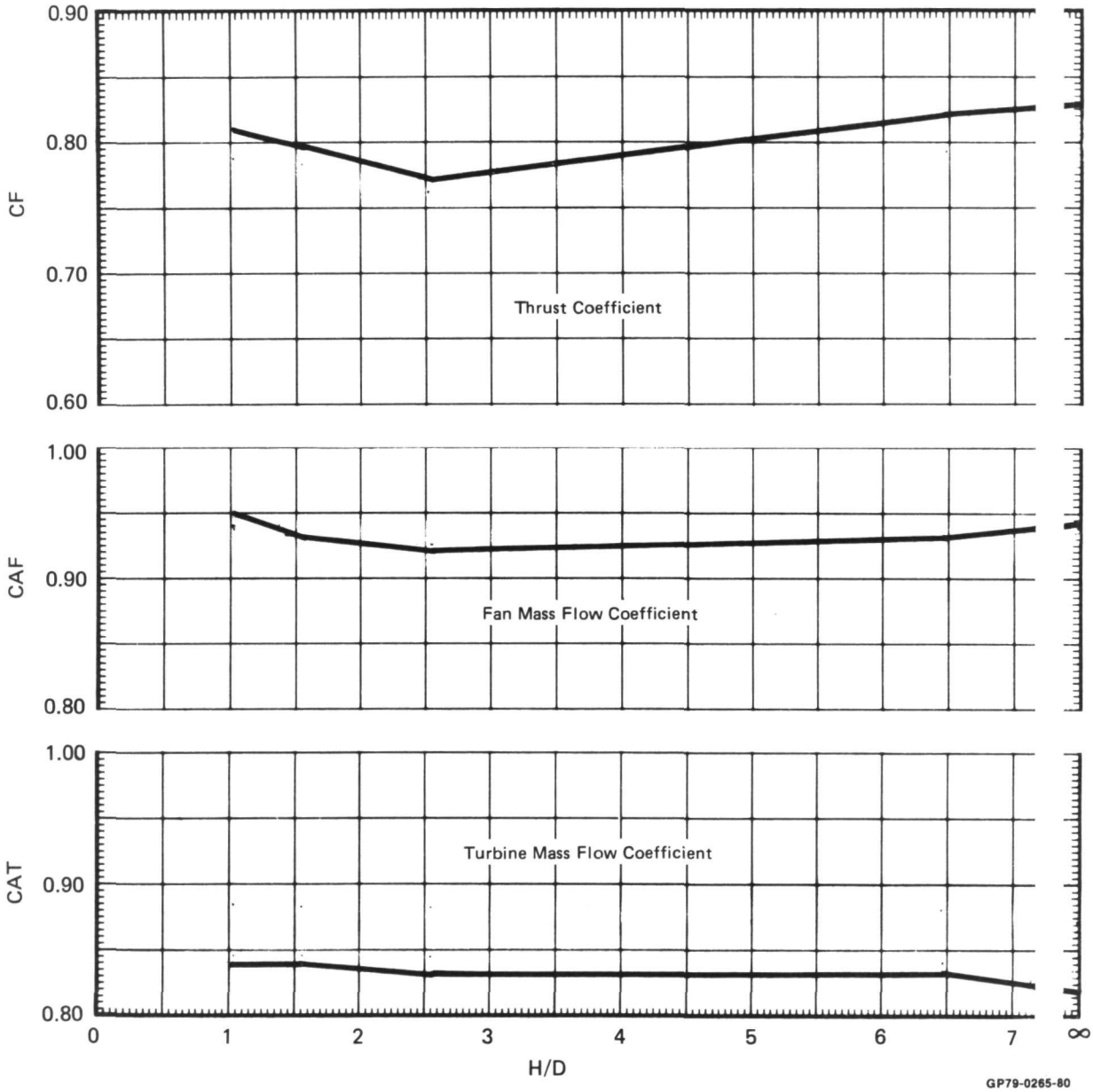

Data taken from reference 6.

FIGURE 3-2
X376B/T58 RIGHT LIFT/CRUISE UNIT
FAN EXIT RAKE THRUST AND MASS FLOW COEFFICIENTS
$\delta_{LC} = 95°$, $\delta_Y = 0°$ $N_F/\sqrt{\theta_{T_i}} = 3600$ RPM

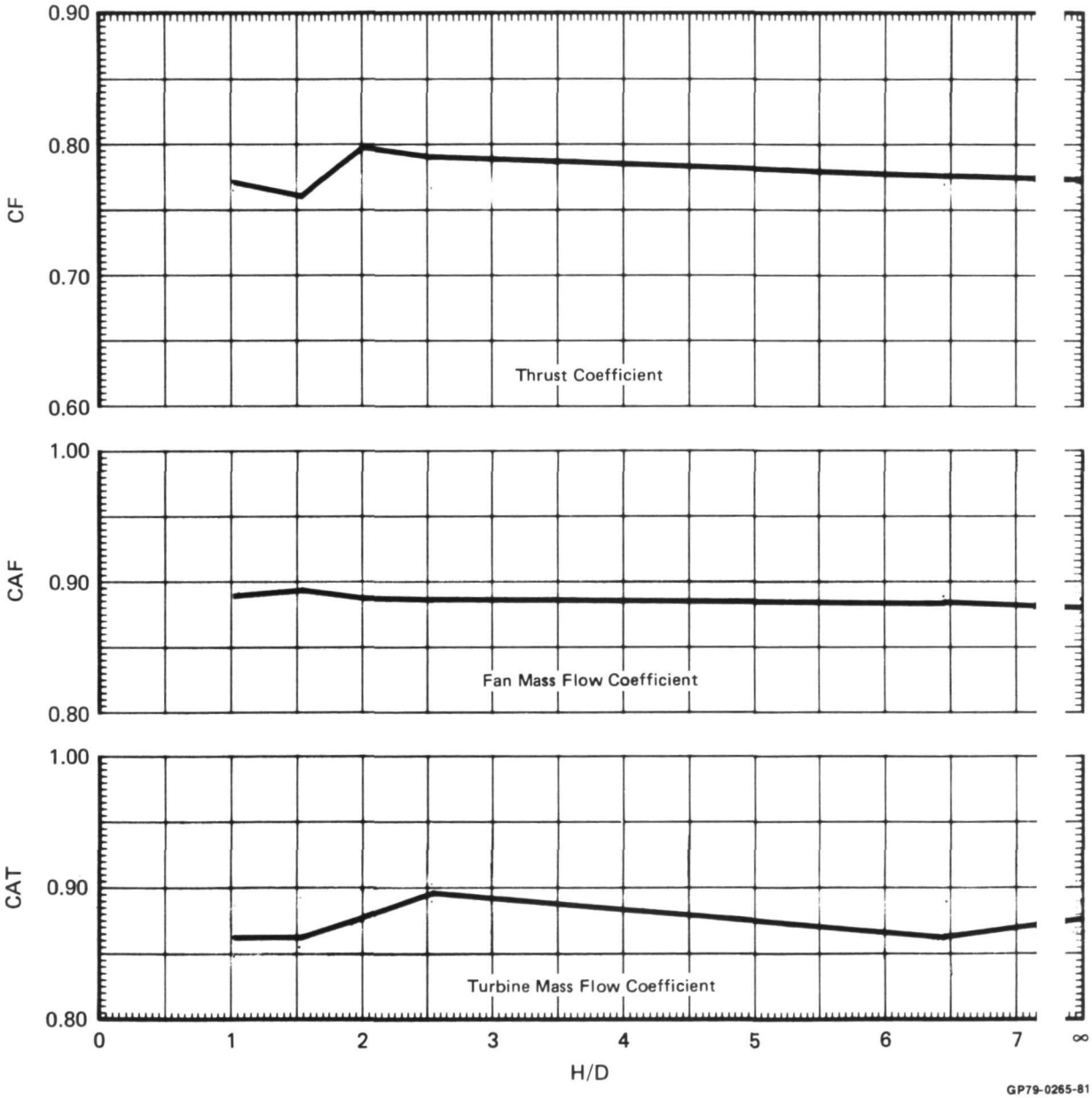

Data taken from reference 6.

FIGURE 3-3
X376B/T58 NOSE LIFT UNIT
FAN EXIT RAKE THRUST AND MASS FLOW COEFFICIENTS
$\delta_{NL} = 95°$ $\delta_y = 0°$ $N_F/\sqrt{\theta}_{T_i} = 3600$ RPM
Flat Plate Hub

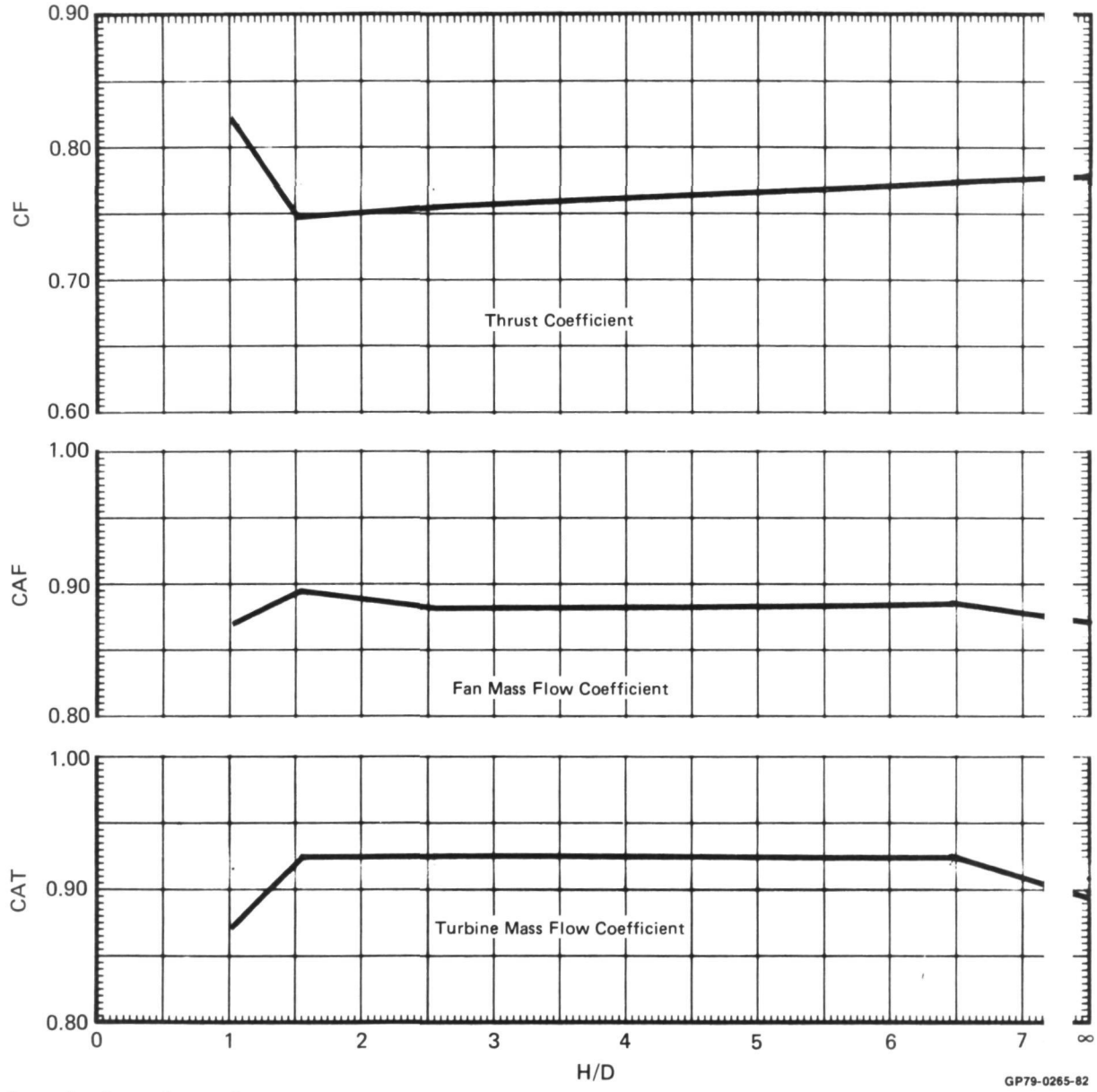

Data taken from reference 6.

shown in Figures 3-3 and 3-4, exhibited little change for H/D values down to 1.55; however, an increase of 5 to 10% in thrust coefficient was measured at 1.02. This performance characteristic was recorded on both fan exit hub geometries. The flat plate hub showed the largest increase at the lowest ground height. The improvement in thrust performance was correlated with an increase in hub base pressure levels. A detailed test report of the fan calibrations over the RPM range of 2000 to 4100 is presented in Reference 6. **MCDONNELL AIRCRAFT COMPANY**

FIGURE 3-4
X376B/T58 NOSE LIFT UNIT
FAN EXIT RAKE THRUST AND MASS FLOW COEFFICIENTS
$\delta_{NL} = 95°$ $\delta_Y = 0°$ $N_F/\sqrt{\theta T_i} = 3600$ RPM
Hemispherical Hub

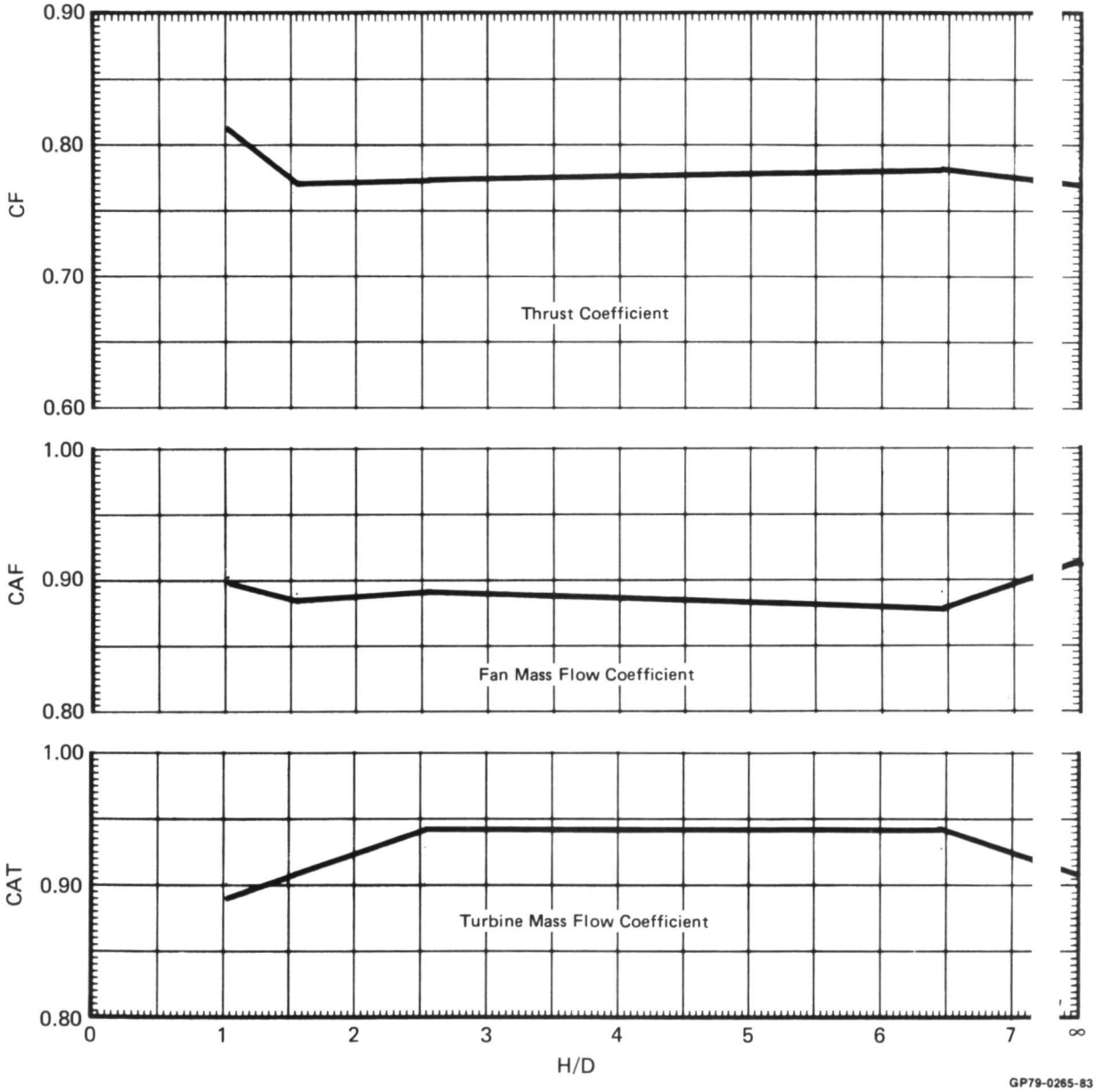

Data taken from reference 6.

3.2 LSPM LOAD CELL CHECKS

Application of known loads to the LSPM test apparatus was carried out at the three lowest model H/D's of 0.95, 1.53 and 3.06. Figures 3-5 is a photograph of the loading rig arrangement at the 3.05 meter height. A single axis load cell was used to establish the model applied loads. This cell was calibrated against known standards at NASA-Ames to an accuracy of ±0.25% at 13,350 newtons. Figures 3-6 through 3-9 show comparisons of the measured and applied loads for nose position loadings at the three heights and a mid fuselage loading at the 3.05 meter height. The check loadings indicate that the load cell units provide data within a ±2 percent uncertainty band with none of the engines operating.

FIGURE 3-5
LOAD CELL CHECK LOADING APPARATUS

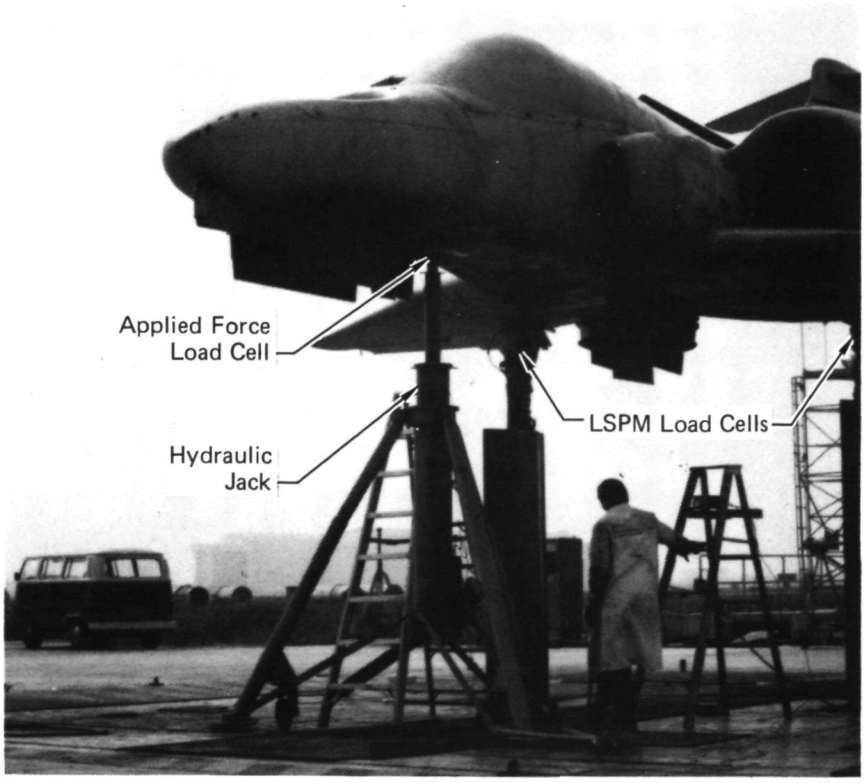

GP79-0265-1

FIGURE 3-6
LOAD CELL CHECKS
Nose Loading H/D = 0.95

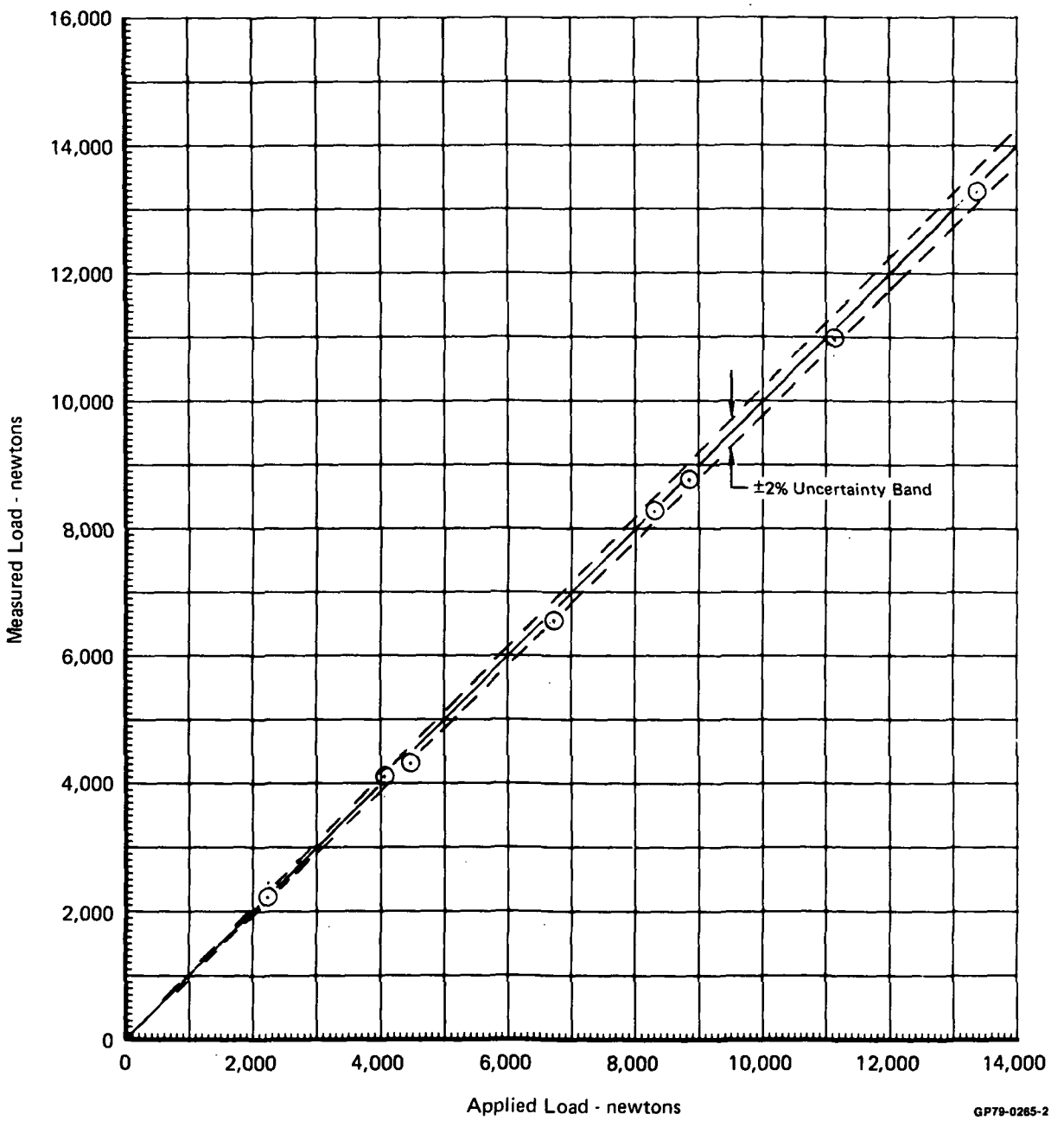

FIGURE 3-7
LOAD CELL CHECKS
Nose Loading H/D = 1.53

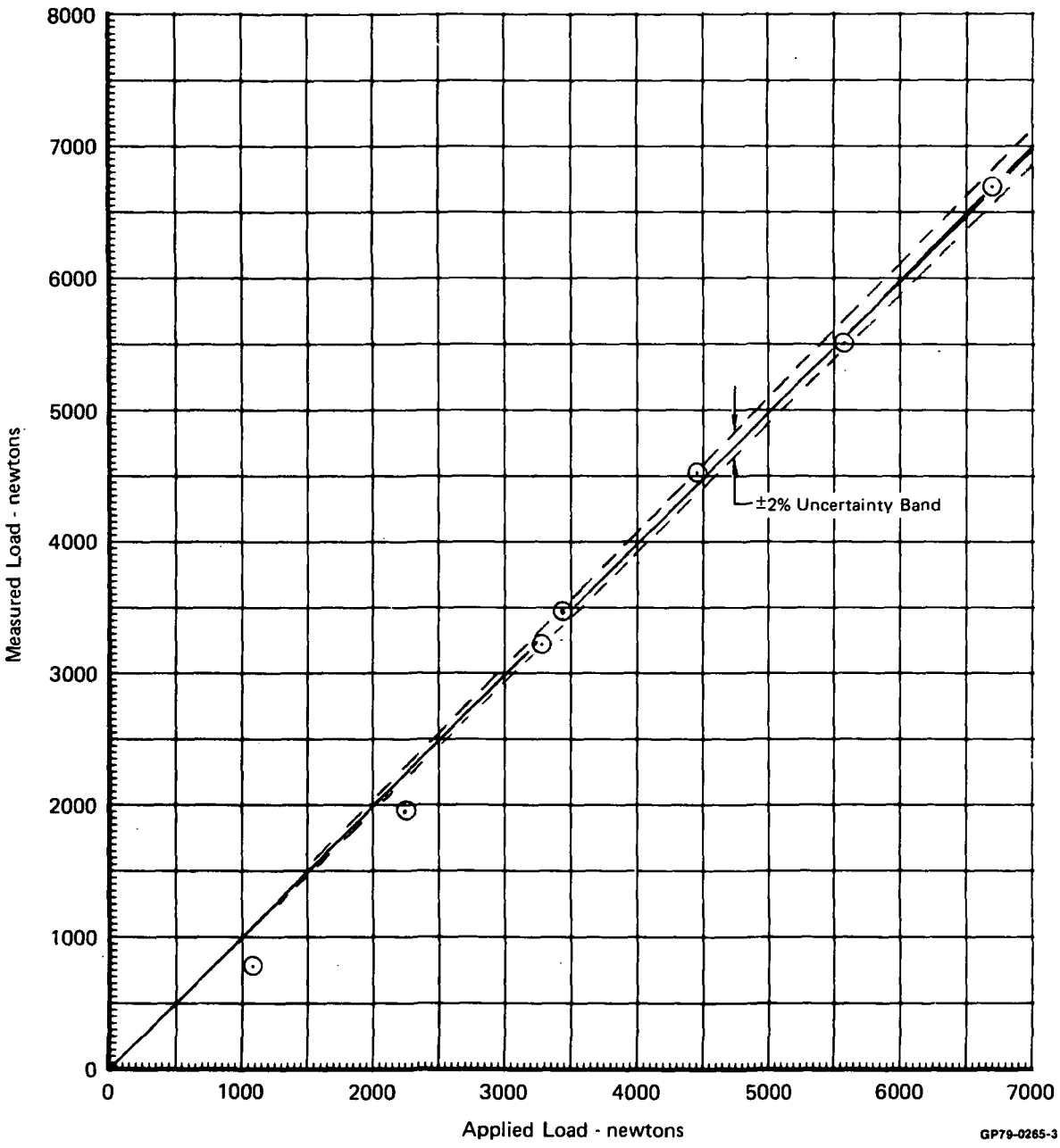

FIGURE 3-8
LOAD CELL CHECKS
Nose Loading H/D = 3.06

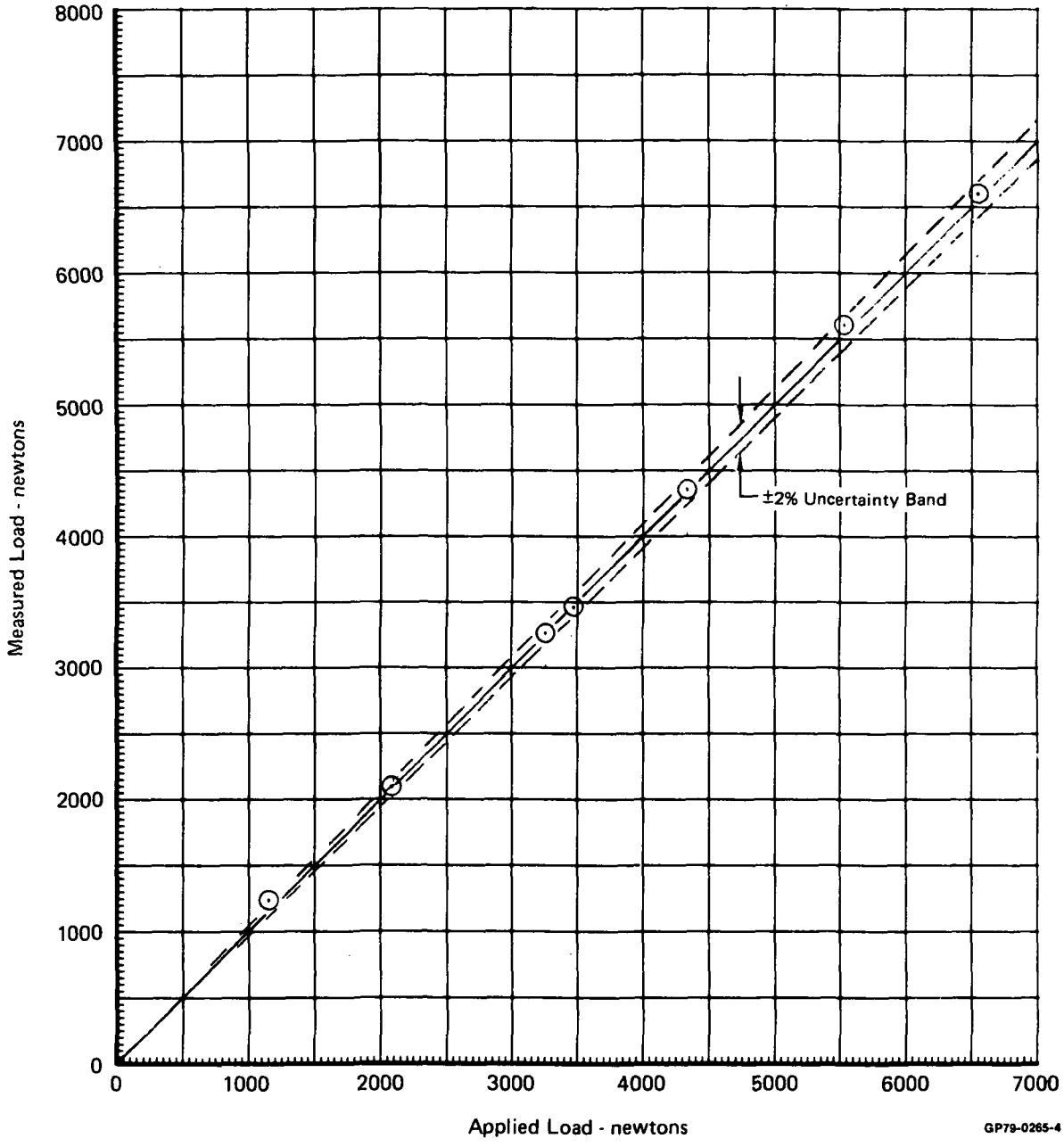

FIGURE 3-9
LOAD CELL CHECKS
Mid Fuselage Loading H/D = 3.06

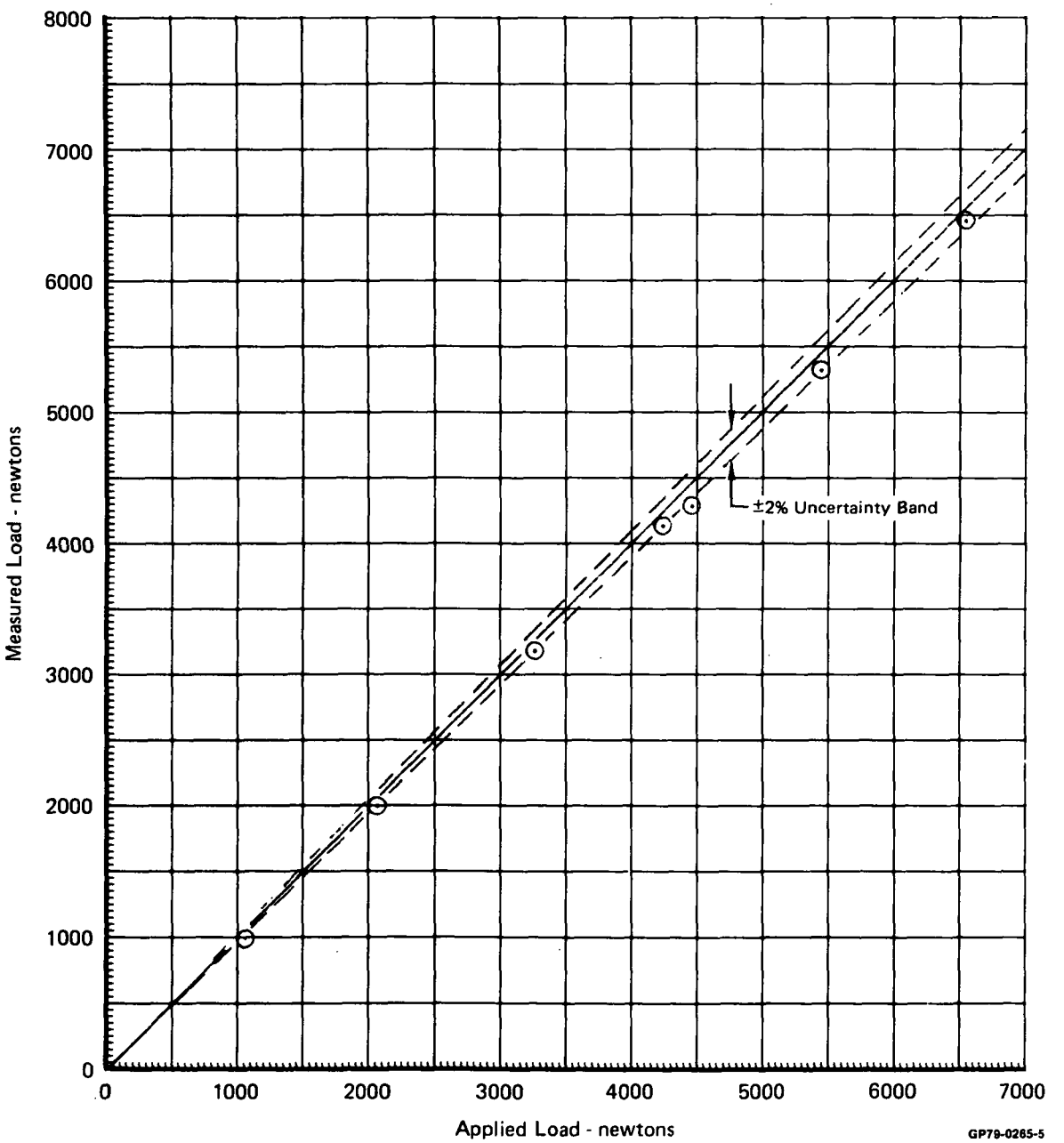

3.3 4.1 PERCENT SCALE MODEL NOZZLE CALIBRATIONS

Induced aerodynamics are dependent upon the lift system characteristics and for comparative purposes the induced forces are non-dimensionalized by the total system thrust. For this reason, the nose and two lift/cruise nozzles used during the small scale jet interaction tests were calibrated in MCAIR Nozzle Thrust Stand Facility prior to the induced lift tests.

The nozzles were calibrated over a range of pressure ratio representative of the operating range of the turbotip fans in the LSPM. The thrust vector angle generated by the lift/cruise nozzle is presented in Figure 3-10 as a function of nozzle pressure ratio. The lift/cruise nozzles were provided with 5 degree inserts so that hood deflection angles of 90 degrees and 95 degrees could be achieved. The data indicates that the 90 degree hood deflection generated a thrust angle of 80 to 82 degrees, while the 95 degree configuration produced 86 to 88 degrees of thrust vectoring. Nozzle velocity coefficient and discharge coefficient data for the nose and lift/cruise nozzles are presented in Figure 3-11. Over the range of LSPM fan operation the velocity and flow coefficients were relatively insensitive to pressure ratio.

Nozzle performance variations in ground effect were investigated during the calibration tests. A comparison of corrected thrust as a function of nozzle pressure ratio for H/D values of 0.95 and ∞ is illustrated in Figure 3-12 and indicates no change in nozzle performance.

FIGURE 3-10
LIFT/CRUISE NOZZLE THRUST VECTORING CHARACTERISTICS
4.1% Model

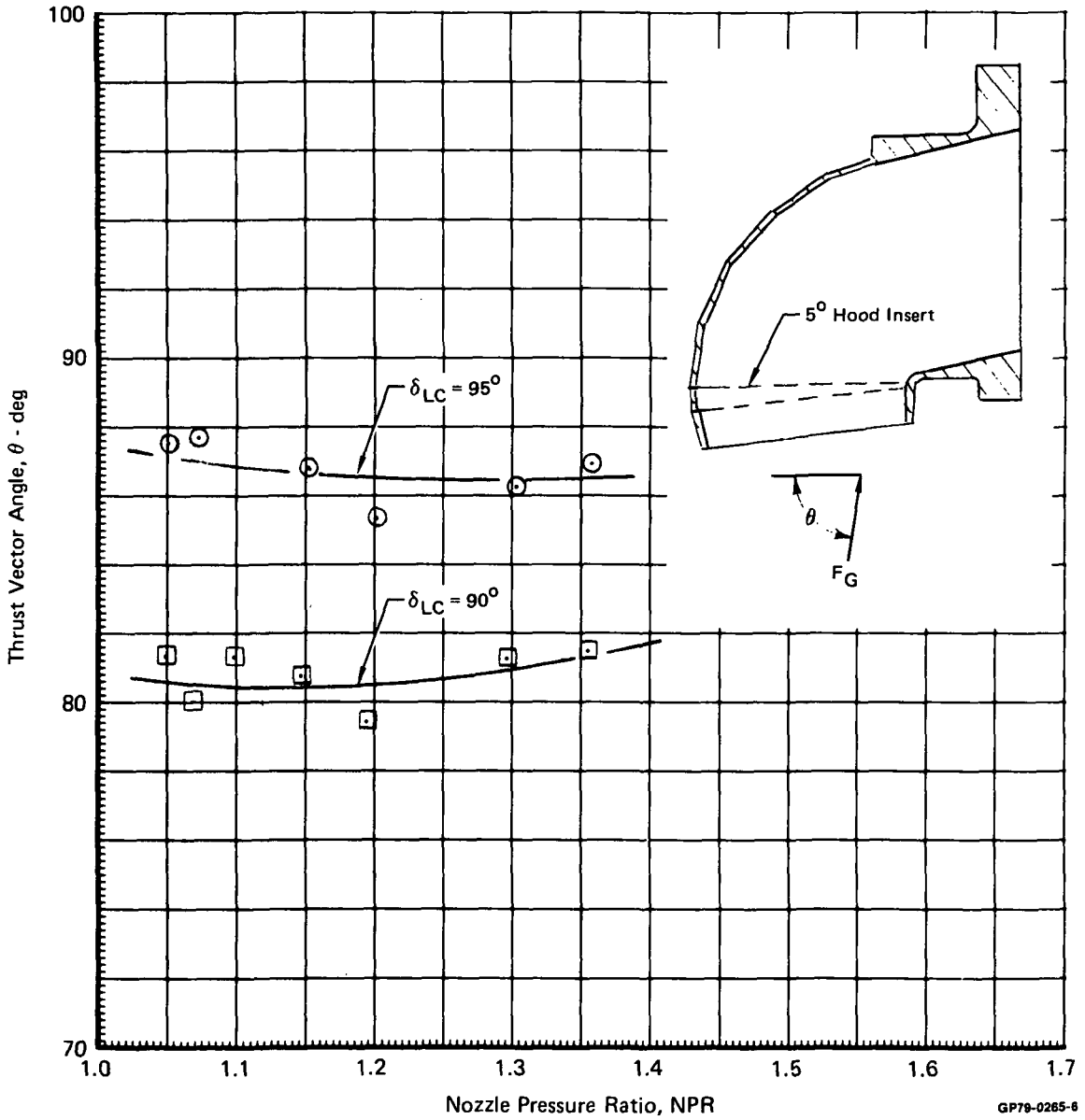

FIGURE 3-11
VELOCITY AND DISCHARGE COEFFICIENTS
4.1% Model Nozzles H/D = ∞

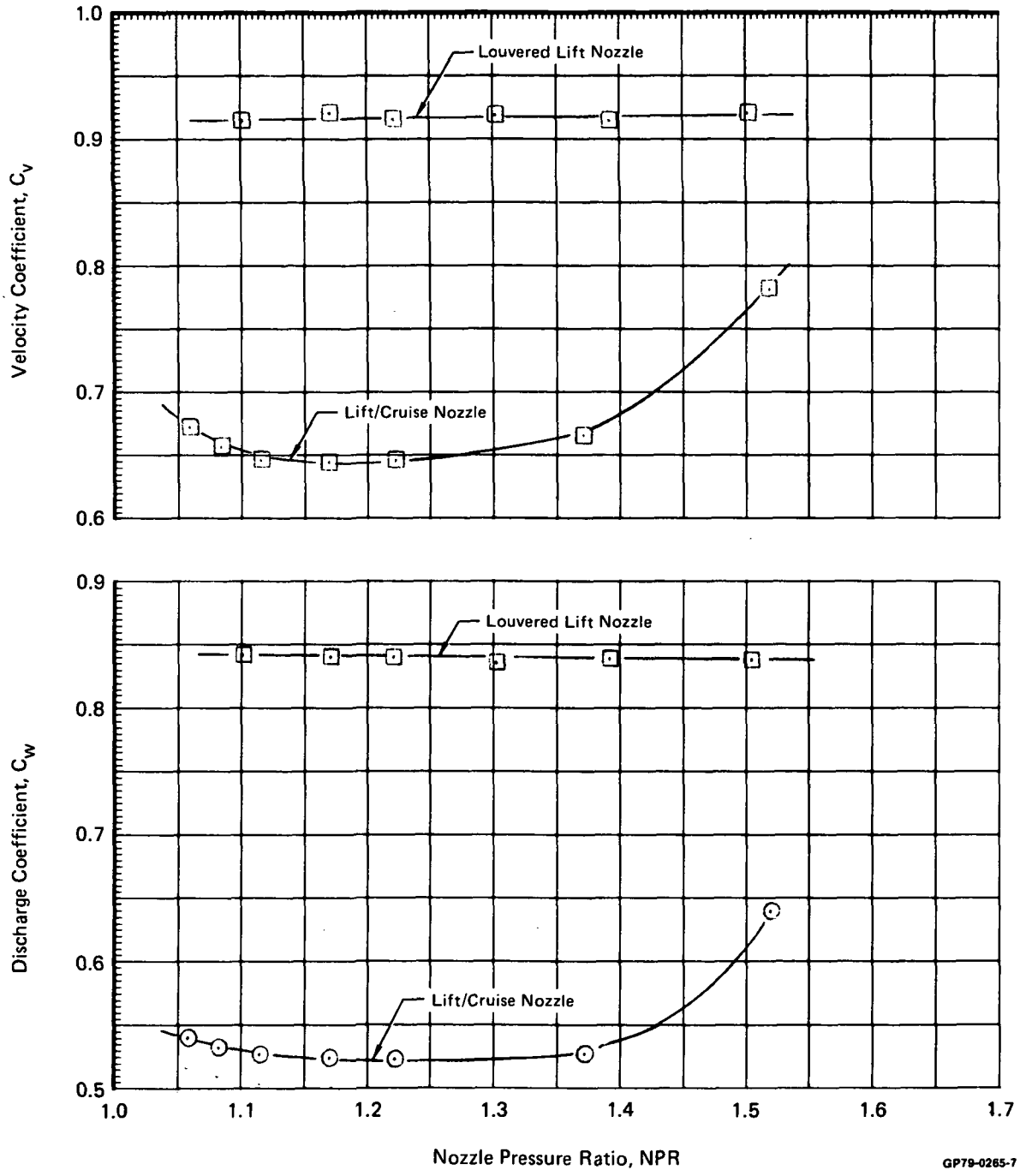

FIGURE 3-12
THRUST PERFORMANCE IN GROUND EFFECT
4.1% Model Nozzles

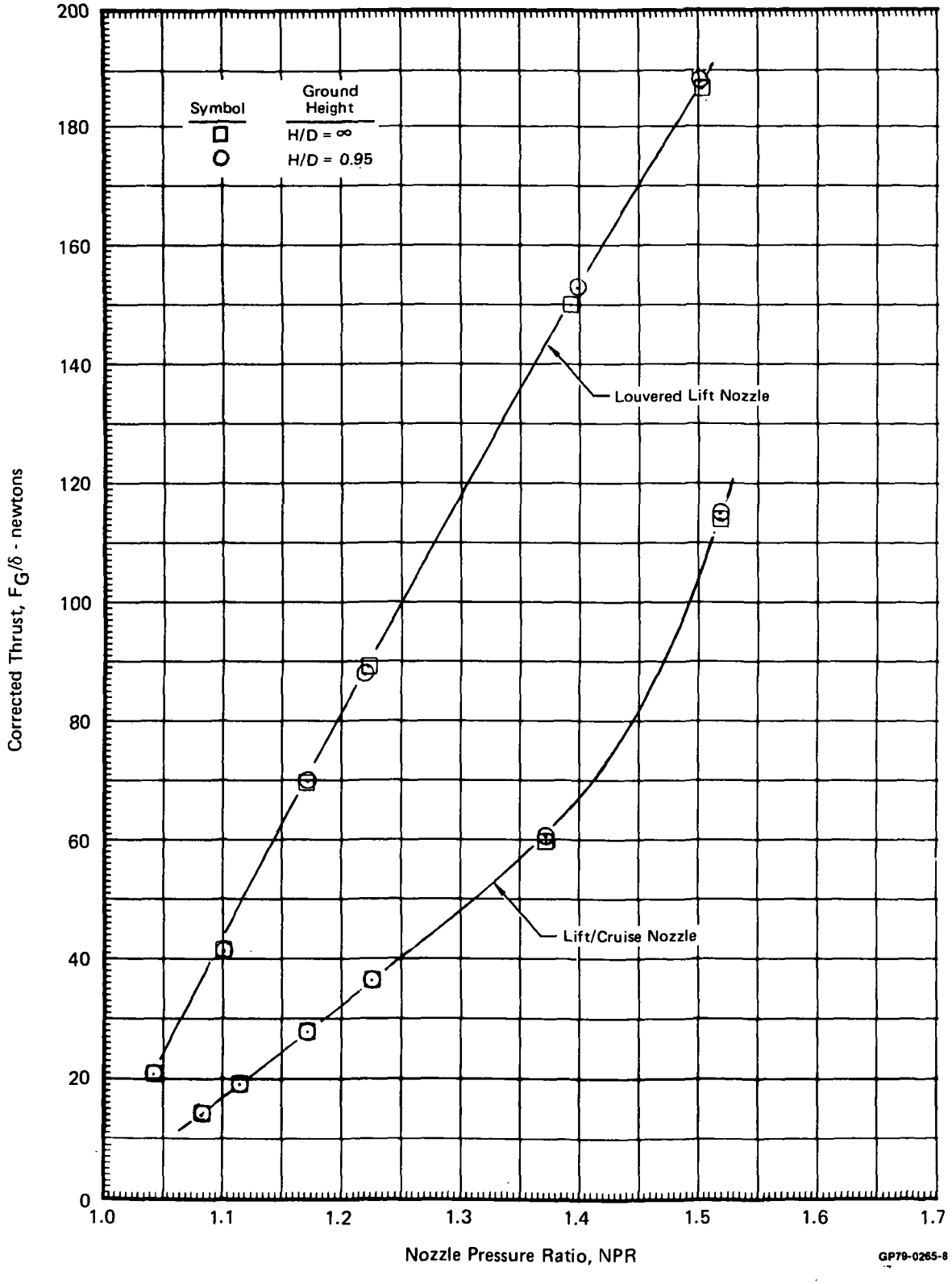

4. TEST RESULTS AND DISCUSSION

The results of the Large Scale Powered Model (LSPM) static test program cover propulsion induced lift effects in ground proximity, inlet reingestion, and airframe surface pressures and temperatures. In the following sections, induced force and moment data are presented for a number of model configurations, attitudes and heights above the ground. For selected model geometries, induced lift characteristics and airframe surface pressure data for the corresponding 4.1 percent scale model are included for comparison with the large scale model test results. Unusual results are then discussed in greater detail. Finally, model lower surface temperatures are presented with the hot gas reingestion data for the nose fan, left lift/cruise fan and left gas generator inlets.

4.1 INDUCED LIFT PERFORMANCE

The baseline configuration consisted of the large scale model aircraft geometry with lift/cruise nozzle rails, 95 degree lift/cruise vectoring hoods and flat plate nose fan exit hub. Alternate configurations included lift improvement devices (LID), lift/cruise nozzle perimeter plates, a hemispherical nose fan exit hub and several model pitch and roll attitudes. A run summary of the model configurations, model heights and fan speeds tested is presented in Appendix A.

The balance measured total lift and calculated ideal thrust are presented herein for average inlet corrected fan speeds. The left lift/cruise fan and nose fan inlet temperatures were measured with fan face temperature rakes. The right lift/cruise fan, however, was equipped with only a fan exit temperature rake. The right lift/cruise fan inlet temperature was determined using the fan exit average temperature and subtracting the temperature rise through the fan, determined from the left lift/cruise fan, to obtain the fan face average temperature.

The ideal thrust was calculated for each unit using fan exit rake pressure and temperature measurements. Thrust coefficients, determined from isolated fan calibrations, were applied to calculate total fan installed thrust.

The large scale model induced lift was calculated by subtracting the total fan installed thrust from the balance measured lift and then nondimensionalizing this result with the total fan installed thrust. The induced lift for a constant corrected fan speed is usually expressed as a function of model height ratio, H/D, where D is based on the average exit flow area diameter of all three lift units, (39.25 inches, 99.7 cm).

Both models were instrumented with lower surface pressure taps to locate positive and negative pressure areas on the model and to calculate an overall induced

force. Each pressure tap was assigned a specific area, the pressure force computed for each area and the forces summed to obtain a total induced force acting on the model. The total force was then nondimensionalized with respect to total fan installed thrust. Pressure contour plots were generated to outline positive and negative pressure areas.

Small scale induced model forces were measured directly independent of nozzle thrust with a six component force balance. Induced lift measurements were nondimensionalized with respect to the calibrated total thrust of all nozzles operating.

4.1.1 BASELINE CONFIGURATION - ONE AND TWO UNIT OPERATION

Single Unit Operation - Static testing was performed with individual lift/cruise fans and nose fan operating alone. This procedure allows for investigation of suckdown effects without fountain upwash and for examination of the interactions resulting from three and two unit operation.

The ideal thrust and balance measured lift for each lift unit are presented in Figures 4-1 through 4-4 as a function of corrected fan speed for H/D values of 0.95, 1.53, 3.06 and 6.45. The ideal thrusts were found to be essentially independent of H/D. The balance measured lift increased with increasing H/D for the lift/cruise units. The same trend is indicated for the nose unit except for a sizeable decrease in lift indicated at H/D of 6.45.

The induced lift characteristics due to the left lift/cruise unit operating alone are presented in Figure 4-5 for a constant corrected fan speed of 3600 RPM. The balance measured total lift decreased with decreasing H/D whereas the installed thrust is essentially independent of H/D. The induced lift increases with decreasing H/D, with a lift loss of 29 percent at a H/D of 0.95. The small scale model induced lift characteristics are also shown in Figure 4-5. Both models show the same trend of induced lift with H/D. The large scale model, however, indicates a consistently greater lift loss than the small scale model at all model heights tested.

The induced lift characteristic due to the right hand lift/cruise fan operating alone is presented in Figure 4-6 and exhibits the same trends as the left lift/cruise fan operating alone. A comparison of the induced lift characteristics for each individual lift/cruise fan operation is presented in Figure 4-7. Due to the symmetry of the two units about the model centerline, the same induced lift characteristics are expected for each single unit operation. The figure shows the characteristics to be similar but not identical.

FIGURE 4-1
EFFECT OF MODEL ALTITUDE ON TOTAL MEASURED LIFT
Left Lift/Cruise - Single Unit Operation
Baseline Configuration

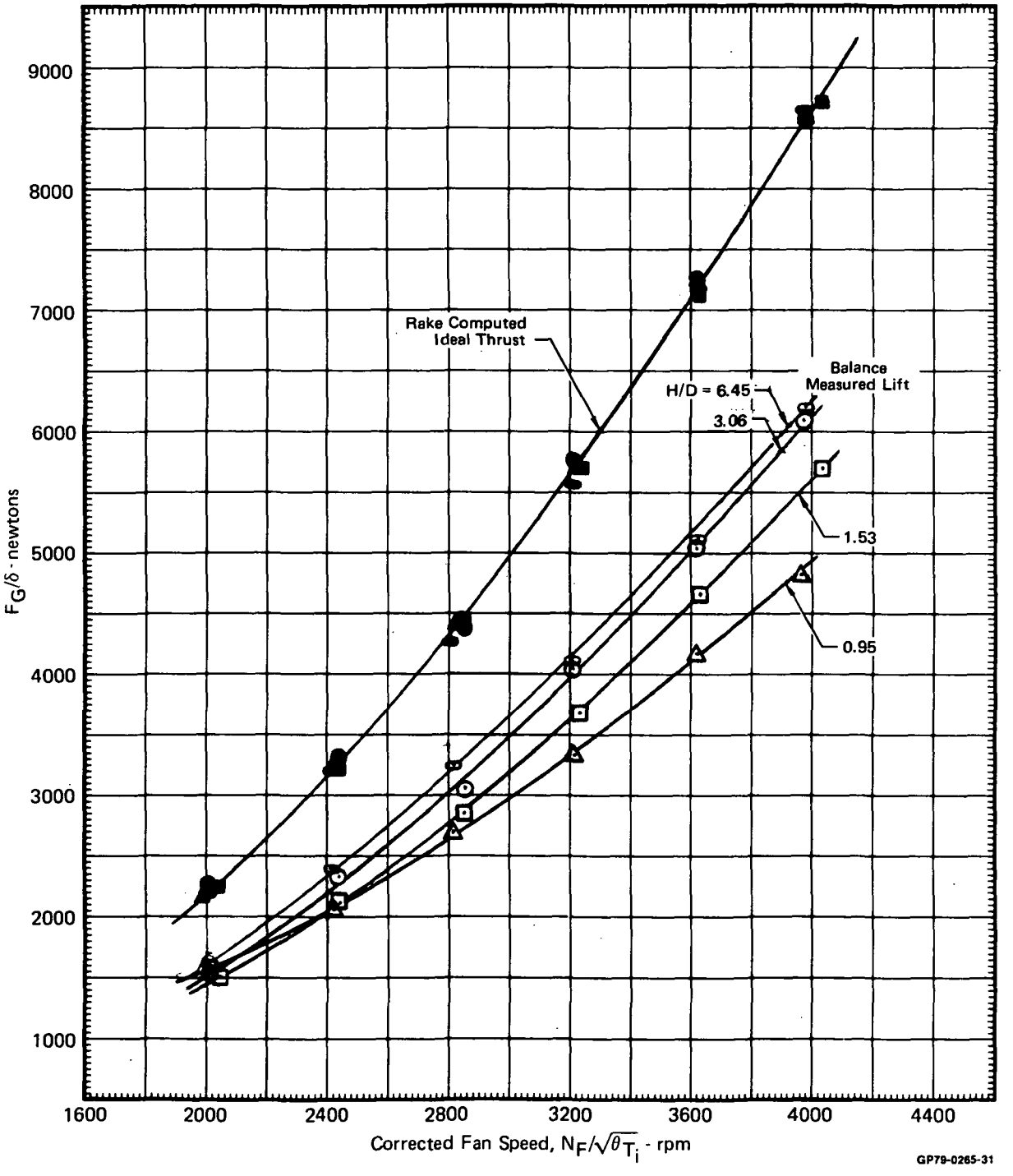

FIGURE 4-2
EFFECT OF MODEL ALTITUDE ON TOTAL MEASURED LIFT
Right Lift/Cruise - Single Unit Operation Baseline Configuration

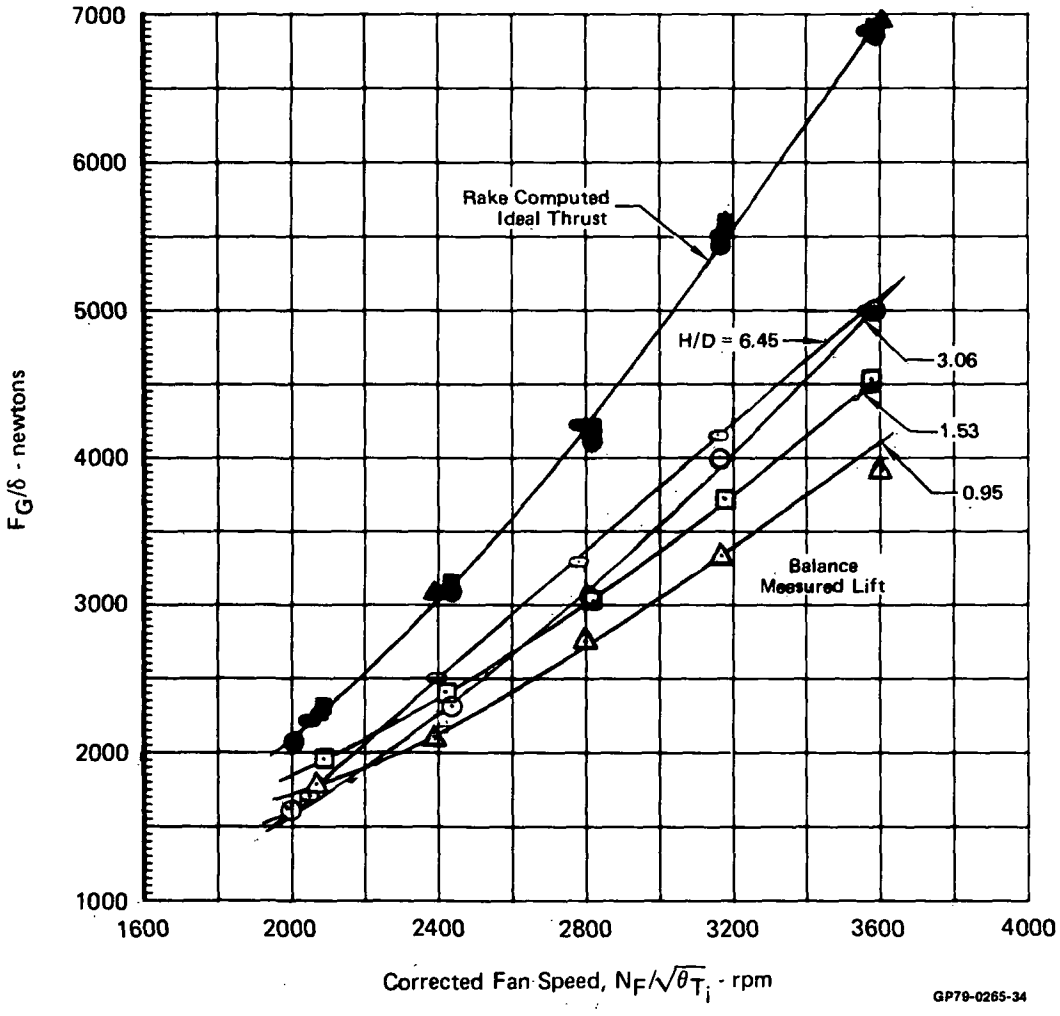

FIGURE 4-3
EFFECT OF MODEL ALTITUDE ON TOTAL MEASURED LIFT
Nose - Single Unit Operation Baseline Configuration

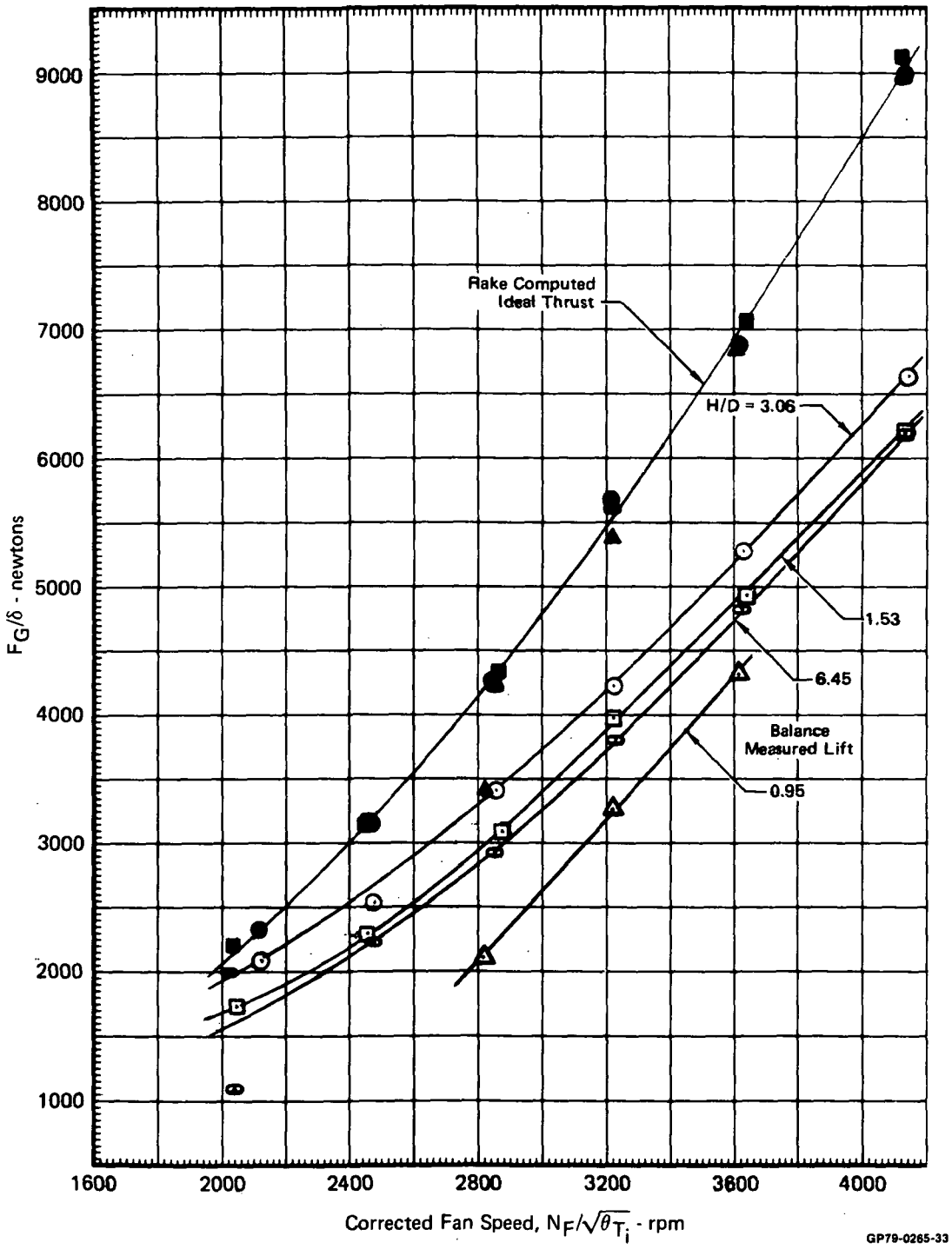

FIGURE 4-4
EFFECT OF MODEL ALTITUDE ON TOTAL MEASURED LIFT
Nose - Single Unit Operation
Baseline Configuration Plus Hemispherical Nose Fan Exit Hub

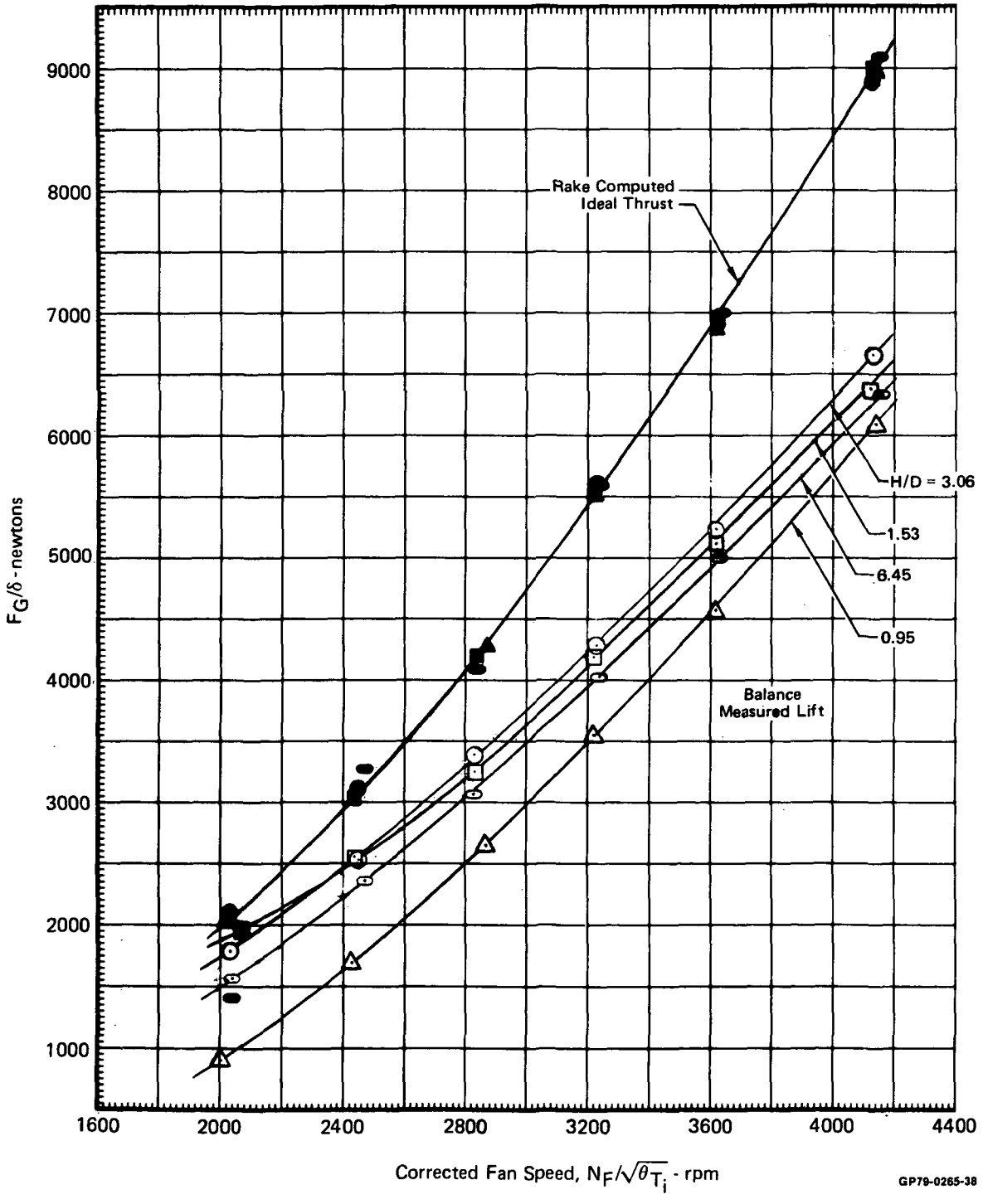

FIGURE 4-5
INDUCED LIFT COMPARISONS
Baseline Configuration Left Lift/Cruise - Single Unit Operation

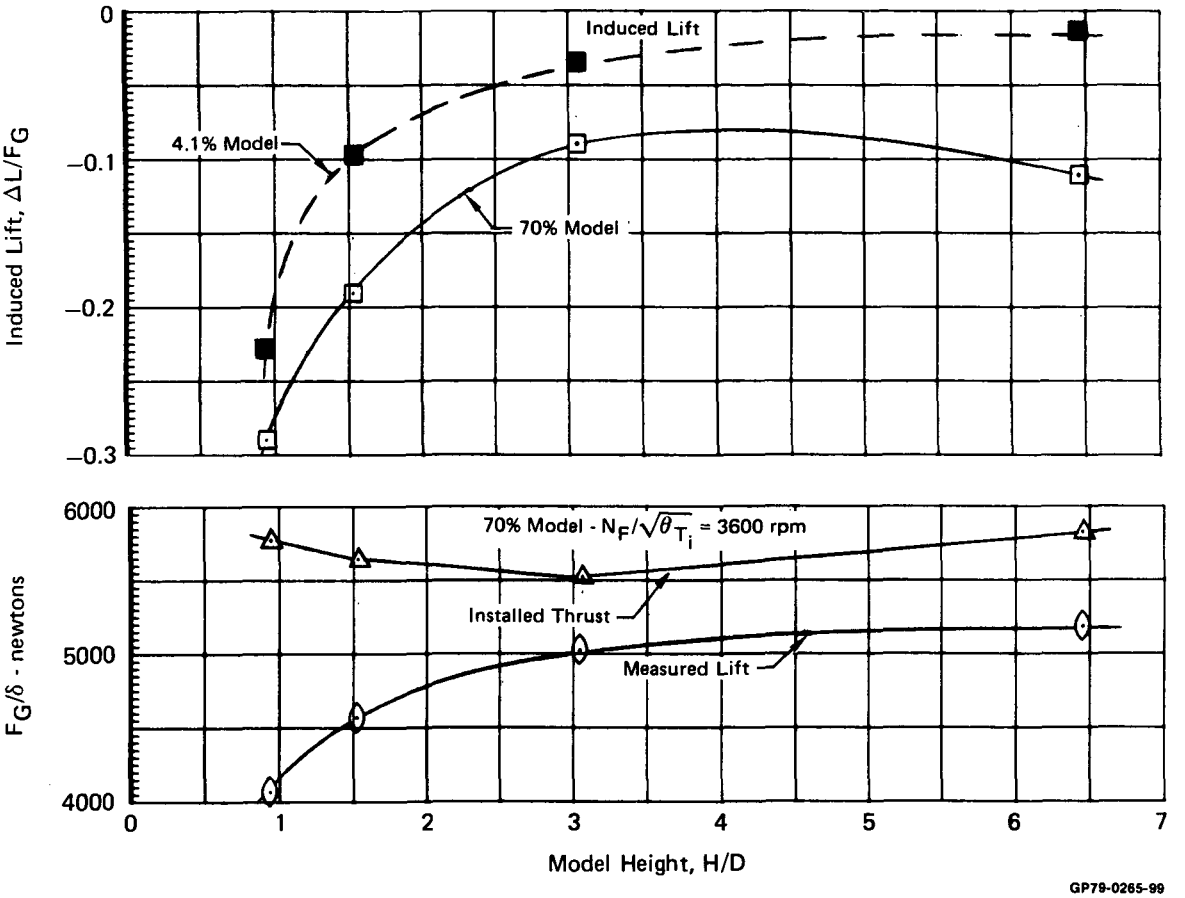

FIGURE 4-6
INDUCED LIFT COMPARISONS
Baseline Configuration Right Lift/Cruise - Single Unit Operation

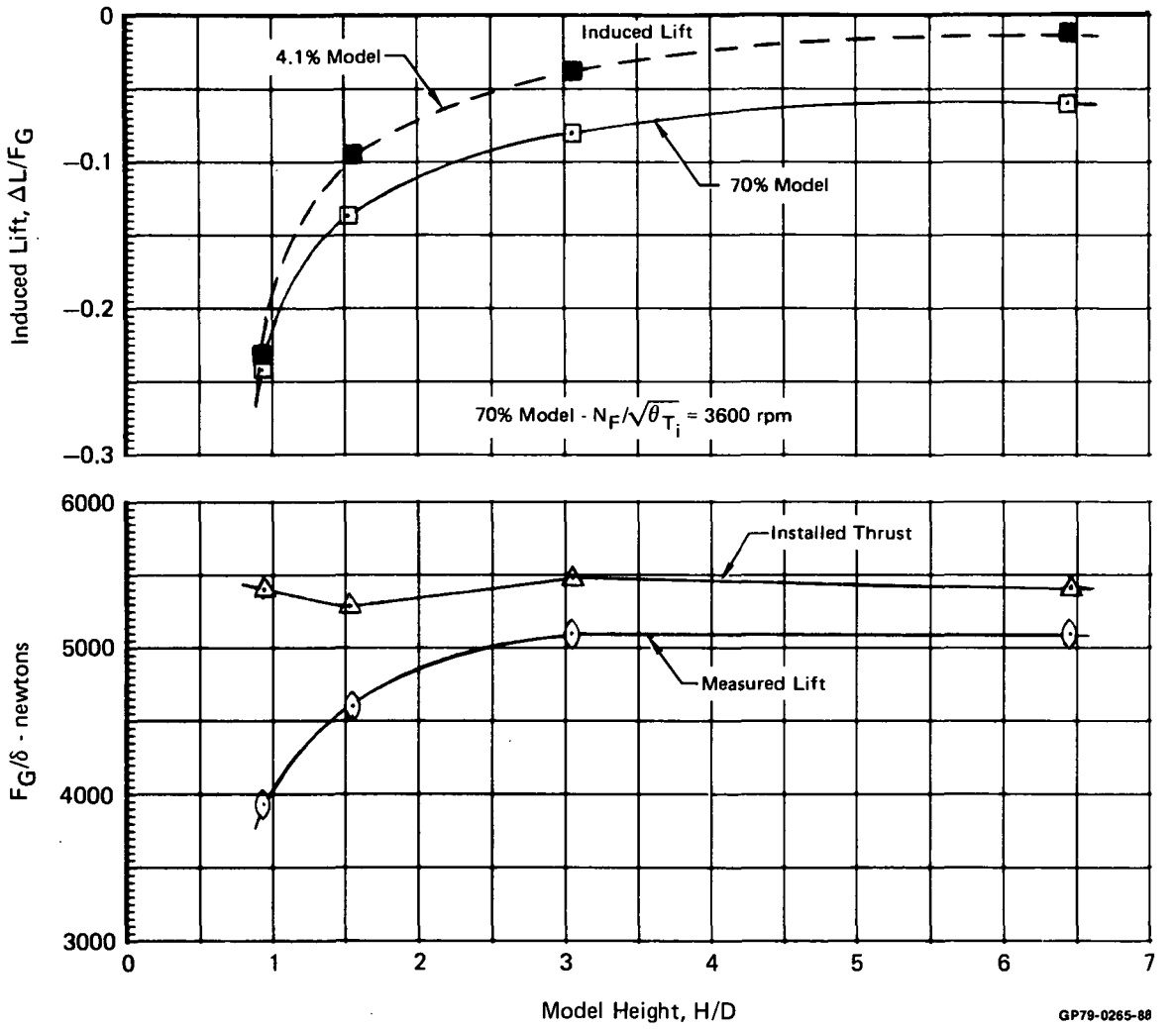

FIGURE 4-7
INDUCED LIFT COMPARISONS
Baseline Configuration Lift/Cruise Single Unit Operation
$N_F/\sqrt{\theta_{T_i}}$ = 3600 RPM

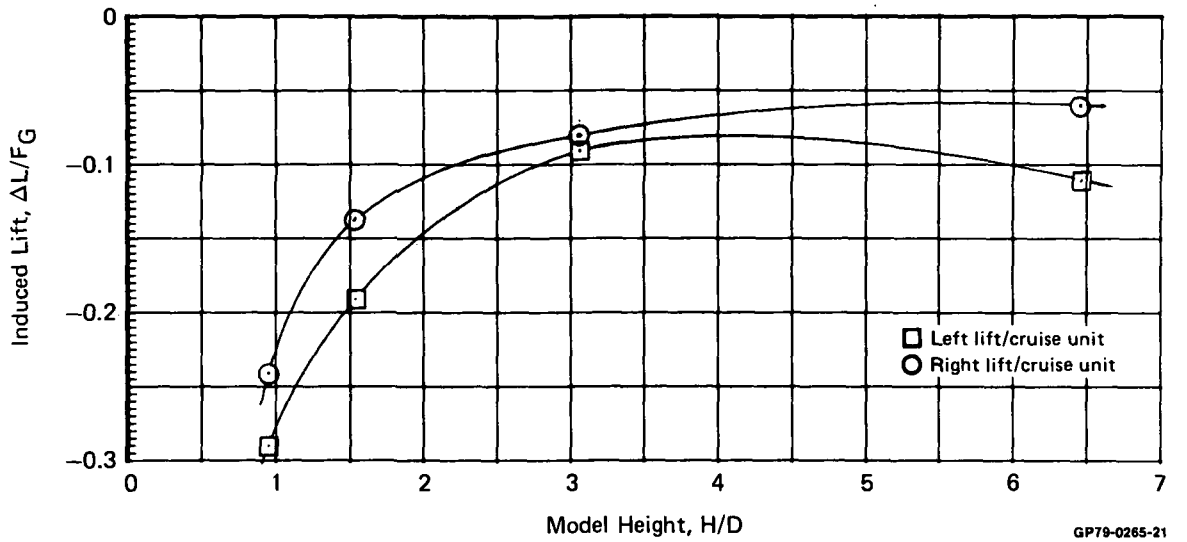

The induced pitching moment expressed as a dimensionless coefficient is presented in Figure 4-8 for single lift/cruise unit operation. The induced pitching moment coefficient is defined as the induced moment about the theoretical center of gravity of the aircraft configuration nondimensionalized with respect to the product of total installed thrust and mean aerodynamic chord. The small scale model exhibits no induced moment out of ground effect and a slight nose up moment at H/D of 0.95. This is probably due to the negative pressure area around the lift/cruise nozzle aft of the center of graivty. The large scale model shows the same general trend of pitching moment coefficient with respect to H/D. The magnitude of the induced moment, however, is greater than for the small scale model at all H/D's tested. Due to the symmetry of the left and right lift/cruise units about the model centerline, the induced moment characteristics were expected to be, and are, the same for each unit. The differences between the two curves is indicative of the uncertainty in calculating the induced pitching moment from the test data.

FIGURE 4-8
INDUCED PITCHING MOMENT COMPARISON
Baseline Configuration Single Lift/Cruise Unit Operation

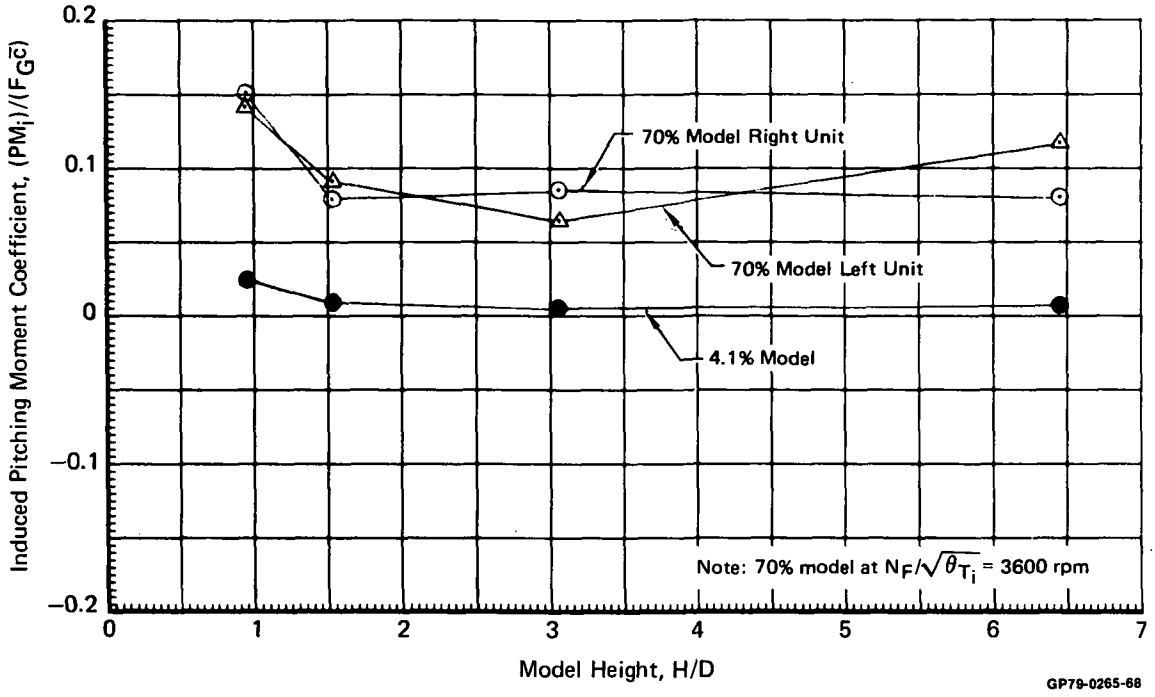

The induced lift characteristics due to the nose fan operating alone is presented in Figure 4-9. The total balance measured lift increases with H/D up to a value 3.06, then decreases at H/D of 6.45. Installed fan thrust is essentially constant except for an 11% increase at H/D = 0.95. Both models show the same trend of induced lift with model height up to H/D of 3.06. At H/D = 6.45, however, the small scale model indicates approximately 1 percent lift loss and the large scale model 12 percent lift loss.

The calculated pressure force for both models is also shown in Figure 4-9. The small scale pressure data indicates the same trend and approximately the same value of lift loss as the balanced measured data. The large scale pressure data, however, indicates significantly less induced lift loss than the balance data for all model heights tested except at H/D = 3.06.

The induced lift characteristics due to the nose fan operating alone with a hemispherical exit hub is presented in Figure 4-10. The installed thrust is essentially the same as that for the nose fan with the flat plate exit hub. The balance measured lift and induced lift are similar to the flat plate hub nose fan operation in both trend and magnitude versus H/D.

FIGURE 4-9
INDUCED LIFT COMPARISON
Baseline Configuration Nose - Single Unit Operation

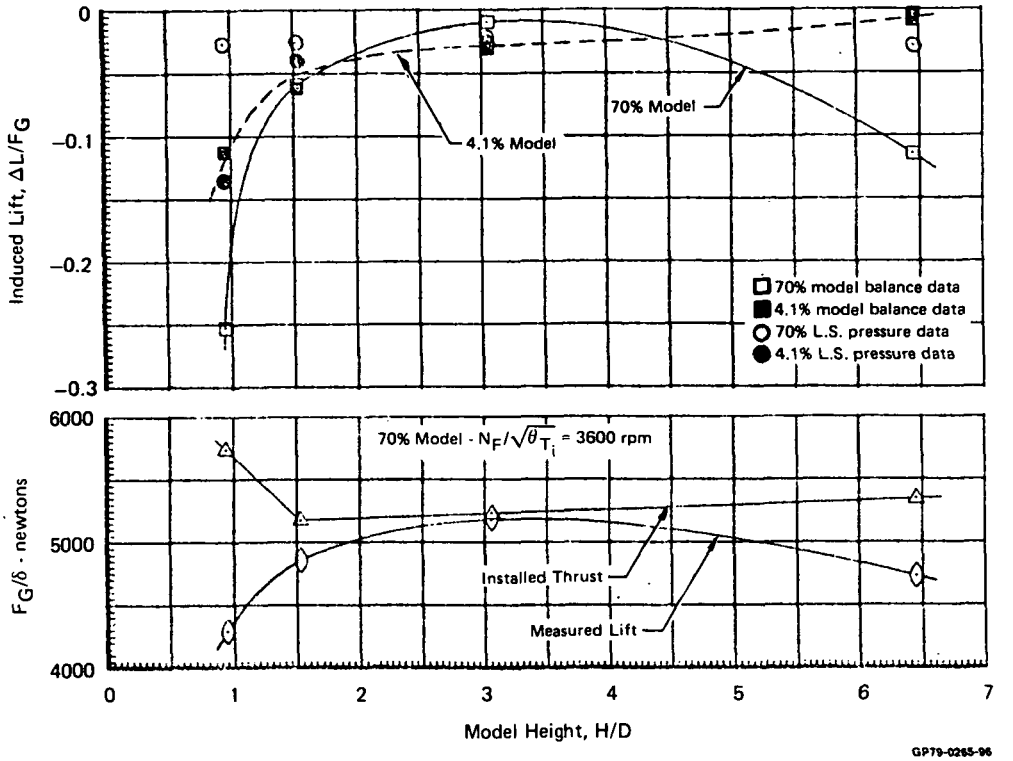

FIGURE 4-10
INDUCED LIFT COMPARISON
Baseline Configuration with Hemispherical Nose Fan Exit Hub
Nose - Single Unit Operation

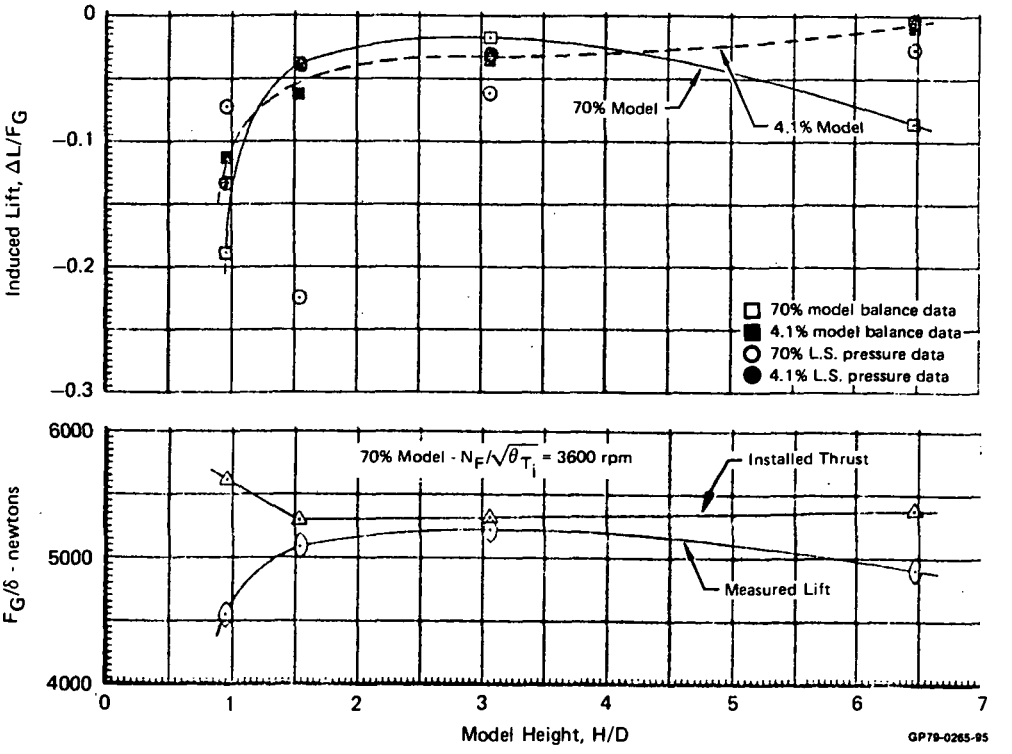

A comparison of the induced lift characteristics for the nose fan operating alone with the flat plate exit hub and hemispherical exit hub is presented in Figure 4-11. The induced lift characteristics are expected to be the same because of the same nozzle exit arrangement with respect to the model. Both curves indicate the same trend of induced lift versus H/D including a large lift loss at H/D = 6.45.

FIGURE 4-11
INDUCED LIFT COMPARISONS
Nose - Single Unit Operation
Hemispherical vs Flat Plate Exit Hub
$N_F/\sqrt{\theta_{T_i}}$ = 3600 RPM

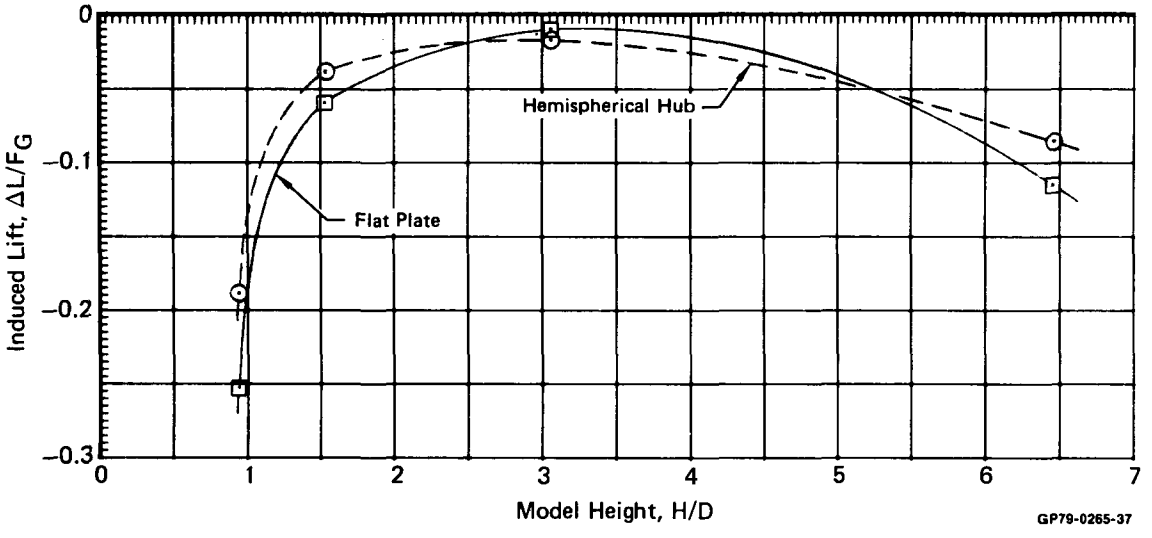

The 70% model nose fan induced lift characteristics are not typical, particularly the trend of increased lift loss from H/D = 3.06 to H/D = 6.45. Tests of various models with single nozzle operation indicate a monotonic decreasing induced lift with increasing altitude above the ground (Gentry and Margason, Reference 1). The large scale model follows this trend from H/D = 0.95 to 3.06. With single unit operation, only suckdown forces exist and there is no fountain upwash to influence the results. A lift loss of 12 percent at H/D of 6.45 was not expected. At this height, the model is essentially out of ground effect and suckdown is caused by moving air entrained by the nozzle exhaust. Other single unit operations at this height show less lift loss for both models. The small scale model shows 1-2 percent lift loss for both nose and lift/cruise single unit operation and the large scale model shows 6-11 percent lift loss for single lift/cruise unit operation. The nose unit would be expected to show less lift loss than a lift/cruise unit since less planform area is located near the nozzle on which negative pressure can act.

The induced pitching moment coefficient for nose unit only operation is presented in Figure 4-12. The small scale model indicates no significant induced pitching moment as a function of H/D. The large scale model indicates a negative or nose down pitching moment for all H/D values.

Two Unit Operation - The large scale model induced lift characteristics for two lift/cruise unit operation are presented in Figure 4-13. The induced lift generally decreases with increasing H/D. At the two lowest H/D's tested, the induced lift is less negative than the corresponding single lift/cruise unit operation.

The induced pitching moment as a function of H/D for two lift/cruise unit operations is presented in Figure 4-14. A positive induced moment is indicated for all H/D's tested. The positive pitching moment is probably due to the suckdown created around the lift/cruise nozzles aft of the center of gravity.

FIGURE 4-12
INDUCED PITCHING MOMENT COMPARISONS
Nose Unit - Single Unit Operation

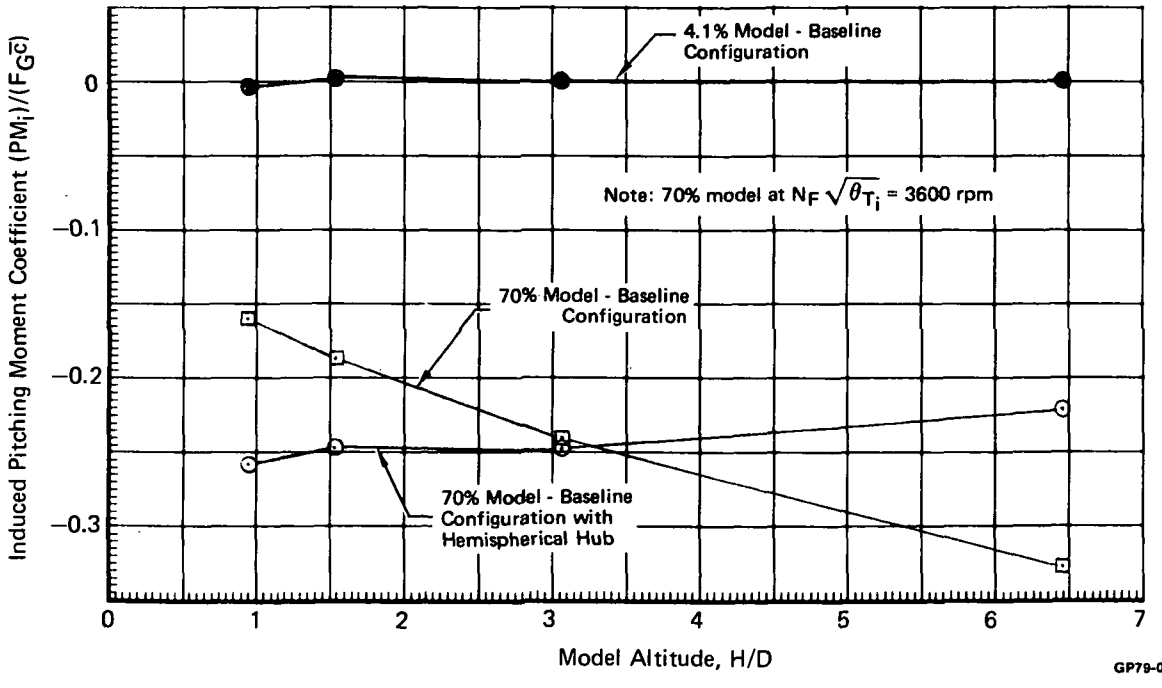

FIGURE 4-13
INDUCED LIFT CHARACTERISTICS
Baseline Configuration 2-Lift/Cruise Unit Operation

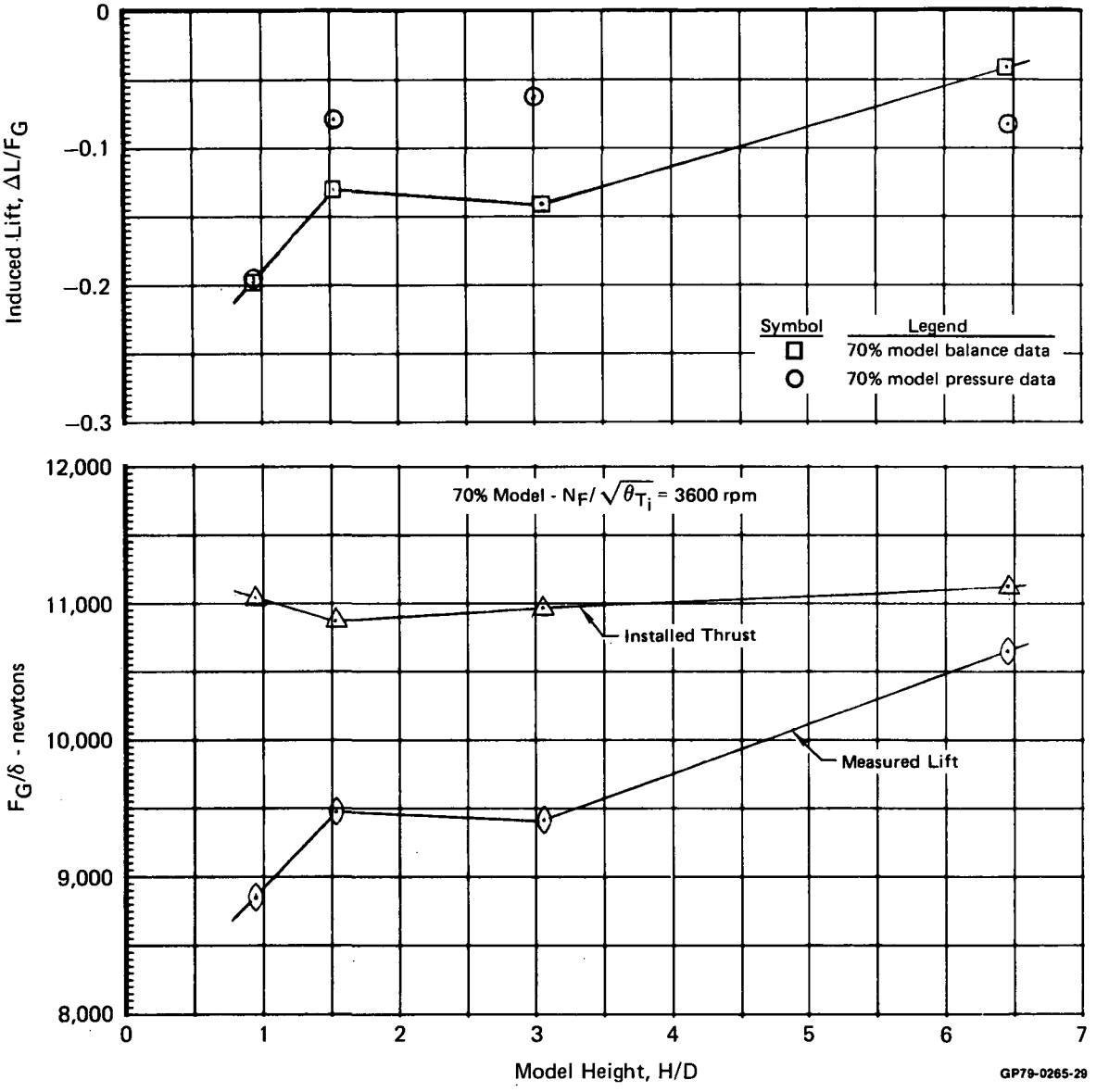

FIGURE 4-14
INDUCED PITCHING MOMENT
Baseline Configuration 2-Lift/Cruise Unit Operation

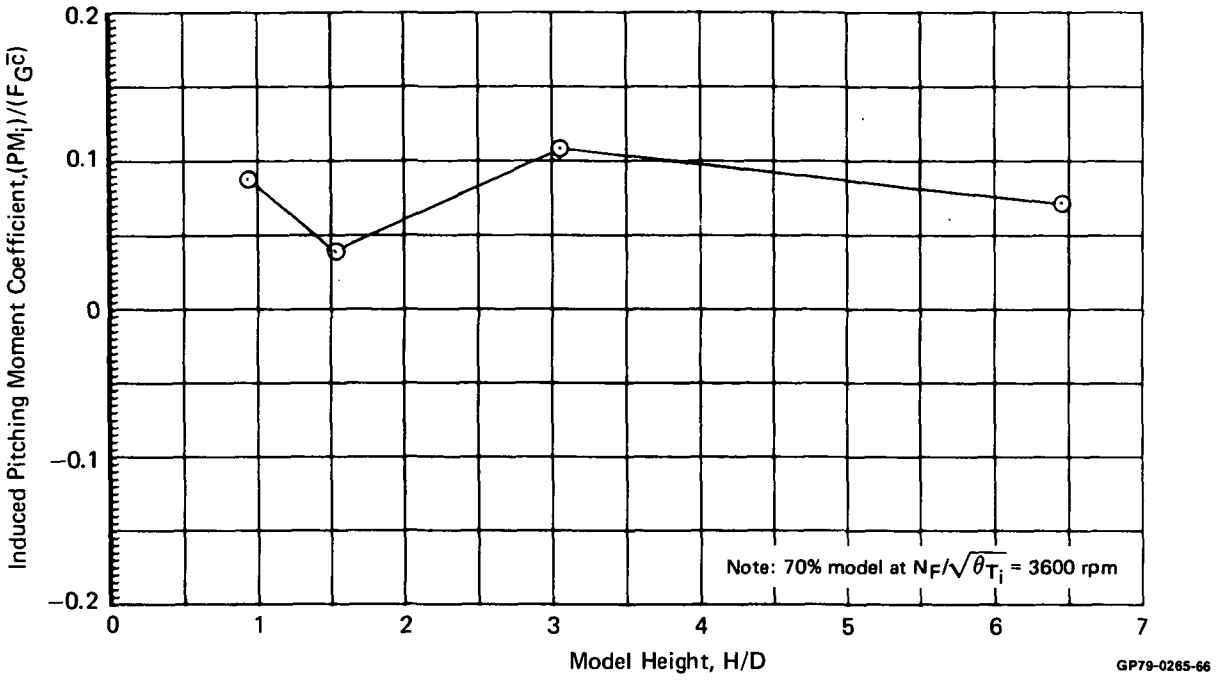

4.1.2 BASELINE CONFIGURATION - THREE UNIT OPERATION - Extensive ground effects testing of the baseline configuration was performed for three fan operation for both large and small scale models, particularly at H/D = 0.95.

The balance measured totallifts at the four model altitudes tested are presented in Figure 4-15 as a function of corrected fan speed. The balance measured lift increases with increasing height except for H/D = 6.45, where the measured lift is less than that measured for H/D of 3.06. The total fan installed thrust is essentially constant with model altitude except at H/D of 0.95. At this height, the increase in thrust is primarily due to the improvement in nose fan thrust coefficient.

The induced lift characteristics of the baseline configuration are presented in Figure 4-16. The induced lift decreases with increasing height up to H/D of 3.06. Approximately 9 percent lift loss is indicated at H/D = 6.45.

FIGURE 4-15
EFFECT OF MODEL ALTITUDE ON TOTAL MEASURED LIFT
3-Unit Operation Baseline Configuration

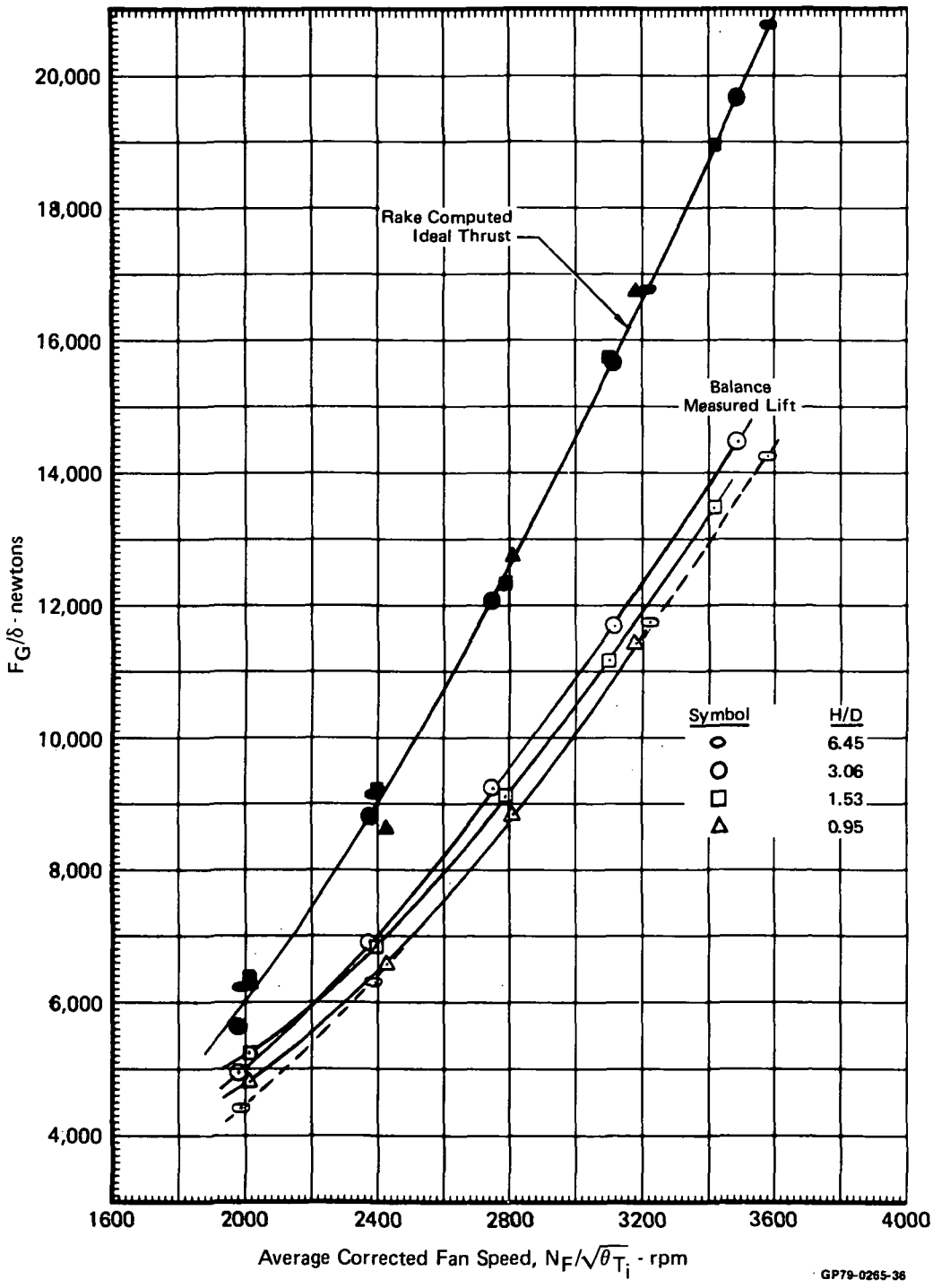

FIGURE 4-16
INDUCED LIFT EFFECT
Baseline Configuration 3-Unit Operation 70% Model
$N_F/\sqrt{\theta T_i}$ = 3200 RPM

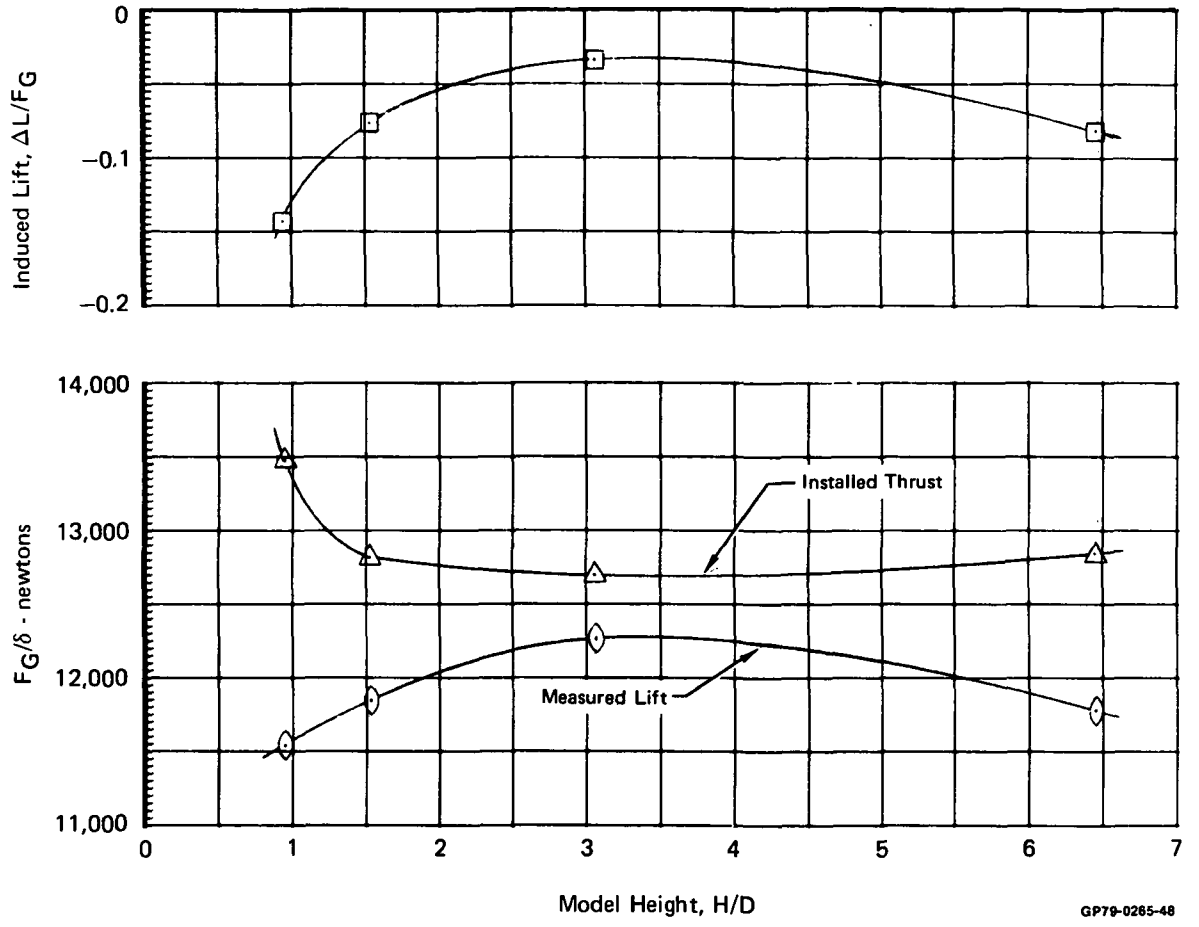

The small scale model duplicated the large scale model geometry, including model support struts. Since the small scale model is supported by its force balance, the simulated support struts can be removed to determine their effects on the induced lift measurements. Only small effects on the order of 1-2 percent are indicated at the intermediate values of H/D as shown in Figure 4-17. The small scale test results presented hereafter were obtained with support struts.

The small scale model induced lift was measured as a function of nozzle thrust for a constant H/D as shown in Figure 4-18. Nozzle thrust was changed by varying nozzle pressure ratio and maintaining equal thrust among all three nozzles. The induced lift was essentially independent of nozzle pressure ratio (nozzle thrust) for a fixed H/D.

FIGURE 4-17
EFFECT OF MODEL SUPPORT STRUTS
Baseline Configuration 3-Unit Operation 4.1% Model

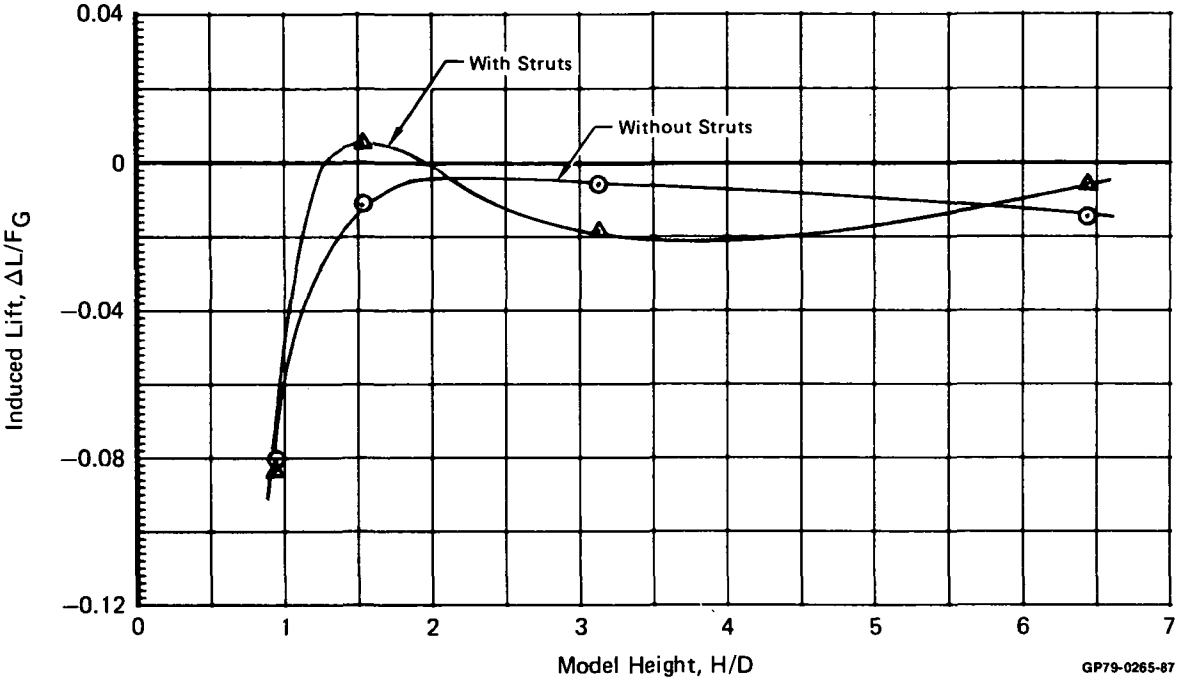

FIGURE 4-18
EFFECT OF NOZZLE PRESSURE RATIO
Baseline Configuration 3-Unit Operation 4.1% Model

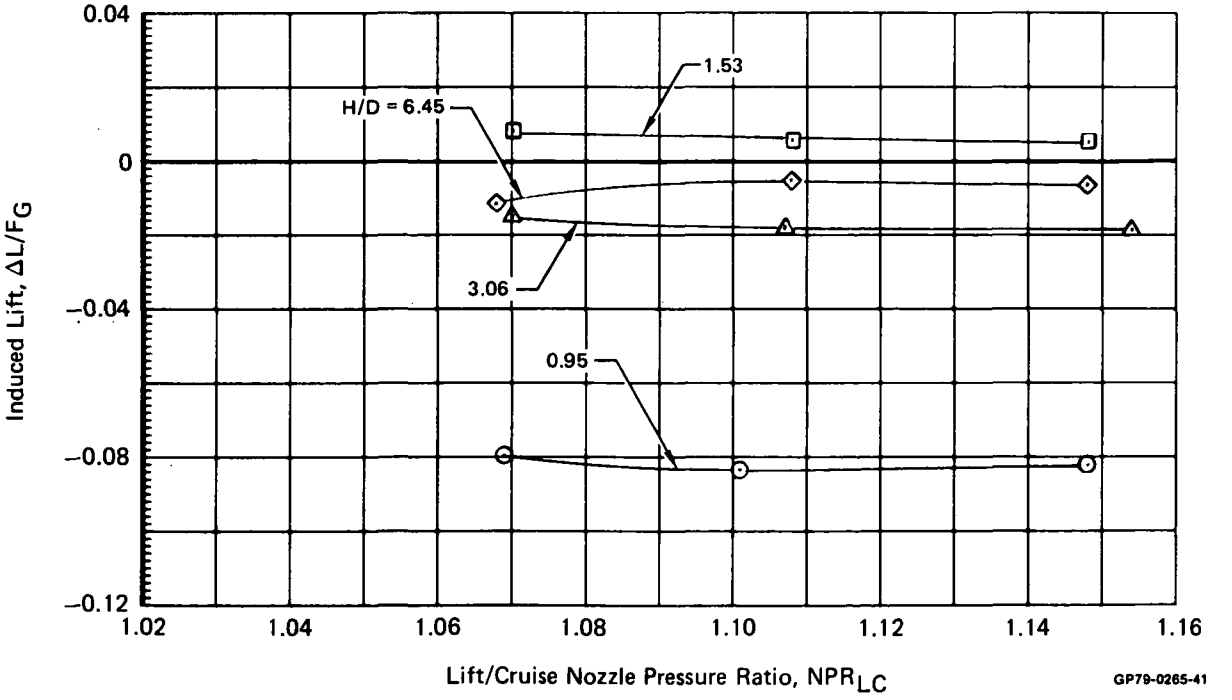

The large and small scale model induced lift characteristics are presented in Figure 4-19. The small scale model results indicated little overall induced lift above H/D of 1.5. A lift loss of 8 percent occurs at H/D = 0.95. The large scale model data indicates more lift loss than the small scale model, particularly at H/D of 6.45.

The small scale model pressure calculated induced lift agrees well with the corresponding balance measured induced lift. The large scale model pressure data is generally less negative than its corresponding balance measured data.

The baseline configuration was also tested with a hemispherical nose fan exit hub and the results are shown in Figure 4-20. The total installed thrust is essentially the same as for the flat plate nose fan exit hub. The induced lift characteristics for both cases are expected to be the same because the external model geometry is the same. The comparison of the two induced lift curves, shown in Figure 4-21 indicate very similar trends with H/D.

FIGURE 4-19
INDUCED LIFT COMPARISON
Baseline Configuration 3-Unit Operation
$N_F/\sqrt{\theta_{T_i}}$ = 3200 RPM

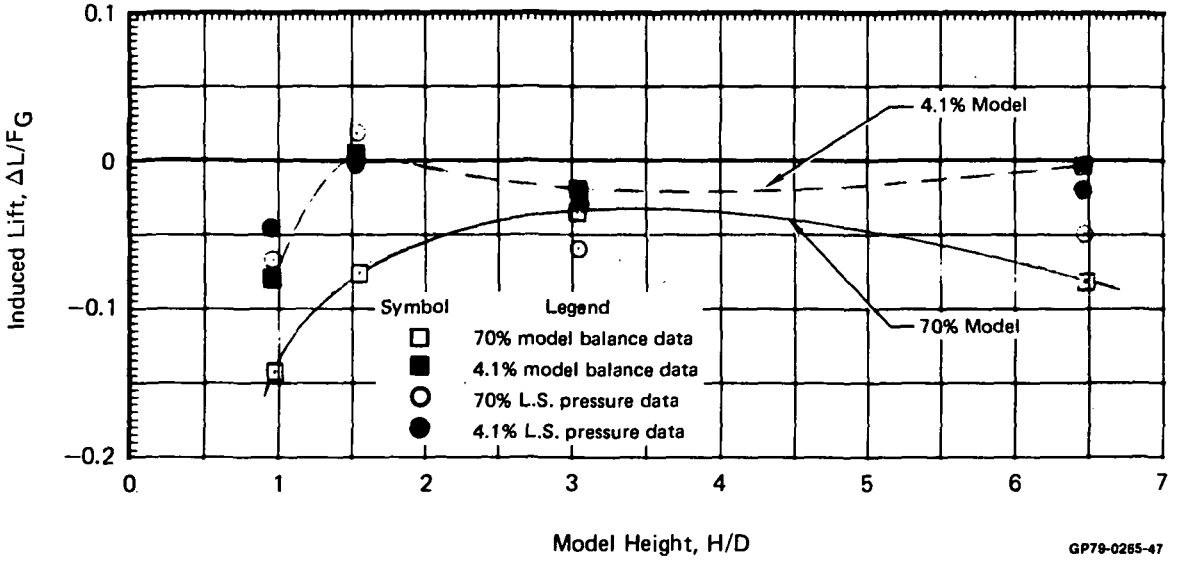

FIGURE 4-20
THREE UNIT OPERATION
Baseline Configuration Plus Hemispherical Nose Fan Hub

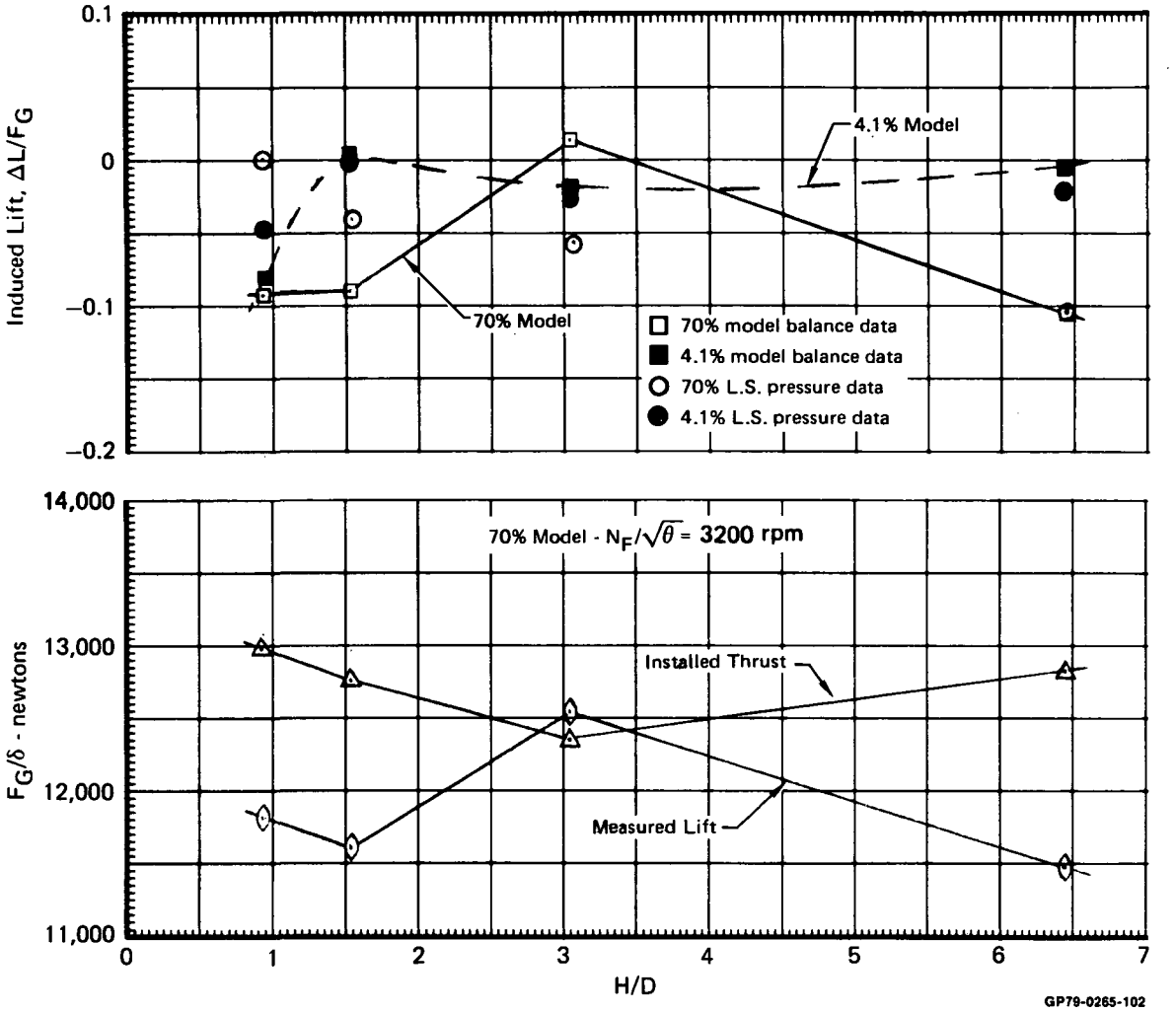

FIGURE 4-21
INDUCED LIFT COMPARISON
3-Unit Operation
$N_F/\sqrt{\theta_{Ti}}$ = 3200 RPM

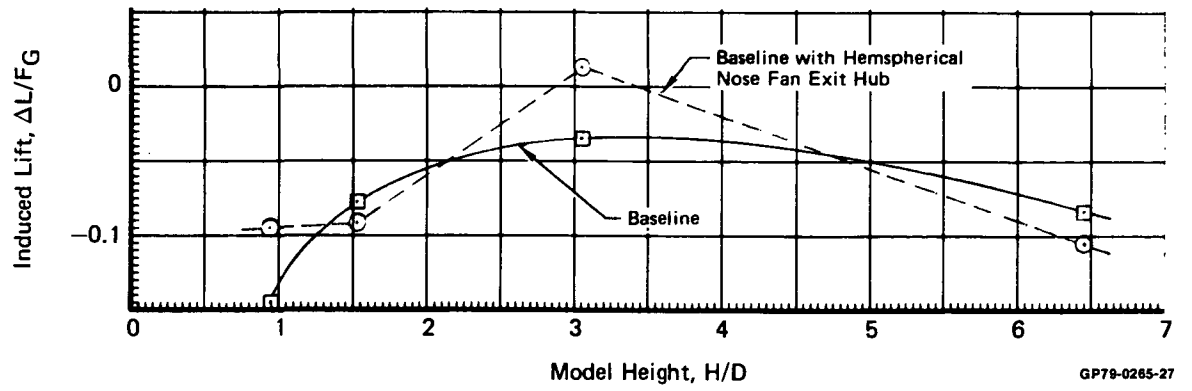

A large lift loss was indicated by the large scale model test data at H/D of 6.45. At this height the model is essentially out of ground effect and suckdown forces are due to the ambient air entrainment by the nozzle efflux. Previous 10% scale powered model tests of similar three fan configurations indicate an out of ground effect lift loss significantly less than the 9 percent lift loss exhibited by the large scale model (Reference 3).

The induced pitching moment coefficients for three unit operation are presented in Figure 4-22. The small scale model indicates no significant induced moments except for a slight nose up moment at H/D of 1.53. The large scale model baseline data is similar, while the baseline with hemispherical hub shows some data scatter.

The lower surface pressure contour plots outlining the positive and negative pressure areas for both models are shown in Figure 4-23. Positive pressure areas exist above the stagnation lines where the upwash impinges on the airframe. The peak positive pressure occurs on the fuselage between the lift/cruise nozzles. Negative pressure areas are located around the nozzles and underneath the wing where air is flowing along the lower surface. The small scale model pressure contour plot shows the same general locations of positive areas as on the large scale model at H/D of 0.95.

FIGURE 4-22
INDUCED PITCHING MOMENT COMPARISON
3-Unit Operation

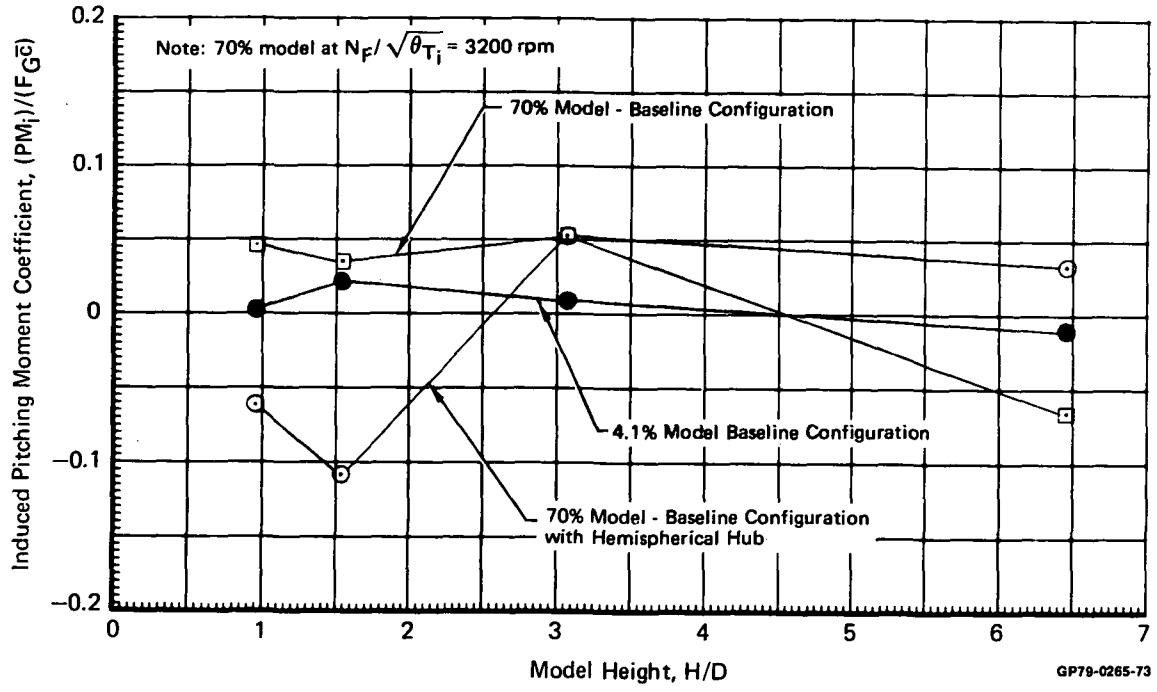

FIGURE 4-23
LOWER SURFACE PRESSURE DISTRIBUTION
Baseline Configuration H/D = 0.95

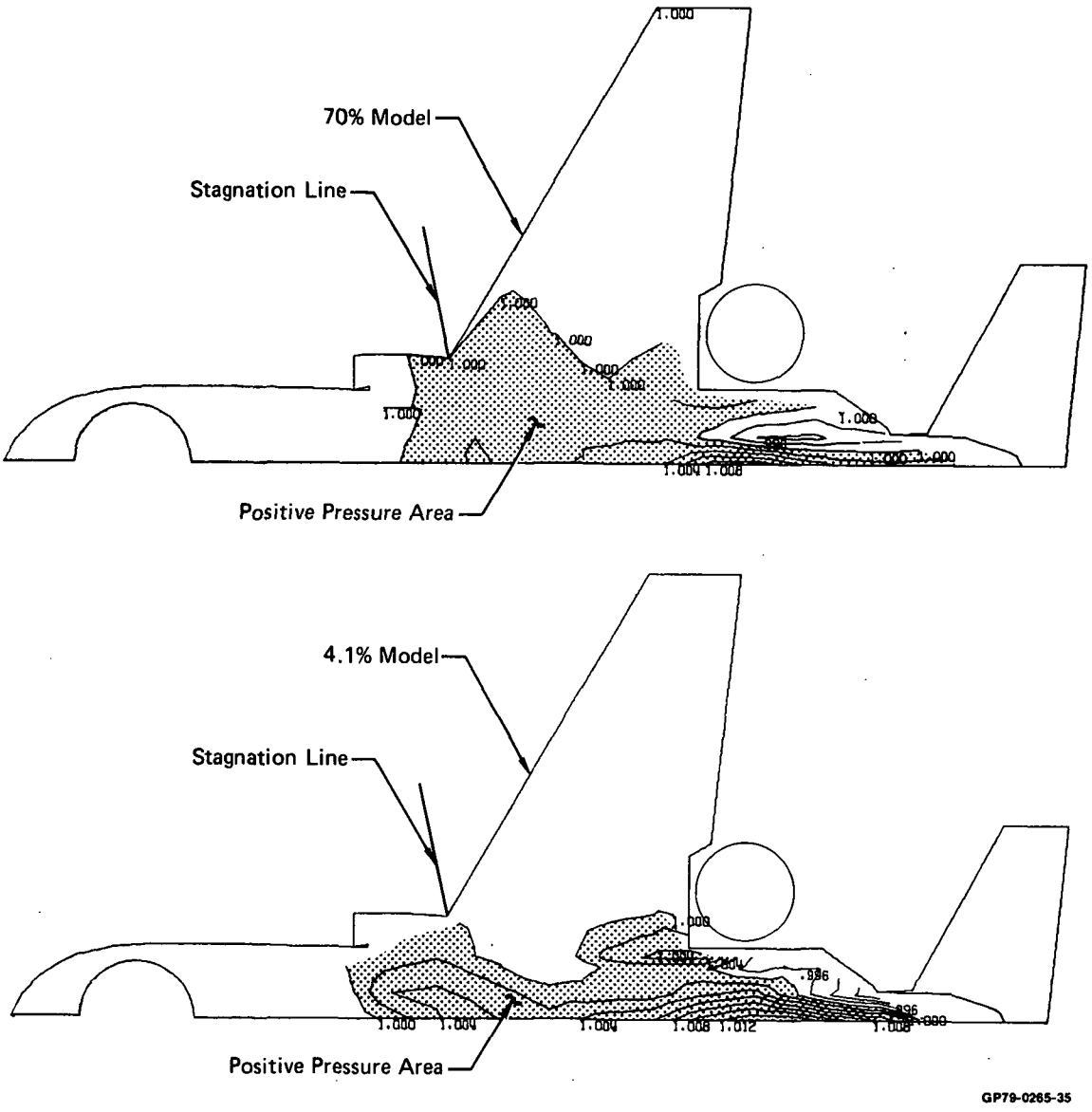

The large scale model integrated pressure force for 3 fan operation is presented in Figure 4-24 as a function of fan speed. Generally the calculated pressure force indicates increasing suckdown with increasing fan speed, however, the data are not sufficiently accurate to substantiate the balanced determined induced lift. This is a consequence of the extremely low model surface pressures created by the low pressure ratio fans.

FIGURE 4-24
LARGE SCALE MODEL INDUCED PRESSURE FORCE
3-Unit Operation Baseline Configuration

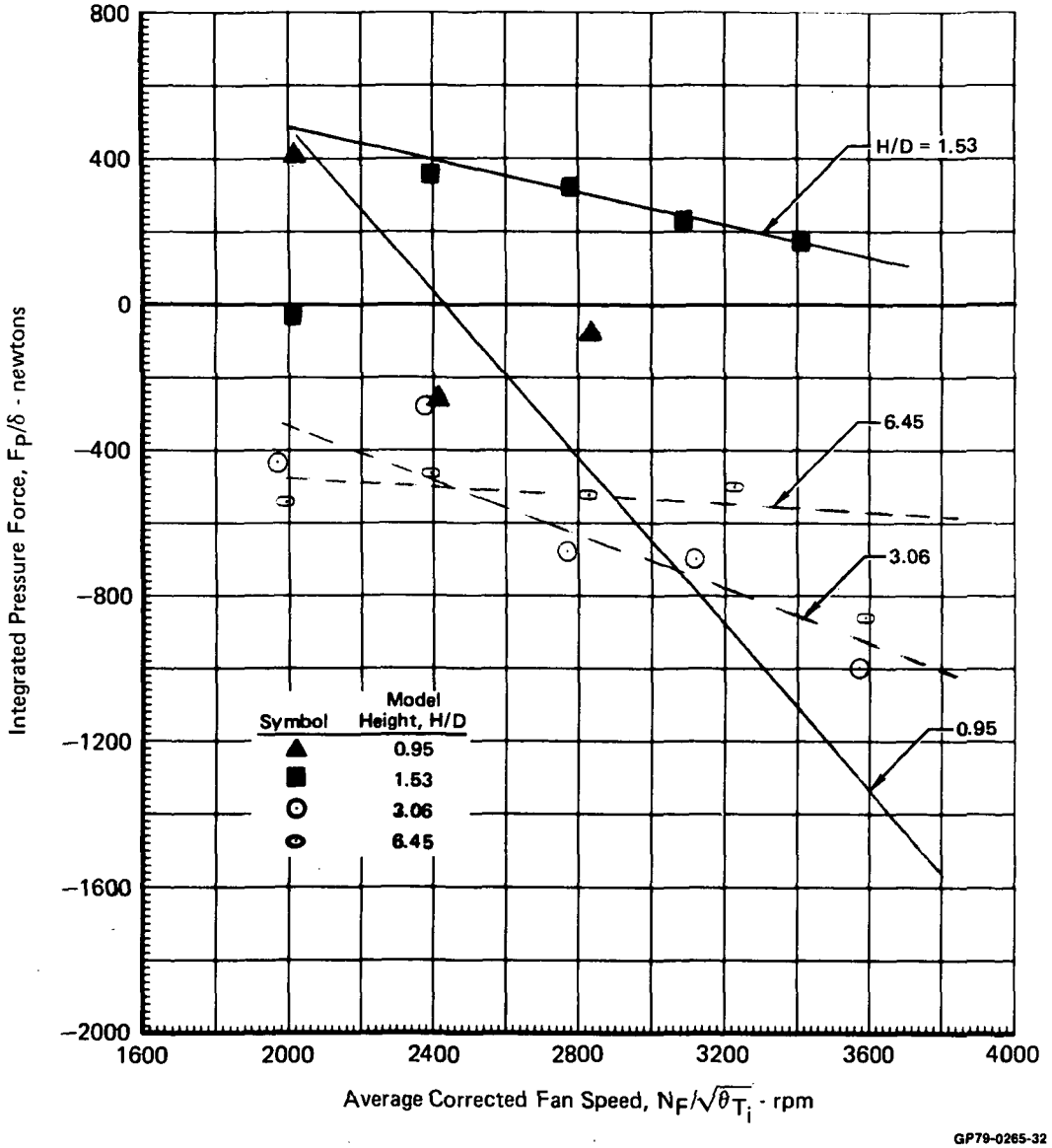

4.1.3 ALTERNATE CONFIGURATIONS - TWO AND THREE UNIT OPERATION

LIDs - Both large and small scale models were tested with identical lift improvement devices. The effect of a four-sided LID is presented in Figure 4-25 for three unit operations. Both models indicate a 12-14 percent improvement in induced lift at H/D of 0.95. The models show the same trend of induced lift vs H/D, however, the large scale model indicates greater lift loss than the small scale model.

FIGURE 4-25
INDUCED LIFT COMPARISONS
4-Sided LID Configuration 3-Unit Operation

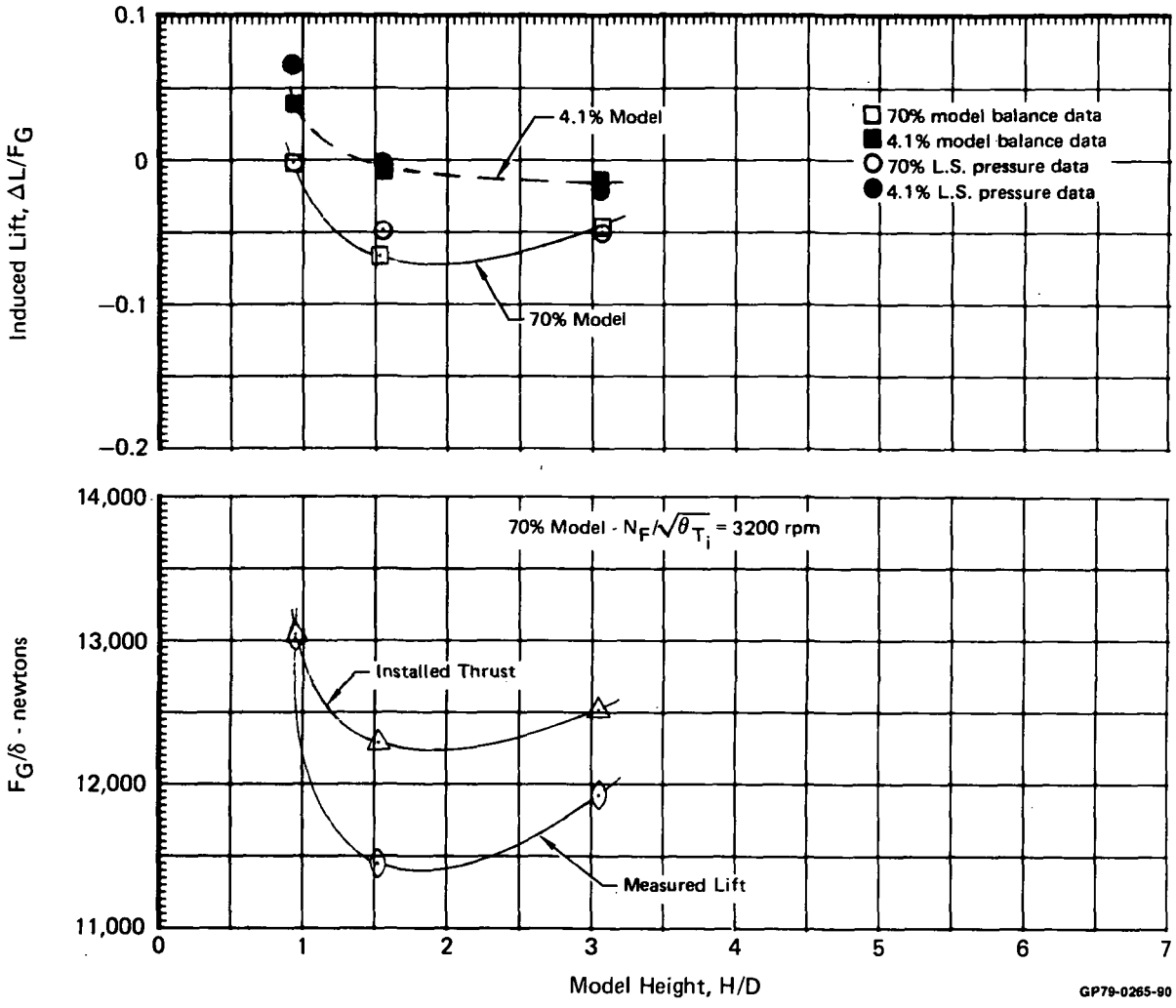

The lower surface pressure contours for the two models with the four-sided LID are presented in Figure 4-26. In both cases, the area enclosed by the LID has been pressurized by the fountain upwash creating a positive pressure area. Simultaneously, the magnitude of the negative pressure areas around the lift/cruise nozzles and underneath the wing has been reduced. This is probably due to the reduction of airflow along the model lower surface since the fountain upwash is unable to turn and flow underneath the model because of the LID walls. The overall effect is an increase in induced lift.

FIGURE 4-26
LOWER SURFACE PRESSURE DISTRIBUTION
Baseline + 4-Sided LID H/D = 0.95

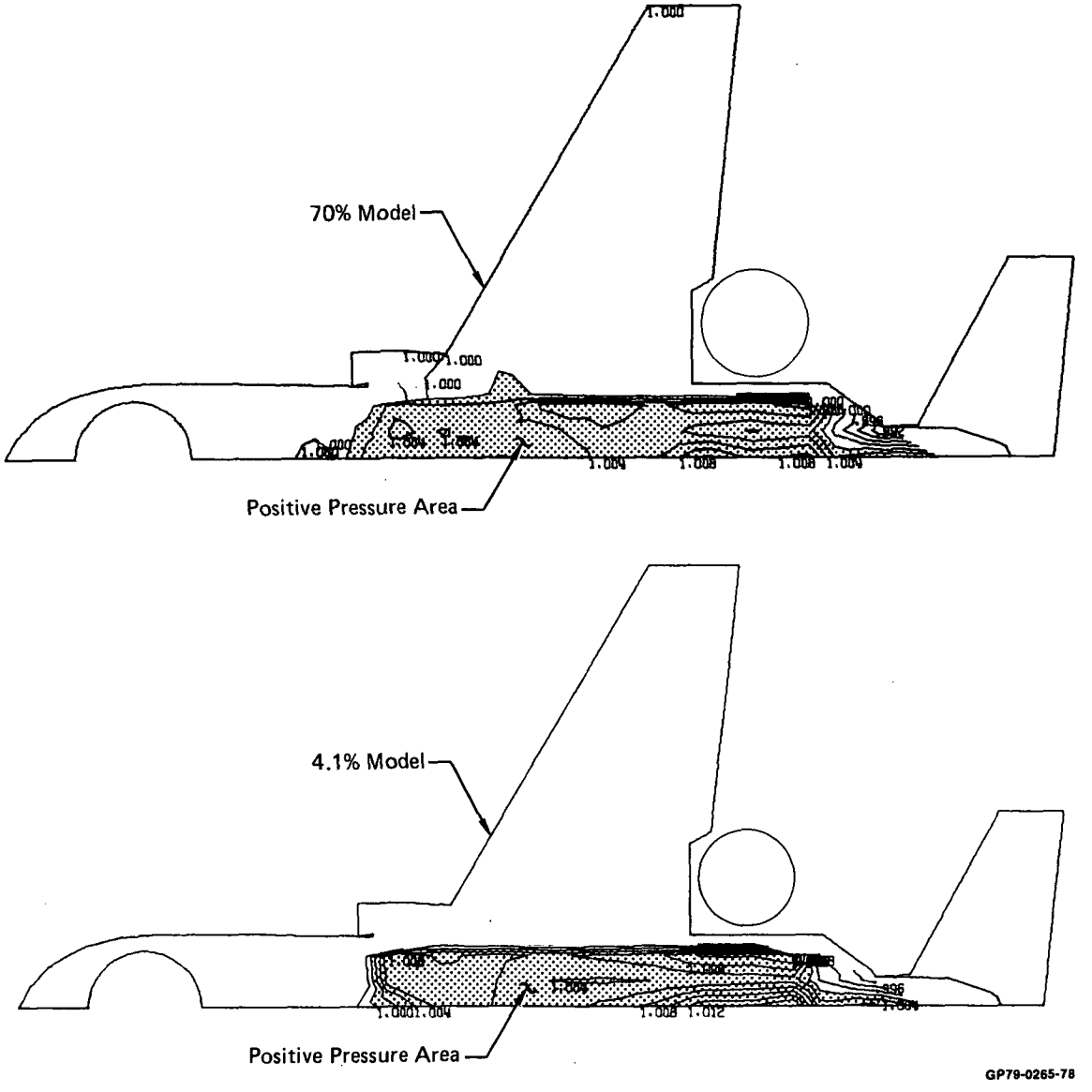

The induced lift for a three-sided LID is presented in Figure 4-27. The small scale model indicates a larger improvement in induced lift at H/D of 0.95 than the large scale model. Also, the large scale model indicates consistently larger induced lift loss than the small scale model.

FIGURE 4-27
INDUCED LIFT COMPARISONS
3-Sided LID Configuration 3-Unit Operation

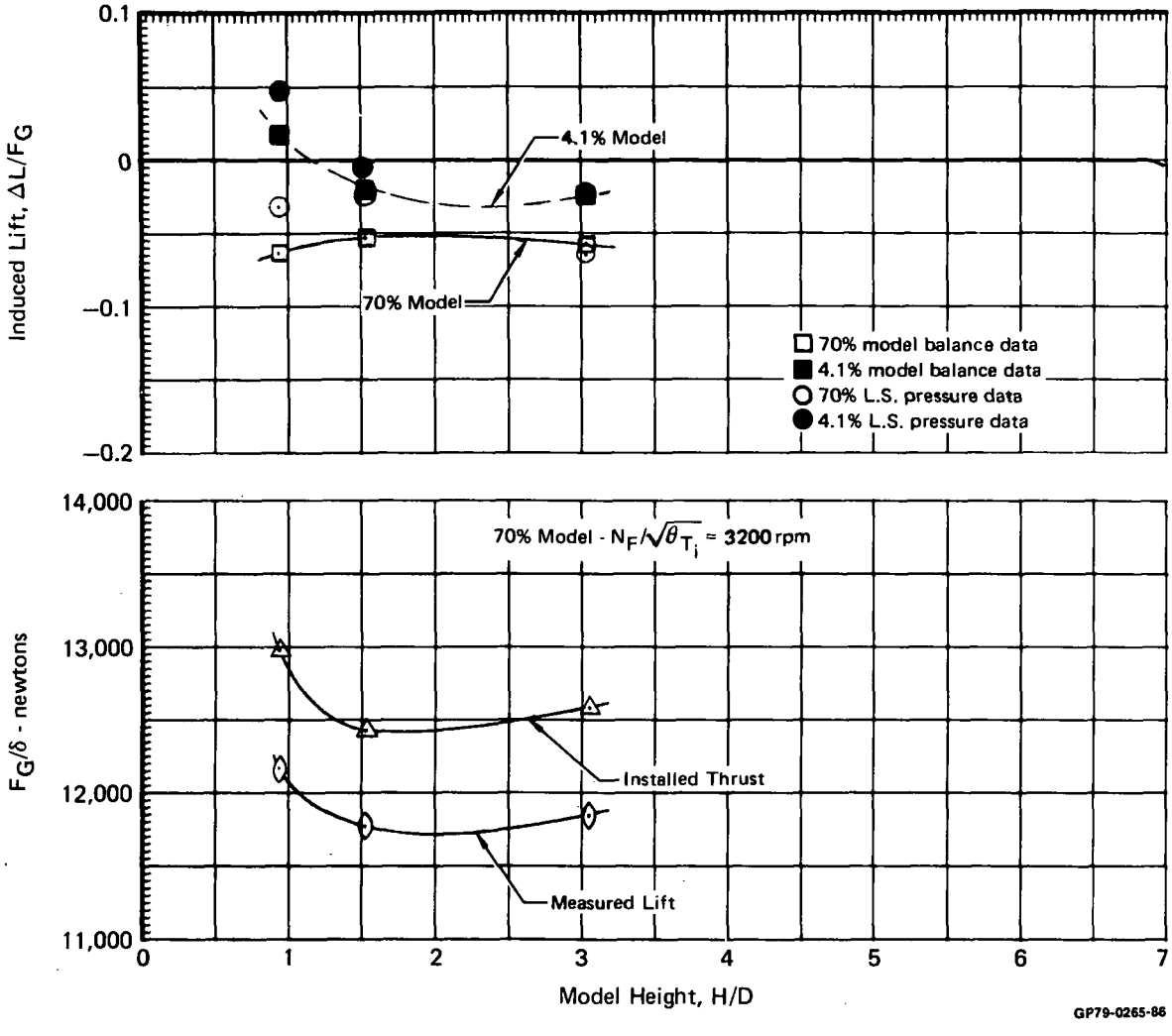

The two-sided LID configuration was investigated at H/D of 0.95. A comparison of two, three and four-sided LID performance is presented in Figure 4-28. All three LID's provide various amounts of lift increase at H/D of 0.95 for both models. Above an H/D of 1.5, the LID's have essentially no effect on the baseline induced lift characteristics.

The two fan induced lift characteristics with a four-sided LID are shown in Figure 4-29. The LID provides a large positive change in the induced lift at H/D's of 0.95 and 1.53 compared to the baseline configuration. The LID is ineffective at an H/D of 3.06.

FIGURE 4-28
SUMMARY OF LID PERFORMANCE
3-Unit Operation 2 , 3 , and 4-Sided LID

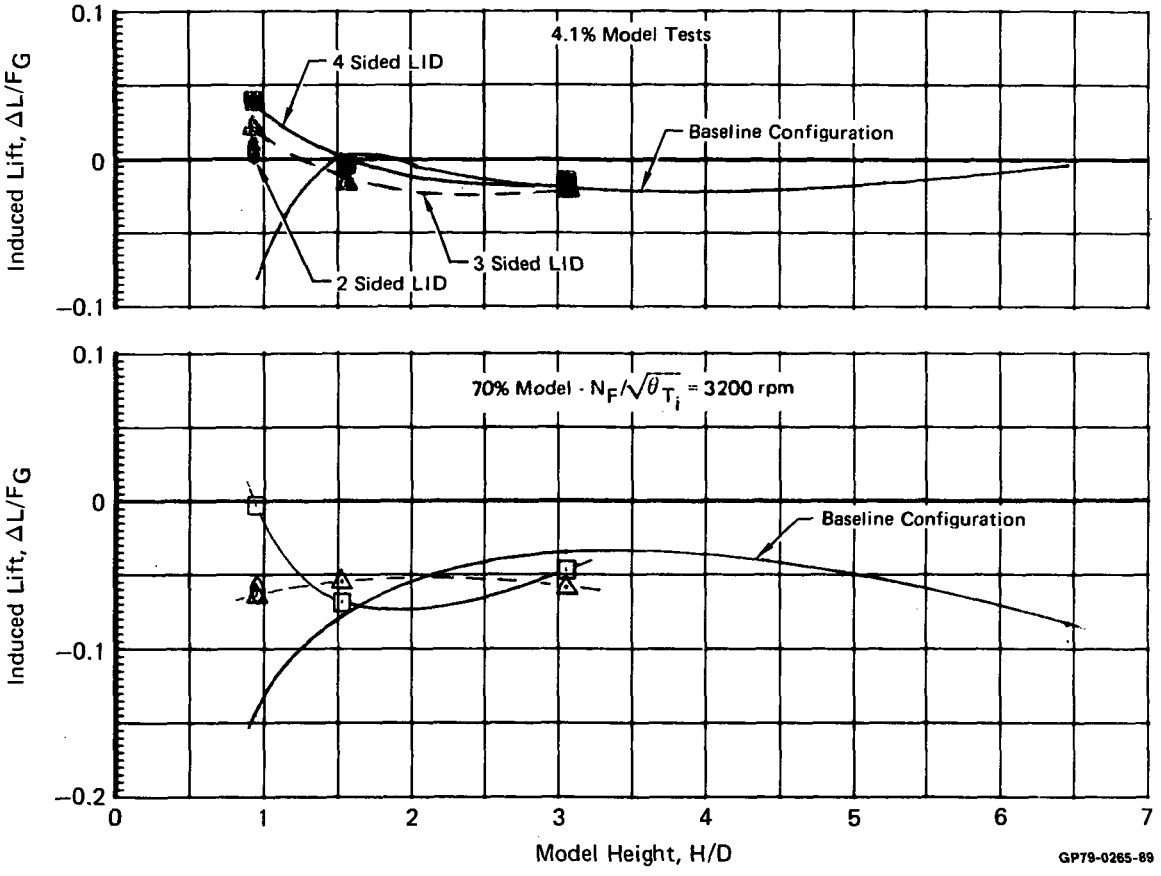

FIGURE 4-29
INDUCED LIFT COMPARISONS
4-Sided LID Configuration 2-Lift/Cruise Unit Operation

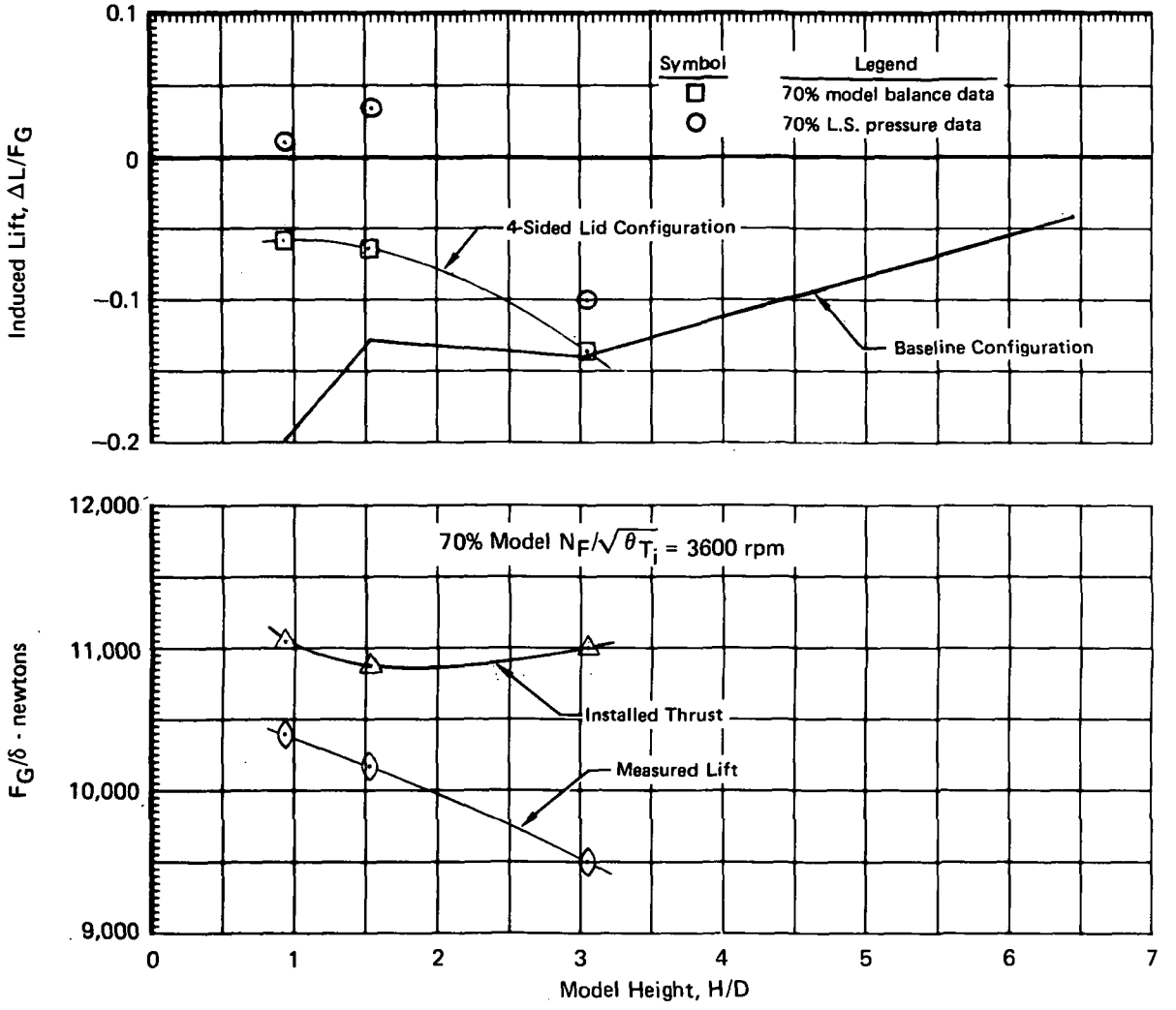

Lift/Cruise Nozzle Rails - The test data obtained on the baseline configuration with and without the lift/cruise nozzle rails are presented in Figure 4-30. Both models indicate an improvement in lift with the rails, with the large scale model showing the largest induced lift change.

Perimeter Plates - Perimeter plates were installed around the lift/cruise nozzles to determine if gaps around the nozzle provided a significant venting area for air to be entrained by the nozzle exhaust. A small to negligible increase in lift loss was measured for both models as shown in Figure 4-31. It is surmised that with the installation of the perimeter plates, a larger fraction of the air entrained by the nozzle exhaust is induced to flow underneath the model, creating a higher lift loss.

FIGURE 4-30
EFFECTS OF LIFT/CRUISE NOZZLE RAILS
3-Unit Operation

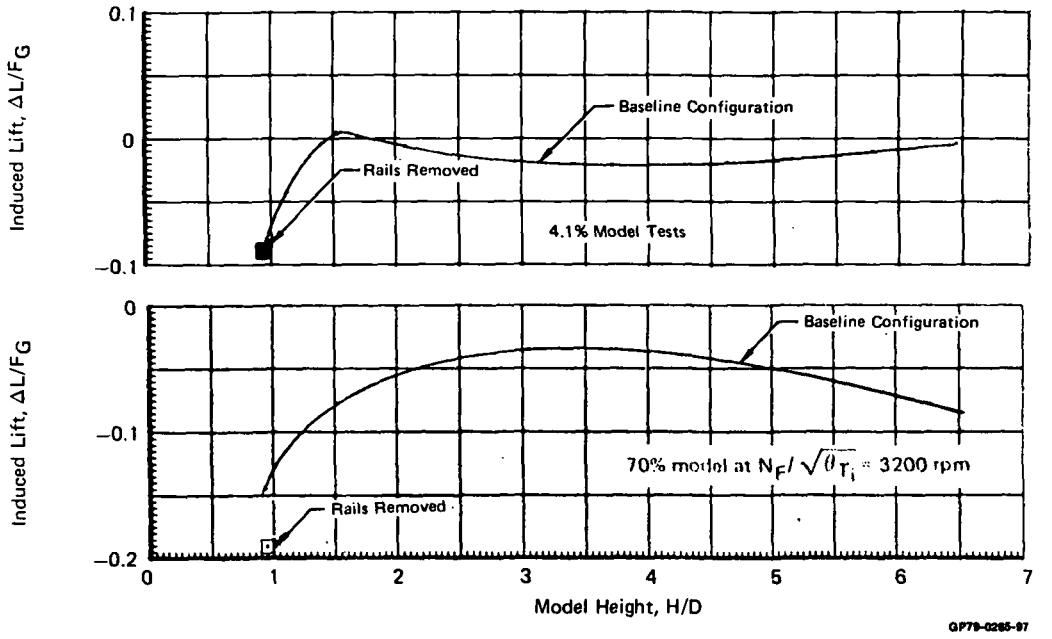

FIGURE 4-31
EFFECT OF LIFT/CRUISE NOZZLE PERIMETER PLATES
3-Unit Operation

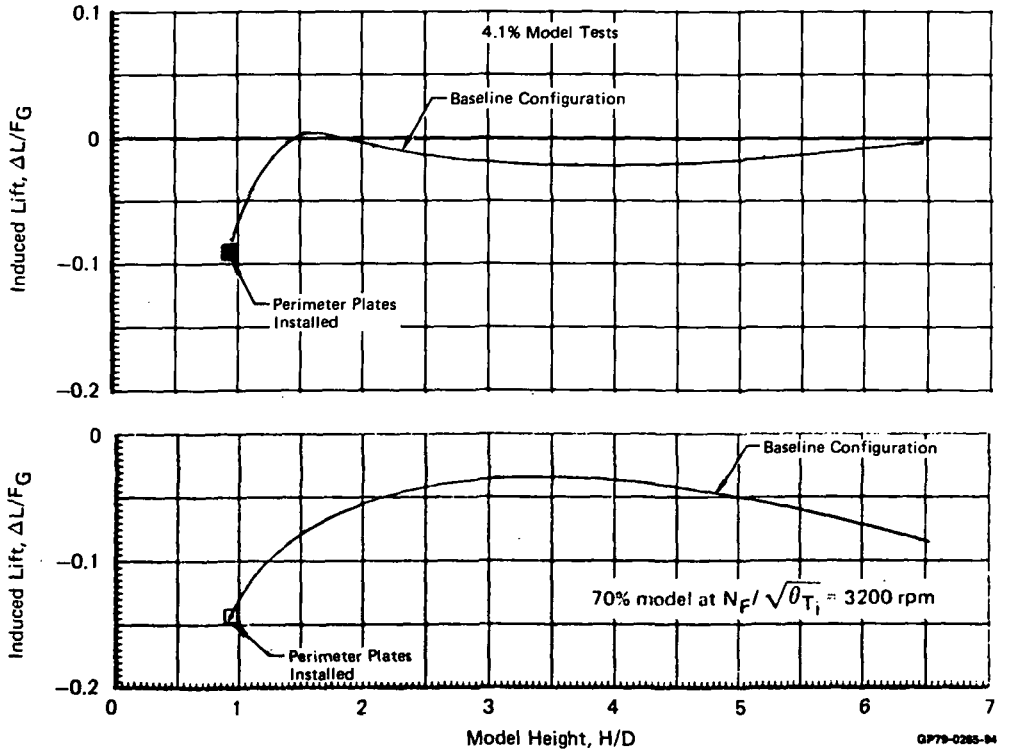

Model Pitch and Roll Attitude - The baseline configuration was investigated for several model pitch angles at an H/D of 0.95. The induced lift effects for pitch angles of -5, +5 and +7.5 degrees are presented in Figure 4-32. The small scale test showed a 4 percent increase in lift at the -5 degree pitch angle while the large scale test exhibited a 9 percent increase. Note that in both tests induced lift improvement decreases as the model nose is raised.

The baseline configuration with four-sided LID was also investigated at + and -5° pitch angle at H/D = 0.95. The results are shown in Figure 4-33. The large scale model shows a larger sensitivity to pitch angle changes than the small scale model.

FIGURE 4-32
PITCH ANGLE EFFECTS
Baseline Configuration 3-Unit Operation

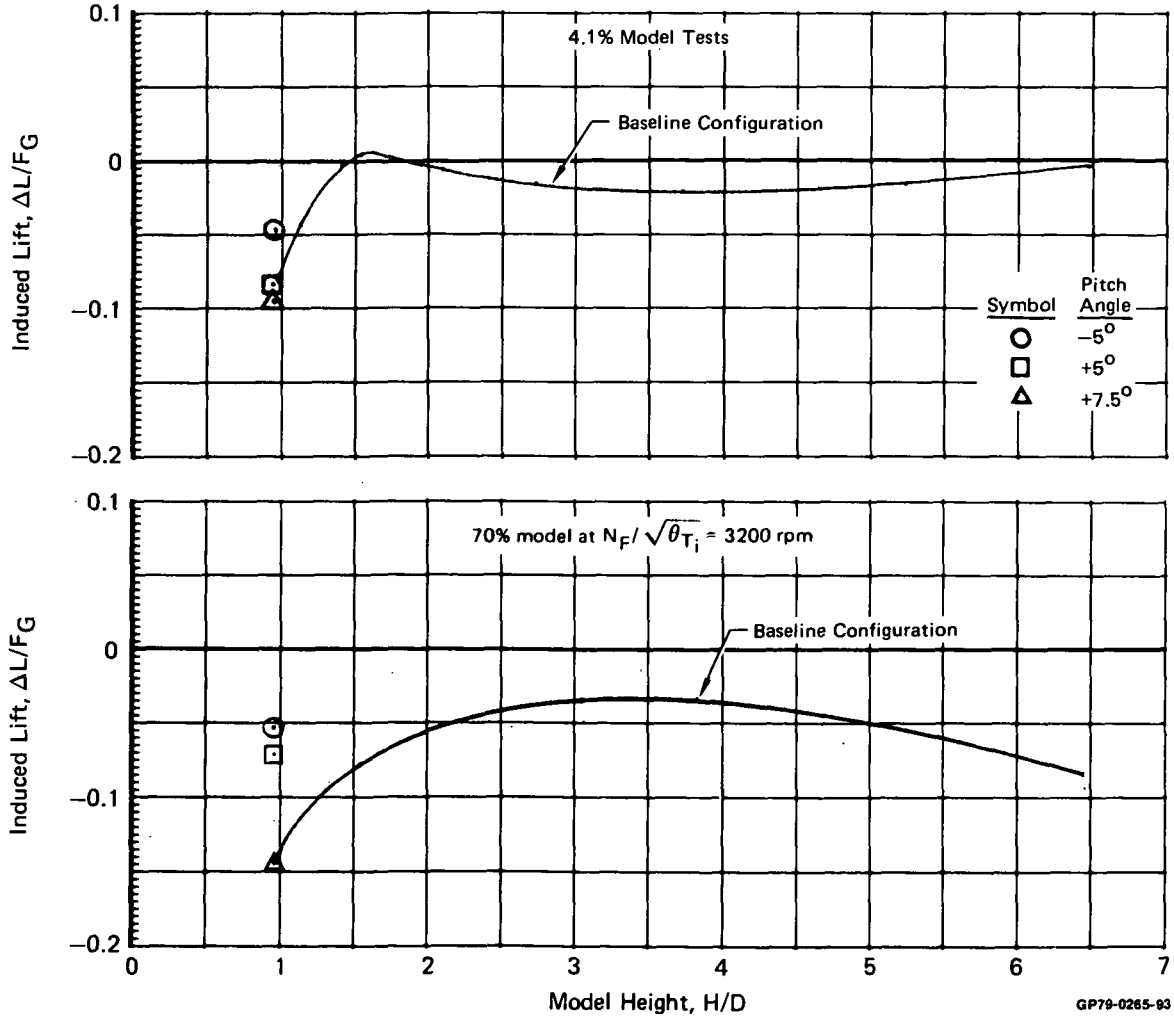

FIGURE 4-33
4-SIDED LID CONFIGURATION
3-Unit Operation

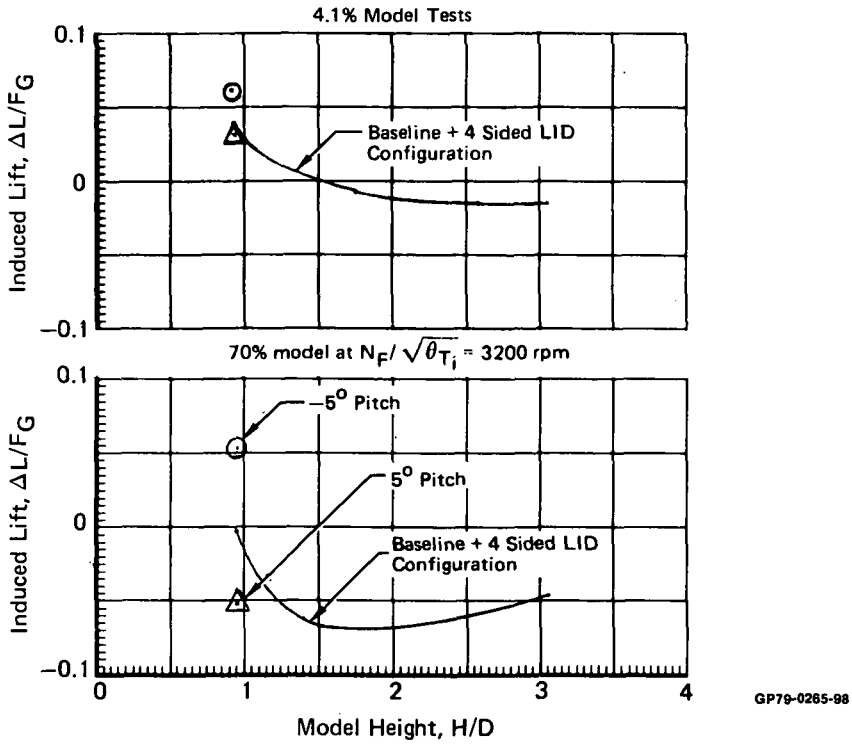

The effect of model bank angle on induced lift was investigated at an H/D of 1.25. A 10 degree bank angle reduced the lift by 7 to 9 percent for both models in the baseline configuration as shown in Figure 4-34.

A similar decrease in lift was measured for both models with the four-sided LID as shown in Figure 4-35.

The effect of a 10 degree bank attitude on the large scale baseline and four-sided LID configuration is shown in Figure 4-36 at H/D of 0.95 for two unit operation. Both configurations indicate a significant lift loss at the 10 degree banked attitude.

4.1.4 NOSE FAN EXIT HUB PRESSURIZATION EFFECTS - The initial LSPM ground tests, Reference 5, indicated an increase in thrust of the horizontally mounted nose fan in ground effect which was attributed to pressurization of the fan exit hub. In this program, both flat plate and hemispherical exit hubs were instrumented with static pressure taps to evaluate the hub force as a function of fan speed and H/D.

The integrated pressure-area force as a function of fan speed for the flat plate and hemispherical exit hubs is presented in Figures 4-37 and 4-38 respectively.

FIGURE 4-34
EFFECT OF MODEL BANK ATTITUDE
Baseline Configuration 3-Unit Operation

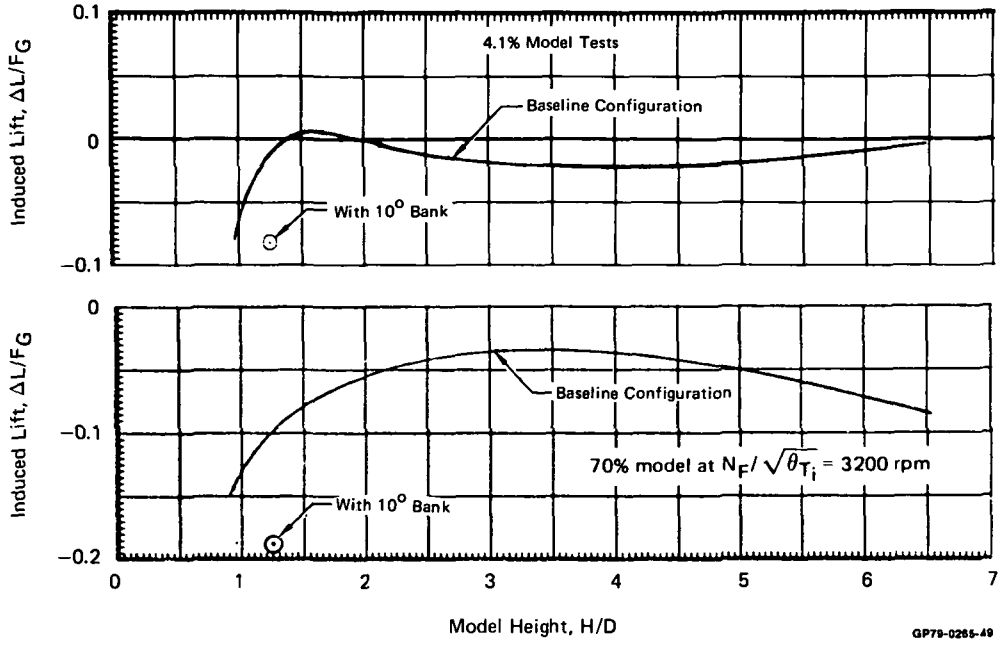

FIGURE 4-35
EFFECT OF MODEL BANK ATTITUDE
4-Sided LID Configuration 3-Unit Operation

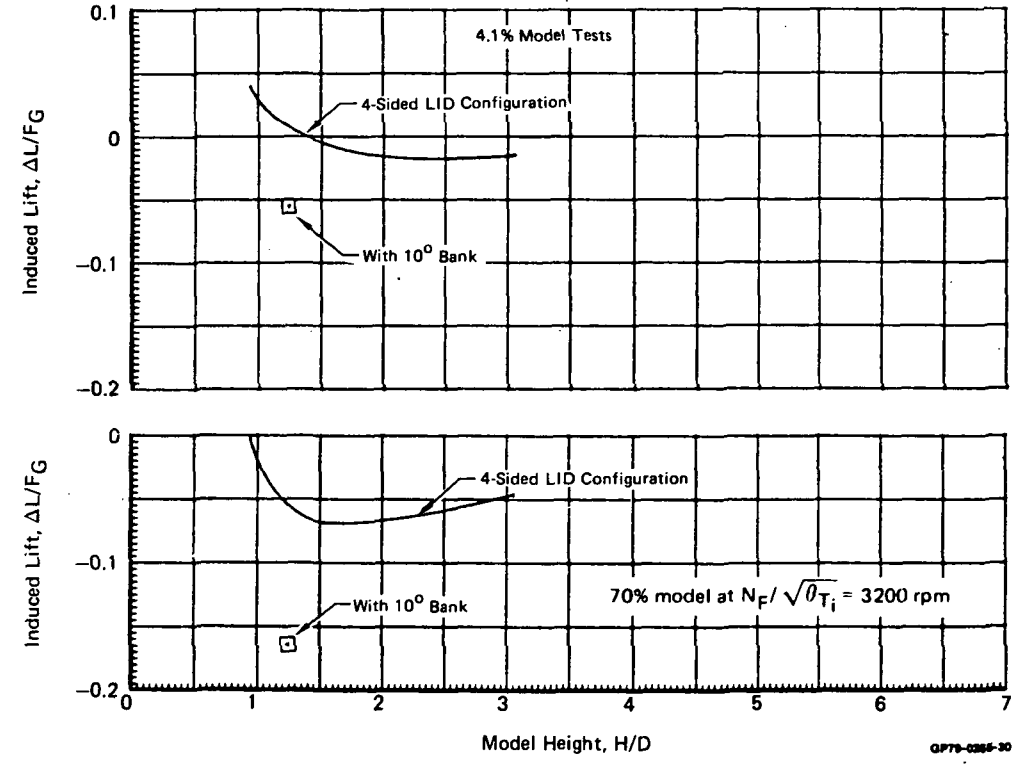

FIGURE 4-36
EFFECT OF MODEL BANK ATTITUDE
Baseline Configuration 2-Lift/Cruise Unit Operation
70% Model $N_F/\sqrt{\theta_{T_i}}$ = 3600 RPM

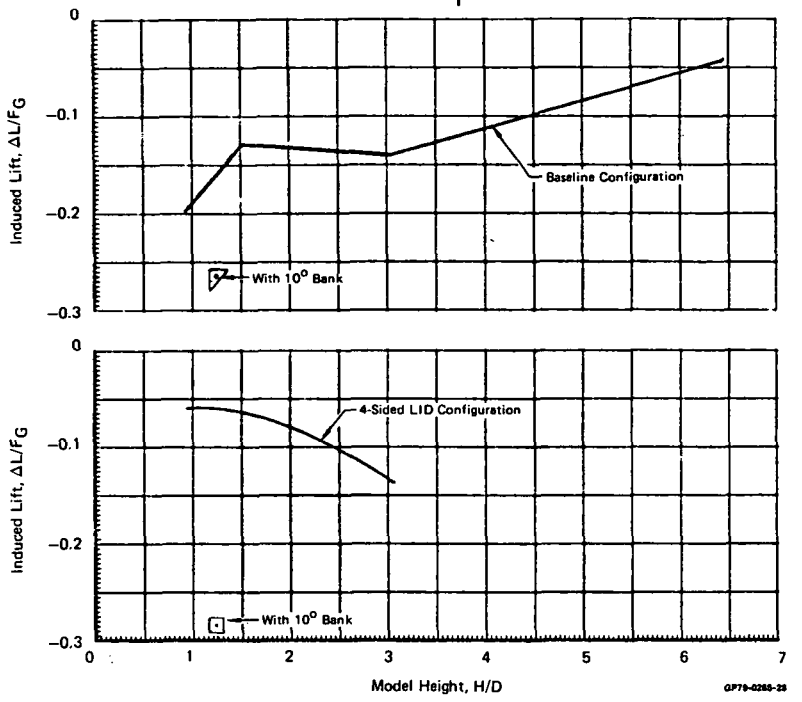

FIGURE 4-37
NOSE UNIT EXIT HUB FORCE
Single Unit Operation Flat Plate Hub

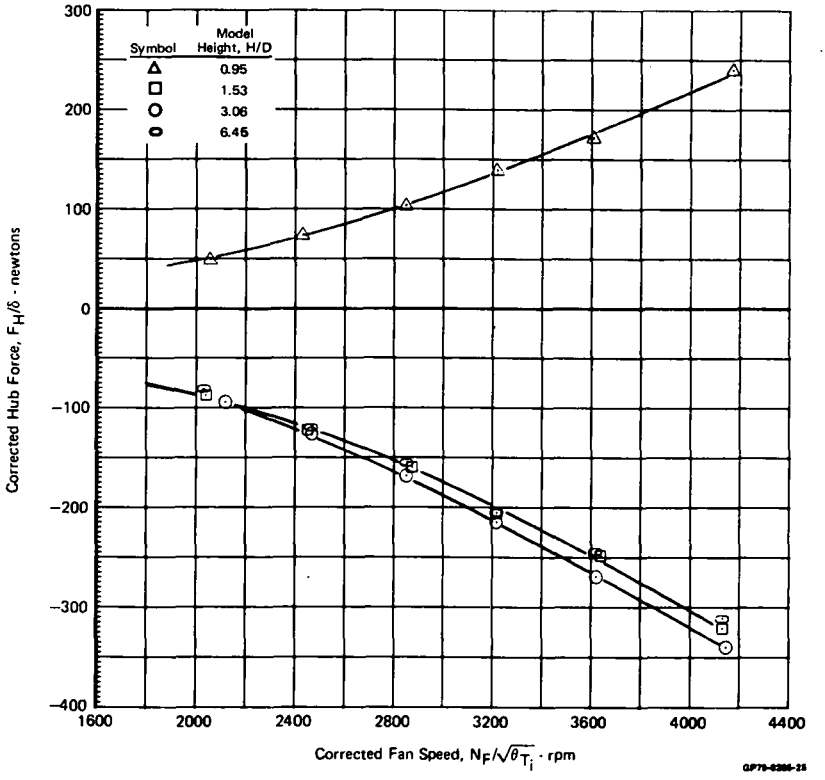

FIGURE 4-38
NOSE UNIT EXIT HUB FORCE
Single Unit Operation Hemispherical Hub

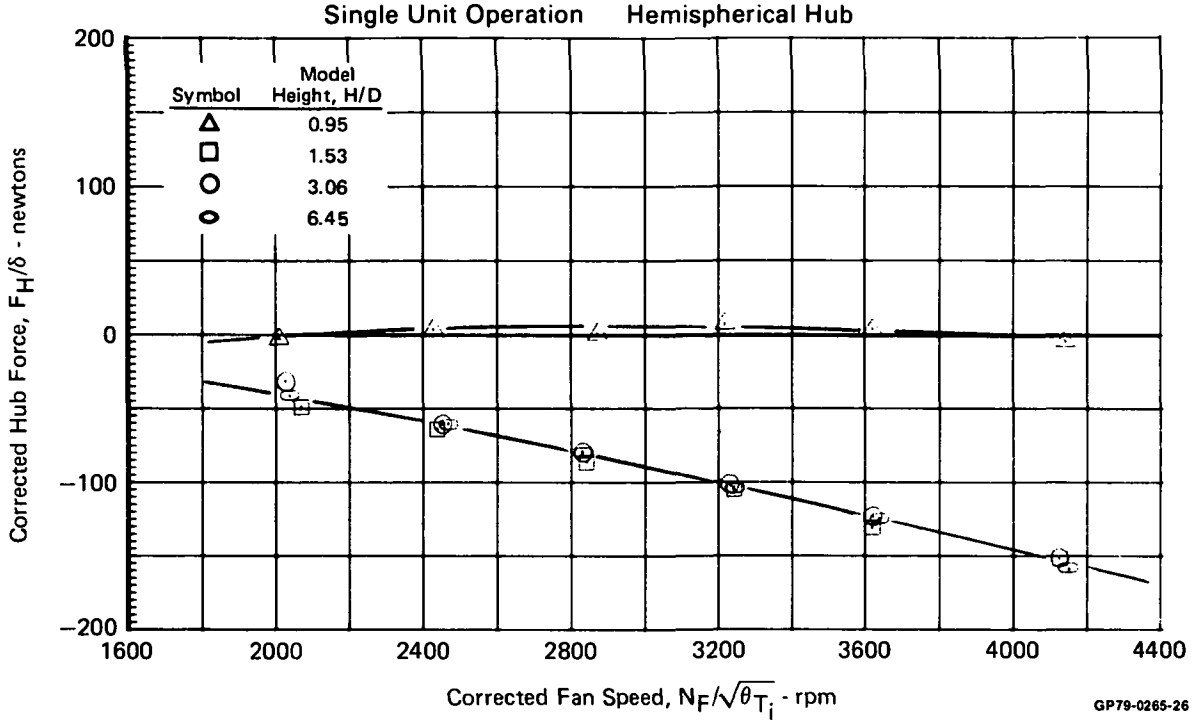

For both hubs, the force becomes more negative with increasing fan speed for heights above H/D = 0.95. At H/D = 0.95, the flat plate hub experiences a continual increase in force with fan speed whereas the hemispherical hub force is essentially zero for all fan speeds.

In both cases, an abrupt increase in force at the lowest H/D tested was recorded as shown in Figure 4-39. The hemispherical hub exhibited a lower incremental force than the flat plate hub in ground effect but it also shows a more positive force out of ground effect.

The static pressure profiles for the two types of exit hub are presented in Figures 4-40 and 4-41. The hemispherical hub exhibits larger negative pressures at the periphery than the center of the hub. In ground effect, the negative pressures are reduced and some positive pressure exists in the middle of the hub. The flat plate hub exhibits negative pressures across the hub out of ground effect and essentially uniform positive pressures in ground effect.

4.2 DISCUSSION OF LARGE SCALE MODEL DATA UNCERTAINTY

The induced lift data obtained during the large scale model test program and presented in Section 4.1 show unexpected results for both single and multiple unit operation. The results are atypical because of the magnitudes of the induced lift loss recorded at a model nondimensional height of 6.45. At this height, single unit operation of the lift/cruise fans yielded lift loss values of 6 and 11 percent

FIGURE 4-39
EFFECT OF GROUND HEIGHT ON NOSE UNIT EXIT HUB FORCE
Single Unit Operation $N_F/\sqrt{\theta_{T_i}}$ = 3600 RPM

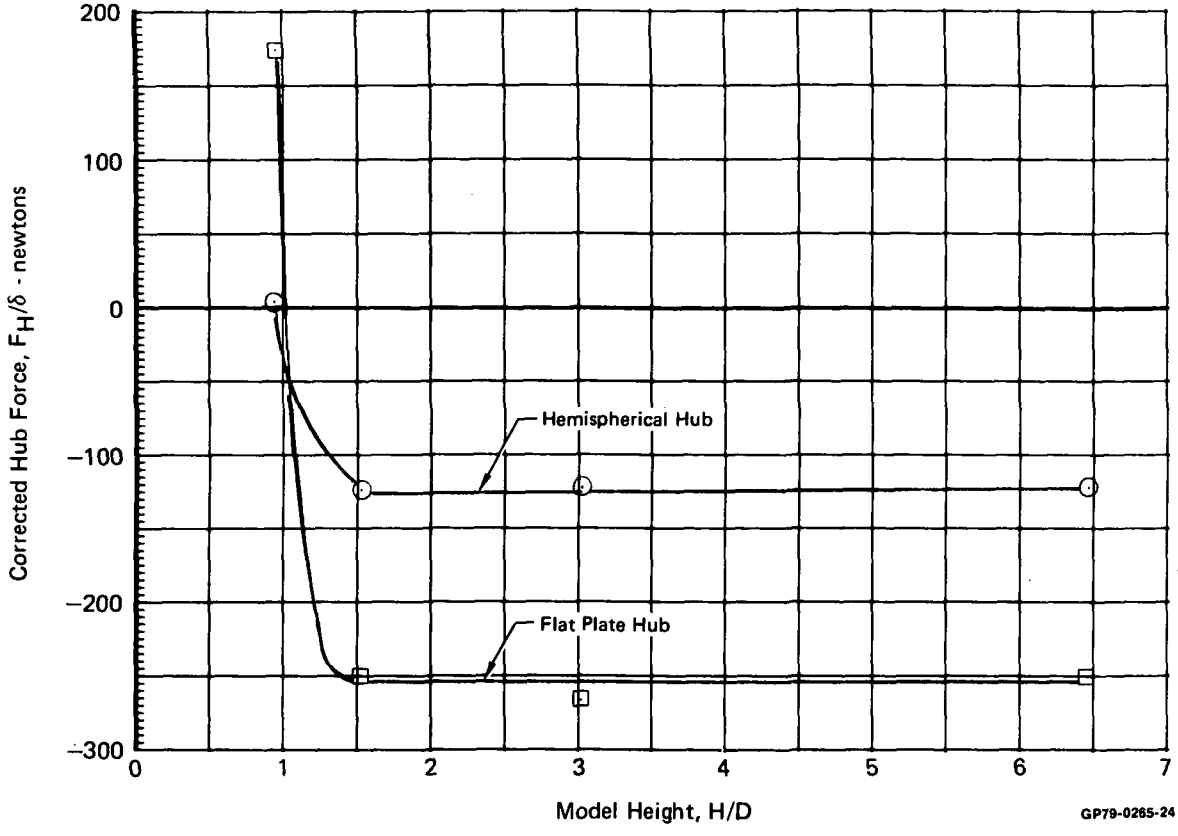

FIGURE 4-40
NOSE UNIT EXIT HUB PRESSURE PROFILES
Single Unit Operation Flat Plate Hub
$N_F/\sqrt{\theta_{T_i}}$ = 3600 RPM

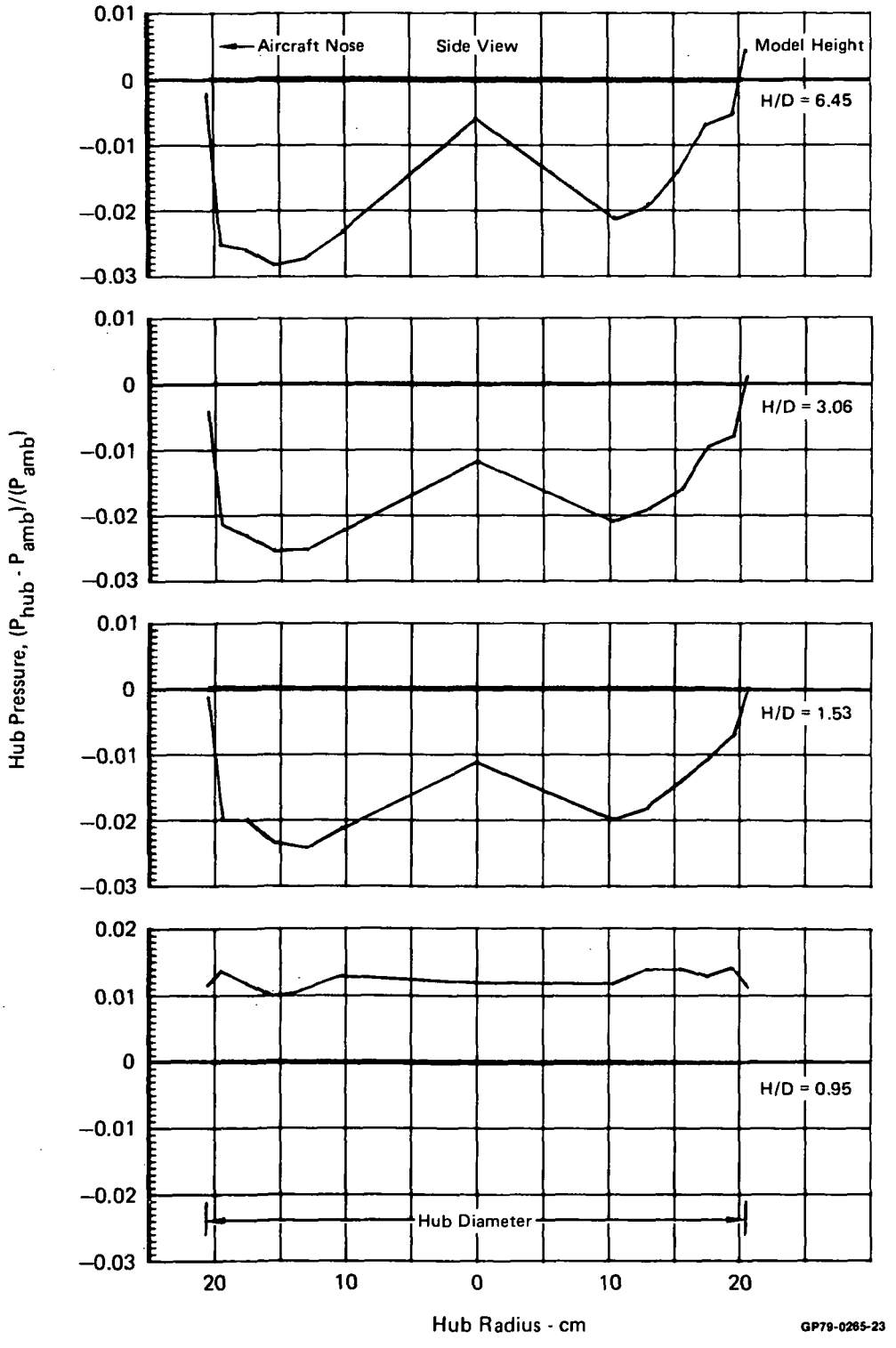

FIGURE 4-41
NOSE UNIT EXIT HUB PRESSURE PROFILES
Single Unit Operation Hemispherical Hub
$N_F/\sqrt{\theta_{T_i}}$ = 3600 RPM

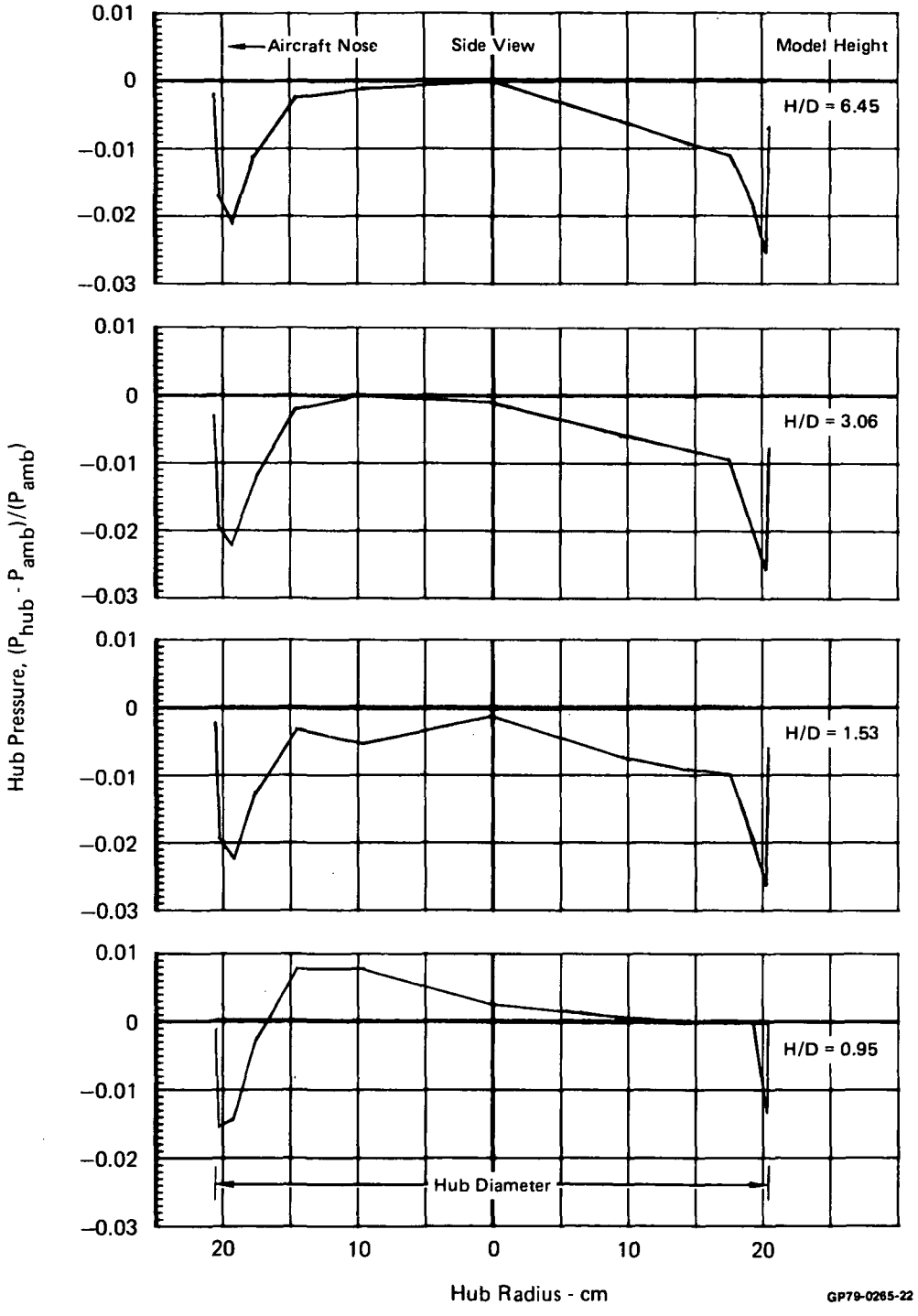

whereas a 12 percent loss was measured with the nose fan operating alone. For 3 unit operation a 8.3 percent lift loss was recorded. These results are quite different than the 4.1 percent scale model test results which show a nominal one percent lift loss for each of these cases. In addition, these results are at variance with all other induced lift information reported in the literature for small scale aircraft models with similar planform to jet area ratios.

An important question arises as to the cause of the differences in induced lift values recorded on the 4.1 and 70 percent scale models. That is, are the differences indicative of model scale effects, the differences in model detail or are the differences within an uncertainty band for the experimental measurements? There is not sufficient data available to evaluate uncertainties due to differences in the model such as the absence of inlet on the small model or the difference in nozzle flow exit shape and turbulence level. It was anticipated that these differences would be quite small. However, a closer examination of test data for the LSPM was carried out to investigate possible uncertainties associated with large scale induced lift measurements. Since induced lift is determined by subtracting the model measured lift (load cells) from the installed thrust (calibrated rake measurements), an uncertainty in either of these measurements can cause substantial percentage change in induced effects.

4.2.1 SINGLE UNIT OPERATION - Program scope limitations did not permit acquisition of data repeatability information on a particular model configuration. However, a number of tests were conducted for which the model geometry changes were slight or were in a location such that the induced lift characteristics for single unit operation would not be expected to be different. Comparisons of these single unit test runs were made to assess data repeatability.

At a model ground height of 0.95 nozzle diameters, single unit tests of the lift/cruise and nose fans were made on the baseline model configuration, baseline minus the lift/cruise nozzle rails and the baseline configuration plus the 4-sided LID. Single nose unit operation was also obtained with the hemispherical fan exit hub installed. Figures 4-42 through 4-44 illustrate the measured lift, rake ideal thrust and installed thrust data as a function of fan speed for the left and right lift/cruise and nose units respectively. For single unit operation no fountain or reflected upwash is present and thus the balance measured lift should be indicative of the sum of the installed thrust and the suckdown forces due to entrained flow by the nozzle exhaust and ground jet. The installed thrust was determined from the product of rake ideal thrust and nozzle thrust coefficient established via the isolated fan calibrations.

FIGURE 4-42
SINGLE UNIT LIFT MEASUREMENTS
Left Lift/Cruise H/D = 0.95

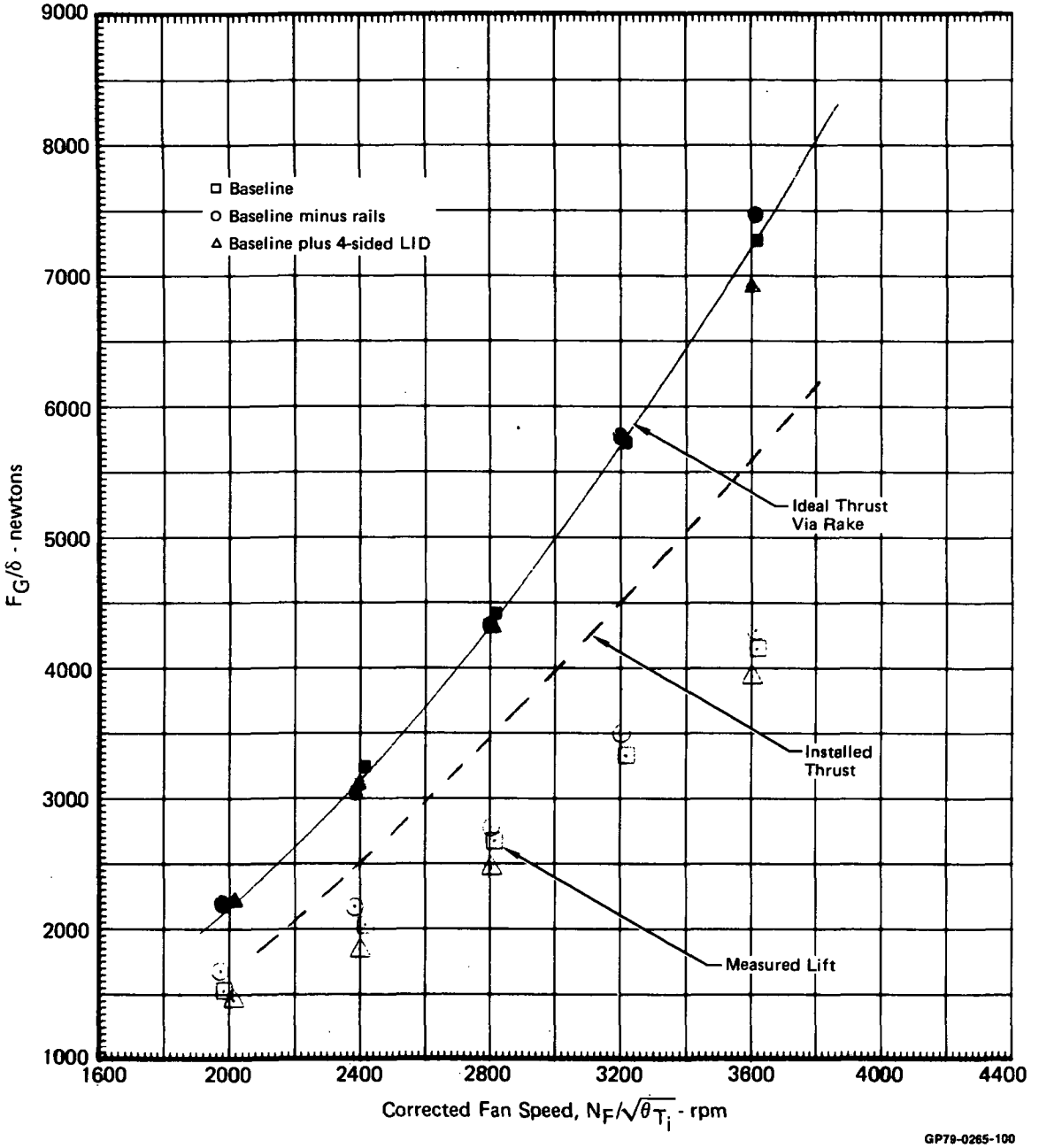

In general the ideal thrust data for the three fan units exhibit an uncertainty band in the range of ±2 with the exception of two data points recorded at 3600 RPM on the left lift/cruise unit (Figures 4-42). The balance measured lift data shows a larger band of scatter in the range of ±5% with the exception of the nose fan test with the 4-sided LID (Figure 4-44) which appears to contain a bias. For this case the bal-

FIGURE 4-43
SINGLE UNIT LIFT MEASUREMENTS
Right Lift/Cruise H/D = 0.95

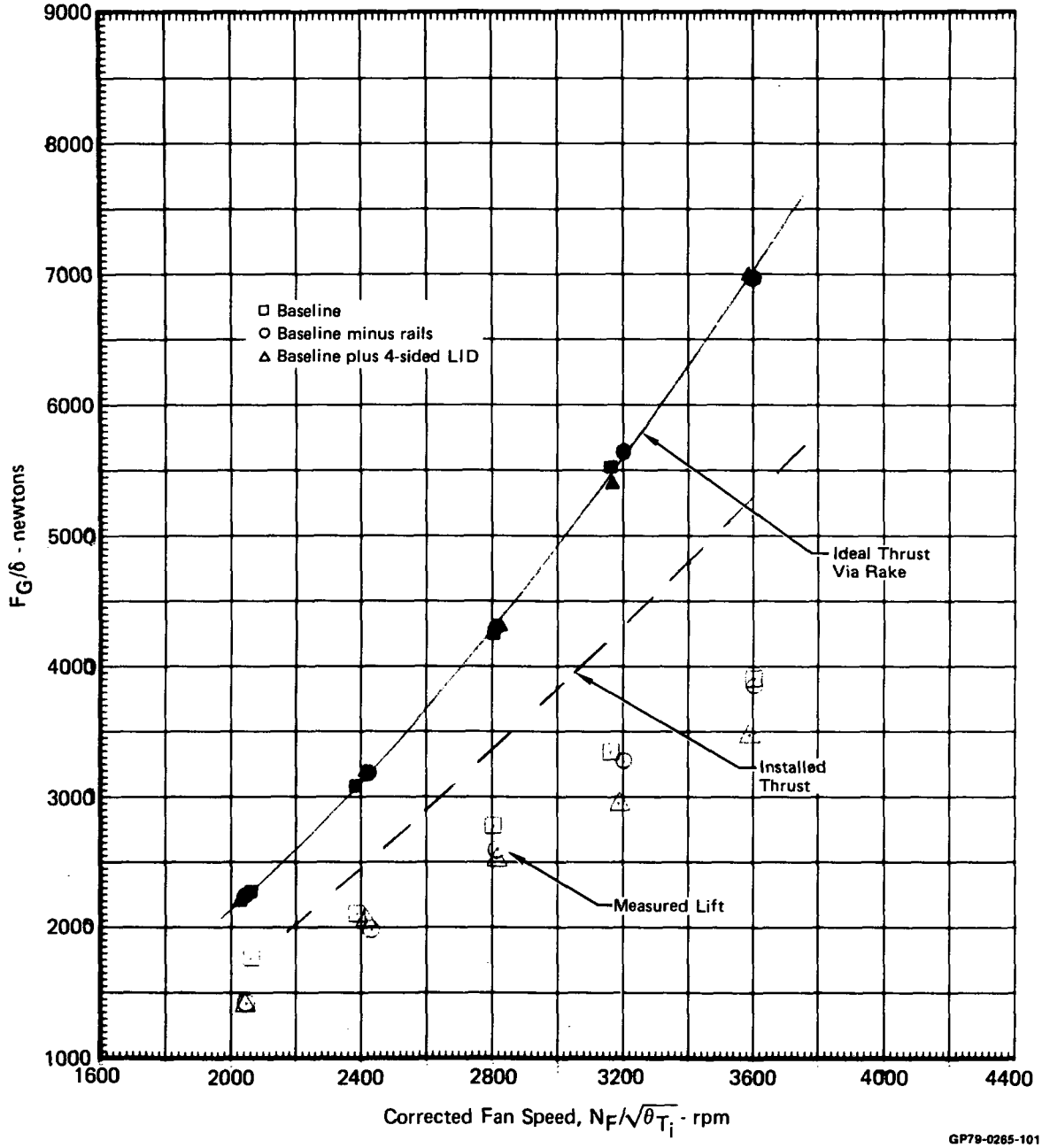

ance data, although well behaved, is greater than the installed thrust at fan speeds below 3400 RPM which implies a positive induced lift effect below 3400 RPM. Since the induced effect should be negative for single unit operation it is concluded that a balance error existed.

Figures 4-45 through 4-47 provide single unit data for the nose fan at model heights of 1.53, 3.06 and 6.45. For these test runs the ideal thrust data again shows an uncertainty band in the range of ±2%. The scatter in the measured lift data

FIGURE 4-44
SINGLE UNIT LIFT MEASUREMENTS
Nose Unit H/D = 0.95

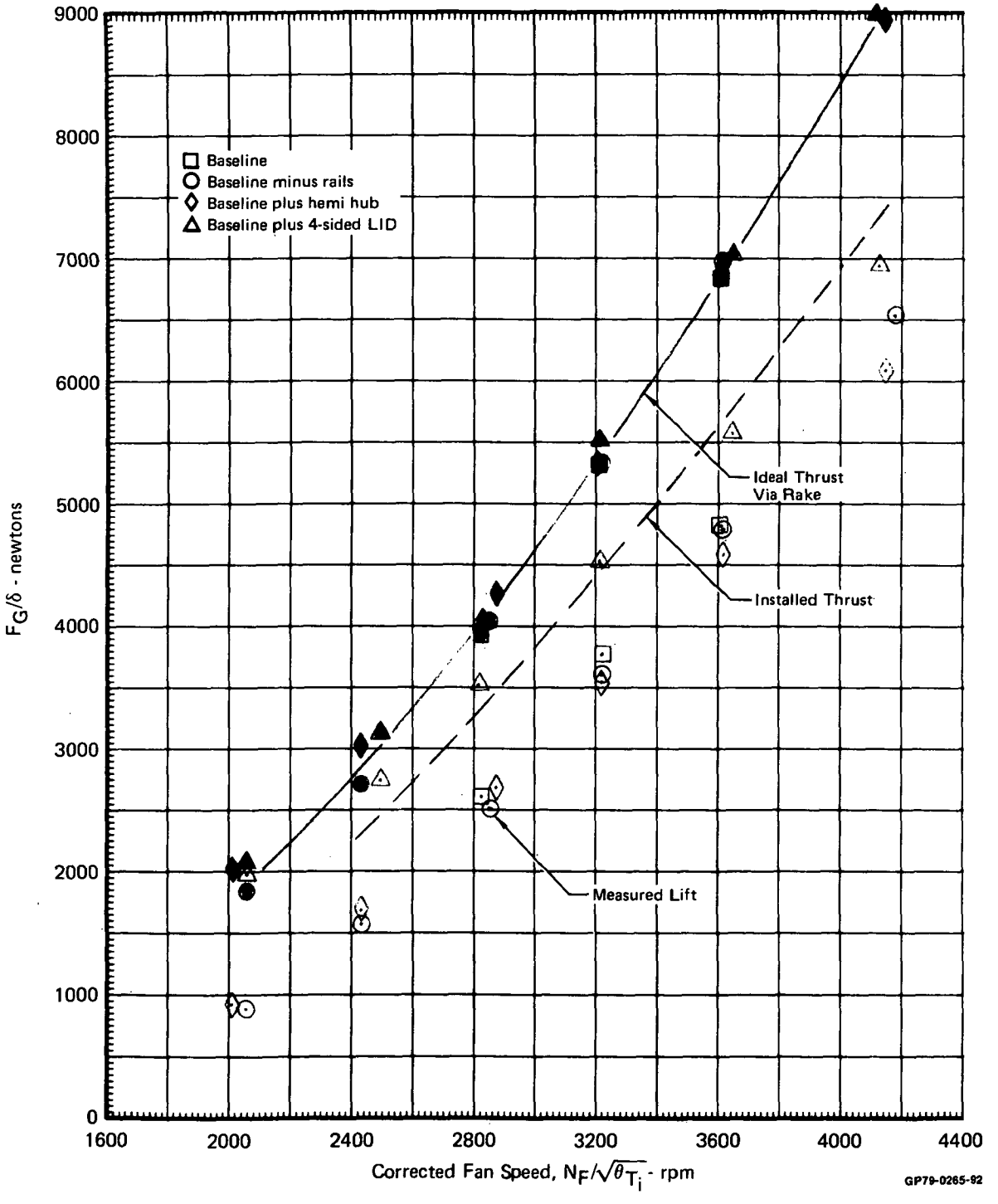

FIGURE 4-45
SINGLE UNIT LIFT MEASUREMENTS
Nose Unit H/D = 1.53

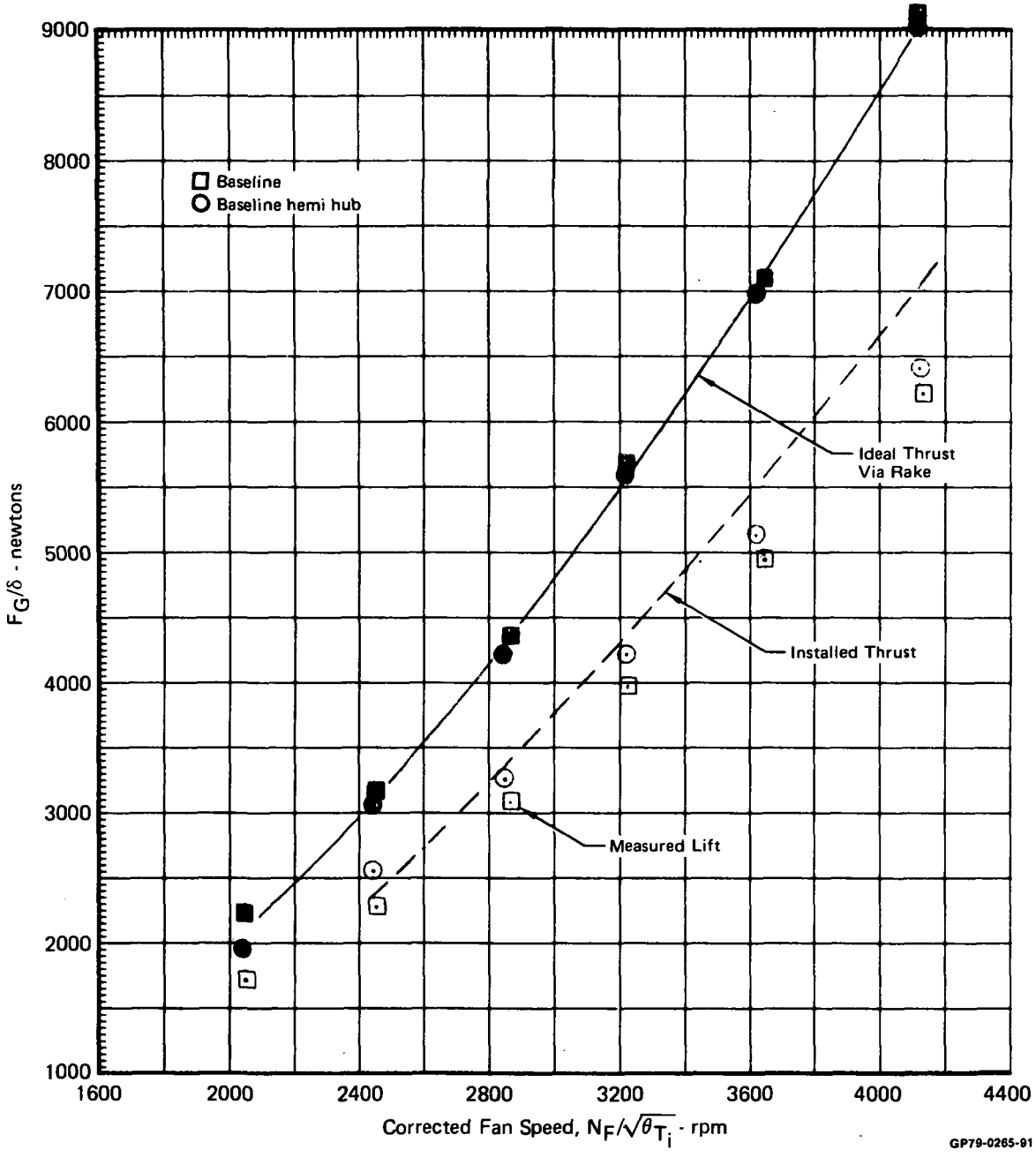

appears to be reduced from that recorded at H/D = 0.95 however, still greater than the ideal thrust data uncertainty.

Single nose unit operation tests were conducted on the large scale model during the initial test program in 1976 (Reference 5). A comparison of the nose fan data obtained in 1976 with the present test program is shown in Figures 4-48 and 4-49. For this program the lift/cruise nozzle rails were installed. However, as mentioned

FIGURE 4-46
SINGLE UNIT LIFT MEASUREMENTS
Nose Unit H/D = 3.06

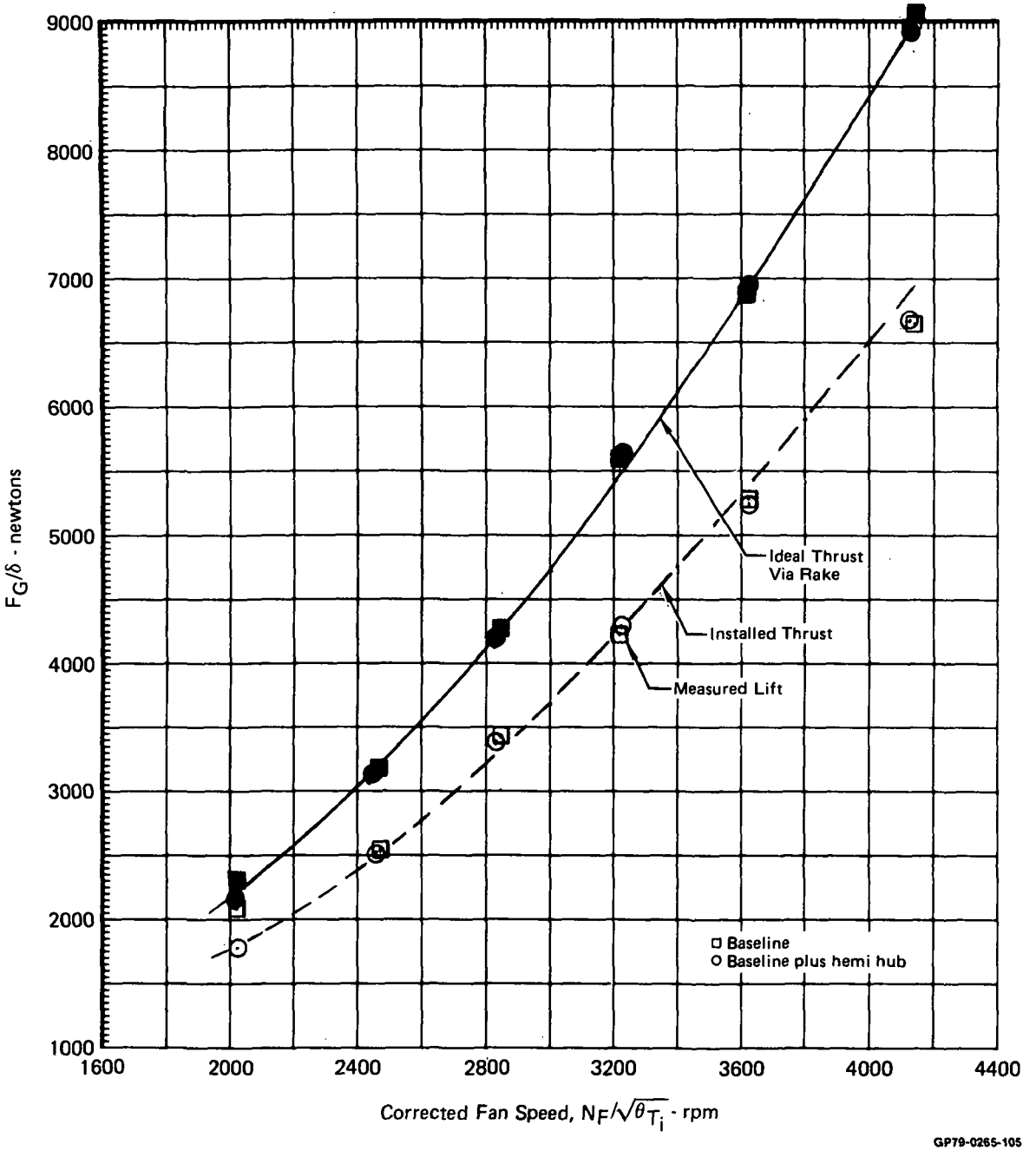

before, these rails should not influence the induced lift data since they are far removed from the nose nozzle. At the lowest H/D tested, Figure 4-48, the ideal thrust data agree fairly well except at 2800 RPM where the 1978 test point is significantly lower. The balance measured lift also appears low at this point and an

FIGURE 4-47
SINGLE UNIT LIFT MEASUREMENTS
Nose Unit H/D = 6.45

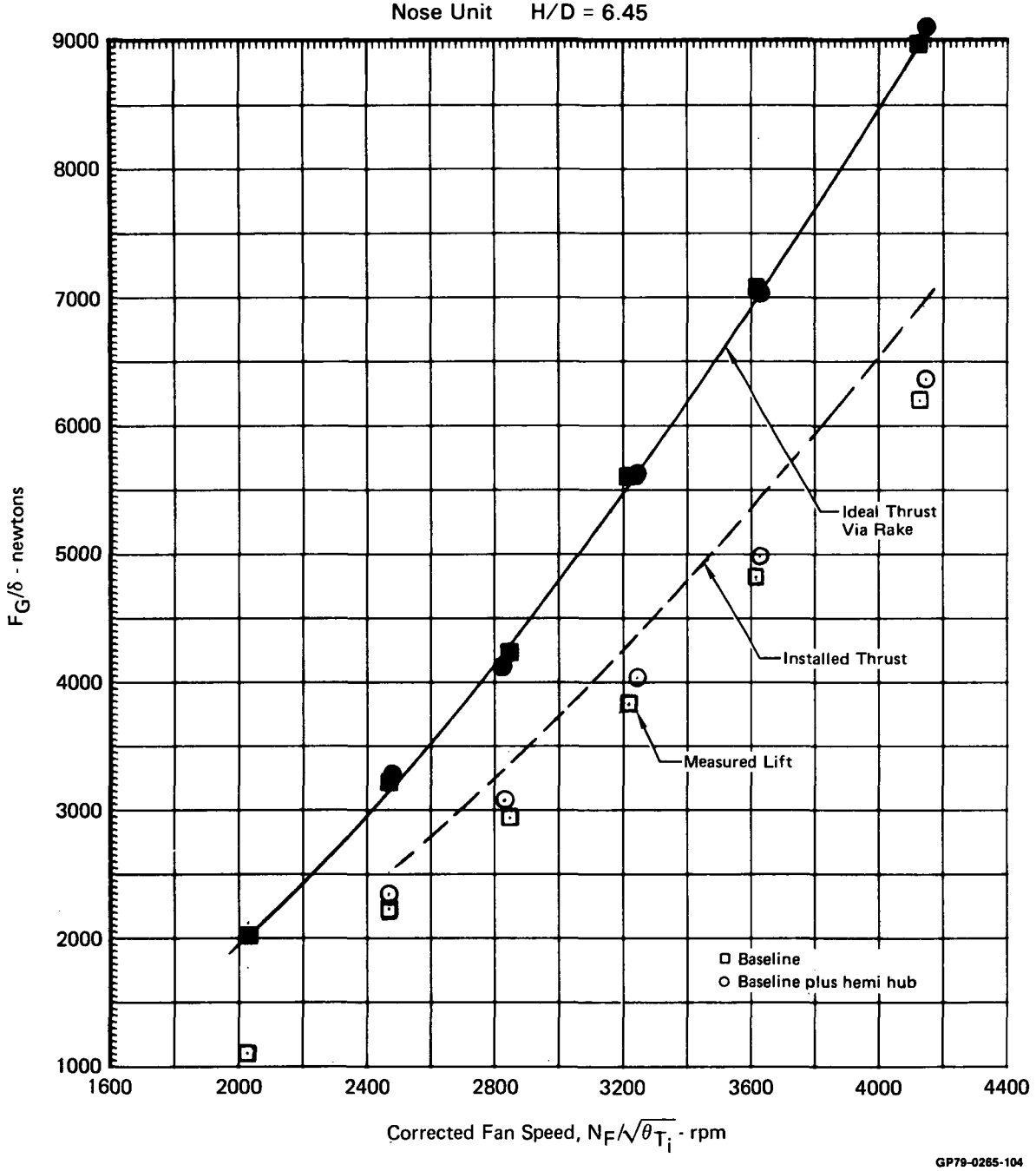

error in fan speed measurement is suspected here. However, the general difference in the balance data appears to be approximately 10 percent with the 1978 data being lower. The data obtained at H/D = 6.45, Figure 4-49, shows good agreement between both the rake computed ideal thrust and the balance lift data.

4.2.3 THREE UNIT OPERATION - The availability of large scale model, three fan operation test data for comparative evalaution is limited. The data obtained during this program for the two different nose fan exit hub shapes was presented in Section 4.1 and showed agreement within ±3 percent. One test of the model in its 1976 configuration was conducted at the lowest model height. This data comparison is provided in Figure 4-50. As with single unit operation, the rake ideal thrust levels for the two tests are in good agreement, however the balance measured lift recorded in 1976 is significantly higher. At higher fan speeds up to a 6 percent difference in total lift is indicated between the two tests.

4.2.4 GENERAL COMMENTS - The data comparisons presented in the above paragraphs do not satisfy the requirements for establishing an uncertainty band for the large scale model balance data primarily because the model geometries in all the cases except one were not identical. It is felt however, that the geometrical variances which existed were minor factors and that agreement in the lift measurement within a percent or two should have been achieved if the ±2 percent uncertainty band established during the check loadings of the load cells (Section 3.0) was maintained during the actual tests with fans operating. The comparisons suggest that the uncertainty band for the balance measured lift data could be as high as 10 percent in some cases.

As a consequence it is concluded that the differences between the large and small model induced lift data should not be interpreted as the effects of model scale and geometry but a consequence of the uncertainty in the large scale model lift measurement. The cause for the increase in lift measurement uncertainty between the check loading runs and the test runs with fans operating is not understood. Variations in ambient wind conditions and/or instrumentation anomalies caused by fan operation are two possible causes for higher uncertainty levels. The well behaved trends of the lift data with fan speed and model configuration changes at a given model height suggest that the uncertainty levels are characteristic of a systematic or bias error rather than a random error source.

4.3 INLET REINGESTION

The following sections present the large scale model inlet temperature rise data for the three instrumented inlets; the left gas generator, left lift/cruise fan and the nose fan. The data are shown for a variety of configurations for two and three unit operation. Nozzle geometries are fixed at zero degree yaw angle, 95 degree lift/cruise hood angle and 95 degree nose nozzle louver angle.

Inlet reingestion is expressed in terms of a temperature rise index. This nondimensionalized quantity is the ratio of the inlet total temperature rise above

FIGURE 4-48
SINGLE UNIT LIFT MEASUREMENTS
Nose Unit 1976 and 1978 Test Program Comparisons

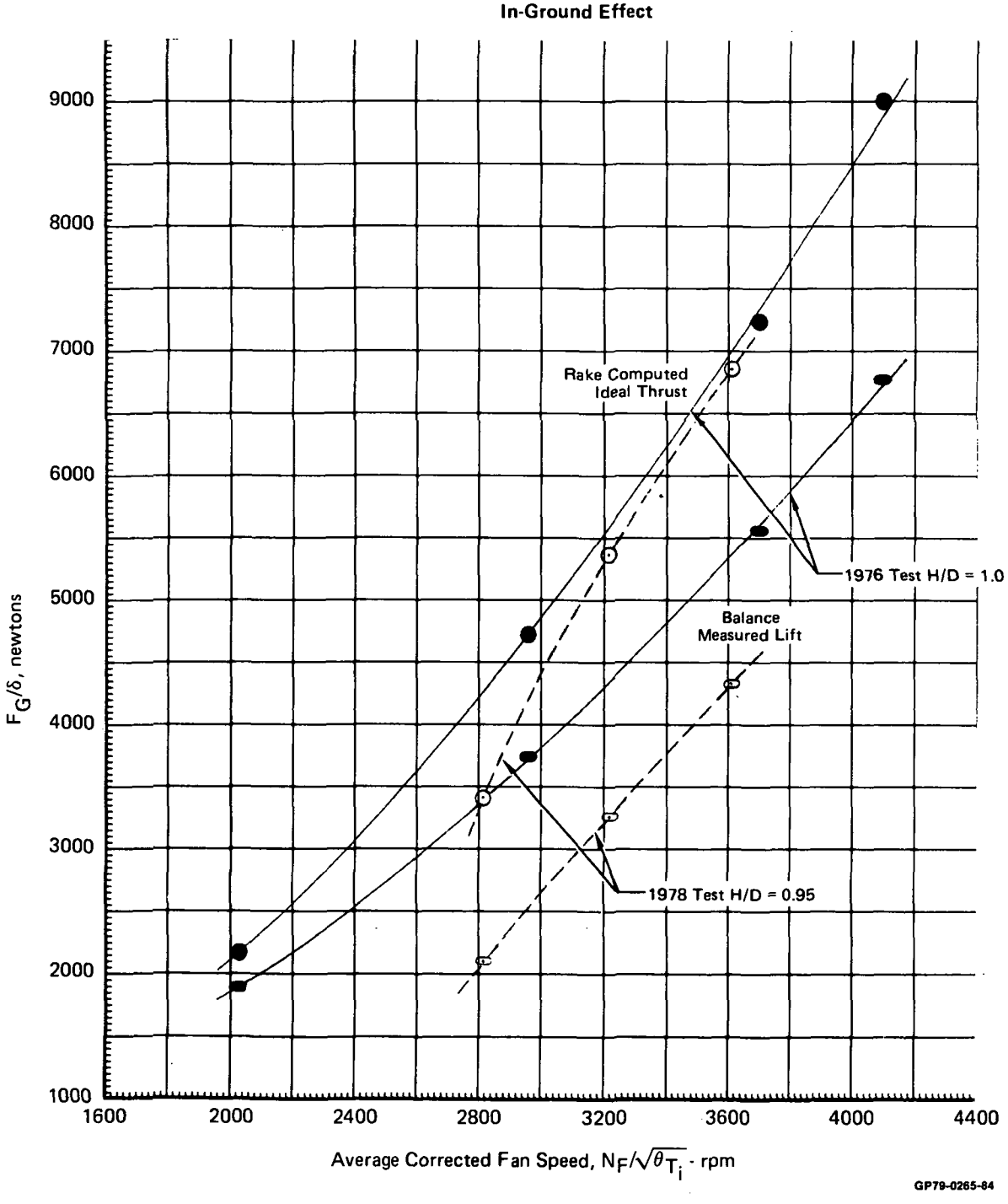

FIGURE 4-49
SINGLE UNIT LIFT MEASUREMENTS
Nose Unit 1976 and 1978 Test Program Comparisons

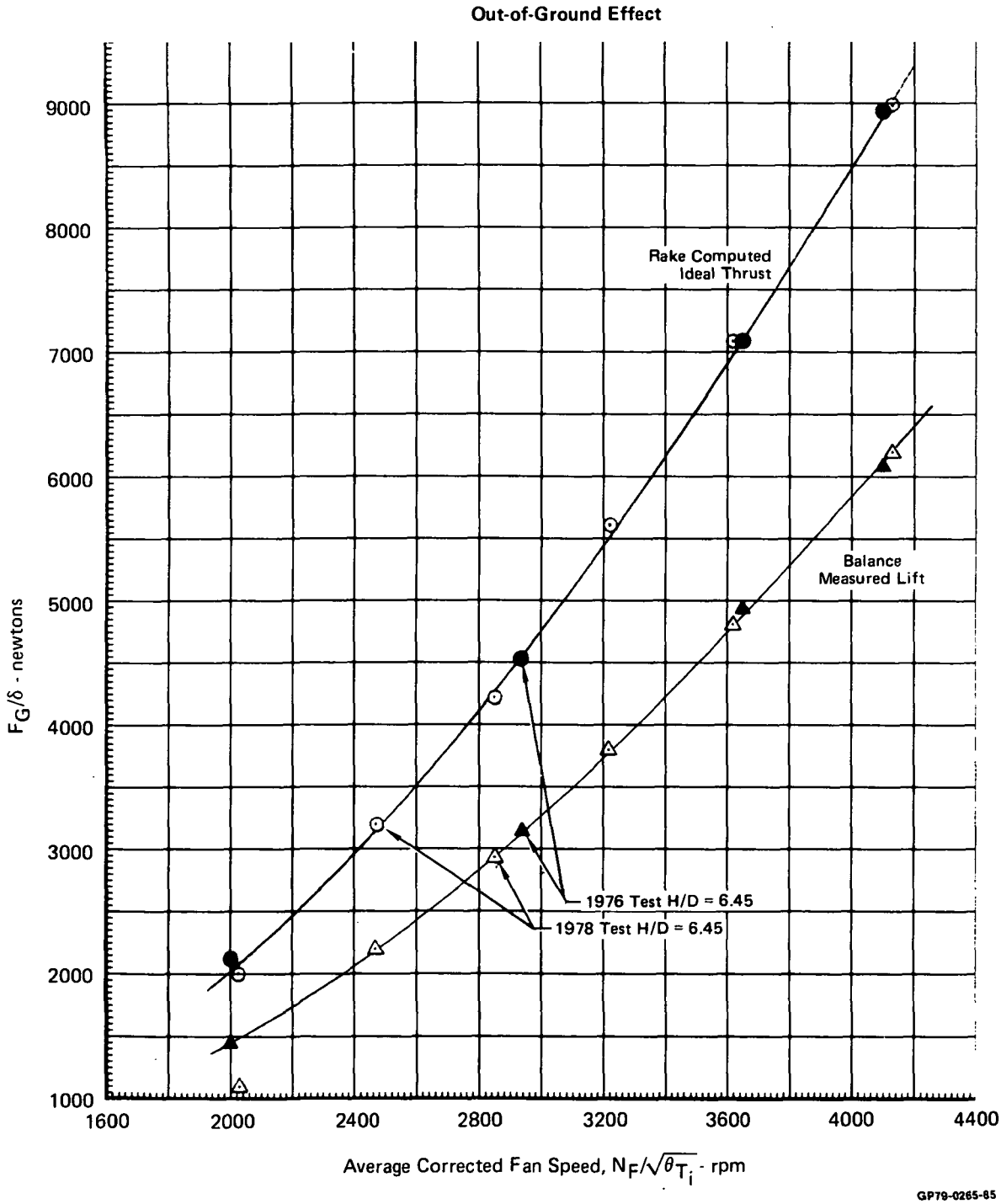

FIGURE 4-50
TOTAL MEASURED LIFT COMPARISON
3-Unit Operation 1976 70% Model Configuration

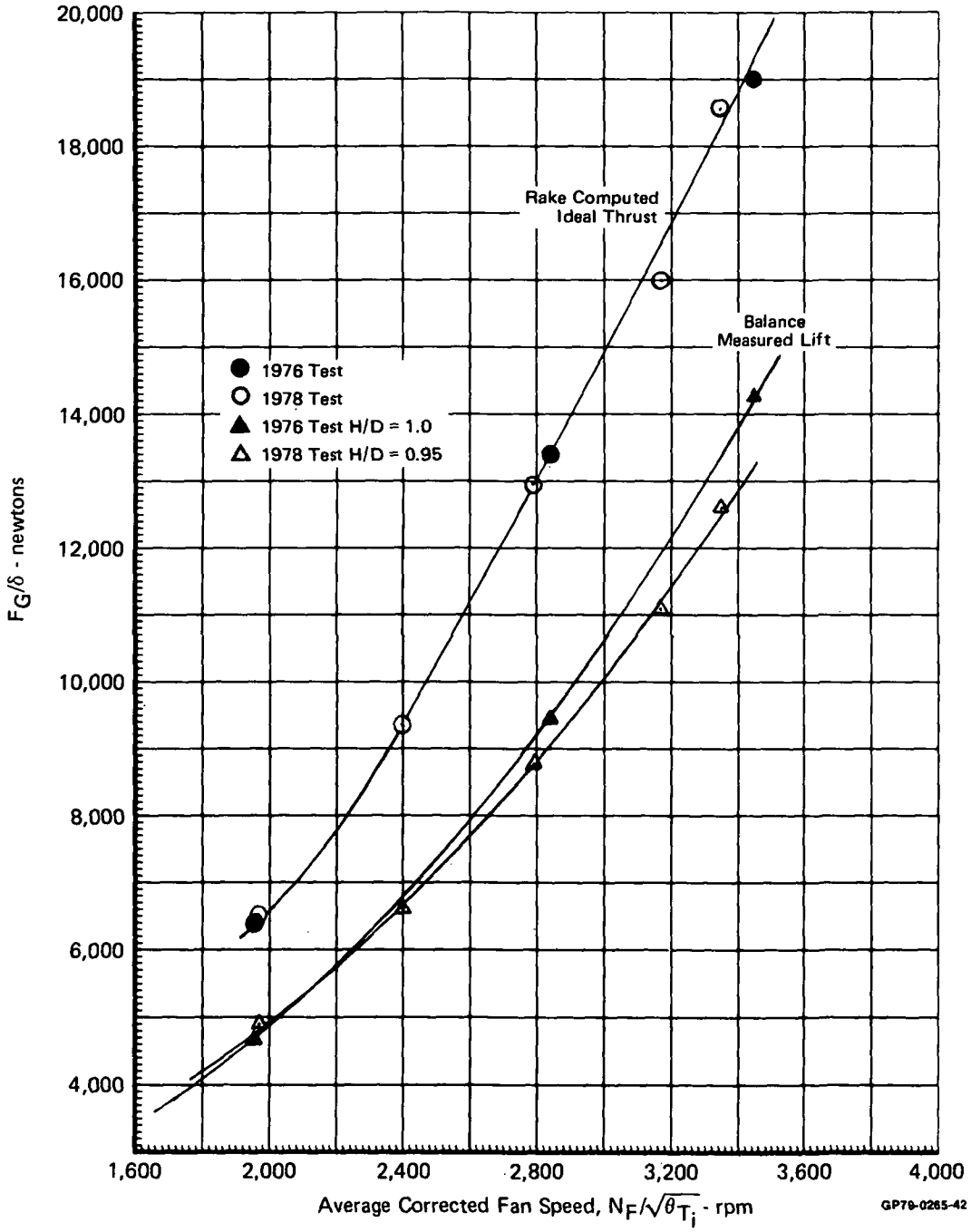

ambient ($T_I - T_{AMB}$) to the mass averaged jet temperature rise above ambient ($T_J - T_{AMB}$) for each unit. In general, the value of ($T_J - T_{AMB}$) varied from 80 to 100 degrees Fahrenheit.

4.3.1 BASELINE CONFIGURATION - The effect of model height on inlet temperature rise is presented in Figure 4-51. The left lift/cruise and nose fan inlets indicate a temperature rise with decreasing height, except for H/D of 0.95. The left gas generator inlet indicates a consistently increasing temperature rise with decreasing model attitudes.

Inlet reingestion as a function of fan speed is presented in Figures 4-52 through 4-55. The temperature rise index is not independent of fan speed for the 4 heights tested. Different trends of inlet reingestion as a function of H/D occur at different fan speeds.

Lower surface temperature distributions are presented in Figures 4-52 through 4-55. The temperature rise index is not independent of fan speed for the 4 heights tested. Different trends of inlet reingestion as a function of H/D occur at different fan speeds.

Lower surface temperature distributions are presented in Figures 4-56 through 4-59. At H/D of 0.95, the highest temperatures are located above the three-jet fountain, near the gas generator inlets. A large temperature gradient appears from the center fuselage to the wingtips where the temperature is ambient. At H/D of 1.53 and 3.06, smaller temperature gradients exist between various locations on the lower surface. At H/D of 6.45, temperatures are expected to be very close to ambient since no fountain upwash is present. The temperatures over 100°F shown at this height are suspected to be caused by internal heating of the model by the interconnect ducting between the gas generators and fans.

The effect of model pitch and bank angle on inlet temperature rise is presented in Figures 4-60 and 4-61 respectively. Negative pitch angle was beneficial to all three inlets by moving the three jet fountain aft underneath the wings.

The effect of model height on inlet temperature rise is presented in Figure 4-62 for two fan operation. Both inlets show less hot gas reingestion than for three fan operation.

Positive roll angle effects are shown in Figure 4-63. With the right wing tilted down, the fountain is tilted to the left, increasing the reingestion for the left inlets.

FIGURE 4-51
INLET REINGESTION vs MODEL HEIGHT
Baseline Configuration 3-Unit Operation
$N_F/\sqrt{\theta T_i}$ = 3200 RPM

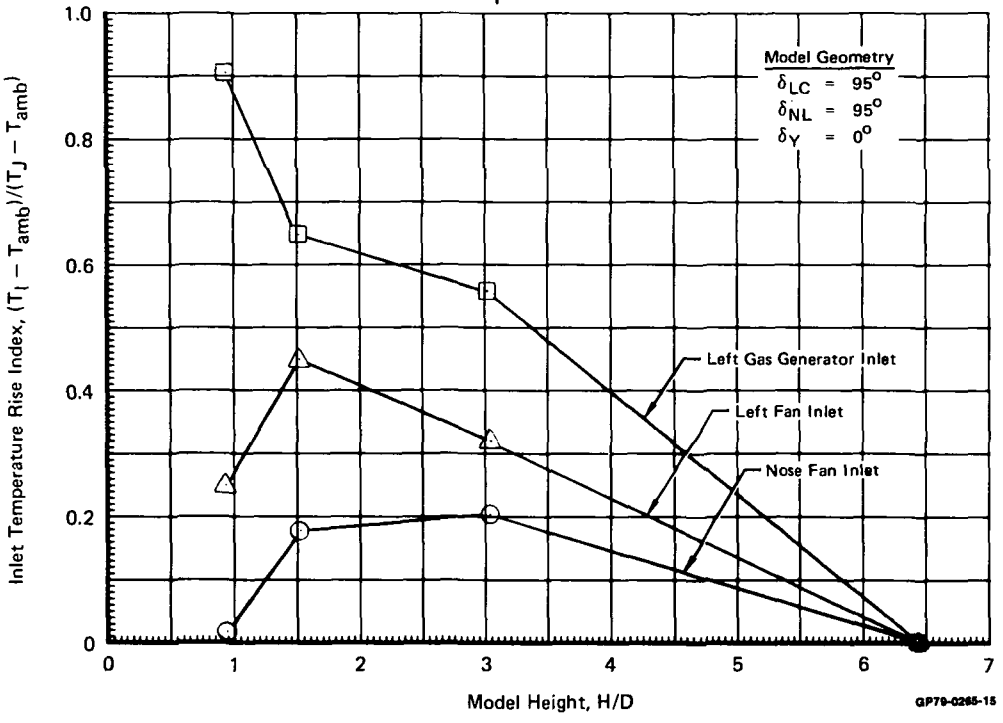

FIGURE 4-52
EFFECT OF FAN SPEED ON INLET REINGESTION
Baseline Configuration 3-Unit Operation H/D = 0.95

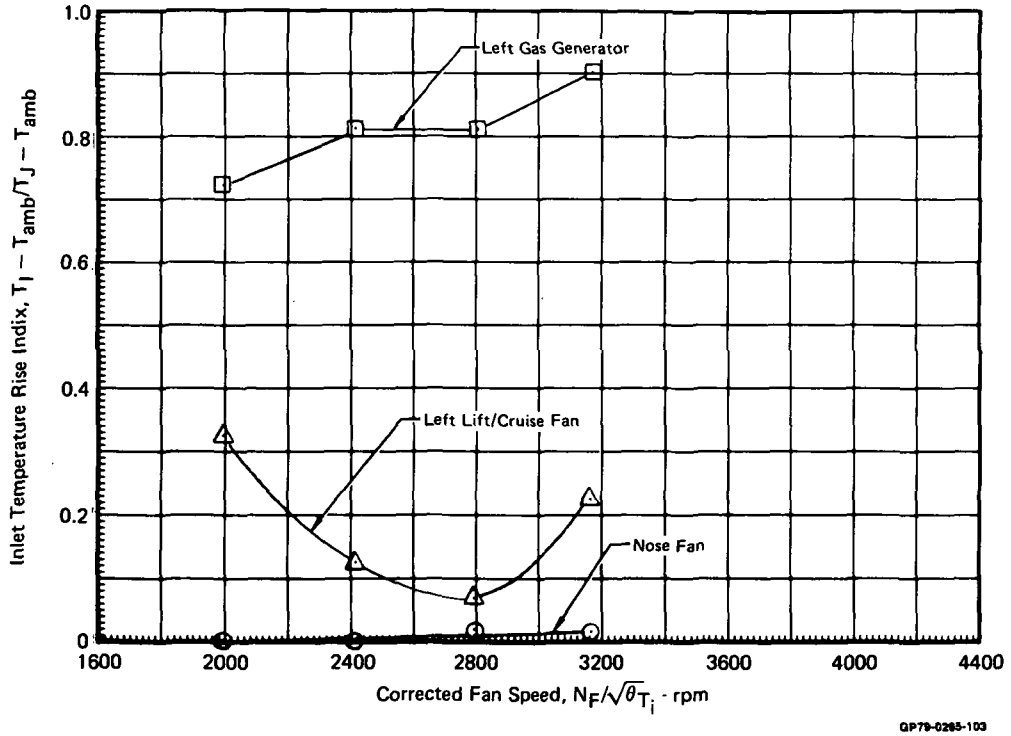

FIGURE 4-53
EFFECT OF FAN SPEED ON INLET REINGESTION
Baseline Configuration 3-Unit Operation H/D = 1.53

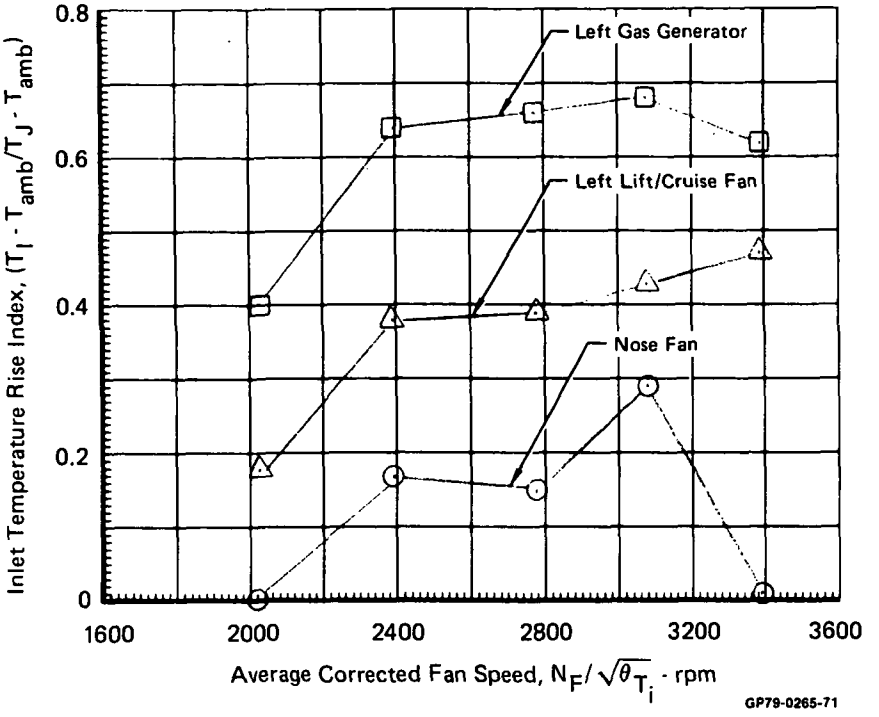

FIGURE 4-54
EFFECT OF FAN SPEED ON INLET REINGESTION
Baseline Configuration 3-Unit Operation H/D = 3.06

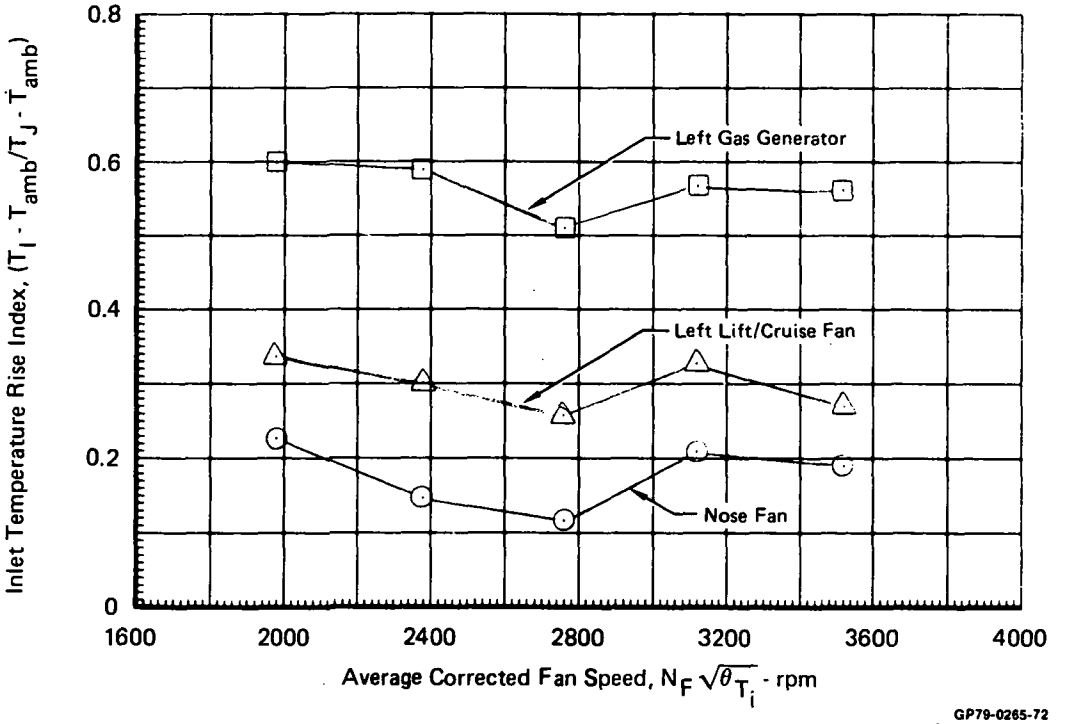

FIGURE 4-55
EFFECT OF FAN SPEED ON INLET REINGESTION
Baseline Configuration 3-Unit Configuration H/D = 6.45

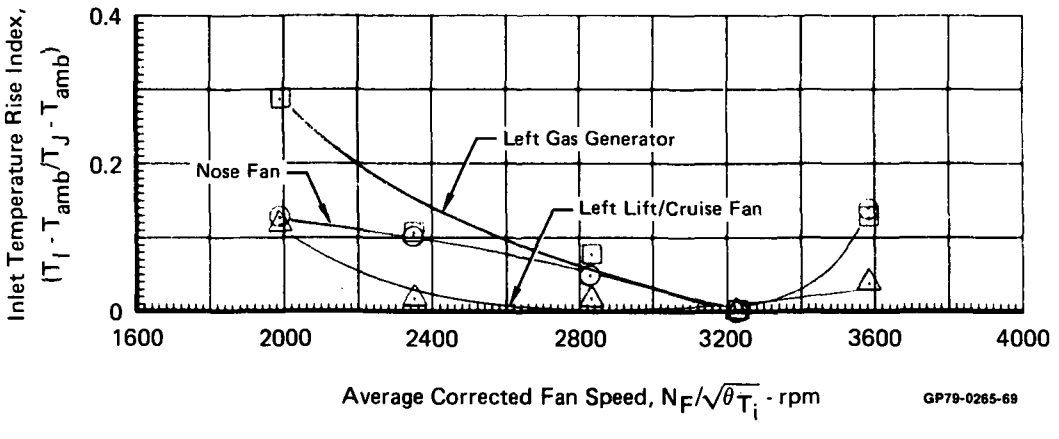

4.3.2 ALTERNATE CONFIGURATIONS - The effect of a 4-sided LID on inlet temperature rise is presented in Figure 4-64. Reduced reingestion levels are indicated for the left gas generator inlet. No significant change is indicated for the left lift/cruise and nose fan inlets.

FIGURE 4-56
LOWER SURFACE TEMPERATURE DISTRIBUTION
Baseline Configuration H/D = 0.95

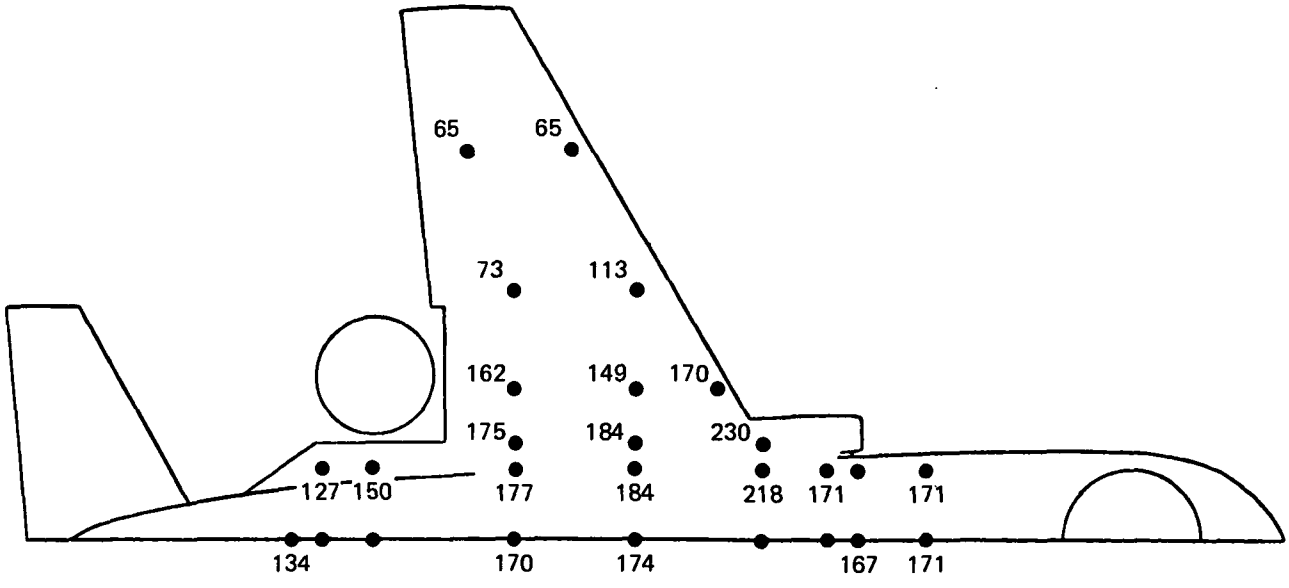

Note:
Temperature in ^{o}F
$T_{ambient} = 65^{o}F$

GP79-0265-74

FIGURE 4-57
LOWER SURFACE TEMPERATURE DISTRIBUTION
Baseline Configuration H/D = 1.53

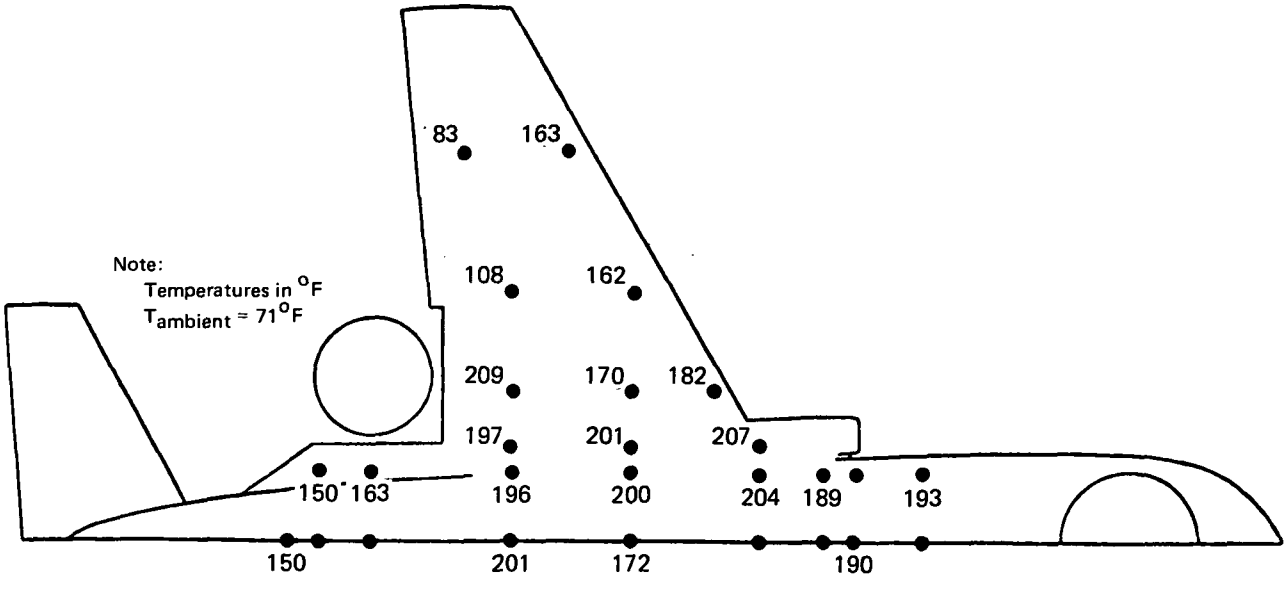

GP79-0265-75

FIGURE 4-58
LOWER SURFACE TEMPERATURE DISTRIBUTION
Baseline Configuration H/D = 3.06

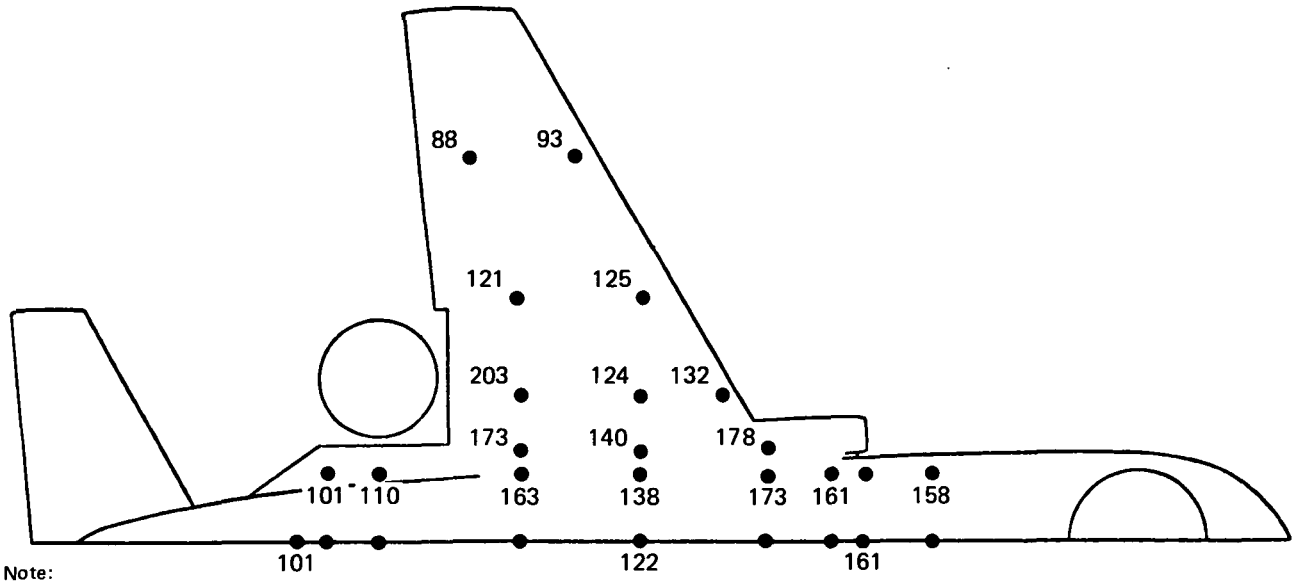

Note:
Temperatures in ^{o}F
$T_{ambient} = 67^{o}F$

FIGURE 4-59
LOWER SURFACE TEMPERATURE DISTRIBUTION
Baseline Configuration H/D = 6.45

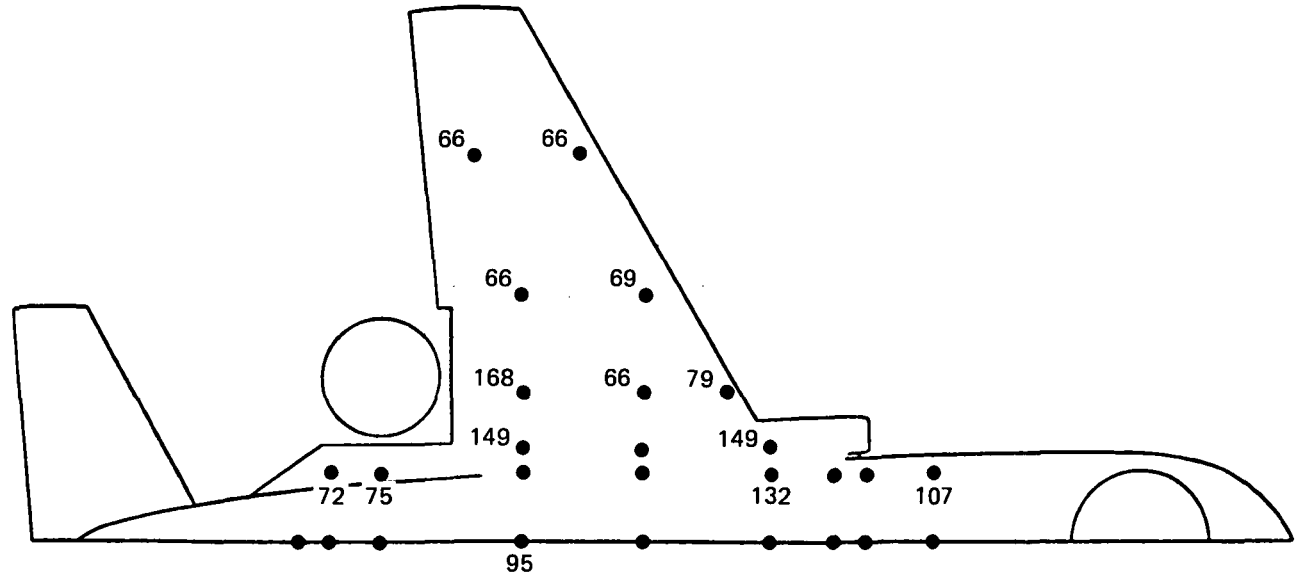

Note:
Temperature in ^{o}F
$T_{ambient} = 66^{o}F$

FIGURE 4-60
INLET REINGESTION vs PITCH ANGLE
Baseline Configuration 3-Unit Operation
H/D = 0.95 $N_F/\sqrt{\theta_{T_i}}$ = 3200 RPM

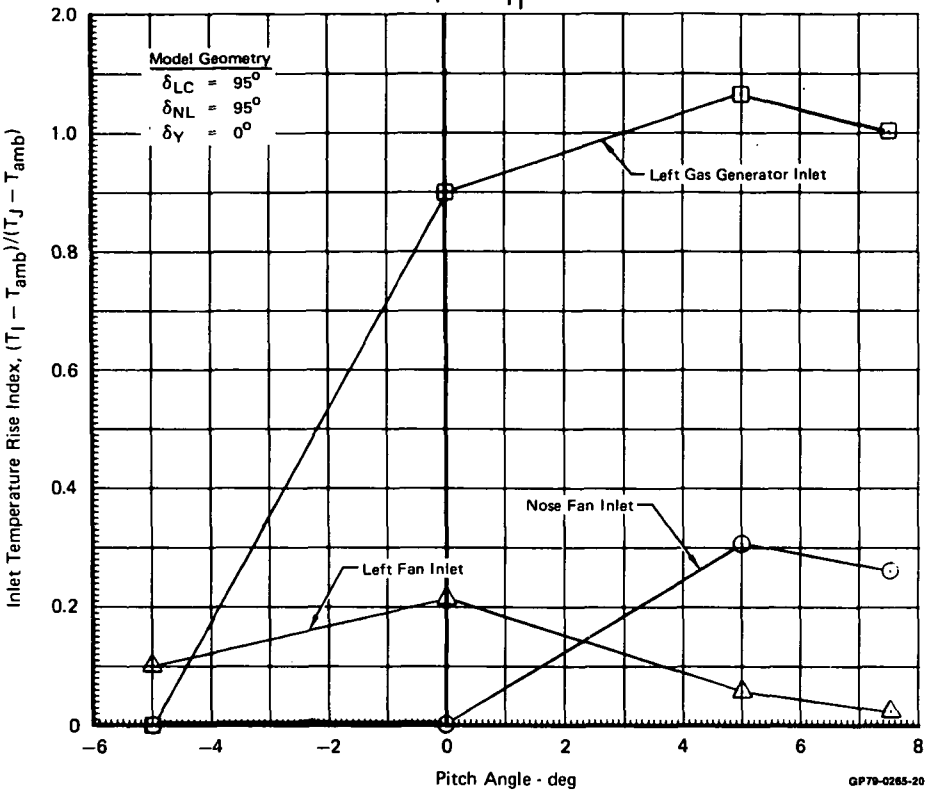

FIGURE 4-61
INLET REINGESTION vs BANK ANGLE
Baseline Configuration 3-Unit Operation
H/D = 1.24 $N_F/\sqrt{\theta_{T_i}}$ = 3200 RPM

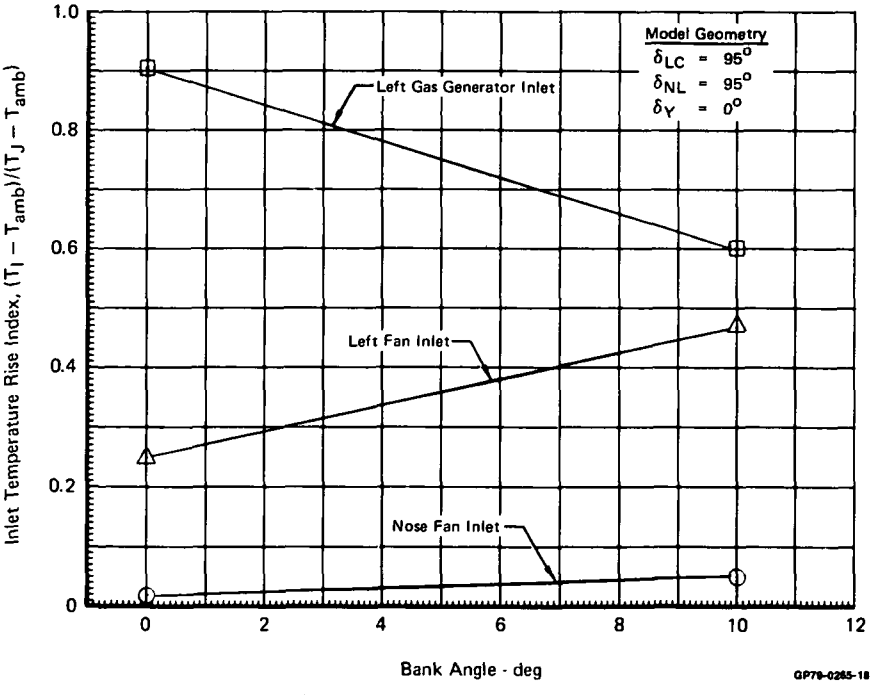

FIGURE 4-62
INLET REINGESTION vs MODEL HEIGHT
Baseline Configuration 2-Unit Operation
$N_F/\sqrt{\theta_{T_i}}$ = 3200 RPM

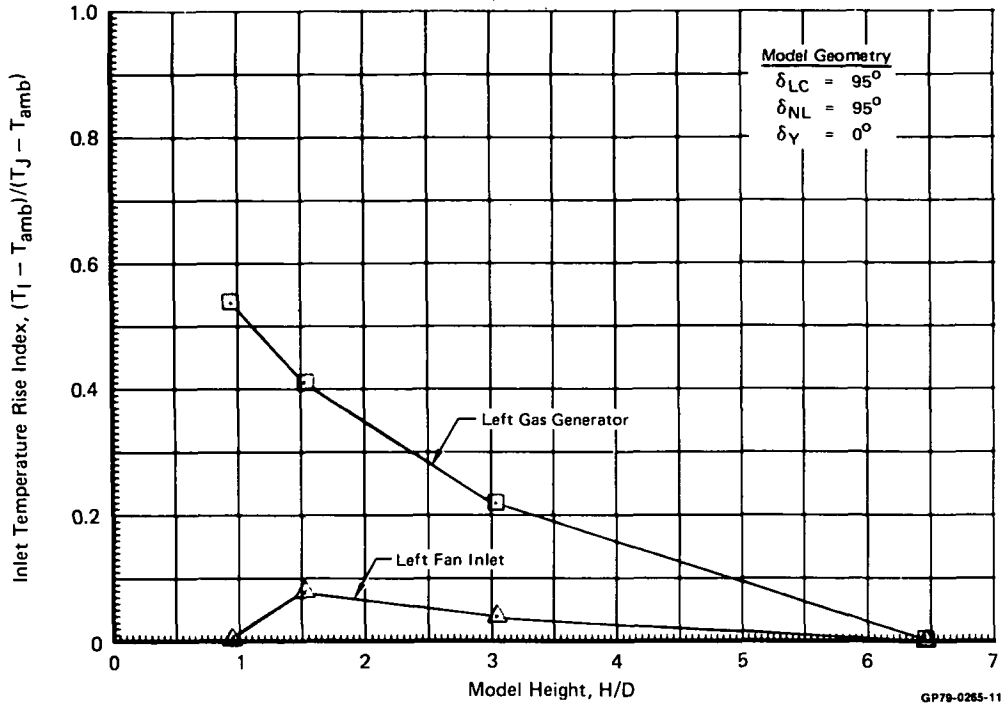

FIGURE 4-63
INLET REINGESTION vs BANK ANGLE
Baseline Configuration 2-Unit Operation
H/D = 1.24 $N_F/\sqrt{\theta_{T_i}}$ = 3200 RPM

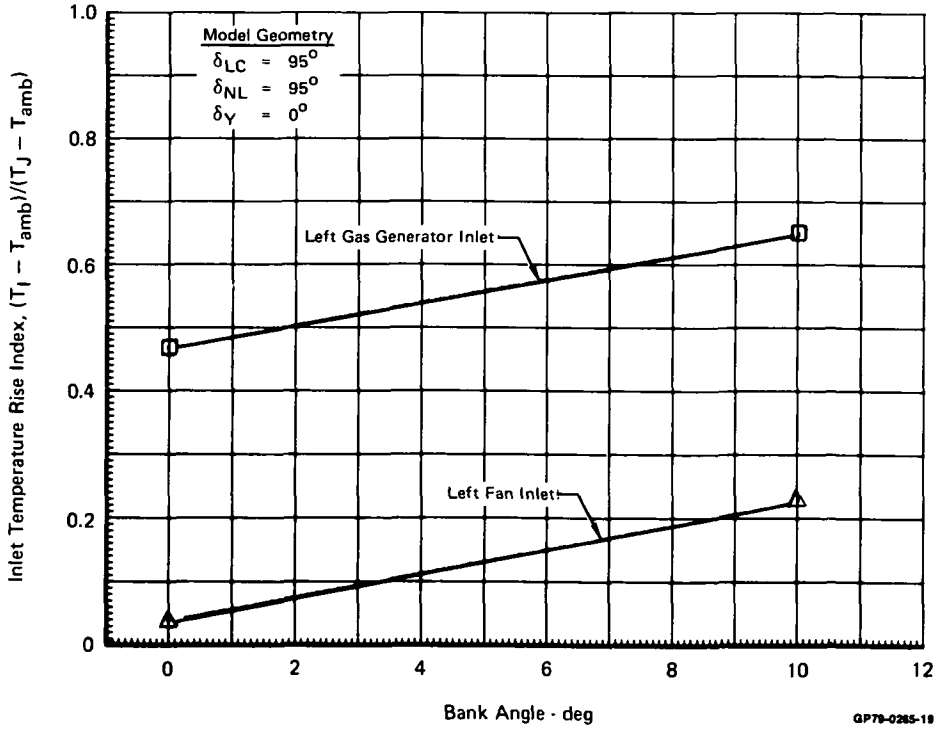

FIGURE 4-64
INLET REINGESTION vs MODEL HEIGHT
3-Unit Operation $N_F/\sqrt{\theta T_i}$ = 3200 RPM

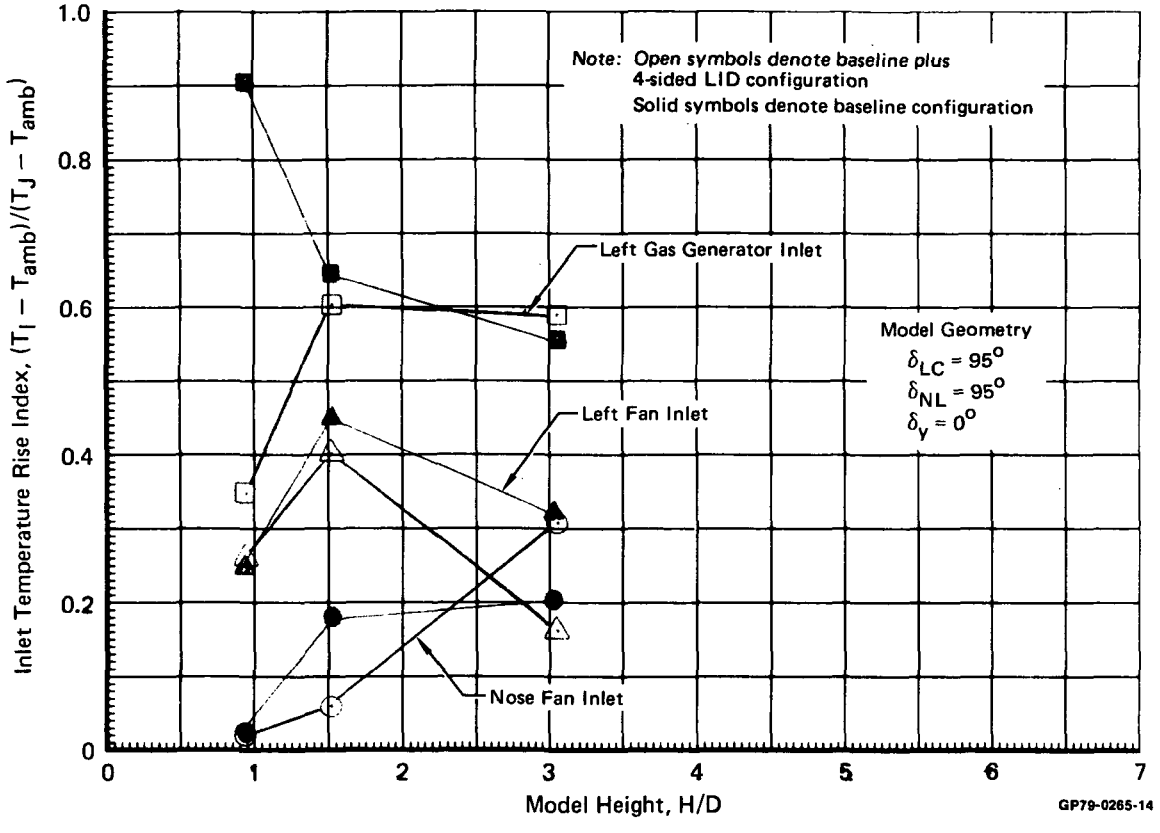

The 4-sided LID does not provide improved reingestion levels at various pitch attitudes as shown in Figure 4-65. Reingestion levels remained constant with the 4-sided LID at 10° bank attitude as shown in Figure 4-66.

The effect of a 4-sided LID for two fan operation is presented in Figure 4-67. The LID reduced reingestion to a small level. However with 10° bank, a large temperature rise occurs for the left gas generator inlet as shown in Figure 4-68. The fountain upwash apparently is not contained by the LID at the 10° bank angle.

The three-sided LID produces much the same effect as the four-sided LID as shown in Figure 4-69. Reingestion levels are reduced for the left gas generator and little improvement is indicated for the left lift/cruise and nose fan inlets.

FIGURE 4-65
INLET REINGESTION vs PITCH ANGLE
3-Unit Operation $N_F/\sqrt{\theta T_i}$ = 3200 RPM
H/D = 0.95

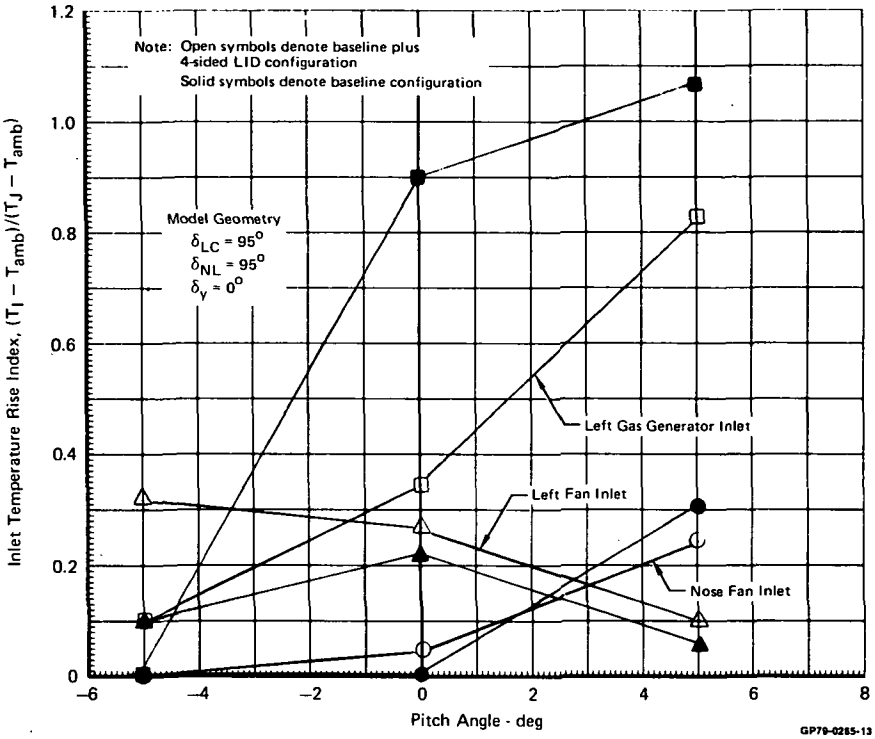

FIGURE 4-66
INLET REINGESTION vs BANK ANGLE
Baseline + 4-Sided LID Configuration 3-Unit Operation
H/D = 1.24 $N_F/\sqrt{\theta T_i}$ = 3200 RPM

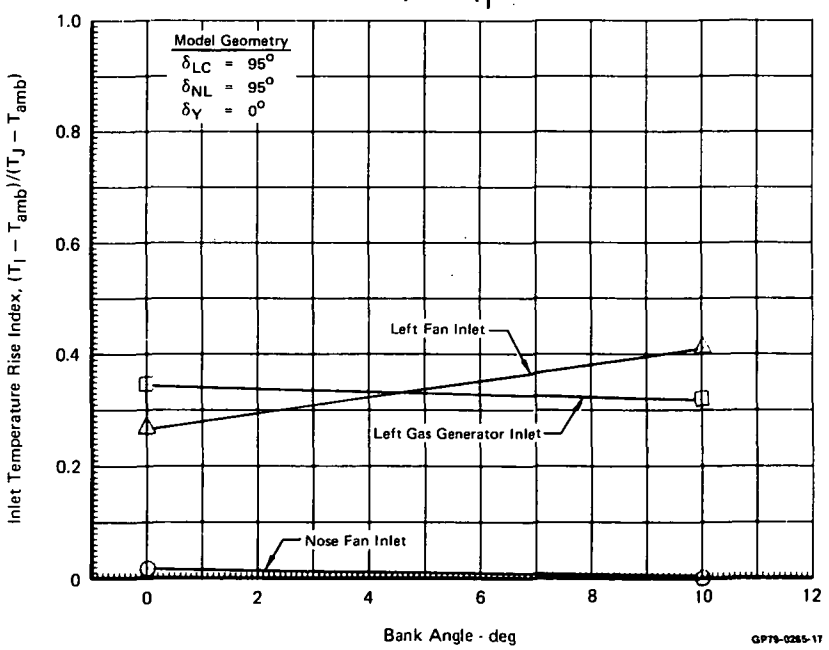

FIGURE 4-67
INLET REINGESTION vs MODEL HEIGHT
2-Unit Operation $N_F/\sqrt{\theta T_i}$ = 3600 RPM

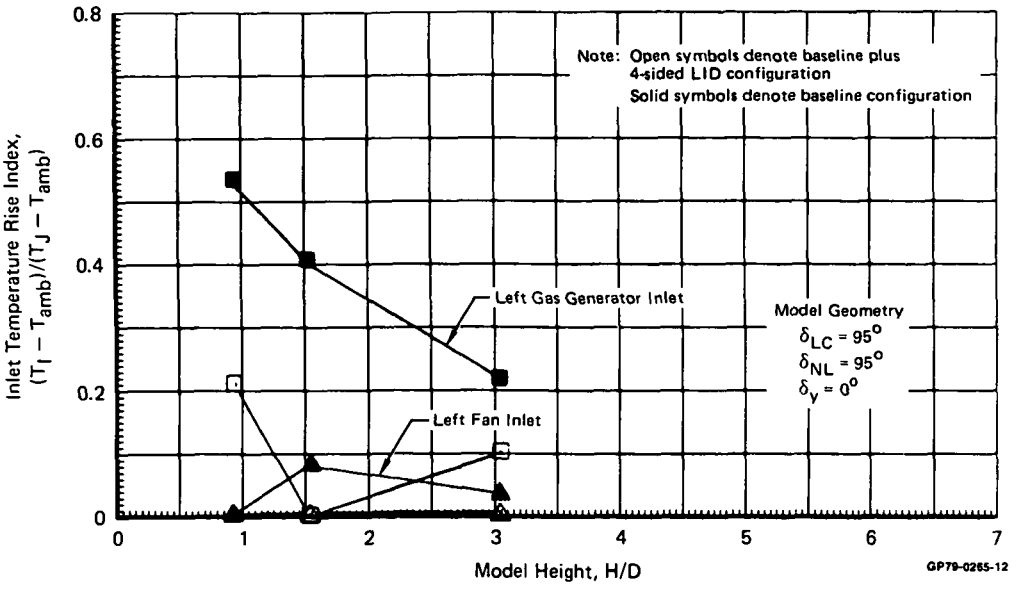

FIGURE 4-68
INLET REINGESTION vs BANK ANGLE
Baseline + 4-Sided LID Configuration 2-Unit Operation
$N_F/\sqrt{\theta T_i}$ = 3200 RPM

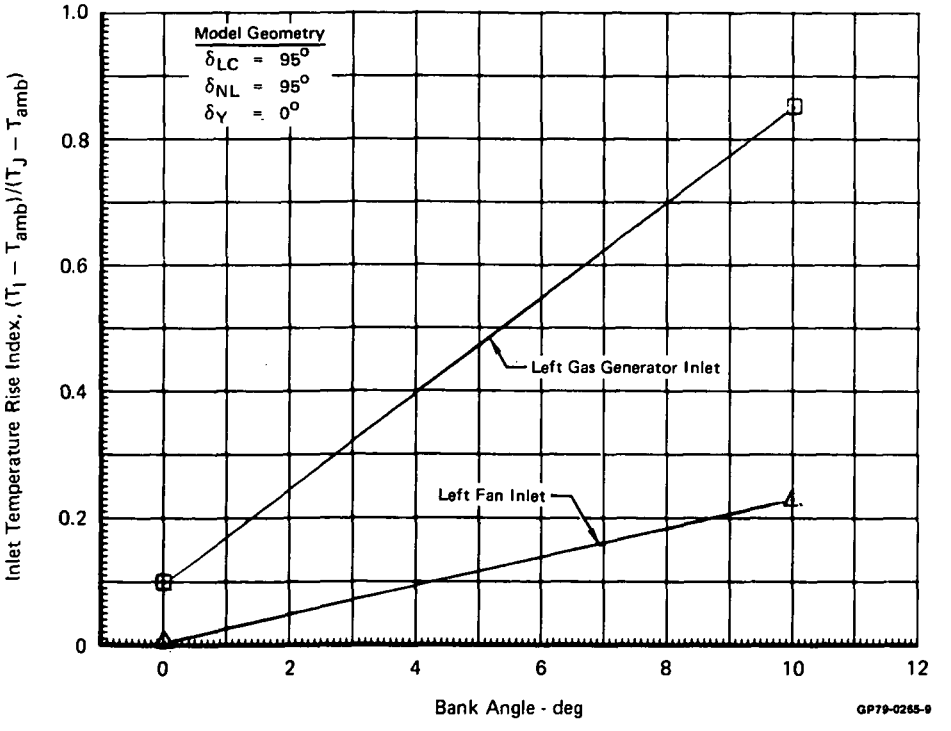

FIGURE 4-69
INLET REINGESTION vs MODEL HEIGHT
3-Unit Operation $N_F/\sqrt{\theta_{T_i}}$ = 3200 RPM

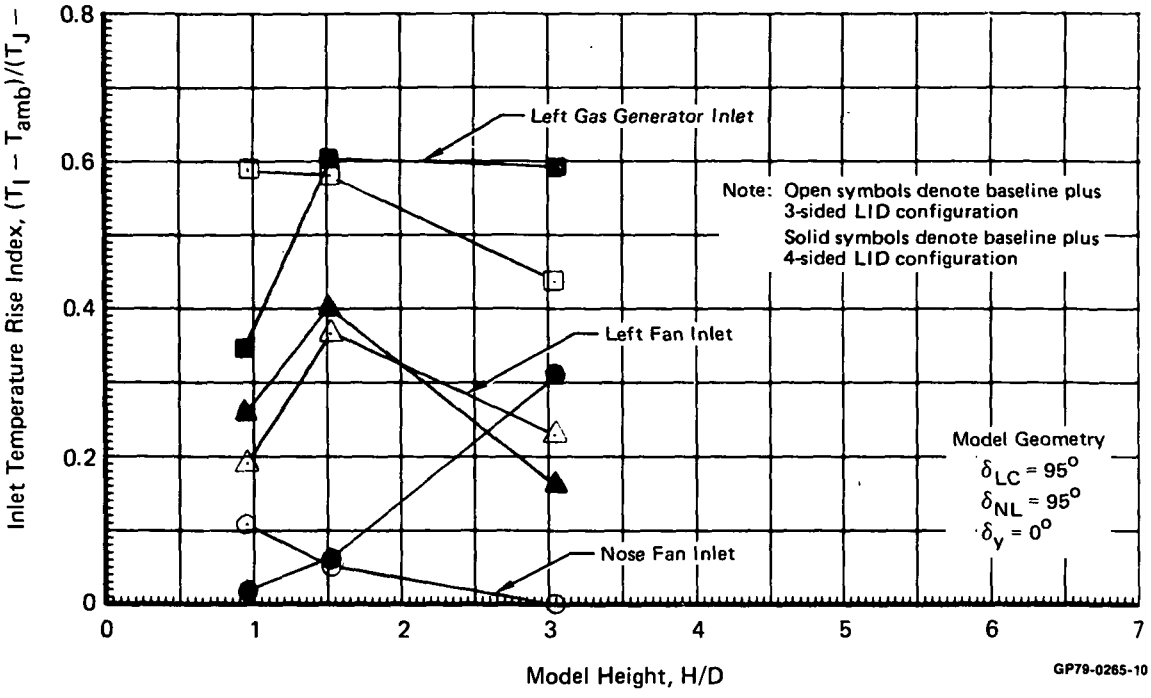

The reingestion characteristics for the baseline plus hemispherical nose fan exit hub is shown in Figure 4-70. These characteristics are similar to those for the baseline configuration except for H/D of 0.95. At this height, reingestion levels are very small. The thrust levels are essentially the same for the nose fan with a flat plate or hemispherical exit hub according to isolated fan calibrations and consequently similar inlet reingestion was expected. The lack of repeatability at the lowest height is not the only case found as discussed below.

4.3.3 COMPARISON WITH 1976 TEST DATA - Inlet reingestion testing was performed for the 70 percent scale model in 1976. In this test program, the identical configuration was again tested at the lowest H/D. A comparison of the data from the two tests is shown in Figure 4-71. The previous test indicated consistently lower levels of reingestion. The left gas generator inlet, for example exhibits only half the temperature rise in the 1976 test as in the 1978 test. In both cases, the wind was a headwind below 5 knots. The differences in the indicated temperature rise levels may be indicative of a significant reingestion sensitivity to wind, however the data base is not sufficient to substantiate this or rule out instrumentation anomalies as a factor.

FIGURE 4-70
INLET REINGESTION vs MODEL HEIGHT
Baseline + Hemispherical Hub Configuration 3-Unit Operation
$N_F/\sqrt{\theta_{T_i}}$ = 3200 RPM

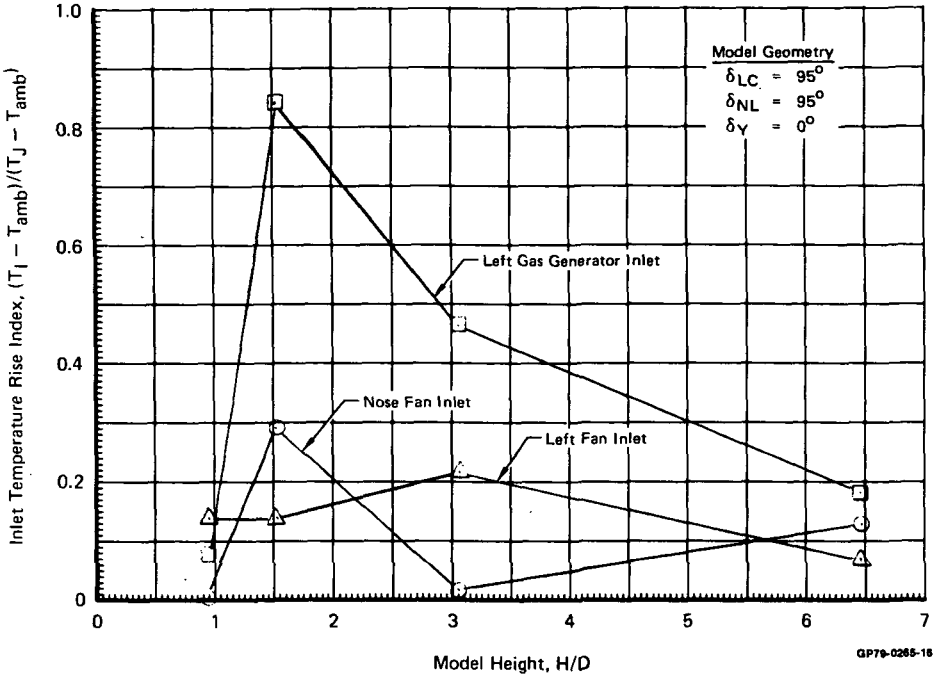

FIGURE 4-71
INLET REINGESTION vs FAN SPEED
1976 Baseline Configuration
1976 and 1978 Test Program Comparisons
3-Unit Operation

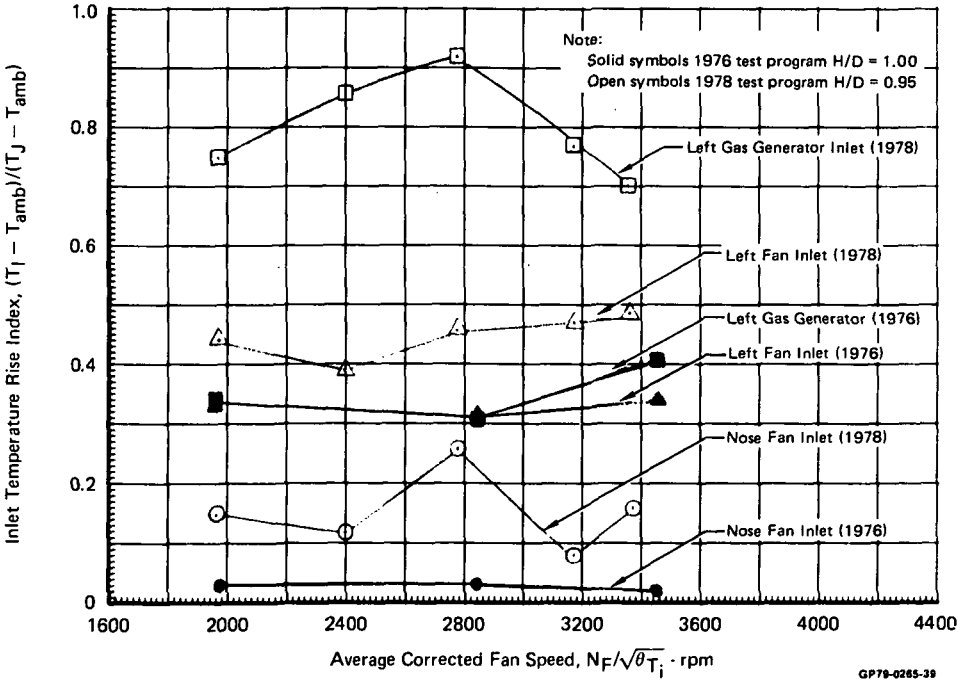

5.0 CONCLUSIONS

Tests of a 70 percent scale model and a 4.1 scale model of a three fan VTOL aircraft have been conducted in the hover mode in proximity to the ground. The following conclusion and observations can be made from the results of the tests.

- The 4.1 percent scale model test results showed induced lift for the three fan V/STOL configuration varies less than one percent for H/D values above 1.5 and at assumed landing gear height (H/D = 1.2) is estimated to be a negative three percent thrust loss with a 6 percent loss at H/D of 1.0.
- Simulated large scale model struts on the small scale model did not significantly change the balance measured forces at constant nozzle thrusts.
- The results of the large scale (70 percent) model tests with three fans operating indicated lift loss of about 8 percent at the highest H/D of 6.45. At assumed landing gear height of H/D = 1.2 the loss was about 10 percent. The lowest loss of about 3 percent was at an H/D of about 3.0. Lift loss of 6 to 12 percent at H/D of 6.45 (6.4M) with single fan operating was also evidenced.
- The large difference between large and small scale model data is believed to be due to not only model scale and differences in the models (the small scale model did not include inlet flow and the nozzle exit flow profile and turbulence levels were not matched), but also due to uncertainties in the large scale model lift measurements.
- Comparison of large and small scale induced lift and pitching moment data shows agreement with respect to trends resulting from variations in ground height and model lower purpose geometry.
  - Two, three, and four sided lift improvement devices (LID's) provide positive lift increments for H/D values below 1.5.
  - Rails located between the lift/cruise nozzles are effective in generating positive lift increments at H/D = .95.
  - Gaps around the lift/cruise nozzle periphery are not significant factors in induced lift.
  - The induced lift performance for three fan V/STOL configuration is sensitive to model pitch and bank angles at H/D = .95.
- The horizontally mounted nose fan thrust level increases three to five percent in close ground proximity due to pressurization of the fan exit hub region.

The large scale model test provided inlet reingestion information which is the basis for the following conclusions.

- o The side mounted gas generator inlets are located in a region of high temperature upwash formed by the three jet fountain and are subject to relatively high reingestion levels.
- o Operation of the two lift/cruise units alone result in lower fan and gas generator ingestion levels than are obtained during three unit operation.
- o Negative model pitch angles reduce reingestion levels on the side mounted gas generator inlets and all fan inlets.

6. REFERENCES

1. Gentry, G. L., and Margason, R. J., "Jet-Induced Lift Losses on VTOL Configurations Hovering In and Out of Ground Effect," NASA TN D-3166, 1966.
2. Margason, R. J., "Review of Propulsion Induced Effects on Aerodynamics of Jet V/STOL Aircraft," NASA TN D-5617, 1970.
3. Weber, W. B. and Williams, R. W., "Experimental Determination of Propulsion Induced Ground Effects of Typical Three Fan Type A V/STOL Configurations," AIAA Paper 78-1507, August 1978.
4. Schuster, E. P. and Flood, J. D., "Important Simulation Parameters for Experimental Testing of Propulsion Induced Lift Effects," AIAA/SAE Paper 78-1078, July 1978.
5. "Wind Tunnel and Ground Static Investigation of a Large Scale Model of a Lift/Cruise Fan V/STOL Aircraft," NASA CR 137916, August 1976.
6. Roddiger, H. A. and Esker, D. W., "Thrust and Mass Flow Characteristics of Four 36-Inch Diameter Turbotip Fan Thrust Vectoring Systems In and Out of Ground Effect", NASA CR 152239, March 1979.
7. Zalay, A. D., et al, "Investigation of a Laser Doppler Velocimeter System to Measure the Flowfield of a Large Scale V/STOL Aircraft in Ground Effect", AIAA Paper 79-1184, June 1979.

APPENDIX A

TEST RUN SCHEDULES

RUN SUMMARY

4.1% Model

MODEL CONFIGURATION DEFINITIONS

LID - Lift Improvement Device
- 4S - 4-Sided LID
- 3S - 3-Sided LID
- 2S - 2-Sided LID

PRMTR Plate - Lift/Cruise Nozzle Perimeter Plate

Operating Nozzles
- L - Louvered Nose Nozzle
- 90 - 90° Lift/Cruise Hood Angle
- 95 - 95° Lift/Cruise Hood Angle

α - Model Angle of Attack

β - Model Bank Angle

RUN SUMMARY
4.1% MODEL TEST

RUN	H/D	OPERATING NOZZLES FWD	L/H	R/H	MODEL CONFIGURATION α	β	LID	PRMTR PLATE	L/C NOZZLE RAILS	GROUND STRUTS
1	0.95	L	95	95	0	0	No	Yes	Yes	Yes
2	↓	↓	↓	↓	↓	↓	↓	↓	↓	↓
3	↓	↓	↓	↓	↓	↓	↓	↓	No	↓
4	3.06	↓	↓	↓	↓	↓	↓	↓	↓	↓
5	↓	↓	↓	↓	↓	↓	↓	↓	Yes	↓
6	0.95	↓	↓	↓	↓	↓	↓	No	No	No
7	0.95-3.06	↓	↓	↓	↓	↓	↓	↓	↓	↓
8	↓	↓	↓	↓	↓	↓	↓	↓	↓	↓
9	6.42	↓	↓	↓	↓	↓	↓	↓	↓	↓
10	0.95-6.42	L	-	-	↓	↓	↓	↓	↓	↓
11	↓	-	95	95	↓	↓	↓	↓	↓	↓
12	↓	-	-	95	↓	↓	↓	↓	↓	↓
13	↓	-	-	90	↓	↓	↓	↓	↓	↓
14	↓	-	90	90	↓	↓	↓	↓	↓	↓
15	0.95-3.06	L	↓	↓	↓	↓	↓	↓	↓	↓
16	↓	↓	↓	↓	↓	↓	↓	↓	↓	↓
17	↓	↓	↓	↓	↓	↓	↓	↓	↓	↓
18	6.42	↓	↓	↓	↓	↓	↓	↓	↓	↓
19	0.95	↓	↓	↓	↓	↓	↓	↓	↓	Yes
20	↓	L	-	-	↓	↓	↓	↓	↓	↓

RUN SUMMARY
4.1% MODEL TEST

RUN	H/D	OPERATING NOZZLES FWD	L/H	R/H	MODEL CONFIGURATION α	β	LID	PRMTR PLATE	L/C NOZZLE RAILS	GROUND STRUTS
21	0.95	-	90	90	0	0	No	No	No	Yes
22	1.53									
23		L	-	-						
24		L	90	90						
25	3.06									
26		L	-	-						
27		-	90	90						
28	6.42									
29		L	-	-						
30		L	90	90						
31		L	95	95						
32										
33		L					2S			
34							3S			
35							4S			
36							No		Yes	
37	3.06									
38							2S		No	
39							3S			
40							4S			

RUN SUMMARY
4.1% MODEL TEST

RUN	H/D	OPERATING NOZZLES FWD	L/H	R/H	MODEL CONFIGURATION α	β	LID	PRMTR PLATE	L/C NOZZLE RAILS	GROUND STRUTS
41	3.06	L	95	95	0	0	No	No	No	Yes
42	↓	–	↓	↓	↓	↓	↓	↓	↓	↓
43	1.53	↓	↓	↓	↓	↓	↓	↓	↓	↓
44	↓	L	↓	↓	↓	↓	↓	↓	↓	↓
45	↓	↓	↓	↓	↓	↓	2S	↓	↓	↓
46	↓	↓	↓	↓	↓	↓	3S	↓	↓	↓
47	↓	↓	↓	↓	↓	↓	4S	↓	↓	↓
48	↓	↓	↓	↓	↓	↓	No	↓	Yes	↓
49	0.95	↓	↓	↓	↓	↓	↓	↓	↓	↓
50	↓	↓	↓	↓	↓	↓	2S	↓	No	↓
51	↓	↓	↓	↓	↓	↓	3S	↓	↓	↓
52	↓	↓	↓	↓	↓	↓	4S	↓	↓	↓
53	↓	↓	↓	↓	↓	↓	No	↓	↓	↓
54	↓	–	↓	↓	↓	↓	↓	↓	↓	↓
55	↓	L	↓	↓	+5	↓	↓	↓	↓	↓
56	↓	↓	↓	↓	↓	↓	↓	↓	Yes	↓
57	↓	↓	↓	↓	↓	↓	4S	↓	No	↓
58	↓	↓	↓	↓	+7½	↓	↓	↓	↓	↓
59	↓	↓	↓	↓	↓	↓	No	↓	Yes	↓
60	↓	↓	↓	↓	↓	↓	↓	↓	No	↓

RUN SUMMARY
4.1% MODEL TEST

RUN	H/D	OPERATING NOZZLES FWD	L/H	R/H	MODEL CONFIGURATION α	β	LID	PRMTR PLATE	L/C NOZZLE RAILS	GROUND STRUTS
61	0.95	L	95	95	-5	0	No	No	No	Yes
62									Yes	
63							4S		No	
64	1.24				0	10				
65							No		Yes	
66									No	
67	10.0					0				No
68			-	-						
69		-	95	95						
70		L							Yes	
71							4S		No	
72	15.0									
73							No		Yes	
74									No	
75			-	-						
76		-	95	95						
77	0.95	L						Yes		Yes
78									Yes	
79	3.06									
80									No	

RUN SUMMARY

70% MODEL

MODEL CONFIGURATION PARAMETERS

Ailerons = 10°
Flaps = 15°
Stabilator = 0°
δ_y = 0° (all nozzles)
δ_{NL} = 95°

MODEL CONFIGURATION DEFINITIONS

LID = Lift Improvement Device
  4S - 4-Sided LID
  3S - 3-Sided LID
  2S - 2-Sided LID
PRMTR Plate - Lift/Cruise Nozzle
  Perimeter Plate
Nose Fan Hub - Nose Fan Exit Hub
  HEM1 - Hemispherical Hub
  FLAT - Flat Plate Hub
α - Model Angle of Attack
β - Model Bank Angle

TEST NOTES

- Bad R/H Load Cell Runs 0-8.
  R/H Load Cell Replaced After Run 8
- Load Cell Calibration Check Loadings
  Runs 0, 3, 4, 5, 9, 29, 35, 36

RUN SUMMARY
70% MODEL TEST

RUN.	PNT	H/D	FAN RPM FWD	FAN RPM L/H	FAN RPM R/H	MODEL CONFIGURATION α	β	LID	PRMTR PLATE	L/C NOZZLE RAILS	NOSE FAN HUB	L/C HOOD ANGLE
0		0.95	Check Loading									
1	0	0.95	0	0	0	0	0	No	No	No	Flat	90
	1	↓	↓	↓	↓	↓	↓	↓	↓	↓	↓	↓
	2				2000							
	3				2900							
2	0	0.95	0	0	0							
	1	↓	↓	↓	↓							
	2			2000								
	3			3000								
	4			3600								
3		0.95	Check Loading									
4		0.95	Check Loading									
5		0.95	Check Loading									
6	0	0.95	0	0	0							
	1	↓	↓	↓	↓							
	2			2000								
	3			2800								
	4			3200								
	5			3600								
	6			MAX								
	7			0	2000							
	8			↓	2800							
	9				3200							
	10		↓		3600							
	11		2000		0							
	12		2400		↓							
	13		2800									
	14		3200									
	15		3600									
	16		MAX									
	17		0									
	99	↓	↓	↓	↓	↓	↓	↓	↓	↓	↓	↓

RUN SUMMARY
70% MODEL TEST

RUN.	PNT	H/D	FAN RPM FWD	FAN RPM L/H	FAN RPM R/H	MODEL CONFIGURATION α	β	LID	PRMTR PLATE	L/C NOZZLE RAILS	NOSE FAN HUB	L/C HOOD ANGLE
7	0	0.95	0	0	0	0	0	No	No	No	Flat	90
	1	↓	↓	↓	↓	↓	↓	↓	↓	↓	↓	↓
	3			2000	2000							
	4			2800	2800							
	5			3200	3200							
	6		2000	2000	2000							
	7		2800	2800	2800							
	8		3200	3200	3200							
	9		3350	3350	3350							
	10		0	0	0							
	99		0	0	0							
8	0	0.95	0	0	0							95
	1		0	0	0							
	2			2000								
	3			2400								
	4			2800								
	5			3200								
	6			3600								
	7			3600								
	8			3890								
	9			0	2000							
	10				2000							
	11				2400							
	12				2800							
	13				3200							
	14				3600							
	15			2000	2000							
	16			2700	2700							
	17			3000	3000							
	18			3200	3200							
	19			3450	3450							
	20		2000	2000	2000							
	21		2800	2800	2800							
	22		3200	3200	3200							
	23		3000	3000	3000							
	24		0	0	0							
	99	↓	0	0	0	↓	↓	↓	↓	↓	↓	↓
		0.95	Check Loading									

RUN SUMMARY
70% MODEL TEST

RUN.	PNT	H/D	FAN RPM FWD	FAN RPM L/H	FAN RPM R/H	MODEL CONFIGURATION α	β	LID	PRMTR PLATE	L/C NOZZLE RAILS	NOSE FAN HUB	L/C HOOD ANGLE
10	0	0.95	0	0	0	0	0	No	No	No	Flat	95
	1		0	0	0							
	2			2000								
	3			2400								
	4			2800								
	5			3200								
	6			3600								
	7			3900								
	8			0	2000							
	9				2400							
	10				2800							
	11				3200							
	12				3600							
	13			2000	2000							
	14			2400	2400							
	15			2800	2800							
	16			3200	3200							
	17			3400	3400							
	18		2000	2000	2000							
	19		2400	2400	2400							
	20		3200	3200	3200							
	21		2800	2800	2800							
	22		2000	0	0							
	23		2400									
	24		2800									
	25		3200									
	26		3600									
	27		4100									
	28		0	0	0							
	99		0	0	0							
11	0	0.95	0	0	0					Yes		
	1		0	0	0							
	2			2000								
	3			2400								
	4			2800								
	5			3200								
	6			3600								
	7			3900								

RUN SUMMARY
70% MODEL TEST

RUN.	PNT	H/D	FAN RPM FWD	FAN RPM L/H	FAN RPM R/H	MODEL CONFIGURATION α	β	LID	PRMTR PLATE	L/C NOZZLE RAILS	NOSE FAN HUB	L/C HOOD ANGLE
11	8	0.95	0	2000	2000	0	0	No	No	Yes	Flat	95
	9	↓	↓	2400	2400	↓	↓	↓	↓	↓	↓	↓
	10			2800	2800							
	11			3200	3200							
	12		↓	MAX	MAX							
	13		0	0	0							
	99	↓	0	0	0							
12	0	0.95	0	0	0							95
	1	↓	0	0	0							↓
	2		↓	↓	2000							
	3				2400							
	4				2800							
	5				3200							
	6		↓	↓	MAX							
	7		2000	2000	2000							
	8		2400	2400	2400							
	9		2800	2800	2800							
	10		3200	3200	3200	↓						
	11		2000	2000	2000	+5						
	12		2400	2400	2400	↓						
	13		2800	2800	2800							
	14		3200	3200	3200							
	15		2000	2000	2000	+7 1/2						
	16		2400	2400	2400	↓						
	17		2800	2800	2800							
	18		3200	3200	3200	↓						
	19		2000	2000	2000	-5						
	20		2400	2400	2400	↓						
	21		3800	2800	2800							
	22		3200	3200	3200							
	23		3600	3600	3600	↓						
	24		2800	0	0	0						
	25		3200	↓	↓	↓						
	26		3600	↓	↓	↓						
	27		0	0	0	↓						
	99	↓	0	0	0	↓	↓	↓	↓	↓	↓	↓

RUN SUMMARY
70% MODEL TEST

RUN.	PNT	H/D	FAN RPM FWD	FAN RPM L/H	FAN RPM R/H	MODEL CONFIGURATION α	β	LID	PRMTR PLATE	L/C NOZZLE RAILS	NOSE FAN HUB	L/C HOOD ANGLE
13	0	0.95	0	0	0	0	0	No	Yes	Yes	Flat	95
	1		0	0	0							
	2			2000								
	3			2400								
	4			2800								
	5			3200								
	6			3600								
	7			3900								
	8		0	0	0							
	99		0	0	0							
14	0	0.95	0	0	0			2S	No	No		
	1		0	0	0							
	2		2000	2000	2000							
	3		2400	2400	2400							
	4		2800	2800	2800							
	5		3200	3200	3200							
	6		3500	3500	3500							
	7		0	0	0							
	99		0	0	0							
15	0	0.95	0	0	0			3S				
	1		0	0	0							
	2		2000	2000	2000							
	3		2400	2400	2400							
	4		2800	2800	2800							
	5		3200	3200	3200							
	6		3500	3500	3500							
	7		0	0	0							
	99		0	0	0							
16	0	0.95	0	0	0			4S				
	1		0	0	0							
	2			2000								
	3			2400								
	4			2800								
	5			3200								
	6			3600								
	7			MAX								

RUN SUMMARY
70% MODEL TEST

RUN.	PNT	H/D	FAN RPM FWD	FAN RPM L/H	FAN RPM R/H	MODEL CONFIGURATION α	β	LID	PRMTR PLATE	L/C NOZZLE RAILS	NOSE FAN HUB	L/C HOOD ANGLE
16	8	0.95	0	2000	2000	0	0	4S	No	No	Flat	95
	9	↓	↓	2400	2400	↓	↓	↓	↓	↓	↓	↓
	10			2800	2800							
	11			3200	3200							
	12		↓	3600	3600							
	13		0	0	0							
	99		0	0	0							
17	0	0.95	0	0	0							
	1	↓	0	0	0							
	2		2000	0	0							
	3		2400	↓	↓							
	4		2800									
	5		3200									
	6		3600									
	7		4100	↓	↓							
	8		2000	2000	2000							
	9		2400	2400	2400							
	10		2800	2800	2800							
	11		3200	3200	3200							
	12		MAX	MAX	MAX	↓						
	13		2000	2000	2000	+5						
	14		2400	2400	2400	↓						
	15		2800	2800	2800							
	16		3200	3200	3200							
	17		3400	3400	3400	↓						
	18		2000	2000	2000	-5						
	19		2400	2400	2400	↓						
	20		2800	2800	2800							
	21		3200	3200	3200	↓						
	22		0	0	0	0						
	99	↓	0	0	0	↓	↓	↓	↓	↓	↓	↓
18	0	0.95	0	0	0							
	1	↓	↓	↓	0							
	2				2000							
	3				2400							
	4				2800							
	5	↓	↓	↓	3200	↓	↓	↓	↓	↓	↓	↓

RUN SUMMARY
70% MODEL TEST

RUN.	PNT	H/D	FAN RPM FWD	FAN RPM L/H	FAN RPM R/H	MODEL CONFIGURATION α	β	LID	PRMTR PLATE	L/C NOZZLE RAILS	NOSE FAN HUB	L/C HOOD ANGLE
18	6	0.95	0	0	3600	0	0	4S	No	No	Flat	95
	7	↓	↓	↓	0	↓	↓	↓	↓	↓	↓	↓
	99	↓	↓	↓	0	↓	↓	↓	↓	↓	↓	↓
19	0	0.95	0	0	0	↓	↓	No	↓	↓	↓	90
	1	↓	0	0	0	↓	↓	↓	↓	↓	↓	↓
	2	↓	2000	2000	2000	↓	↓	↓	↓	↓	↓	↓
	3	↓	2400	2400	2400	↓	↓	↓	↓	↓	↓	↓
	4	↓	2800	2800	2800	↓	↓	↓	↓	↓	↓	↓
	5	↓	3200	3200	3200	↓	↓	↓	↓	↓	↓	↓
	6	↓	3500	3500	3500	↓	↓	↓	↓	↓	↓	↓
	7	↓	0	0	0	↓	↓	↓	↓	↓	↓	↓
	99	↓	0	0	0	↓	↓	↓	↓	↓	↓	↓
20	0	0.95	0	0	0	↓	↓	↓	Yes	Yes	↓	95
	1	↓	0	0	0	↓	↓	↓	↓	↓	↓	↓
	2	↓	2000	2000	2000	↓	↓	↓	↓	↓	↓	↓
	3	↓	2400	2400	2400	↓	↓	↓	↓	↓	↓	↓
	4	↓	2800	2800	2800	↓	↓	↓	↓	↓	↓	↓
	5	↓	3200	3200	3200	↓	↓	↓	↓	↓	↓	↓
	6	↓	3500	3500	3500	↓	↓	↓	↓	↓	↓	↓
	7	↓	0	0	0	↓	↓	↓	↓	↓	↓	↓
	8	↓	0	0	0	↓	↓	↓	↓	↓	↓	↓
	9	↓	0	0	0	↓	↓	↓	↓	↓	↓	↓
	10	↓	↓	↓	↓	↓	↓	↓	↓	↓	↓	↓
21	0	0.95	0	0	0	↓	↓	↓	No	↓	Hemi	↓
	1	↓	0	0	0	↓	↓	↓	↓	↓	↓	↓
	2	↓	2000	2000	2000	↓	↓	↓	↓	↓	↓	↓
	3	↓	2400	2400	2400	↓	↓	↓	↓	↓	↓	↓
	4	↓	2800	2800	2800	↓	↓	↓	↓	↓	↓	↓
	5	↓	3200	3200	3200	↓	↓	↓	↓	↓	↓	↓
	6	↓	3600	3600	3600	↓	↓	↓	↓	↓	↓	↓
	7	↓	2000	0	0	↓	↓	↓	↓	↓	↓	↓
	8	↓	2400	↓	↓	↓	↓	↓	↓	↓	↓	↓
	9	↓	2800	↓	↓	↓	↓	↓	↓	↓	↓	↓
	10	↓	3200	↓	↓	↓	↓	↓	↓	↓	↓	↓
	11	↓	3600	↓	↓	↓	↓	↓	↓	↓	↓	↓

RUN SUMMARY
70% MODEL TEST

RUN.	PNT	H/D	FAN RPM FWD	FAN RPM L/H	FAN RPM R/H	MODEL CONFIGURATION α	β	LID	PRMTR PLATE	L/C NOZZLE RAILS	NOSE FAN HUB	L/C HOOD ANGLE
21	12	0.95	4100	0	0	0	0	No	No	Yes	Hemi	95
	13	↓	0	↓	↓	↓	↓	↓	↓	↓	↓	↓
	99	↓	0	↓	↓	↓	↓	↓	↓	↓	↓	↓
22	0	1.24	0	0	0	↓	10	↓	↓	↓	Flat	↓
	1	↓	0	0	0	↓	↓	↓	↓	↓	↓	↓
	2	↓	2000	2000	2000	↓	↓	↓	↓	↓	↓	↓
	3	↓	2400	2400	2400	↓	↓	↓	↓	↓	↓	↓
	4	↓	2800	2800	2800	↓	↓	↓	↓	↓	↓	↓
	5	↓	3200	3200	3200	↓	↓	↓	↓	↓	↓	↓
	6	↓	MAX	MAX	MAX	↓	↓	↓	↓	↓	↓	↓
	7	↓	0	2000	2000	↓	↓	↓	↓	↓	↓	↓
	8	↓	↓	2400	2400	↓	↓	↓	↓	↓	↓	↓
	9	↓	↓	2800	2800	↓	↓	↓	↓	↓	↓	↓
	10	↓	↓	3200	3200	↓	↓	↓	↓	↓	↓	↓
	11	↓	↓	MAX	MAX	↓	↓	↓	↓	↓	↓	↓
	12	↓	↓	0	0	↓	↓	↓	↓	↓	↓	↓
	99	↓	↓	0	0	↓	↓	↓	↓	↓	↓	↓
23	0	1.24	0	0	0	↓	↓	4S	↓	No	↓	↓
	1	↓	0	0	0	↓	↓	↓	↓	↓	↓	↓
	2	↓	2000	2000	2000	↓	↓	↓	↓	↓	↓	↓
	3	↓	2400	2400	2400	↓	↓	↓	↓	↓	↓	↓
	4	↓	2800	2800	2800	↓	↓	↓	↓	↓	↓	↓
	5	↓	3200	3200	3200	↓	↓	↓	↓	↓	↓	↓
	6	↓	MAX	MAX	MAX	↓	↓	↓	↓	↓	↓	↓
	7	↓	0	2000	2000	↓	↓	↓	↓	↓	↓	↓
	8	↓	↓	2400	2400	↓	↓	↓	↓	↓	↓	↓
	9	↓	↓	2800	2800	↓	↓	↓	↓	↓	↓	↓
	10	↓	↓	3200	3200	↓	↓	↓	↓	↓	↓	↓
	11	↓	↓	3600	3600	↓	↓	↓	↓	↓	↓	↓
	12	↓	↓	0	0	↓	↓	↓	↓	↓	↓	↓
	99	↓	0	0	0	↓	↓	↓	↓	↓	↓	↓
24	0	1.53	0	0	0	↓	0	↓	↓	↓	↓	↓
	1	↓	0	0	0	↓	↓	↓	↓	↓	↓	↓
	2	↓	0	0	0	↓	↓	↓	↓	↓	↓	↓
	3	↓	2000	2000	2000	↓	↓	↓	↓	↓	↓	↓

RUN SUMMARY
70% MODEL TEST

RUN.	PNT	H/D	FAN RPM FWD	FAN RPM L/H	FAN RPM R/H	MODEL CONFIGURATION α	β	LID	PRMTR PLATE	L/C NOZZLE RAILS	NOSE FAN HUB	L/C HOOD ANGLE
24	4	1.53	2400	2400	2400	0	0	4S	No	No	Flat	95
	5	↓	2800	2800	2800	↓	↓	↓	↓	↓	↓	↓
	6		3200	3200	3200							
	7		3600	3600	3600							
	8		0	2000	2000							
	9		↓	2400	2400							
	10			2800	2800							
	11			3200	3200							
	12			3600	3600							
	13			0	0							
	99		0	0	0							
25	0	1.53	0	0	0			3S				
	1	↓	0	0	0			↓				
	2		2000	2000	2000							
	3		2400	2400	2400							
	4		2800	2800	2800							
	5		3200	3200	3200							
	6		MAX	MAX	MAX							
	7		0	0	0							
	99		0	0	0							
26	0	1.53	0	0	0			No		Yes		
	1	↓	0	0	0			↓		↓		
	2		2000	↓	↓							
	3		2400									
	4		2800									
	5		3200									
	6		3600									
	7		4100									
	8		0	2000								
	9		↓	2400								
	10			2800								
	11			3200								
	12			3600								
	13			4000	↓							
	14			2000	2000							
	15	↓	↓	2400	2400	↓	↓	↓	↓	↓	↓	↓

RUN SUMMARY
70% MODEL TEST

RUN.	PNT	H/D	FAN RPM FWD	FAN RPM L/H	FAN RPM R/H	MODEL CONFIGURATION α	β	LID	PRMTR PLATE	L/C NOZZLE RAILS	NOSE FAN HUB	L/C HOOD ANGLE
26	16	1.53	0	2800	2800	0	0	No	No	Yes	Flat	95
	17	↓		3200	3200	↓	↓	↓	↓	↓	↓	↓
	18			3500	3500							
	19		0	0	0							
	99		0	0	0							
27	0	1.53	0	0	0							
	1	↓	0	0	0							
	2		↓	↓	2000							
	3				2400							
	4				2800							
	5				3200							
	6				3600							
	7		2000	2000	2000							
	8		2400	2400	2400							
	9		2800	2800	2800							
	10		3200	3200	3200							
	11		3600	3600	3600							
	12		0	0	0							
	99		0	0	0							
28	0	1.53	0	0	0						Hemi	
	1	↓	0	↓	↓						↓	
	2		2000									
	3		2400									
	4		2800									
	5		3200									
	6		3600									
	7		4100	↓	↓							
	8		2000	2000	2000							
	9		2400	2400	2400							
	10		2800	2800	2800							
	11		3200	3200	3200							
	12		MAX	MAX	MAX							
	13		0	0	0							
	99	↓	0	0	0							
29		1.53	Check Loading			↓	↓	↓	↓	↓	↓	↓

RUN SUMMARY
70% MODEL TEST

RUN.	PNT	H/D	FAN RPM FWD	FAN RPM L/H	FAN RPM R/H	MODEL CONFIGURATION α	β	LID	PRMTR PLATE	L/C NOZZLE RAILS	NOSE FAN HUB	L/C HOOD ANGLE
30	0	3.06	0	0	0	0	0	No	No	Yes	Hemi	95
	1		0	0	0							
	2		2000									
	3		2400									
	4		2800									
	5		3200									
	6		3600									
	7		4100									
	8		2000	2000	2000							
	9		2400	2400	2400							
	10		2800	2800	2800							
	11		0	0	0							
	99		0	0	0							
31	0	3.06	0	0	0						Flat	
	1		0	0	0							
	2		2000									
	3		2400									
	4		2800									
	5		3200									
	6		3600									
	7		4100									
	8		2000	2000	2000							
	9		2400	2400	2400							
	10		2800	2800	2800							
	11		3200	3200	3200							
	12		3600	3600	3600							
	13		0	0	0							
	99		0	0	0							
32	0	3.06	0	0	0							
	1		0	0	0							
	2			2000								
	3			2400								
	4			2800								
	5			3200								
	6			3600								
	7			4000								

RUN SUMMARY
70% MODEL TEST

RUN.	PNT	H/D	FAN RPM FWD	FAN RPM L/H	FAN RPM R/H	MODEL CONFIGURATION α	β	LID	PRMTR PLATE	L/C NOZZLE RAILS	NOSE FAN HUB	L/C HOOD ANGLE
32	8	3.06	0	2000	2000	0	0	No	No	Yes	Flat	95
	9			2400	2400							
	10			2800	2800							
	11			3200	3200							
	12			3600	3600							
	13			0	2000							
	14				2400							
	15				2800							
	16				3200							
	17				3600							
	18				0							
	99				0							
33	0	3.06	0	0	0			3S		No		
	1		0	0	0							
	2		2000	2000	2000							
	3		2400	2400	2400							
	4		2800	2800	2800							
	5		3200	3200	3200							
	6		3600	3600	3600							
	7		0	2000	2000							
	8		0	2400	2400							
	9			2800	2800							
	10			3200	3200							
	11			3600	3600							
	12			0	0							
	99			0	0							
34	0	3.06	0	0	0			4S				
	1		0	0	0							
	2		2000	2000	2000							
	3		2400	2400	2400							
	4		2800	2800	2800							
	5		3200	3200	3200							
	6		3600	3600	3600							
	7		0	2000	2000							
	8			2400	2400							
	9			2800	2800							

RUN SUMMARY
70% MODEL TEST

RUN.	PNT	H/D	FAN RPM FWD	FAN RPM L/H	FAN RPM R/H	MODEL CONFIGURATION α	β	LID	PRMTR PLATE	L/C NOZZLE RAILS	NOSE FAN HUB	L/C HOOD ANGLE
34	10	3.06	0	3200	3200	0	0	4S	No	No	Flat	95
	11	↓	↓	3600	3600	↓	↓	↓	↓	↓	↓	↓
	12			0	0							
	99			0	0							
35		6.45	Check Loading									
36		6.45	Check Loading									
37	0	6.45	0	0	0			No		Yes	Hemi	
	1		0	0	0			↓		↓	↓	
	2		2000	↓	↓							
	3		2400									
	4		2800									
	5		3200									
	6		3600									
	7		4100									
	8		2000	2000	2000							
	9		2400	2400	2400							
	10		2800	2800	2800							
	11		3200	3200	3200							
	12		3600	3600	3600							
	13		0	0	0							
	99	↓	0	0	0							
38	0	6.45	0	0	0						Flat	
	1		0	0	0						↓	
	2		2000	↓	↓							
	3		2400									
	4		2800									
	5		3200									
	6		3600									
	7		4100									
	8		2000	2000	2000							
	9		2400	2400	2400							
	10		2800	2800	2800							
	11		3200	3200	3200							
	12	↓	3600	3600	3600	↓	↓	↓	↓	↓	↓	↓

RUN SUMMARY
70% MODEL TEST

RUN.	PNT	H/D	FAN RPM FWD	FAN RPM L/H	FAN RPM R/H	MODEL CONFIGURATION α	β	LID	PRMTR PLATE	L/C NOZZLE RAILS	NOSE FAN HUB	L/C HOOD ANGLE
38	13	6.45	0	2000	2000	0	0	No	No	Yes	Flat	95
	14			2400	2400							
	15			2800	2800							
	16			3200	3200							
	17			3600	3600							
	18			0	0							
	99		0	0	0							
39	0	6.45	0	0	0							
	1			0								
	2			2000								
	3			2400								
	4			2800								
	5			3200								
	6			3600								
	7			4000								
	8			0	2000							
	9				2400							
	10				2800							
	11				3200							
	12				3600							
	13				0							
	99		0	0	0							
40	0	6.45	0	0	0					No		90
	1			0								
	2			2000								
	3			2400								
	4			2800								
	5			3200								
	6			3600								
	7			4000								
	8			0	2000							
	9				2400							
	10				2800							
	11				3200							
	12		0	0	900							
	13		0	0	0							
	14		0	0	0							